SYNTHESIS OF GEOPOLYMER FROM SOUTH AFRICA CFA FOR CONSTRUCTION APPLICATION

EVRAL NTSA

Thesis submitted in fulfilment of the requirements for the degree of

Master of Engineering: Chemical Engineering

Department of Chemical Engineering

Faculty of Engineering & the Built Environment

Cape Peninsula University of Technology

Bellville Campus

Supervisor: Prof T.V. Ojumu

Co-Supervisor: Prof Leslie Petrik

December 2023

Declaration

I, Evral Ntsa, declare that the contents of this thesis/dissertation represent my unaided work and that the thesis/dissertation has not previously been submitted for academic examination towards any qualification. Furthermore, it represents my own opinions and not necessarily those of the Cape Peninsula University of Technology.

2023-09-16

Signature

Date

Abstract

In compliance with sustainable development goal nine, new construction materials' impact becomes increasingly important in the 21st century. This is because of the anthropogenic activities related to cement production and concrete casting, which have led to high levels of CO_2 emissions. Coal fly ash (CFA) from coal combustion during energy production is a waste product that is costly to dispose of in an open environment and is also associated with air and land pollution.

The use of waste CFA as raw material for the synthesis of geopolymer has been reported as a route to convert this waste into value-added products, simultaneously remediating its environmental impact as well as eliminating additional greenhouse gas emissions associated with the production of cement and concrete. As a result of improved formulations, good mechanical and durability characteristics have been achieved that meet concrete standards; however, the 24-hour oven heating curing regime may not favour energy savings, which in turn affects the cost of the product, CO_2 emissions, and other applications.

As a raw material, CFA was physiochemically examined and characterised to understand its properties in the mix design process. Formulations were designed based on the effect of fine and coarse aggregates on CFA-based geopolymer paste properties and then cured at different regimes: room curing with plastic cover, room curing without plastic cover, along with the reference oven heating method. These formulation's properties were investigated using concrete standards such as fresh properties, mechanical strength, durability and thermal profiles based on the optimised formulations. The best formulations at different curing conditions were characterised using XRF, SEM, XRD, and FTIR analytical techniques to understand the material's composition, morphology, and mineral phases and identify organic or inorganic bonds in the materials. Radon and gamma measurements were also performed to determine whether CFA-based geopolymer formulations are carcinogenic. It was essential to quantify greenhouse emissions for the optimised formulations as well as understand all the fundamental chemistry and the link from material composition to its behaviour and the cost associated with the most suitable curing regime.

The XRF, XRD and particle size analysis of CFA indicate its properties that comply with ASTM 618, using low calcium CFA based on silica, aluminium and calcium oxide content, with high particle size. CFA and products synthesised using CFA-based geopolymer formulations exhibited

high quantities of crystalline structures with quartz and mullite minerals. The effect of sodium hydroxide concentration and variation of formulations at the fresh state impacted the initial and final setting time, and consistency resulted. Better setting properties using 12 molarity (M) of 170- and 230 minutes with GPP-M2A formulation on initial and final setting time with a consistency of 7 mm penetration was achieved compared to other NaOH concentrations tested. Adding fine and coarse aggregates to GPP-M2A to create GPC-M2C as an optimised formulation led to a density increase of 1748.6 to 2182.2 kg/m^3, lowering compressive strength from 29.7 to 26.7 MPa. Considering flexural, tensile, and modulus of elasticity tests, these formulations with fine aggregates showed greater ductility and increased yield than those with no fine and coarse aggregates. Based on curing regimes, the given conditions of oven curing resulted in early strength similar to that standard of concrete of being 25 MPa at three days of curing, while this strength is achieved more slowly after 21 and 28 days of ageing, respectively, using room curing, with and without a plastic cover respectively. After three months of ageing, products of room curing with plastic covered had similar compressive strength to oven curing. CFA-based GPC cured room curing without plastic-covered resulted in heavy efflorescence, while high early shrinkage was observed from that cured at oven condition of 60 ^oC. All formulations resulted in good durability properties. A panel of about 60 mm thick cured under plastic-covered conditions achieved an excellent thermal fire rating of 1 hour. An oven curing condition at 60 ^oC for 24 hours is unfavourable for industrialisation due to its CO_2 emissions factor of 0.684 kg CO_2 eq and yearly utility costs of R1 361 933.35 compared to 0.094 kg CO_2 eq and R33 146.79 associated with room curing, which is also lower than the CO_2 emissions factor of 0.132 kg CO_2 eq associated with conventional Ordinary Portland Cement (OPC) concrete. CFA-based geopolymer formulations may be recommended for open infrastructure, but the average total radon and gamma activities must be controlled for housing. CFA showed 684 Bq/kg of average total activity in this study, which is above the world average of 420 Bq/Kg, while the synthesised formulations produced 408 to 459 Bq/kg on average.

The GPC-M2C formulation cured at room temperature under a plastic covering condition, being considered the optimised formulation, resulted in comparable standard properties to that of normal OPC concrete. The results of this study indicate that synthesised CFA-based geopolymer formulations that cure at room temperature with plastic cover are recommended as being an environmentally friendly, lower cost and feasible process with suitable early strength, as most strength decisions are reached after 28 days of ageing.

Acknowledgements

First, I wish to express my gratitude to Prof TV Ojumu and Prof Leslie Petrik for being assiduous and passionate supervisors throughout this research. They have been the driving forces behind this accomplishment.

To all my lovely family members in the name of Dr Marcel Ollion, Ontso Veronique, Victor Ntsa, Adalie Ntsa (Adalie Notyhanga), Hyacinth Mbourangon, Zita Mviri, Jule Ombou Mbani, Gael Mparambo, Atipo Bordonow, Mardochee Ollion, Christ Ollion, Gael Omiere, Bubien Ntsa Ollion, Debien Ntsa, Dejanvinelle Ollion, Theresia Ollion, Heldia Mparampo and others, I am grateful for your interminable supports, love, and word of encouragement.

I acknowledge the help of my chemical engineer colleagues in the name of Vinny Ndjate, Etienne Beya, and Rosicky Kalombe in this project.

I also appreciate the support of my friends Alex Mumba, Brel Goliele, Lionel Kandza, Amedee Kampala, Junior Mpho-ina, Benel Hessanguy, Jean Claude Omolombi, Brel Batalou, Iloki Rael, Duval M'fouka, Kely Mouko, Stevhen Dzon and everyone whose names are not mentioned but who supported me: you all deeply believed that I would successfully achieve this. I would like to extend my sincere gratitude to Portia Sobekwa and Hero Qhawekazi Nkungu

Words of blessing to my Pastor, Nathan Johnrock, who serves as a motivator through prayers. May God bless every member of the City of Glory Church.

I am very thankful to people and the following organisation: Big thanks to all the ENS family, Mr Pieter de Wet and William Mathobela of Roadlab. Dirk Oosthuizen and all the team from NES Consult for helping me with testing facilities and equipment. Prof Robert Lindsay and Mr Evan Swartbooi from UWC helped with the radon measurement and sieve particle analysis, respectively. Prof. Philip Janney, Dr Hong Su, Sandeeran, Nassela and Zahra from UCT with the help of XRF, XRD and Particle Analyzer, respectively. I also appreciate the help of the UWC Securities control room team for their access help during the critical period of COVID-19, Kelly Moir from Scientific Services, and Remy Bucher from iThemba labs. My deepest gratitude goes to the following CPUT staff members who were extremely helpful: Ms Taylia Green, Prof Mujahid Aziz, Prof Veruscha Fester, Ms Mtembukazi Sibindlana and Mr Steve Nsenda Tshilumbu.

I gratefully acknowledge the funding provided by the CPUT bursary, which motivated me to pursue and achieve success in this project.

Dedication

I **dedicate** this thesis to the memory of my late partner **Bongi Notyhanga**.

Thank you, mama, your contribution to my life has been incalculable. I think and weep in my heart about you. You have highly blessed my life with Victor and Adalie. You may be gone early, but will never be forgotten. May your soul continue to rest in internal peace.

All the honour and Praise to the most supreme God, Almighty Jesus Christ. You are all that matters**.**

"And LORD JEHOVAH God helped me; because of this, I am not ashamed; because of this, I refuse to give up, and I know that I will not be disgraced."

Isaiah 50:7 "

List of presentations and publications

Oral presentation

Ntsa, E., Petrik L.F. and Ojumu T.V., 2022. Suitability of geopolymer made from waste CFA as replacement for Portland cement concrete. RecycleBIM R&D Project and the SUBLime Network. University of Minho. Guimarães. Portugal. 19 October, 2022.

Ntsa, E. and Petrik, L.F., 2021. Geopolymer production and projects to date SACCA WEBINAR – GEOPOLYMERS. South Africa. 24 February, 2021.

Publication in progress

Ntsa, E., Petrik L.F and Ojumu T.V., 2023. Synthesis of low calcium CFA geopolymer concrete cured at room temperature for structural application.

Ntsa, E., Lindsay, R., Petrik, L.F. and Ojumu, T.V., 2023. Measurement of radon exhalation and emanation in synthesised geopolymer-based South African CFA as a construction material

Table of Contents

List of Figures

List of Tables

List of Abbreviation

ASTM	American Society for Testing and Materials
BFD	Block Flow Diagram
CFA	CFA
EDX	Energy Dispersive X-Ray Analysis
EPA	Environmental Protection Agency
EPD	Environmental Product Declaration
FA	Fly Ash, same as CFA
FTLIR	Fourier Transform Infrared Spectroscopy
GPa	Giga-Pascale
GPC	Geopolymer Concrete
GPM	Geopolymer Mortar
GPP	Geopolymer Paste
GWP100a	Global Warming Potential over 100 years
ICP-OES	Inductively Couple Plasma Optical Emission Spectrometry
ISO	International Organization for Standardization
LCA	Life Cycle Assessment or Analysis
LOI	Loss on Ignition
MPa	Mega-Pascale
PFD	Process Flow Diagram
SA	Department of Energy
RSA/ SA	Republic of South Africa/ South Africa
SABS	South African Bureau of Standards
SANS	South African National Standards
SEM	Scanning Electron Microscopy
USA	United States of America
XRD	X-ray diffraction

XRF	X-ray fluorescence

Chapter 1

General introduction of the study

This chapter contains a brief background to the study and the present research motivation and problem statement. The research aims, objectives, approaches, scope and limitations, and conceptual framework are detailed.

1.1 Background

In the mid-20th century and the commencement of the 21st century, one of the major challenges facing humans is the lack of energy security. Using the current fossil fuels process has led to unsustainability issues, with resources depleting and wastes accumulating. Climate change is real, and its consequences are inevitable. Day-to-day human activity based on coal-based energy contributes to ecosystem degradation as it increases environmentally related human health issues and soil pollution and leads to the extinction of plant and animal populations (Omer, 2018). This is the case in the Republic of South Africa (RSA), where most of the electricity production comes from the combustion of low-grade coal, which leads to a high amount of by-product, Coal fly ash (CFA), considered waste.

Coal is a non-renewable source of energy. South Africa's coal reserves are estimated at 53 billion tons, with almost 200 years of resource supply left based on the present production rate. Coal power stations are responsible for about 72.1 to 77% of primary energy needs by providing about 224 million tons of marketable coal annually (Eskom, 2021, DOE, 2018). This production results in a large amount of CFA waste, of which about 7% is sold. The rest is disposed of in an open dump. Coal burning largely contributes to the country's CO_2 emission, and CFA generated as a by-product has a disposal concern due to the high volume of waste (Reynolds-Clausen and Singh, 2019 Nair and Vishnudas, 2014). Based on a study by EcoMetrix Africa, the total greenhouse gas (GHG) emissions from Eskom's operations amounted to 212,601,425 tCO_2eq in 2019 (Eskom, 2020). In general, as part of the global warming impact, burning 10 tons of carbon (C= 12g /mol) releases 36.66 tons of CO_2 (CO_2= 44 g/mol). However, the heating of coal generates 10% by weight of CFA; therefore, for every 10 tons of coal used, 1 ton of CFA is generated, and

33 tons of CO_2 is emitted (Davidovits, 2021). The use of CFA as a binder to produce construction materials may minimise environmental issues related to the country's construction industries and improve the country's economy and biodiversity.

Portland cement is the usual commodity binder used to produce most construction elements in construction. It provides acceptable fresh hardened and long-term durability properties. Its high production rate leads to global warming and climate changes due to increased CO_2 and greenhouse emissions caused by the calcination process, which requires high energy (reaction starts at 900 ^oC) to decompose calcium carbonate into calcium oxide as the required product. This also results in CO_2 as a by-product (Naqi and Jang, 2019). As Davidovits (2021) explained, the production of 1 ton of cement directly releases 0.55-ton chemical CO_2 and requires carbon base fuel to yield an additional 0.40 ton of CO_2; therefore, the production of 1 ton of cement results in 1 ton of CO_2 emitted.

Presently, research aims to develop alternative green technologies to minimise the usage of cement to diminish carbon emissions. Several technological advancements are being made to reduce costs, CO_2 emissions, and embodied energy in cement by using binding extenders such as fly ash, condensation silica fume, and ground granulated blast-furnace slag. One of the new sustainable technologies considered to become a potential replacement for cement binders with high scientific interest to improve economic, environmental, and social outcomes is the geopolymer process *et al.*, 2016 and *et al.*, 2018), This technology is experiencing a scientific delay due to the effect of parameters such as a higher setting time of the product which requires elevated temperatures for curing which restrains its ease of use in construction, particularly in low weathering condition, 2019). The presence of radionuclides such as enhanced levels of uranium (U), thorium (Th), and Radium 226 (Ra) have been reported and observed in many CFA and soils of some industrial regions (Jaworski and Gryzbowska, 1977; Roy et al., 1981) and Fucic et al., 2011).

Geopolymer is an “environmentally green” material, which has been claimed to excel Portland cement in many aspects, a material that could potentially be the future “cement”. It was proposed by Davidovits in the late 1970s, referring to the amorphous to semi-crystalline three-dimensional silico-aluminate materials activated in a highly alkaline environment (Davidovits, 2008). Geopolymer consists of chains or networks of mineral molecules linked with covalent bonds. From their chemical structure, geopolymers can be used in many applications such as bricks, ceramics,

fire protection board manufacturing, fire-resistant and heat-resistant fibre composites, and many other materials, depending on the silicon and aluminium ratio (Ebewele, 2000).

1.2 Problem statement

The studies of Nyale (2014) and Kalombe et al. (2020) have demonstrated that low calcium CFA can be used to synthesise geopolymer for construction applications, even though geopolymer resulted in high-strength materials. The formulations developed from the mentioned studies were cured at high oven temperatures (60-100^{o}C) for 24 hours. However, the energy expended may not justify the product cost, embodied energy and carbon footprint because high heat curing is an energy-intensive process that directly impacts the product cost, embodied energy and carbon emission. The oven curing method also makes the process unfavourable to the cast-in-situ process. This will be seen as a stumbling block in the large-scale production of construction materials. It is therefore important to develop similar geopolymer formulations of comparable strength under room temperature with the view to minimise the energy cost, which will make the process economically and environmentally friendly.

1.3 Aim and objectives of the study

The goal of this research is to develop processes that are eco-friendly and feasible. Here, formulations will be aimed at structural and durable properties to turn waste (CFA) at power stations for value-added construction materials cost-effectively and energy-efficiently. The objectives of the research are to:

i. Identify the characteristics of CFA to be used, including its physical and chemical properties for suitable geopolymerization.
ii. Determine the effect of high and low sodium hydroxide concentration and the effect of curing at high (oven) and low temperatures (room temperature) on the final product.
iii. Develop optimised formulation of geopolymerisation protocol for manufacturing low environmental impact construction material such as wall panels systems and pipes at low temperatures with structural strength and durability properties that comply with SANS, ASTM, and ISO standards for construction and building elements.
iv. Perform material and energy balances to determine the unit cost of the optimised CFA-based geopolymer product.

1.4 Research questions of the study

Many questions may be posed about using CFA as the main binder to produce construction material by synthesising geopolymer to achieve the above project objectives. These questions will be experimentally answered based on whether the fresh and hardened properties of each formulation developed complied with SANS or SABS, ASTM, and ISO standards by providing information on the following research questions:

i. What are the chemical, physical properties, and mineralogy of Lethabo-classified CFA and its effect on the final product?
ii. What is the minimum sodium hydroxide concentration needed to obtain a durable and adequate strength geopolymer product?
iii. Is it possible to minimise the setting times of any formulation at low and ambient (room) temperatures and produce cement-free construction materials?
iv. What are the appropriate mixing and demoulding times for each formulation?
v. What are the strength increment and durability of these geopolymer formulations made using CFA sourced from the Lethabo power station?
vi. What is the material composition of the final product, the energy used during the process, the environmental effect of the final product, and the cost of formulation per unit kilogram or cubic meter?
vii. Are CFA-based geopolymer products radioactive?

1.5 Significance and contribution of this study

CFA is a solid waste from coal-burning power stations. Solid waste management is a universal issue that affects everyone in the world. In South Africa, CFA can be obtained from Eskom coal power plants. Due to the presence in CFA of toxic metals such as arsenic, lead, mercury, cadmium, chromium, and many others, this waste is classified as hazardous. The Environmental Protection Agency (EPA) has found that living next to a coal ash disposal site can increase the risk of cancer by 50% or cause other diseases such as nervous system impacts, including cognitive deficits, developmental delays, and behavioural problems (Available at: https://www.psr.org/wp-content/uploads/2018/05/coal-ash-hazardous-to-human-health.pdf, Accessed on the 20th September 2021). This project will have as its goal the elimination of the environmental impact of CFA by converting it from powder into a well-bonded material. It will also benefit Eskom by minimising waste from coal mining and energy generation processes. This will

lower the country's CO_2 emissions from cement production by substituting geopolymer for cement.

1.6 Research approach

Many studies have proved the possibility of manufacturing construction materials such as bricks from the synthesis of geopolymer using CFA and alkaline activator (sodium hydroxide, water, and sodium silicate), which resulted in an acceptable strength at a high concentration of 14M NaOH and mixing time not less than 30 minutes with curing temperature around 80 to more than 100 ^{o}C This research consists of developing suitable formulations for materials such as poles and pipes and precast panels at a sodium hydroxide concentration of less than 14M using minimum mixing times and low curing temperatures. The study will investigate the effect of these parameters on strength and durability, including product quality, by measuring cracking due to chemical reactions, shrinkage, water absorption, and penetration. The overall schematic representation of all the steps of the experiments and different techniques of strength, durability, and characterisation tests are represented in the diagram Figure 1-1

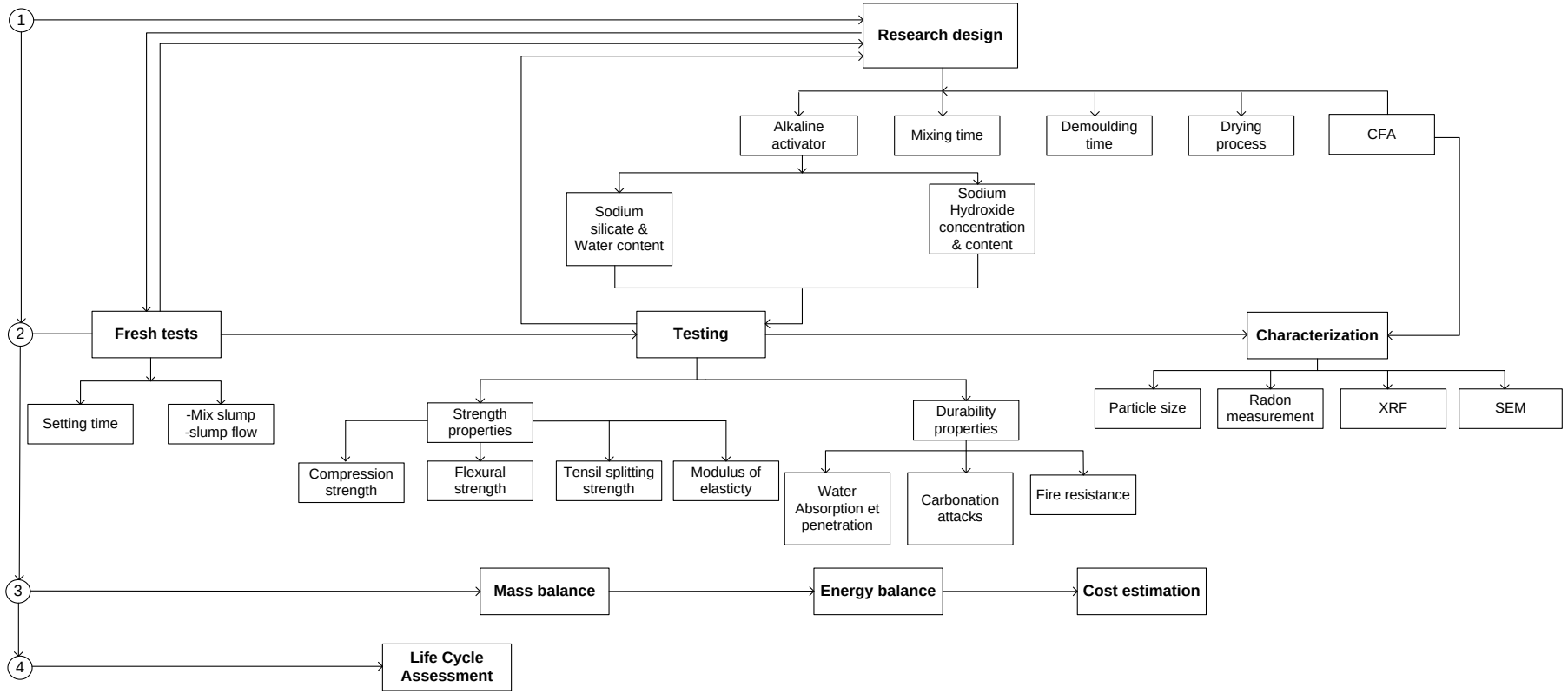

Figure 1-1:Schematic of the research approach

1.7 Scope and delimitation of the study

The experimental work was based on Lethabo CFA; therefore, the results obtained in this study will be a baseline for comparison with other types of CFA in the future. Again, no cementitious experiments will take place in this study as this study is mainly focused on CFA. No additional trial run on any other chemicals apart from sodium hydroxide and sodium silicate was used in this process to improve properties. This avoids additional chemical costs, which may lead to an expensive product. This study will not include a full carbon footprint determination or a lifecycle assessment of the product as the process is not at the industrial level yet.

1.8 Thesis layout

The thesis layout was arranged systematically in six (6) chapters.

Chapter 1: General introduction to the study

This chapter presents a comprehensive background to the study and the problem statement. It also establishes the research aim and objectives. Furthermore, it defines the research approaches, scope, and limitations.

Chapter 2: A literature review on the synthesis of CFA-based geopolymer

This chapter describes the origin, chemical composition, and classification of CFA as a binder. It provides a comprehensive summary of geopolymer. The published articles, journals, theses, and other publications on the geopolymerization process are comprehensively reviewed.

Chapter 3: Experimental methodology for the synthesis of CFA-based geopolymer

This chapter sets out how to develop construction material by synthesising CFA-based geopolymer at low temperatures for industrial benefit by describing the methods used for developing formulations, equipment, and chemicals used. Here, the methods include the pre-test and testing of raw material and geopolymer products using engineering tests and analytical techniques.

Chapter 4: Development of geopolymer for construction application using CFA I: Optimisation and Characterisation

This chapter contains the main findings of the research, followed by a discussion Section that interprets the results of the optimised mix based on strengths, durability, special properties, and analytical techniques and provides the significance of the findings. Proper results discussed in this Section will lead to better conclusions and recommendations

Chapter 5: Development of geopolymer for construction application using CFA III: Life Cycle Assessment

This chapter used a technique based on a certain environmental methodology to evaluate the effects that CFA-based geopolymer paste and concrete products developed at optimum conditions would have on the environment at a laboratory scale. LCA technique can also allow decision makers to compare CFA products with other products, such as normal OPC concerns, therefore, select the product with the lowest environmental impact. This decision-making may be political or business in nature.

Chapter 6: Development of geopolymer for construction using CFA II: Materials and Energy Balances and Economics

In this chapter, the process was audited through the performance of material and energy balances and economic analysis. The material and energy balances helped to determine the mass flow rates and chemical and physical properties of different streams entering or leaving the energy quantities of the process. The economic analysis helped to determine the feasibility of the process, which will help in investment decision-making.

Chapter 7: Conclusion, recommendations, and suggestions for future works

This chapter lists general conclusions and recommendations related to the major findings obtained from this study. Here, the best opinions are provided. Challenges that could not be resolved due to time or being out of the study scope will also be recommended to be investigated as continuity of this research.

Chapter 2

A literature review on the synthesis of CFA-based geopolymer

This chapter presents a background to CFA, such as its origin, availability, and environmental effects related to its dumping. It also provides a general understanding of geopolymer synthesis from previous studies based on structural properties, durability properties, and environmental factors of the product. Here, published articles, theses, and other publications on geopolymer research are reviewed.

2.1 Coal mining and CFA

2.1.1 Coal mining

The most instinctive method to generate heat is the ignition of organic matter, which will continue to generate heat in the presence of oxygen until all this matter has combusted (Keyte, 2009). Coal is vital for producing electrical energy in coal-burning thermal power plants worldwide. Geologically, coal is a sedimentary rock. It is dark brown to black in colour, combustible and consists of a complex heterogeneous mixture of organic and inorganic matter. It is chiefly composed of carbon, hydrogen, and oxygen, with some amount of inorganic matter with a certain moisture content depending on its type. Mineral matter is the non-combustible portion of the materials available in coal, resulting in ash at the end of combustion (Zhang, 2013). Organic matter makes a prime contribution to the use of coal for many purposes, and the inorganic matter influences the corrosion, erosion, and agglomeration that rise during coal utilisation (Susilawati, 2015).

2.1.1.1 Origin of coal mining

Coal is formed by a geological process known as coalification (Figure 2-1a) when plant material (vegetal matter) decays underwater in the absence of oxygen, leading to an increase in carbon. The initial product of this decomposition process is peat, which gradually transforms into different coal types (Figure 2-1b) by the action of moderate temperature (about 773 ^{o}C) and high pressure in a geochemical stage. (Marsh and Rodríguez-Reinoso, 2006).

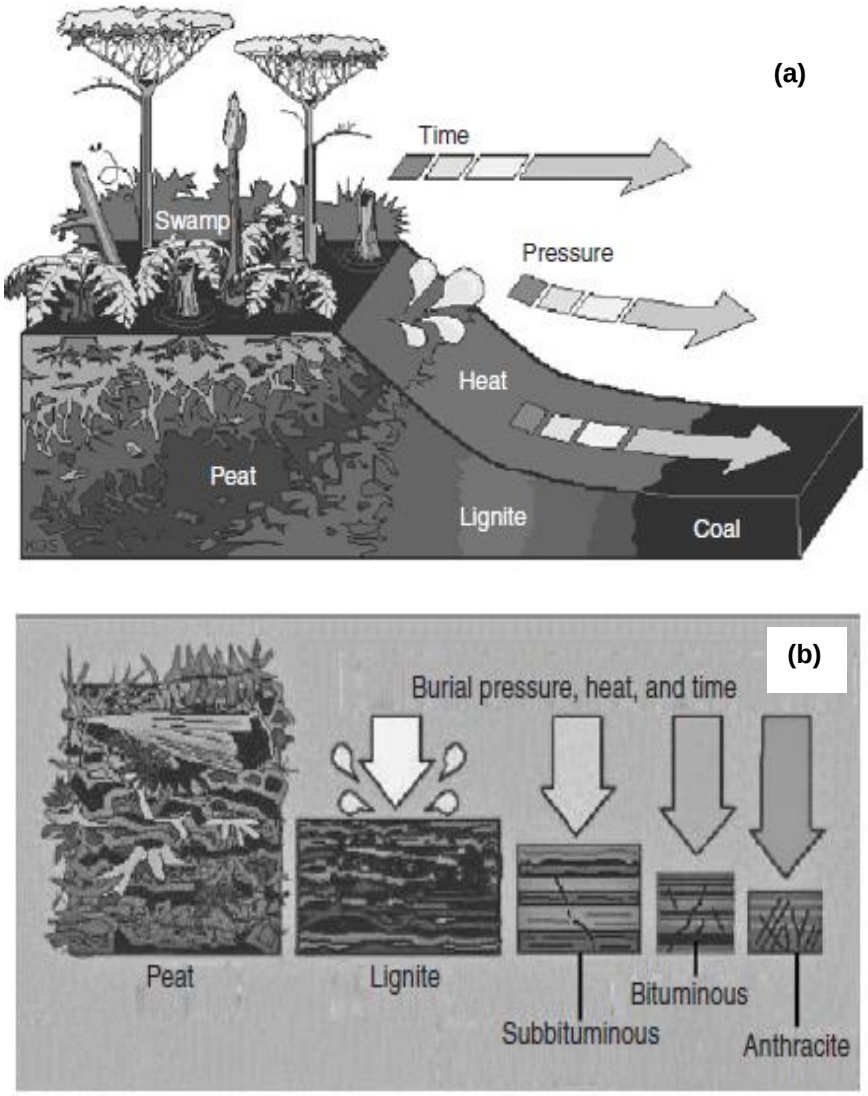

Figure 2-1: Coalification process (a) and types of coal types (b) (source: Speight, 2008:135)

2.1.1.2 Properties of coal mining

According to Kumar et al. (2016), coalification exhibits ample changes in the physical and chemical properties of coal. Different properties are observed from each stage, such as moisture content, carbon content (which also affects the colouring), and calorific value corresponding to different industrial usage. Figure 2-2 and Table 2-1 represent moisture and carbon content in different coals and a typical mass basis composition of bituminous coal, respectively.

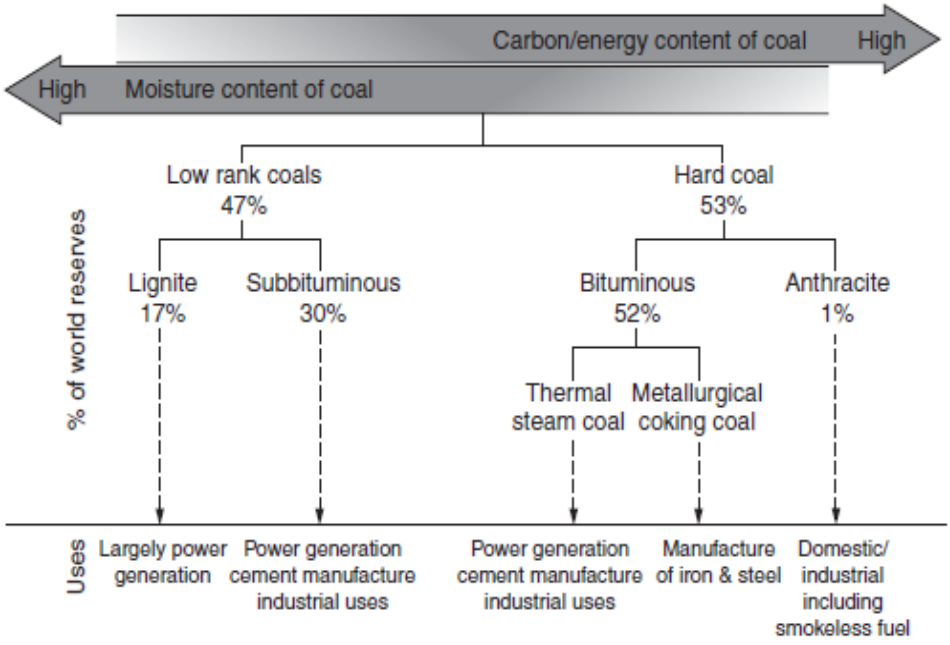

Figure 2-2: Different coal moisture and carbon content and applications (source: Speight, 2008)

Table 2-1: Bituminous coal composition (Source: Weiland and White, 2018; Luo et al., 2019)

Ultimate analysis	**As received wt.%**
Carbon	63.75
Hydrogen	4.5
Nitrogen	1.25
Sulphur	2.51
Chlorine	0.29
Ash	9.7
Moisture	11.12
Oxygen	6.88

2.1.2 Coal fly ash

Coal is first crushed or pulverised into a fine powder, then combusted to heat and purified, demineralised water to generate electricity. Water turned into steam with temperatures ranging from 1200 ^{o}C to 1700 ^{o}C. Coal burning generates heat and by-productsby-product in CFA and various gases such as CO_2, NOx and SOx (Eskom Official, 2015). CFA is grey powder and the end residue of combustion from pulverisation of bituminous, sub-bituminous or lignite coal in the furnace at thermal power plants. It also consists of mineral constituents of coal which are not fully burnt (Basu *et al.*, 2009).

2.1.2.1 Coal fly ash generation and technologies

CFA formed from the inorganic impurities remains suspended in the flue gases during combustion. Some of them coagulate and precipitate to form the bottom ash, whereas the rest are transported by gases and collected by mechanical separators or electrostatic precipitators (Tokyay, 2016). The combustion system of a pulverised-coal-fired power plant is schematically shown in Figure 2.2. The total amount of CFA obtained from combustion may vary from 6% to 40% (by mass) of coal used; however, this depends on the type of coal used and the plant-installed capacity. According to Reynolds-Clausen and Singh (2019), in 2014-2015, Eskom burnt 120 Mt of coal in its 13 power stations, generating 35,000 MW of electricity and resulting in about 30% of CFA as a by-product.

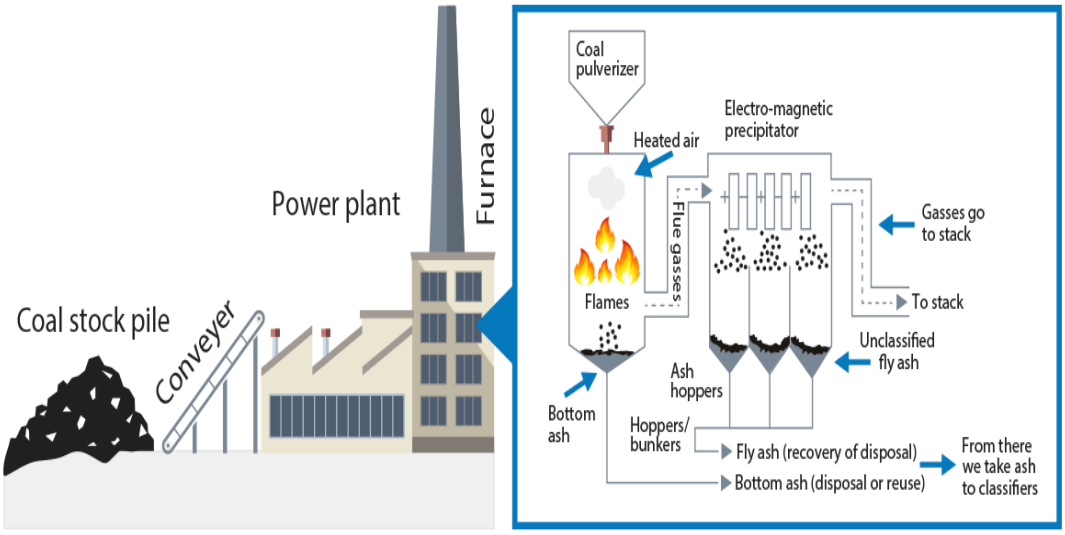

Figure 2-3: Generation of CFA during combustion (source: https://www.sepcement.co.za/Product-Ash.php, Accessed on 1 August 2021).

In terms of burning temperatures, there are various technologies available. Table 2-2 lists them.

Table 2-2: Combustion technologies and operating temperatures (Source: Davidovits, 2008:277)

Technology	Temperature, °C
Fluidised bed	850
Pulverised coal combustion 1	1250
Pulverised coal combustion 2	1500
Coal gasification IGCC	1800

Fly ash reactivity appears to be determined by the nature and proportion of the glass phase present, which, for a given type of coal, is generally dependent on the operating temperatures in the boiler, according to Table 2-3. The chemical reactivity seems to be influenced by glass composition, glass content, and the physical state of the glass. Currently, research in fly ash is aimed at understanding the microstructure of the glass phase due to the complex inter- and intra-particle inhomogeneities of these materials (Davidovits, 2008:279).

Table 2-3: The principal phases found in coals and the phases formed after combustion (Source: Davidovits, 2008:279)

Common coal minerals	**Phases formed after combustion**		
	850^{o}C	**1500^{O}C**	**1800^{O}C**
Quartz	quartz	cristobalite	glass
Kaolinite	metakaolin	glass+mullite	glass
Illite	illite	glass+mullite	glass
Pyrite FeS_2	iron sulphide FeS/FeO	Fe_2O_3 haematite + glass Fe_2O_4 haematite + glass	glass
Calcite	lime CaO	glass	glass

Table 2.4 represents an estimation of the amount of CFA content for a specific type of coal.

Table 2-4: Types of coal and its CFA content (Source: www.purdue.edu/discoverypark/energy/assets/pdfs/cctr/outreach/Basics8-CoalCharacteristics-Oct08.pdf, Accessed on 1 August 2021).

Types of Coal	**CFA content,** % weight
Lignite	10 to 50
Sub-Bituminous	≤10
Bituminous	3 to 12
Anthracite	10 to 20

2.1.2.2 Mineralogy, classification and chemical composition of CFA

CFA has more or less 316 individual minerals with 188 mineral groups, which makes it one of the most complex materials in terms of characteristics. CFA contains SiO_2 (both amorphous and crystalline), Al_2O_3, and F_2O_3 as the major component, followed by minor elements shown in Table 2.5 (Bhatt *et al.*, 2019). The presence of trace elements such as As, B, Be, Cd Cu, Ga, La, Mn, Hg, Ni, Pb, Ag, Sn, Sr, Zn, and Zn are observed, including radioactive elements such as U, Th, Ra and Rn (Fatoba, 2007; Madzivire et al. 2014). Figure 2-4 represents a mineralogy of a CFA sample obtained from the Arnot power station in the RSA.

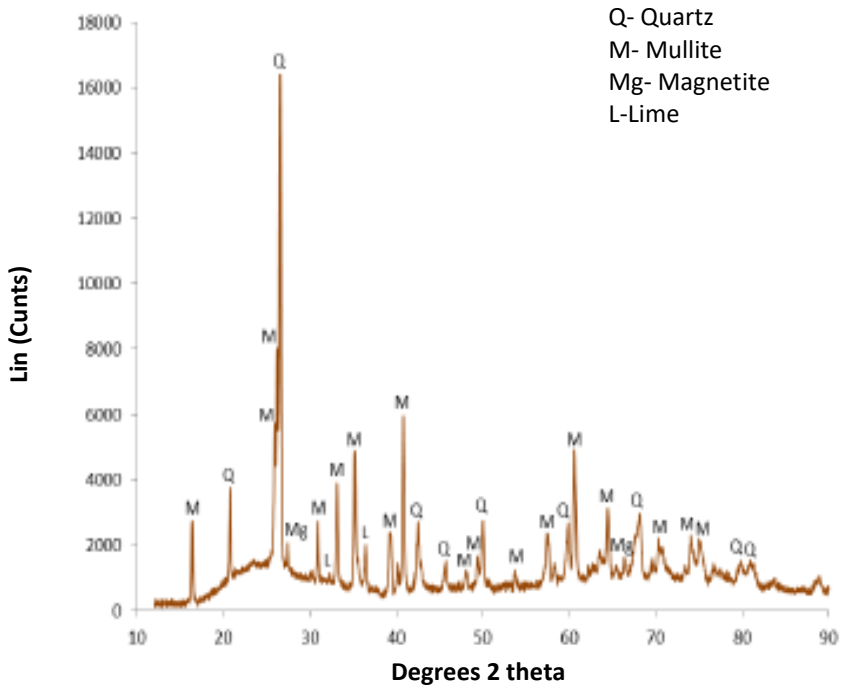

Figure 2-4: An example of the mineralogy of a fresh CFA sample obtained from Arnot power station in South Africa as determined by qualitative XRD (Source: Nyale, 2014:106).

The variation of major elements depends upon the CFA class, where three classes are categorised according to the ASTM C618 (2019). CFA is mainly available in Class F and Class C from different coal roughly, as shown in Table 2-5. Class F may contain double the amount for the loss of ignition fraction than class C (Wallah and Rangan, 2006).

Table 2-5: Range of chemicals of Chemical Composition for low and high-calcium coal fly ashes (Source: Davidovits, 2008:278).

Oxide content	**Class F, %**	**Class C Lignite-based, %**
SiO_2	47.2 - 54	18 - 24.8
Al_2O_3	27.7 - 34.9	12.1 - 14.9
Fe_2O_3	3.6 - 11.5	6.3 - 7.8
CaO	1.3 - 4.1	13.9 - 49
Free lime content	0.1	18 - 25
MgO	1.4 - 2.5	1.9 - 2.8
SO_3	0.1 - 0.9	5.5 - 9.1
Na_2O	0.2 - 1.6	0.5 - 2
K_2O	0.7 - 5.7	1 - 3

Table 2-6: Main categories of coal fly ashes (Source: ASTM C 618, 2019)

Class of CFA	CaO content
Low-calcium fly ash class F	Less than 10 %
High-calcium fly ash class C	Greater than 10 %

2.1.2.3 Particle size distribution and morphology

CFA is an incombustible inorganic and odourless material. It is grey and mainly composed of spherical glassy powder that consists of microparticles with an estimated size range from 0.5 to 100 µm (Figure 2-5) and with a bulk density between 900-1300 Kg/m^3 and ignition loss (%) of 3.82%. It has an amorphous or spherical shape. This also means the morphological CFA is a heterogeneous material with the composition varying from place to place (Figure 2-6).

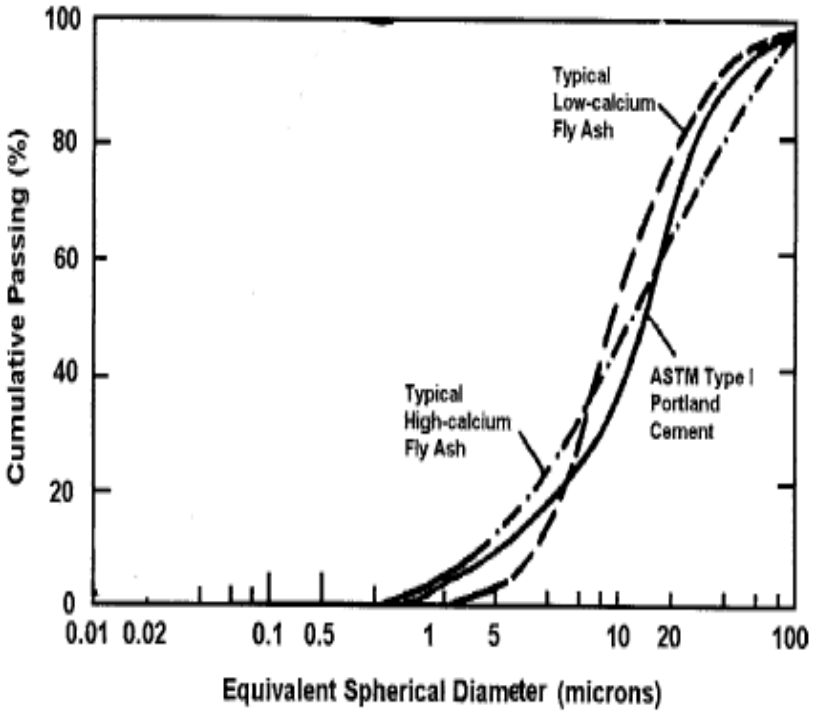

Figure 2-5: Cumulative distribution of low calcium CFA class, high calcium CFA class and Portland cement (Modified from source: Shi et al., 2003: 61)

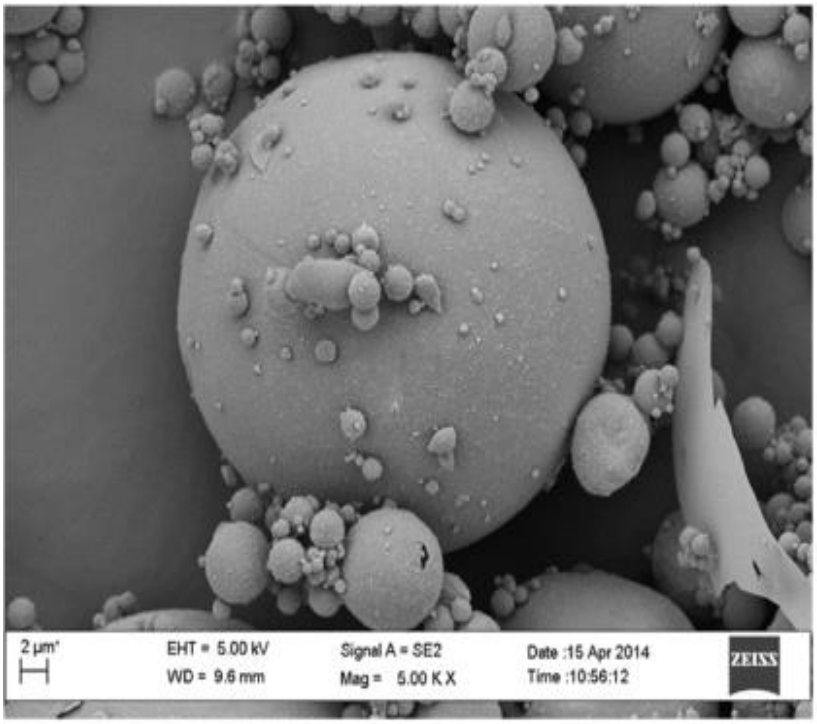

Figure 2-6: Morphology of Eskom Malta plant CFA from unknown firing temperature determined by SEM analysis (Source: Maleka, 2015:53)

2.1.2.4 CFA disposal, environmental impact, and utilisation

Coal power generation is the world's primary energy source, with about 38% of the total energy demand, followed by 23% from hydraulic power (see Figure 2.6). As a result of its production, CFA is generated in large quantities globally as a by-product (fly ash—85% and bottom ash—15%) of nearly 1 billion tons annually (Sultana et al., 2021).

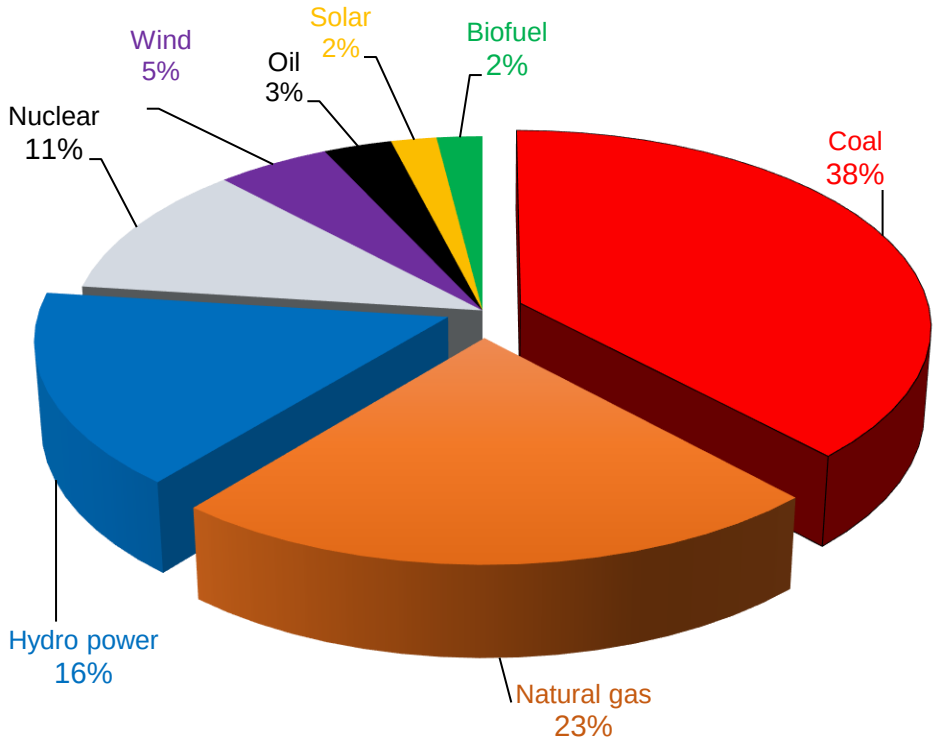

Figure 2-7: Worldwide type of energy production source and accountability (Source: Sultana et al., 2021).

Because of the colossal use of coal to meet growing energy demands, the amount of CFA being generated grew exponentially to approximately 750 million tons in 2015 (Yao *et al*., 2015; Gollakota, Volli and Shu, 2019) Compared to 500 million tons in 2005 (USEIA, 2014; Gollakota, Volli and Shu, 2019). In South Africa, according to the Department of Environmental Affairs, Eskom electricity production results in many kilo-tons of this waste being produced and disposed of in the open dumps annually (Figure 2.8).

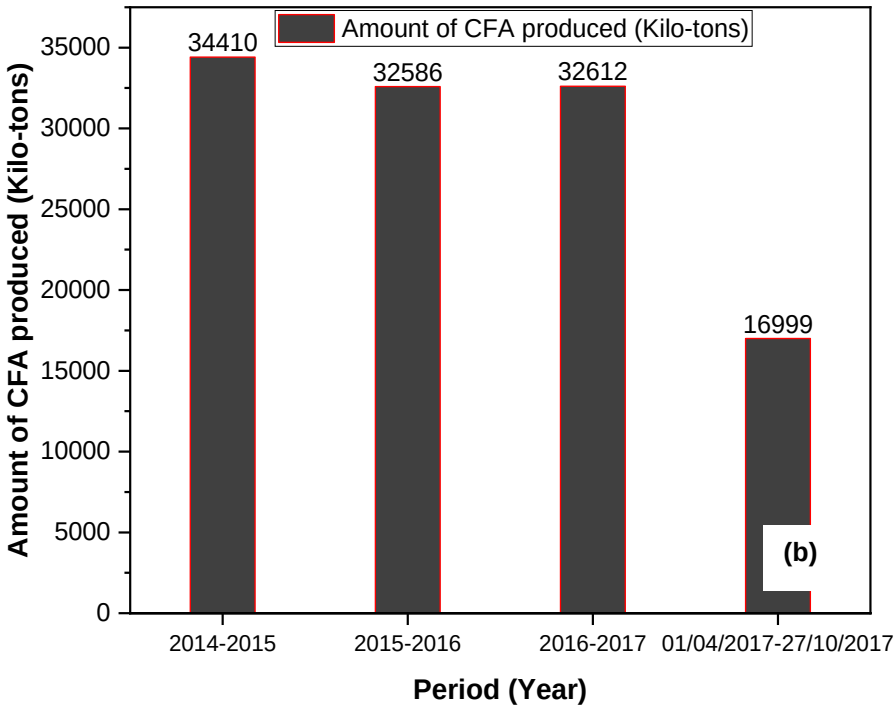

Figure 2-8: CFA dry disposal at one of Eskom power stations in Mpumalanga (Source: https://www.bizcommunity.com/Article/196/493/163979.html, Accessed on the 12 June 2022) (a) and Yearly kilo-tons of CFA produced in South Africa (Source: Department of Forestry, Fisheries and the Environment) (b).

Unsafe disposal of such solid wastes into landfills and other improper waste management practices can harm the environment. Due to their adverse effects on human health and the environment, fine particulate emissions from coal-fired power plants have received widespread attention lately. The presence of toxic elements (such as Se, As, V, Mn, Zn, Cr, Co, and Cd) harms many organisms in various ways. (Waters et al., 1975; Eichorn et al., 1973; Browning, 1969; Hartung, 1973; Roy et al.,1981:29). Consequently, their introduction into the environment through CFA could be a significant health hazard.

According to Roy et al. (1981:29), three distinct hazardous actions can be posed by CFA: (a) direct action with external surfaces (skin, eyes), (b) action in the respiratory tract and (c) action in the alimentary canal (This can be through direct ingestion or expulsion of fly ash from the lungs).

2.1.2.5 CFA utilisation

Although CFA was viewed as a waste product that was deposited in landfills as a source of pollution, in many fields, it has become a valuable resource which created a global market valued at approximately 4 billion US dollars in 2020 with an increase of around 6% annually (Sultana et al.,2021).

Globally, CFA reuse accounts for only one-quarter of total production (Volli and Shu, 2019). As a result of massive coal consumption to meet energy needs, CFA production exponentially increased from 500 million tons in 2005 (USEIA, 2014) to approximately 750 million tons in 2015 (Yao et al., 2015). According to Wang (2008), global CFA utilisation is ranked as follows: Europe ranked first with 47%, followed by the United States with 39% (Gollakota *et al.*, 2019). Based on Figure 2.11, about 500 million tons of CFA were produced globally, and South Africa's utilisation was found to be 1.1% of this global production.

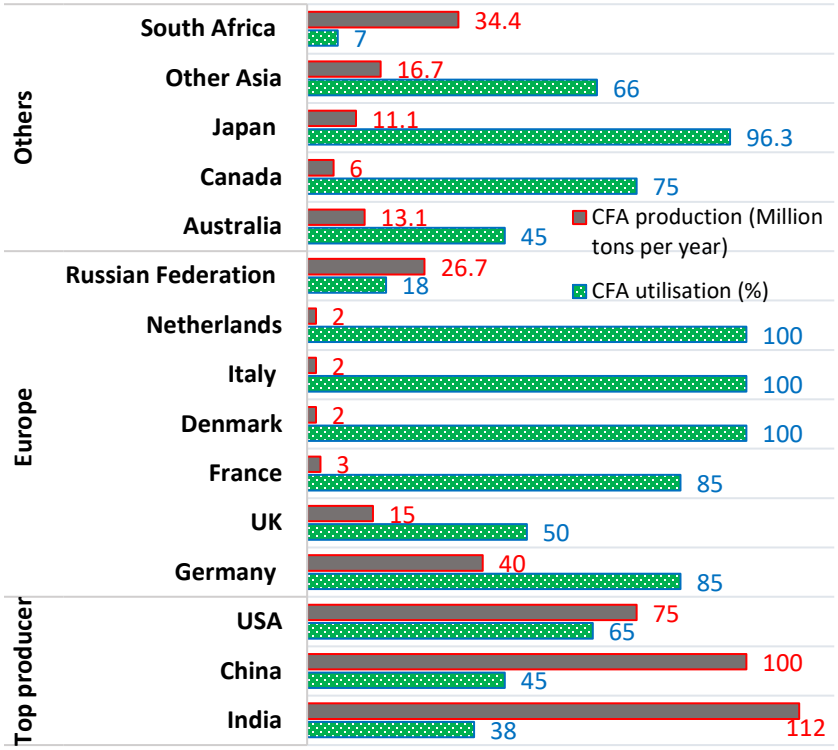

Figure 2-9: CFA production and utilisation countrywide (modified from source: Gollakota et al., 2019).

Over the past two decades, as more sustainable solutions to waste problems such as fly ash have been sought, its utilisation as an industrial by-product has gained attention. CFA offers a range of potential applications as a raw material: to improve soil quality in agriculture, to manufacture glass and ceramics, to manufacture mesoporous materials, to synthesise geopolymers, to serve as catalysts and catalyst supports, and as an adsorbent for gases and wastewater processes, and to extract metals (Blissett and Rowson, 2012).

Based on environmental production, many studies have shown that acid mine drainage can be treated using CFA (Gitari *et al.*, 2006). On the other hand, in the construction industry, CFA

production and use trends and the utilisation of fly ash in concrete and cement in the USA are illustrated in Figure 2.10 from 2000 to 2013. Since 2010, the percentage of fly ash used in cement and concrete products has increased from 19% to 27% due to improved mechanical and durability properties of concrete mixes containing fly ash and the reduction of greenhouse gas emissions by replacing Portland cement in concrete (Gursel, Maryman and Ostertag, 2016).

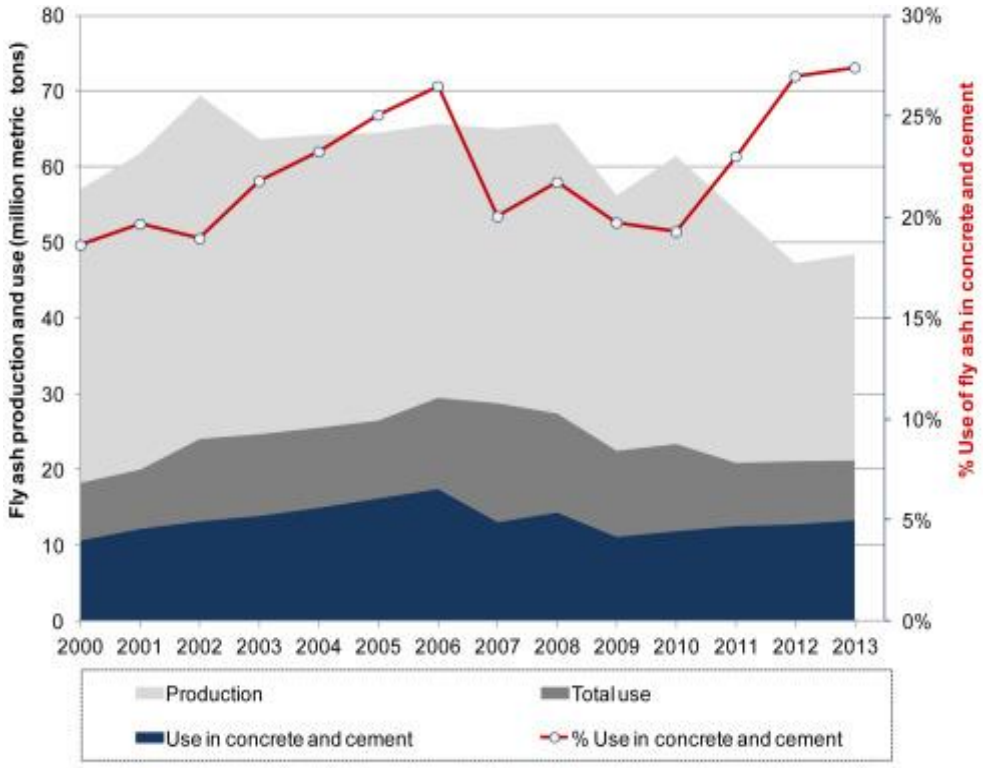

Figure 2-10: US CFA production and utilisation statistics (Source: ACAA, 2014; (Gursel et al., 2016).

2.2 Geopolymer and geopolymerization

2.2.1 Geopolymer definition and history

The term geopolymer is derived from the classical Greek word geo, meaning "earth", and polymers (from poly as many and meres as parts). Geopolymers were first defined by a French materials scientist named Joseph Davidovits in 1978 as long chains of repeating inorganic macromolecules that consist of stable aluminosilicate materials forming a three-dimensional network where their tetrahedral (SiO_4 and AlO_4) are linked together by the sharing of oxygen atoms (see Figure 2.14) (Davidovits, 2020).

Since the early 1980s, Prof. Joseph Davidovits argued that the pyramids and temples of Old Kingdom Egypt were constructed using agglomerated limestone instead of quarried and hoisted natural limestone blocks. He stated that Egyptian workers disaggregated the outcrops of relatively soft limestone with water, then mixed the muddy limestone (including fossilised shells) with lime and other tecto-aluminosilicates (geosynthetic-forming materials such as kaolin clay, silt, and the salt natron (sodium carbonate). During construction, buckets of limestone mud were transported up the pyramid sides and then poured, packed or rammed into wood, stone, clay or brick moulds

to form these pyramid sides. The re-agglomerated limestone hardens into resistant blocks by a geochemical reaction called geopolymer cement. (Available at: www.geopolymer.org/archaeology/pyramids/are-pyramids-made-out-of-concrete, Accessed on the Accessed-on 13 June 2022). As a result of this theory, researchers have been developing a new type of concrete completely devoid of cement, using a variety of waste and energy-saving materials as binders instead of conventional OPC, which emits a significant amount of CO_2. The waste materials used include CFA blast furnace slag, which wastes are difficult to decompose and can have a devastating effect on the environment if untreated.

2.2.2 Geopolymerization

2.2.2.1 Geopolymerization terminology

Geopolymers are ceramic-like inorganic polymers produced at low temperatures, generally below 100 °C resulting in an amorphous to a semi-crystalline three-dimensional polymeric structure based on Si–O–Al bonds (Davidovits, 2017) and (Davidovits, 1999; Abdel-Ghani, Elsayed and AbdelMoied, 2018). They are composed of chains or networks of mineral molecules known as oligomers (Figure 2.15) linked by covalent bonds. As polymers, they should be referred to using polymer terminology, which is very different from ceramic terminology. As an example, kaolinite is one of the major clay minerals with the formula:

- for a ceramicist $Al_2O_3{\cdot}2SiO_2{\cdot}2H_2O$,
- for a chemist, $Si_2O_5Al_2(OH)_4$.

From a geopolymer context, it is written as [≡Si-O-Al- $(OH)_2$]n with the covalent aluminium hydroxyl - Al- $(OH)_2$ side groups branched to the poly(siloxo) hexagonal macromolecule [≡Si-O-] n. In terms of understanding geopolymerization mechanisms, this polymeric approach has profound implications (Davidovits, 2017). Geopolymer oligomers are named according to the atomic ratio of Si to Al, as can be seen in Figure 2.11

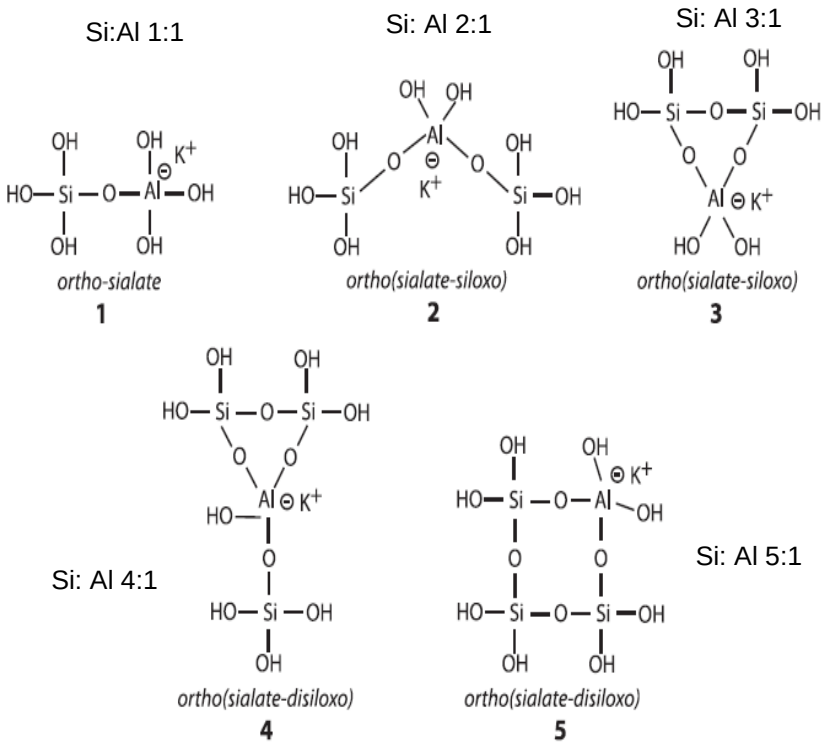

Figure 2-11: Five ortho-sialate oligomers isolated in KOH solutions (Source: North and Swaddle, 2000; Available at https://www.geopolymer.org/science/scientific-means-of-investigation/, Accessed on 27 June 2022).

2.2.2.2 Mechanism of geopolymerization process

Geopolymerization starts with oligomers. An important issue in sialate-based geopolymerization relates to its reaction mechanism. Geopolymer research at the beginning and afterwards, for at least 25 years, was based on the assumption that geochemical syntheses occur through hypothetical oligomers (dimer, trimer) (Davidovits, 2017). This mechanism occurs when Si-Al minerals undergo a substantially fast chemical reaction under alkaline conditions, creating a three-dimensional polymeric chain and ring structure consisting of Si-O-Al-O bonds as followed the equation 2.1 (Source: Van Chanh et al., 2008; Abdullah et al., 2011).

$$M_n[-(SiO_2)_z - AlO_2]_n . wH_2O \qquad \text{Equation 2.1}$$

Where: - M is an alkali element or cation (K, Na, Ca)

- n is the polycondensation degree or polymerisation
- and z is 1,2,3 or higher.

As a result of further polycondensation (polymerisation of monomers into polymeric structures) of these hypothetical building units, actual structures were found for the macromolecular edifice (See following equations reaction principle and Equation 2.2 to 2.5 from Khale and Chaudhary's (2007)

study. The first Geopolymer Conference papers were published in 1988, and the second, 11 years later, in 1999, none of them included scientific details about the reaction mechanism (Davidovits, 2017).

$$\textbf{Si-Al source + Silicates + Water} \xrightarrow{\textbf{Hardener}} \textbf{Geopolymer}$$ Reaction Principe

$$(Si_2O_5, Al_2O_2)n + nH_2O \xrightarrow{NaOH/KOH} n(OH)_3\text{-}Si\text{-}O\text{-}\overset{(-)}{Al}\text{-}(OH)_3$$ Equation 2.2

$$n(OH)_3\text{-}Si\text{-}O\text{-}\overset{(-)}{Al}\text{-}(OH)_3 \xrightarrow{NaOH/KOH} (Na,K)\text{-}\underset{\underset{O}{|}}{Si}\text{-}O\text{-}\underset{\underset{O}{|}}{Al}\text{-}O\text{-})_n + 3H_2O$$ Equation 2.3

Orthosialate (Na,K)-Poly(sialate)

$$(Si_2O_5, Al_2O_2)n + nSiO_2 + 4nH_2O \xrightarrow{NaOH/KOH} n(OH)_3\text{-}Si\text{-}O\text{-}\underset{\underset{(OH)_2}{|}}{\overset{(-)}{Al}}\text{-}(OH)_3$$ Equation 2.4

$$n(OH)_3\text{-}Si\text{-}O\text{-}\underset{\underset{(OH)_2}{|}}{\overset{(-)}{Al}}\text{-}O\text{-}Si\text{-}(OH)_3 \xrightarrow{NaOH/KOH} (K,Na)\text{-}(\underset{\underset{O}{|}}{Si}\text{-}O\text{-}\underset{\underset{O}{|}}{Al}\text{-}O\text{-}\underset{\underset{O}{|}}{Si}\text{-}O\text{-})_n + 4nH_2O$$ Equation 2.5

Oligo(sialate-siloxo) (Na,K)-Poly(sialate-siloxo)

The Orthosialate and Oligo(sialate-siloxo) are seen as geopolymer precursors while ((Na, K)-Poly(sialate) and (Na,K)-Poly(sialate-siloxo) present geopolymer backbone.

Setting, hardening, or geopolymerization takes place at low temperatures below 100 °C. At ambient and medium temperatures, the nature of the hardened geopolymer is either x-ray amorphous, and at temperatures above 500 °C for Na-based, and above 1000 °C for K-based species, respectively, it is x-ray crystalline (Davidovits, 2017). It consists of three stages, as shown in Figure 2.12.

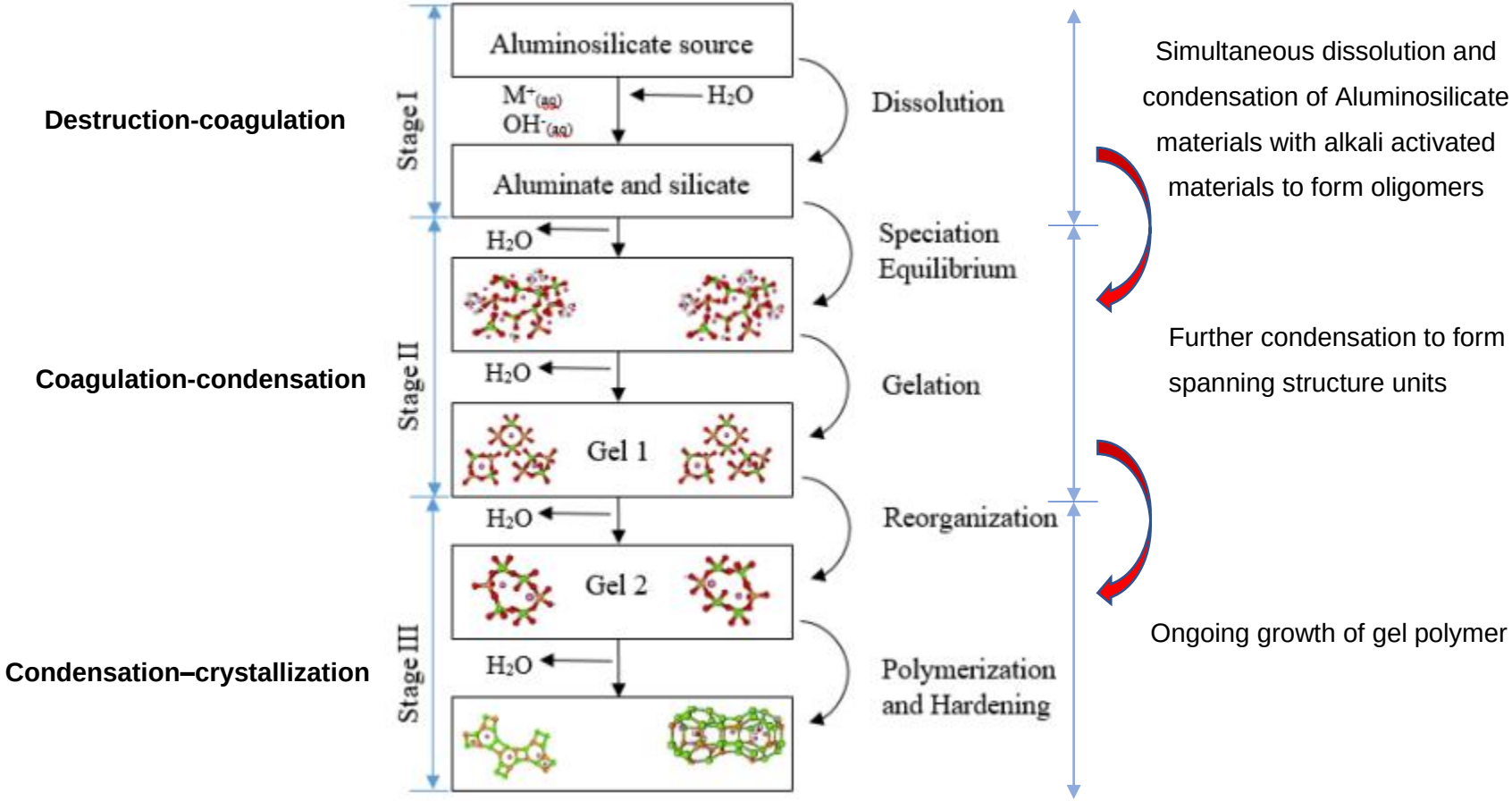

Figure 2-12: Highly simplified reaction mechanism concept for geopolymerization (Modified from source: Fernandez-Jimenez et al., 2006; Mahmood, 2019:12 and Duxson et al., 2007a; Pouhet, 2015:36).

2.2.3 Constituents of geopolymer.

Geopolymer paste is formed by the dissociation of aluminosilicate source materials considered as a binder into an alkaline solution. Similar to cement-based concrete, adding fine and coarse aggregates into geopolymer creates geopolymer concrete, while in some cases, additional chemical or mineral admixture materials may also be added to enhance the fresh or hardener properties of geopolymer concrete. Figure 2-13 illustrates the constituents of geopolymer paste, mortar (plaster) and concrete.

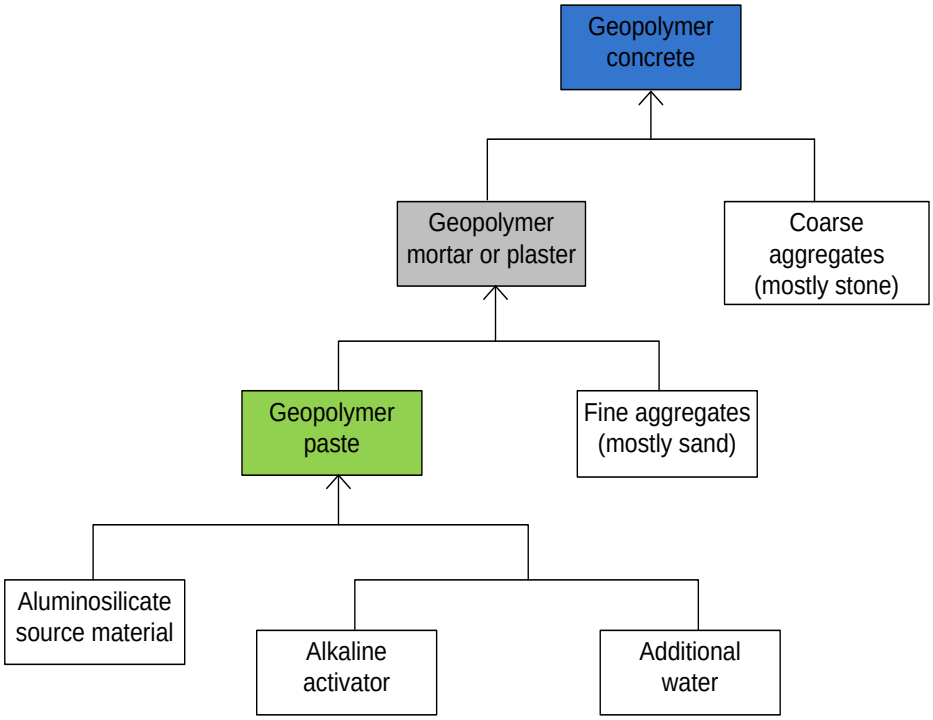

Figure 2-13: Constituents of geopolymer paste, mortar (plaster) and concrete

2.2.3.1 Source materials

Aluminosilicate source materials with a greater part of aluminium and silicon-containing raw materials in amorphous form are preferred for binders. Several minerals and industrial by-product materials have been investigated; due to their availability and desired properties, CFA and ground granulated blast furnace slag (GGBS) are mostly used (Hardjito, 2005). Metakaolin obtained from the calcination of natural source china clay or kaolin at a combustion temperature of 850^{o}C, according to Table 2-3, is one of the most environmentally friendly source materials. In some cases, to obtain a proper Si: Al (SiO_2:Al_2O_3) ratio in the mix design, a certain amount of silica fume (SF) is added, depending on the application. Figure 2-14 describes the CaO-SiO_2-Al_2O_3 ternary phase of most source materials as a binder in geopolymer.

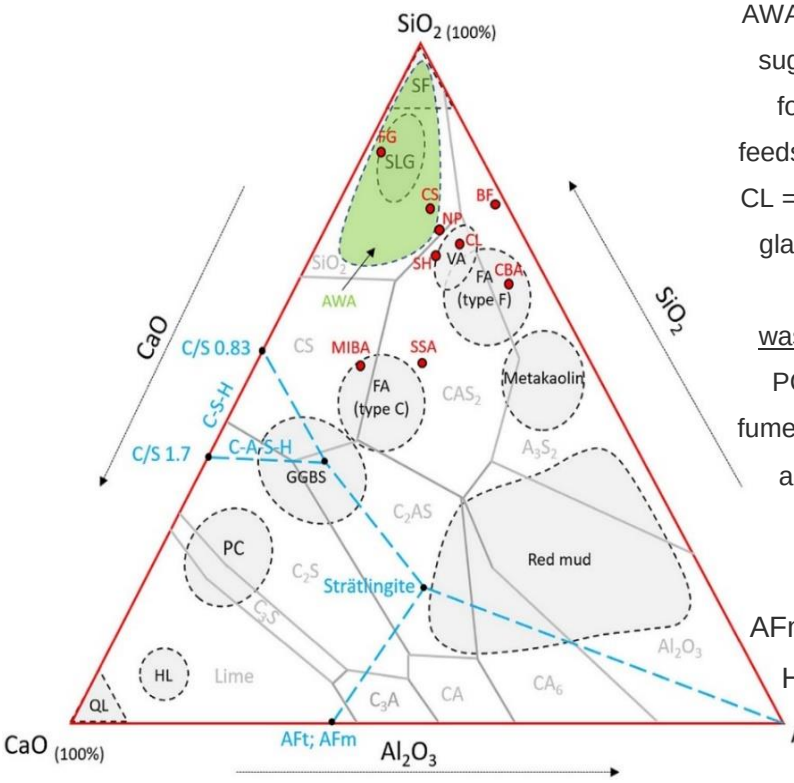

AWA = agricultural wastes (rise husk ash, corn cob ash, sugarcane bagasse ash, straw ash, palm oil fuel ash, forest biomass bottom ash, wood ash), BF = Brick feedstock, BF = brick feedstock, CBA = coal bottom ash, CL = clay, CS = copper slag, FA = coal fly ash, FG = flat glass, GGBS = ground granulated blast furnace slag, HL = hydraulic lime, MIBA = municipal solid waste incinerator bottom ash, NP = natural pozzolan, PC = Portland cement, QL = quick lime, SF = silica fume, SH = shale, SLG = soda lime glass. Texts with red and black colours are average value and range values, respectively. C = CaO, S = SiO_2, A = Al_2O_3 (grey texts). AFt = ettringite, AFm = monosulphate, C–S–H = Calcium-Silicate-Hydrate (blue texts). CS, C2S, C3S, lime are reactive to CO_2

Figure 2-14: CaO-SiO_2-Al_2O_3 ternary phase diagram of different source materials used as a binder (Source: de Brito and Kurda, 2021).

2.2.3.2 Alkali liquids

The alkaline liquids are one of the most important materials for the production of geopolymers. The alkaline liquids play a crucial role in increasing the rate of polymerisation, resulting in stronger geopolymer. In general, sodium hydroxide (NaOH) and potassium hydroxide (KOH), as well as sodium silicate and potassium silicate (Na_2SO_3), are used as alkaline liquids. Adding soluble silicates, such as sodium silicate, to sodium hydroxide enhances the reaction rate. Compared to KOH, NaOH solution caused a greater amount of mineral dissolution, so it is preferred over KOH (Bisarya *et al*.., 2015; Chowdhury et al., 2021). NaOH is the most preferred reagent (hardener) for producing alkali-activated materials due to its high alkalinity (Provis and Van Deventer, 2009; Somna et al., 2011; Nematollahi and Sanjayan, 2014). On the other hand, NaOH is less expensive and more available than KOH.

2.2.3.3 Fine and coarse aggregates

Fine and coarse aggregates comprise a large portion of concrete; depending on the concrete application, they might account for up to 70% of the total concrete volume. The use of locally available aggregates will be economical. Various tests, such as sieve analysis (to determine the

grading and fine modulus), bulk density, relative density and impact tests, should be conducted on fine and coarse aggregates according to prescribed specifications. (Priyanka et al., 2020). In most cases, aggregate is added to concrete to increase the concrete yield as it also lowers the concrete cost and carbon emissions. Excess aggregates in concrete will also create pores, which will have a negative impact on its strength and durability. The following table illustrates the difference between fine and coarse aggregates.

Table 2-7: Different between fine and coarse aggregates materials (ASTM C33-07., 2004)

Type of aggregates	Sieve specification
Fine	Particles passing through a sieve of 4.75 mm square openings
Coarse	Particles retaining on a sieve of 4.75 mm square openings

2.2.4 Factors affecting the properties of geopolymers

In the new construction industry, high-performance materials are needed; however, these new materials must also meet the requirements of low cost, high durability and high strength. Production of new materials from industrial waste may be a sustainable and economically efficient way of using resource materials such as ordinary Portland cement (Chindaprasirt and Chalee, 2014). Like conventional cement concrete, many factors affect the properties of fresh and hardened construction material made from CFA-based geopolymer. Several factors regarding the reactivity of CFA as a precursor for geopolymer concrete have been investigated. (Soutsos *et al.*, 2016). In most studies, investigations were mainly done on the following factors to see their effect on the compressive strength of the geopolymer

2.2.4.1 Sodium hydroxide concentration

To form an alkaline liquid, also called an alkaline activator, a given NaOH concentration is blended with Na_2SO_3. Despite this, every NaOH concentration has a distinct impact on the geopolymer's fresh and hardened properties. Alehyen (2017) stated that the variation in NaOH concentration has an important role in the compressible strength of the material. Furthermore, it was confirmed that the presence of NaOH increases the number of soluble silicates and aluminate in the mixture of through fly ash. The results of a study proved that an increase in NaOH concentration from 4.5 to 14.0 M increased the compressive strength of pastes, as shown in Figure 2-15 (Somna *et al.*,

2011). However, the use of high sodium hydroxide concentration is a high-cost process and may lead to the high heat of hydration, which, in return, can significantly impact fresh and hardened properties at a certain ambient cured temperature.

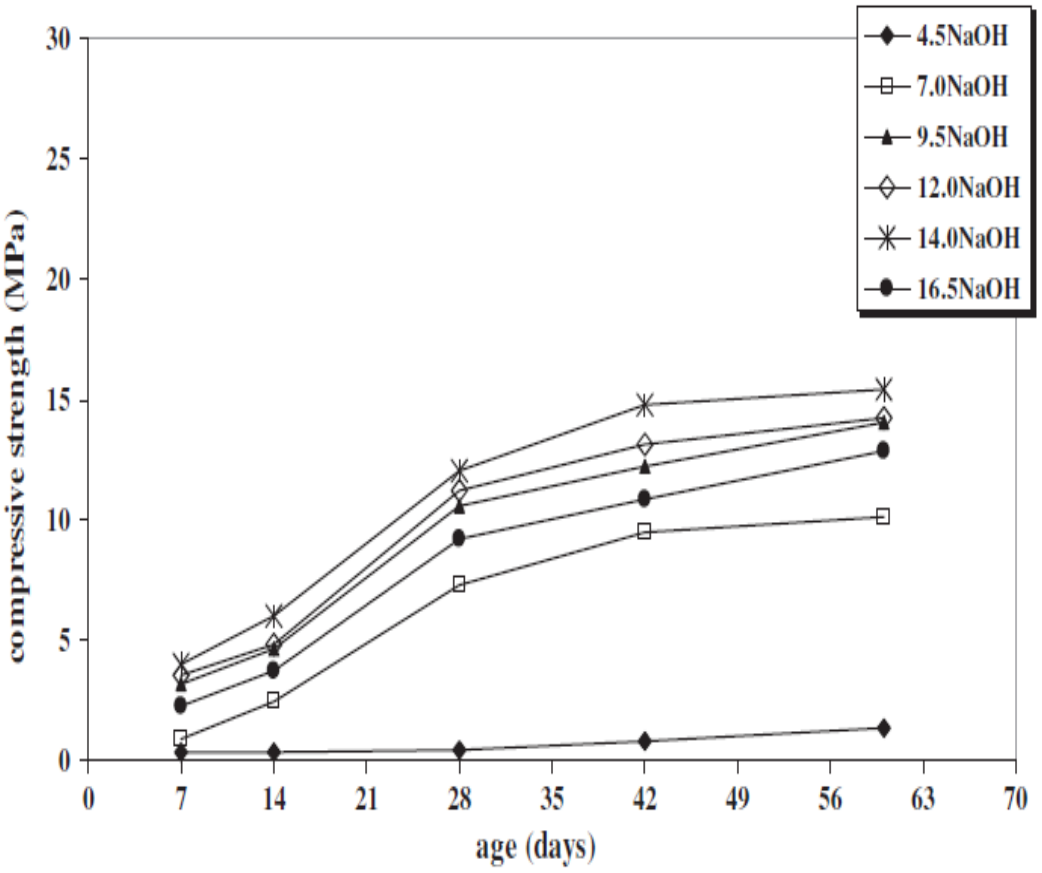

Figure 2-15: Compressive strengths of CFA-based geopolymer pastes using different NaOH concentrations at different (Somna et al., 2011).

2.2.4.2 Silica to alumina ratio

Silica to alumina ratio (Si/Al or SiO_2:Al_2O_3 ratio) and ageing time are the most critical parameters that affect the reaction degree of geopolymerisation process and the reaction time, thereby affecting the final properties (Gao *et al.*, 2020). It has been acknowledged that the alkaline activator dosage and Si/Al are dominant influences on geopolymerisation. (Sindhunata et al., 2006, Duxson *et al.*, 2007; Zheng *et al.*, 2010). According to the results obtained by Timakul et al. (2015) using high calcium CFA (Class C, ASTM 618). By increasing the ratio of SiO_2: Al_2O_3 from 2.60 to 2.65, increased compressive strength increased from 32 MPa to 40 MPa. Despite this, compression strength was decreased when the SiO_2: Al_2O_3 ratio was raised from 2.65 to 3.0. Compressive strength was highest when the SiO_2:Al_2O_3 ratio was 2.65 at 75°C for 96 hrs, and

samples had high densities. The following Figure 2-16 shows the effect of SiO_2: Al_2O_3 on the compression strength of GPP.

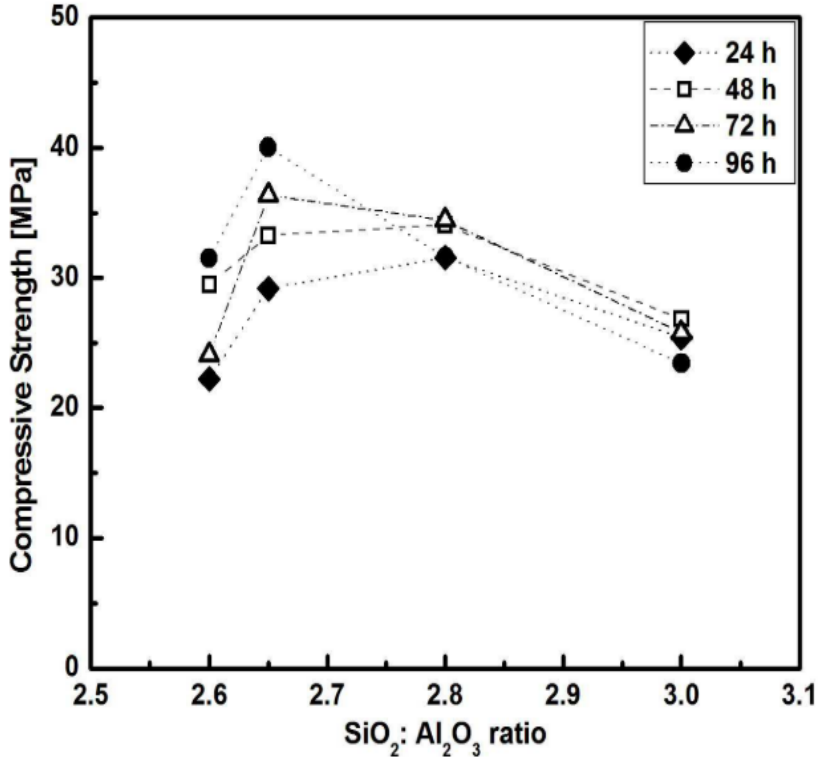

Figure 2-16: Compressive strength development of geopolymer at different SiO2: Al2O3 ratios cured at 75 ^{O}C for a different period in the oven (Timakul et al.,2015).

2.2.4.3 Curing regimes and the effect of water

Curing temperatures and curing time represent the curing conditions that strongly affect the setting and hardening of geopolymer. A study was conducted by Rovnanik (2010) on the effect of curing temperatures on the development of hard structures in metakaolin-based geopolymers. The study was designed to examine the effects of curing temperature (10, 20, 40, 60, and 80°C) and time on metakaolin-based geopolymer based on compressive and flexural strengths, pore distribution, and microstructure. Results showed that treating fresh mixtures at elevated temperatures accelerates strength development, but mechanical properties deteriorate after 28 days compared to mixing at ambient or slightly decreased temperatures. According to other studies, adding water decreased compressive strength, whereas longer curing times and higher curing temperatures increased it (Van Chanh *et al.,* 2008). Therefore, compressive strength is curing time and temperature-dependent, while additional water affects final strength (Heah *et al.*, 2011). In a study by Xie and Ozbakkaloglu (2015), geopolymer concrete (GPC) specimens were

cast at ambient temperature and cured in the open air. The results of that study are shown in Figures 2.17 (a) and (b); visible efflorescence formations were observed in some of the GPC specimens.

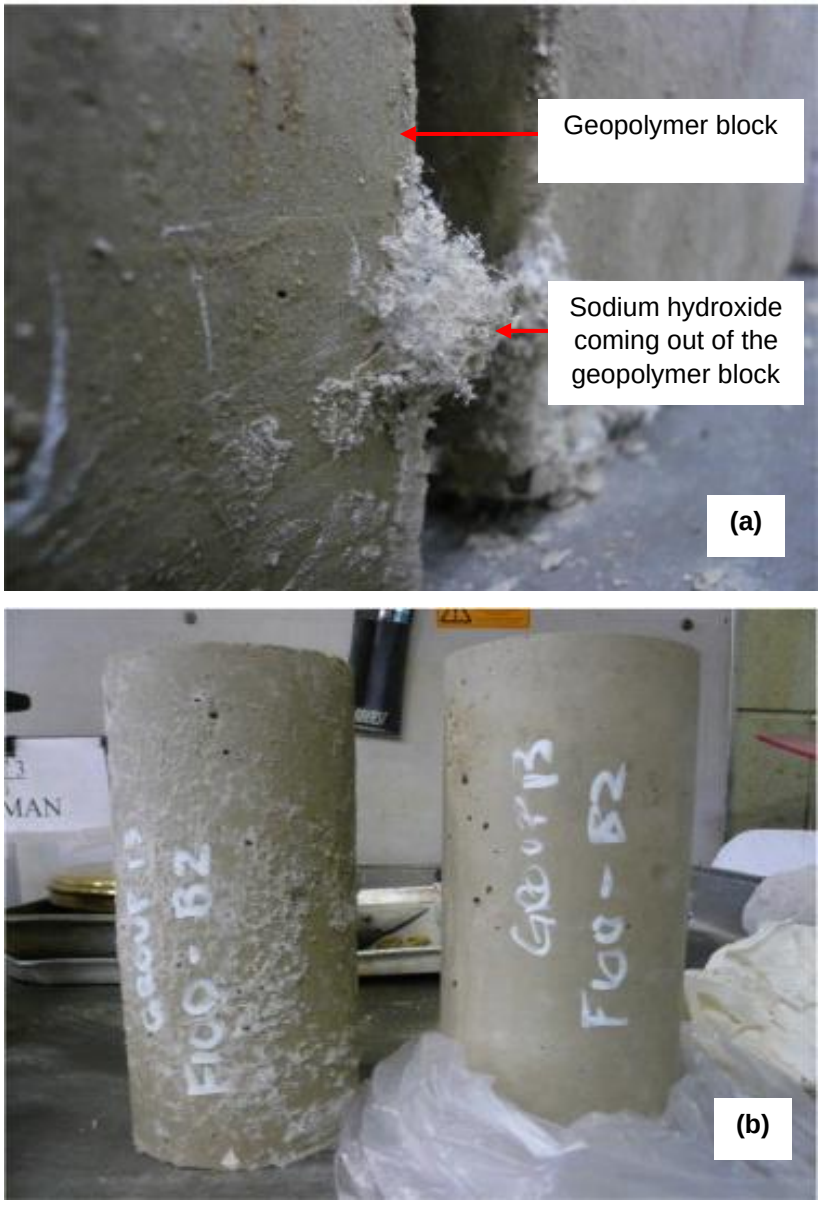

Figure 2-17: Efflorescence in geopolymer block as a result of ambient curing temperature in the open air; (a) efflorescence at the edge of the beam specimen and (b) comparison between a cylinder with efflorescence present (on the left) and a sealed cylinder that exhibits no efflorescence (on the right) (Xie and Ozbakkaloglu, 2015).

Davidovits (2008:284) cited experimental results from US Patent 5061643 about the curing time. A significant correlation exists between curing time and compressive strength of geopolymer

samples. As shown in Figure 2.19, the curing time increases with an increase in compression strength from 2 hours with 36.4 MPa to 24 hours with 108.7 MPa. It is also important to understand that the cost associated with curing the product for 24 hours might be highly expensive and impact carbon emissions.

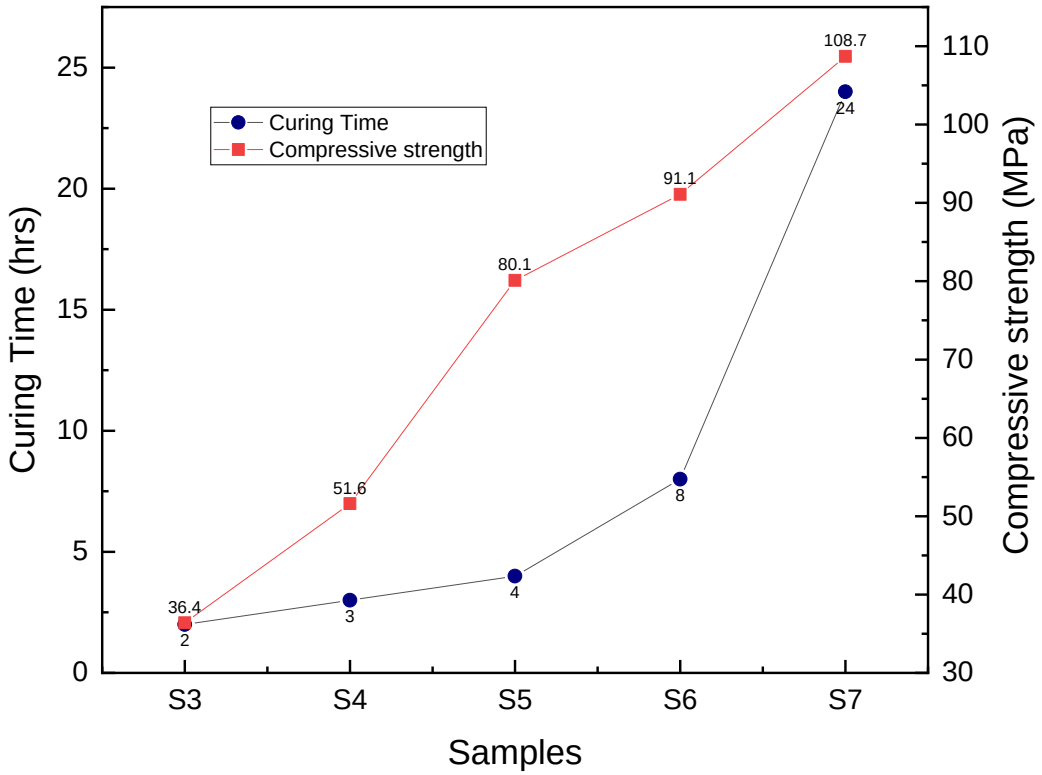

Figure 2-18: Effect of curing time on the compressive strength of geopolymer cure at 80 oC for short and long hours (Source: US Patent 5061643; Davidovits 2008:284).

2.2.5 Uses of geopolymer

Geopolymeric materials have a variety of applications in the field of industries, such as in the automobile and aerospace, nonferrous foundries and metallurgy, civil engineering, and plastic industries (Davidovits, 1989). Production of fire-resistant materials and reduction of CO_2 emissions in construction materials as an alternative to Portland-based (calcium silicate) cement are the earliest and current primary areas of application of geopolymer. Several other properties of geopolymers make them a superior alternative to traditional construction materials, but performance alone is not sufficient to revolutionise construction materials (Duxson et al. 2007a). The market will demand this new material as geopolymers become incorporated into the construction. The use of geopolymer in waste encapsulation, as low-cost ceramics (either directly

or as precursors for calcination), and in fire protection is numerous (Provis and Van Deventer, 2009:6).

The applications of materials made by geopolymerisation are determined according to the chemical structure in terms of the atomic ratio Si: Al in the polysialate (Davidovits, 1999) classified the type of application according to the Si: Al ratio as presented in Table 2.8.

Table 2-8: An example of different applications of geopolymer materials with a focus on Si: Al atomic ratio (Source: Davidovits, 2017).

Si: Al ratio	Polymeric character	Applications	
		Low technology	**High technology**
1:1	3D Network	-Tiles -Ceramics	-Fire protection
2:1		-Low CO_2 cement and concrete	-Radioactive and toxic waste encapsulation
3:1	2D Network	-Fire protection fibreglass composite	-Heat-resistant composites from 200 ^{O}C to 1000 ^{O}C
		-Foundry equipment	-Toolings for the titanium aeronautics process
>3:1		-Sealants for industry from 200 ^{o}C to 600 ^{O}C	-Toolings for Superplastically formed (SPF) aluminium
20 - 35			-Fire resistance & heat resistant fibre composites

2.3 Critical summary

An overview of the geopolymerisation process, including the applications of geopolymer and the generation of CFA as a raw material, has been described. CFA-based geopolymer paste, mortar and concrete have been synthesised by many researchers for construction applications when cured at oven temperature. This study is based on a contradictory approach to previous

geopolymer studies in which the mixes developed were cured with a focus on high oven curing conditions. Although good geopolymer properties were obtained, the high curing temperature is an obstacle to the industrialisation of geopolymer for major construction applications and cannot favour the casting of applications such as cast in situ, foundation casting, and 3D printing. Many researchers have been claiming that geopolymer cured at an oven temperature of about 80^{o}C, results in saving CO_2 emissions by about 40-80% compared to the normal OPC concrete process (van Deventer et al., 2010, Shekhovtsova, 2015 Kalombe et al., 2020). However, in none of these studies no analysis method was defined, neither was the system boundary considered and the energy used in the drying process was not considered during carbon footprint analysis. In the case of South Africa, the oven curing process for 24 hours might be considered a hostile process as the CO_2 emission related to electricity consumption is high (0.95 Kg CO_2e/kWh (Eskom CO_2 emission factor in 2018). Developing polymerisation formulations using CFA in the room curing process has resulted in efflorescence from previous studies (Xie and Ozbakkaloglu, 2015). A review of the room curing process is an area of research that needs further exploration as it seems more cost-effective and sustainable due to the cut-off 24-hour heat curing.

This study also attempts to fill deficiencies found in previous research on the synthesis of CFA-based geopolymer by performing engineering analysis on mechanical and durability properties and environmental analysis. Many properties are needed to introduce a new construction material to the market. According to Table 2.9, this has only been partially defined in many studies, with limited information provided from the synthesis of geopolymer using South African CFA. The difference between CFA-based geopolymer paste, mortar and concrete for structural application will be investigated.

In the case of compression strength as the major test, generally, the compression strength of concrete is determined based on the application, which is related to a certain category of concrete. Concrete strength requirement is classified into four (4) categories, as shown in Table 2.10.

Table 2-9: Investigation parameters of CFA-based geopolymer product from a single formulation in a study.

Study			Fresh properties						Mechanic properties					Durability properties						
			Setting time			Rheology			Strength, MPa			Stress-strain								
Author	Country	CFA-based geopolymer type	Consistency, mm	Initial setting time, min	Final setting time, hr	Flow test, sec	Slump test, mm	Slump flow, mm	Compression	Flexural	Tensile splitting	Modulus of elasticity, GPa	Poisson ratio	TQC Karsten Tube Penetration	Water absorption, %	Capillary water absorption,%	Efflorescence, %	Dry shrinkage, microstrain	Carbonation depth	Fire resistance, time rating
Mallikarjuna Rao et al., 2015	Saudi Arabia	GPP&GPM	✓	✓	✓	✓	x	x	✓	x	x	x	x	x	x	x	x	x	x	x
Wang and Dai, 2020	Spain	GPP		✓	✓	✓	x	x	✓	x	x	x	x	x	x	x	x	x	x	x
Galiano et al., 2017	Spain	GPP	x	x	x	x	x	x	✓	✓	x	x	x	x	✓	x	x	x	x	✓
Nath, 2014	Australia	GPC		✓	✓	x	✓	✓	✓	✓	✓	✓	x	x	x	✓	x	x	✓	x
Xie and Ozbakkaloglu, 2015	Australia	GPC	x	x	x	x	✓	x	✓	✓	x	✓	x	x	x	x	✓	✓	x	x
Kalombe, 2018	South Africa	GPP	x	x	x	x	x	x	✓	x	x	x	x	x	✓	✓	✓	x	x	x
Kalombe et al., 2020	South Africa	GPP	x	x	x	x	x	x	✓	x	x	x	x	x	✓	✓	x	x	x	x
Shekhovtsova, 2015	South Africa	GPC	x	x	x	x	✓	x	✓	✓	✓	✓	✓	x	x	x	✓	✓	x	x
Chen et al., 2022.	China	GPP	x	x	x	x	x	x	✓	✓	x	x	x	x	✓	x	x	✓	x	x
Guo and Xiong, 2021	China	GPM	x	x	x	x	x	x	✓	✓	x	x	x	x	x	x	x	x	x	x

CFA = CFA , GPC = geopolymer concrete , GPP = Geopolymer paste and GPM= geopolymer mortar

Table 2-10: Concrete classified in accordance with compressive strength based on application requirements (Modified from source: SANS 10400, 1990:73 and Li, 2011:16).

Classification		**Compressive strength, MPa**		**Applications**
Low strength concrete	Controlled Low-Strength Material	< 2.1	< 10.0	Generally used as a backfill
	Hollow load-bearing units	3.5		Single-storey building wall. From 7.0 MPa applicable for double-storey buildings, Bulustrate, Parapet and Foundation walls
	Bearing unit	4		
	Lean concrete	5 -7.5		
Ordinary concrete			10.0 -20.0	mass concrete structures, subgrades of roads and partitions
Standard concrete	Moderate-strength concrete A	20.0 -50.0	20.0- 55.0	Construction of slabs, beams, columns, footings, buildings, bridges, Pavements and similar structures
	Moderate-strength concrete B	35.0 -55.0		Runways, Pressurised Concrete Girders
High strength concrete			60 - 150	Tall buildings, columns, bridges, towers, and shear walls
Ultra-high strength concrete			> 150	Not widely used in structural constructions. Only footbridges and girders

Additionally, the following parameters will be investigated at the fresh and hardened state from the synthesis of geopolymer using coal fly ash, as they are crucial for construction applications.

2.3.1 Fresh properties of geopolymer

The fresh properties, also called the dormant period or plastic state (Soroka, 1993:22 and Nagaratnam et al., 2016:274) of geopolymer paste or concrete properties will be defined using methods that applied to a wet ordinary Portland cement paste or concrete. Here, geopolymer concrete or paste has not yet undergone setting and hardening. Geopolymer products (in paste, mortar, or concrete form) might last a few hours in this state, after which they can be poured and deformed into any shape using a specific mould. Figure 2.19 illustrates the behaviour of normal concrete from a plastic state to a hardened state, which was used as an example to define the plastic state of geopolymer.

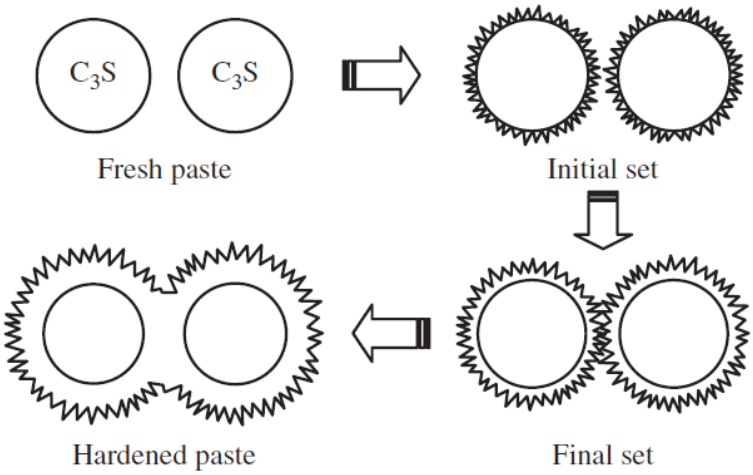

Figure 2-19: An example of setting steps of the fresh cement paste (Li, 2011:43).

2.3.2 Hardened properties

2.3.2.1 Carbonation test

A study conducted by RoofLock (2019) found that the infiltration of carbon dioxide into reinforced concrete causes steel reinforcements to corrode, resulting in expansion cracks and the weakening of the concrete. This will, therefore, lead to the deterioration of the infrastructure and reduce its service period.

2.3.2.2 Radon exhalation and emanation

Radon is a fundamental atomic element, a radioactive noble gas in the ^{238}U decay series that can move from its host material since it is a gas (NRC, 2006; Snead, 2022). It is an invisible, odourless, tasteless, colourless, inert and radioactive gas. Radon generally occurs from the natural

breakdown of uranium in the earth's crust. It usually travels through soil by entering into homes, schools and other buildings element. It is often 10% or less of the actual radon created in the material. Radon is of considerable importance since it is the primary health risk associated with chronic indoor radon exposure and the second most important after smoking for increasing the lifetime risk of lung cancer (NRC, 2006). The mechanism that increases health developing lung cancer is the emission of an alpha particle from radon decay products, causing physical and chemical damage to cells and DNA (Lorenzo-Gonzalez et al., 2019; Grzywa-Celińska et al., 2020). Figure 2-20 illustrates this mechanism.

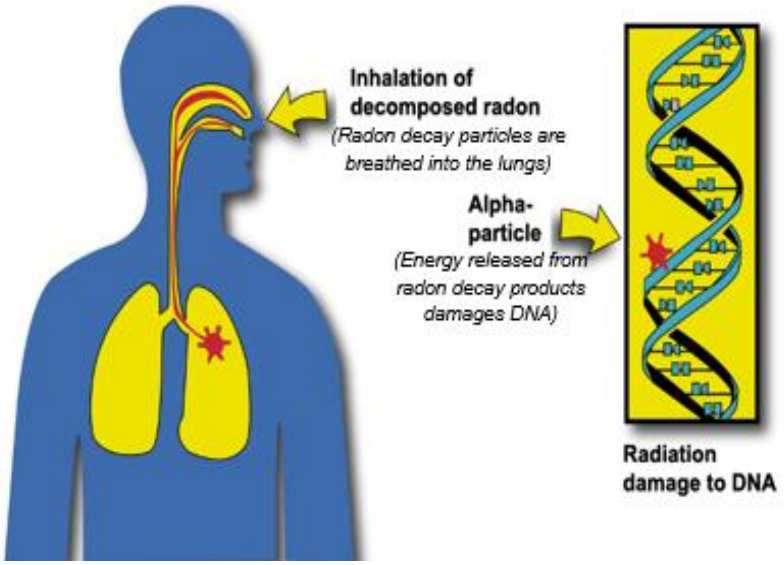

Figure 2-20: Mechanism of DNA damage and lung cancer from radon decay product (Source: Available at: https://www.radonaway.com/radon-health-risks.php, Accessed on 22 October 2021).

2.3.2.3 Life cycle analysis

Life cycle analysis (LCA) is defined as a technique used to determine and assess (evaluate) the environmental loadings and impacts of a product or process as well as upstream effects from the supply chain (Curran 1993; Crawford, 2011:38). Each human action affects the environment, resulting in its degradation. A large number of natural resources is required to sustain the lifestyle. It was found that construction activities have significant environmental impacts due to the high demand for material resources, primarily energy and water, necessary for manufacturing products and resource extraction. As a result, it is important to examine the impact of the process or find a way to reduce it to create a sustainable model in a sector with high raw material demand. Figure 2.21 illustrates the impact categories taken into consideration in the environmental product declaration, from the extraction of raw materials, manufacturing, distribution, use, and end of life

using the environmental product declaration (EPD) method (Available at https://www.youtube.com/watch?v=NCiMDepskSe Accessed on the Accessed-on the 11 August 2022). Furthermore, the stages involved in the life cycle of the building material are illustrated in Figure A-3 in the appendix.

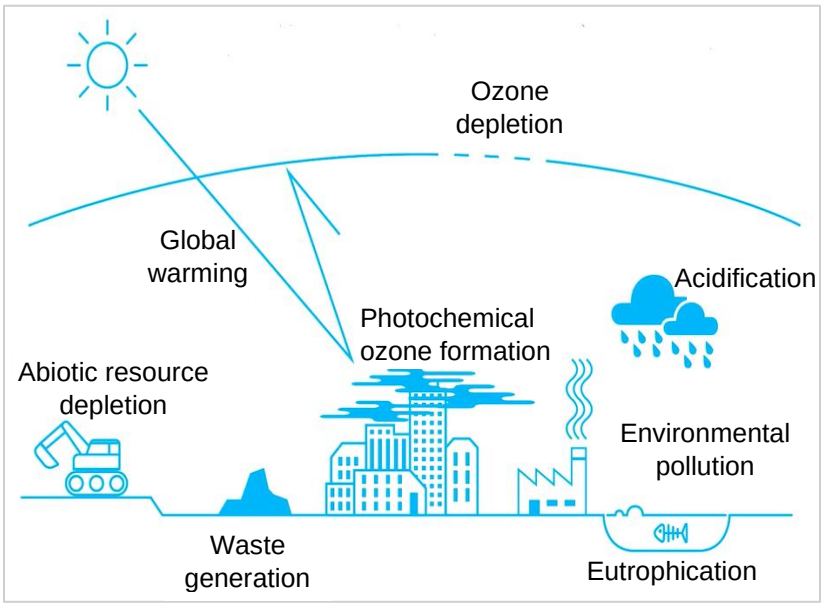

Figure 2-21:Types of environmental impact categories generated on the planet from the extraction of raw materials to the end life of the construction product assessed based on EPD method activities (Available at https://www.youtube.com/watch?v=NCiMDepskSe, Accessed-on 11 August 2022).

Chapter 3

Experimental methodology for the synthesis of CFA-based geopolymer

This chapter will give a better understanding of the process developed for the synthesis of geopolymer using South African CFA for construction applications. Here, the materials and equipment used are listed and described. Standard methods of testing raw materials, products, and analytical techniques are explained. In short, this chapter discusses the workforce process of this study.

3.1 Experimental program

The suitable formulations developed were considered due to their better setting and strength (comparable to a strength obtained from an oven curing regime) properties at ambient temperature. Figure 3.1 illustrates the study's elements, including research questions, aims, and objectives, as well as how these were sequentially achieved. An experimental trial mix design will first be developed with CFA as aluminosilicate source material, then laboratory mix within a cost-acceptable and environmentally friendly alkaline medium to form at a certain mixing time to form a homogeneous geopolymer paste that will be tested for consistency, initial and final setting time. The best trial mix was then cured at given curing regimes (curing conditions), after which it was tested for diverse properties when hardened. Once the geopolymer paste results in acceptable fresh and hardened properties, it can be modified at a later stage by adding fine and coarse aggregate. This will be geopolymer mortar and geopolymer concrete. This research will mainly define the properties of geopolymer paste and concrete.

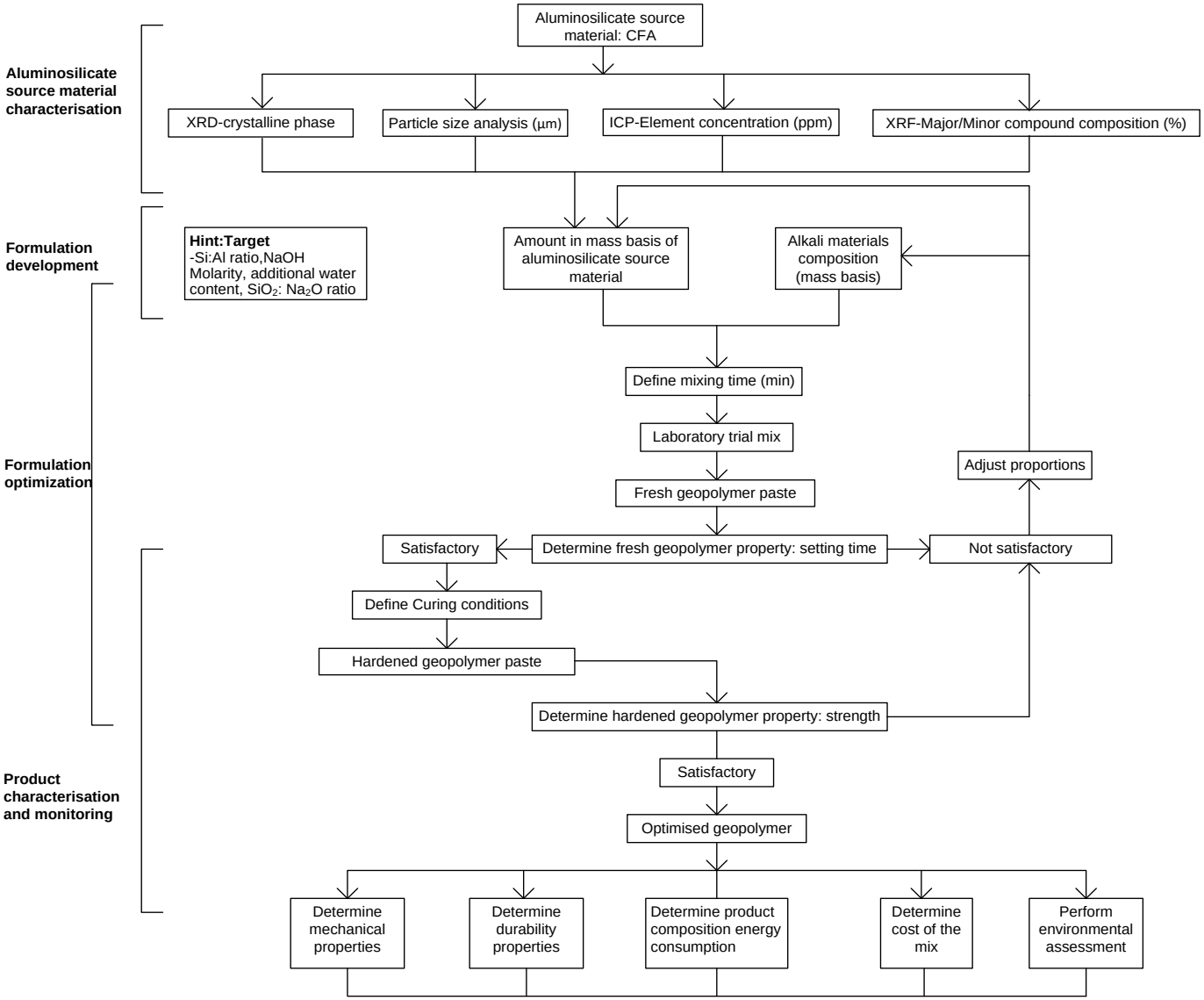

Figure 3-1: Geopolymer paste with the design process with a focus on setting time and strength as main properties.

3.1.1 Chemicals

Chemicals used in this study and their suppliers are shown in the following Table 3.2

Table 3-1: List of chemicals used and their purity on a mass basis.

Chemical		Purity, %	Supplier	Location
Sodium hydroxide pellet		98	Kimix	Cape Town, Western Cape, South Africa
Sodium silicate	SiO_3	30	Protea chemicals	
	Na_2O	9.2		
	H_2O	60.8		
Shutter oil		-	Kimix	
Phenolphthalein solution		1	Kimix	
Isopropyl-alcohol		99.5	Kimix	

3.1.2 Sample collection

CFA used in this study was DURAPOZZ-processed CFA from Lethabo power station located in the Mpumalanga province of South Africa and delivered by Lafarge-Ash resources packed in 50 kg paper with plastic sealed bags and then used as the binding raw material. At the laboratory, bags were stored in a moisture-free area and placed on wooden pallets. A CFA sample from the bag was kept in sealed plastic for different analyses.

3.1.3 Fine and coarse aggregates

Fine and normal-weight coarse aggregates used in this project are Philippi sand and blue stone obtained from builders. Figure 3-2 represent these aggregates.

Figure 3-2: Philippi used as fine aggregate (a) and blue stone as coarse aggregates (b) for the synthesis of CFA-based geopolymer mortar and concrete.

The aggregates properties were determined at the Roadlab Civil Engineering Laboratory, Cape Town facility based on bulk loss density, dust content, and sieve analysis (using sieves 19.0, 14.0, 9.5, 6.7, 4.75, 2.36 and 1.18 for coarse aggregate and 4.75, 2.36, 1.18, 0.6, 0.3, 0.15, and 0.075 for fine aggregates) and fineness modulus. To determine the maximum density gradation of aggregates, Fuller and Thompson developed the following Equation: 3.1 was used (Nagaratnam et al., 2016. P.121).

$$P_i = \left(\frac{d_i}{D_{max}}\right)^n \times 100 \qquad \text{Equation 3.1}$$

where: - P_i is the percentage corresponding to particle size d_i in percentage (%)

- D_{max} is maximum particle size in millimetres (mm)
- d_i is particle size millimetre (mm)
- n is a parameter that adjusts for the fineness and coarseness of the aggregates.
- $n \approx 0.5$, according to Fuller and Thompson.

3.1.4 Effect pigments on CFA-based geopolymer mix

This study also used a fixed percentage of cement pigment oxides obtained from builders as a supplier in certain geopolymer paste, mortar, and concrete mixes. Those cement pigment oxides are shown in the following Figure 3.3 with names related to their colours.

Figure 3-3: CFA and different cement oxides used in certain mixes

3.2 Equipment

Table 3.2 consists of the main equipment used in the synthesis of CFA-based geopolymer in this study from mixing, casting, and curing.

Table 3-2: List of the main equipment used, including suppliers' names and location

		Supplier information	
Equipment	**Capacity**	**Name**	**Location**
Hot air oven (EcoTherm)	1.7 kW /40-330 ^{o}C	Labotec	Cape Town, Western Cape, South Africa
Mixer (stirred tank)	2.1 kWh	-	
Plastic and nylon moulds	100x100x100 mm^3	Scientific Manufacturing	
Beakers	1-2 L	Kimix	
Volumetric Flask Grade A	1L	Kimix	
Brick trowel	275 mm	Builders	

One of the main pieces of equipment was the mixer unit, as shown in Figure 3.7. Some of the equipment was unavailable in the market at the lab scale; therefore, a personal design (PD) of that equipment was made.

3.3 Batch geopolymer processing steps

Synthesis of the CFA-based geopolymer process involves a series of steps to produce an end product: geopolymer paste, mortar, or concrete. Figure 3.4 illustrates the major steps as defined below. The steps in this processing chain are dependent on each other and, at the laboratory scale, are run batch processes while they can be run as continuous processes at the industrial level. The following block flow diagram (BFD) illustrates the process for the production of geopolymer paste while when it can to mortar BFD, the same process is used except CFA was premixed with fine aggregate. The process is followed for concrete mortar, and then the aggregate is added when a homogeneous mortar mix is obtained.

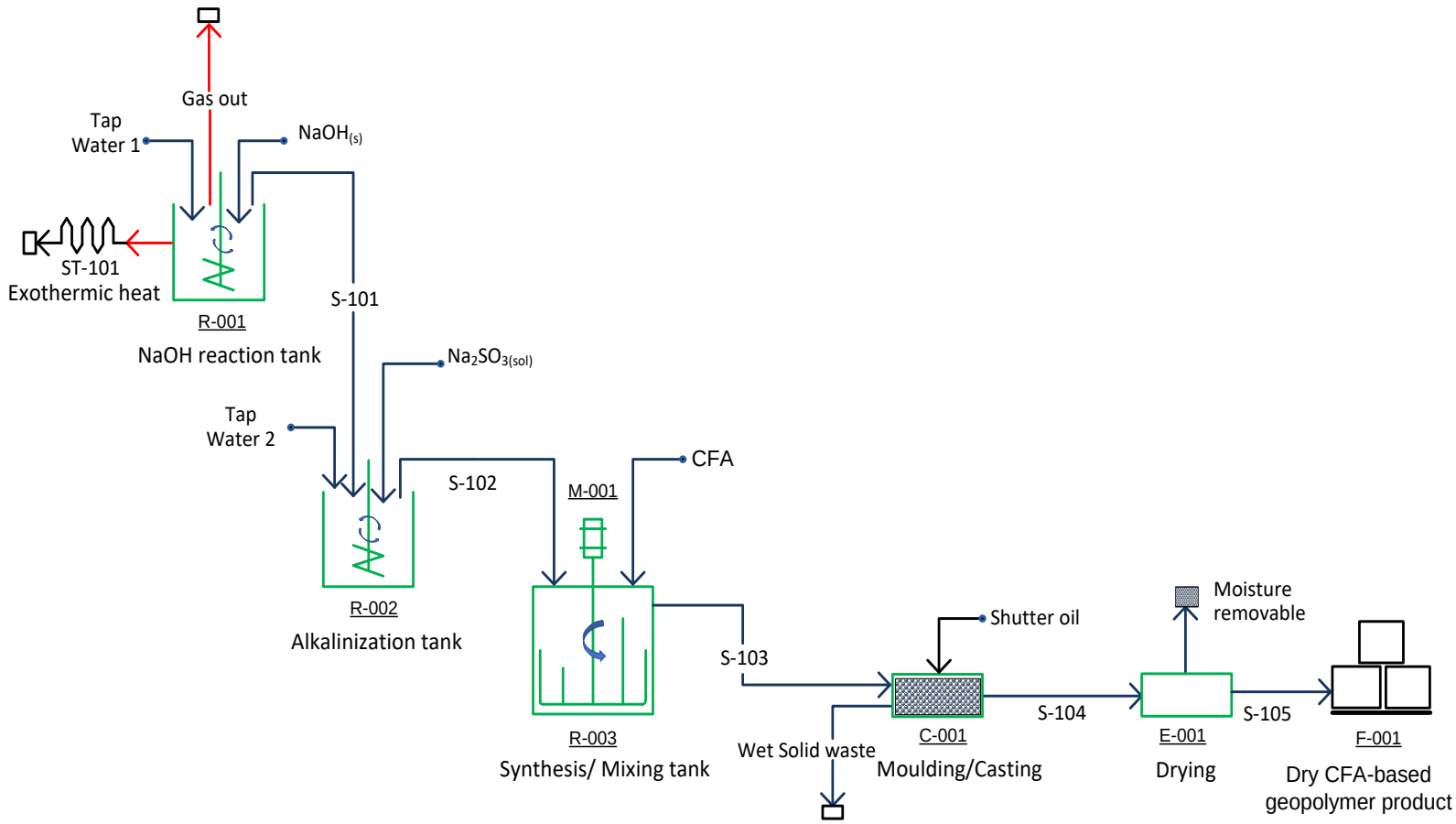

Figure 3-4: Block flow diagram illustrating various processing steps in the geopolymer paste process. In R-001, Sodium hydroxide solution is prepared from the pellet. In R-002, alkaline activators are prepared by mixing a certain amount of sodium hydroxide solution made with a given amount of sodium silicate liquid, after which the alkaline liquids obtained are diluted with water. In R-003, CFA is first poured, and then the R-003 new alkaline liquid obtained is added.

3.3.1 Mixing proportioning

The mixing process consisted of weighing all dry materials coal fly ash, sodium hydroxide pellet, fine and coarse aggregates), water, alkaline liquids (sodium silicate and sodium hydroxide solution), and other ingredients such as cement oxide. These processes were done in batches. Table 3.3 represents the different formulations from geopolymer paste, mortar, and concrete developed with 10, 12, and 14 sodium hydroxide molarity using only South African Lethabo power station CFA as a binder.

Table 3-3: Synthesised CFA-based geopolymer formulations mass composition

Mix series	CFA-based geopolymer formulations composition (w/w %)											Dry mix coloured dye content in w/w		
Formulation code	CFA	Fine aggregate	Coarse aggregates max size (mm)		Alkali-Activated Materials						Amount of additional water			
			13	19	Sodium Hydroxide (NaOH), Molarity					Sodium silicate (Na_2SiO_3)		Yellow	green	Black
					8	10	12	14	16					
GPP-M1A	68.97	0.00	0.00	0.00	6.90	0.00	0.00	0.00	0.00	17.24	6.90	0.00	0.00	0.00
GPP-M2A	68.97	0.00	0.00	0.00	0.00	6.90	0.00	0.00	0.00	17.24	6.90	0.00	0.00	0.00
GPP-M3A	68.97	0.00	0.00	0.00	0.00	0.00	6.90	0.00	0.00	17.24	6.90	0.00	0.00	0.00
GPP-M4A	68.97	0.00	0.00	0.00	0.00	0.00	0.00	6.90	0.00	17.24	6.90	0.00	0.00	0.00
GPP-M5A	68.97	0.00	0.00	0.00	0.00	0.00	0.00	0.00	6.90	17.24	6.90	0.00	0.00	0.00
GPP-SMR1	84.27	0.00	0.00	0.00	0.00	0.00	7.87	0.00	0.00	7.87	0.00	0.00	0.00	0.00
GPP-SMR2	82.53	0.00	0.00	0.00	0.00	0.00	7.70	0.00	0.00	7.70	0.00	2.06	0.00	0.00
GPM-M1	50.45	41.70	0.00	0.00	0.00	0.00	2.52	0.00	0.00	5.33	0.00	0.00	0.00	0.00
GPP-SM1A	74.05	0.00	0.00	0.00	0.00	0.00	3.70	0.00	0.00	18.55	3.70	0.00	0.00	0.00
GPP-SM2A	74.05	0.00	0.00	0.00	0.00	0.00	7.40	0.00	0.00	18.55	0.00	0.00	0.00	0.00
GPC-M2C	29.47	24.36	40.67	0.00	0.00	0.00	1.77	0.00	0.00	3.73	0.00	0.00	0.00	0.00
GPC-M2E	32.40	21.40	40.70	0.00	0.00	0.00	1.77	0.00	0.00	3.73	0.00	0.00	0.00	0.00
GPC-M2F	37.92	12.51	43.67	0.00	0.00	0.00	1.90	0.00	0.00	4.00	0.00	0.00	0.00	0.00
GPC-M2G	37.59	13.53	42.49	0.00	0.00	0.00	2.05	0.00	0.00	4.33	0.00	0.00	0.00	0.00
GPC-M2I	39.66	13.09	41.09	0.00	0.00	0.00	1.98	0.00	0.00	4.19	0.00	0.00	0.00	0.00

3.3.1.1 Preparation of stock solution

NaOH solutions at specific molarity were prepared by reacting NaOH pellets at 98% purity, as shown in Figure 3.4 and water in a 1 litre (1000ml) volumetric flask grade A. NaOH pellets were gradually added to the volumetric flask.

Figure 3-5: 98% purity Sodium hydroxide pellet used.

The mass of sodium hydroxide pellet for a given solution's molarities was calculated according to Equation 3.2, and Table 3.4 illustrates the amount used for the different solutions used in this study.

$$m_{solids} = C \times M_m \times V_{sol} \qquad \text{Equation 3.2}$$

Where: - m_{solids} is the mass of sodium hydroxide pellets required in grams (g)

- C is the required molarity, also called concentration in molarity (M)
- Mm is the sodium hydroxide molar mass, given as 40g/mol
- V_{sol} is the volume of the solution taken as 1 litre (L) of water.

Table 3-4: Sodium hydroxide pellet mass (g) to make a 1L volume of sodium hydroxide solution at the given Molarity obtained from Equation 3.1

Sodium hydroxide concentration, M	Sodium hydroxide pellet, g
8	320
10	400
12	480
14	560
16	640

3.3.2 Alkaline activator preparation

The NaOH solution prepared was then stored at room temperature. The alkaline activator was made by mixing NaOH solution with Na_2SO_3 liquid in grams. The alkaline solution was further diluted with water. Figure 3.6 shows chemicals used for the making of alkaline solution.

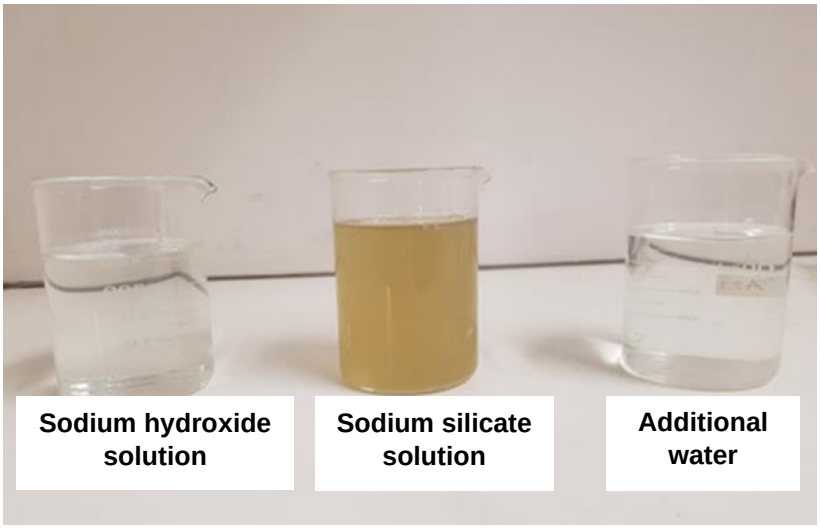

Figure 3-6: Alkaline activator components and additional water used in a real image (top) and thermal infrared image (bottom)

3.3.3 Synthesis of CFA-based geopolymer

All ingredients from CFA and the alkaline solution prepared, including fine and coarse aggregates for certain mixes, were measured in kilograms. First, a trial mixing time was set, and the mixture was monitored during the mixing to observe the homogenisation of the mix. Figure 3-7 presents the mixer used for the geopolymerization.

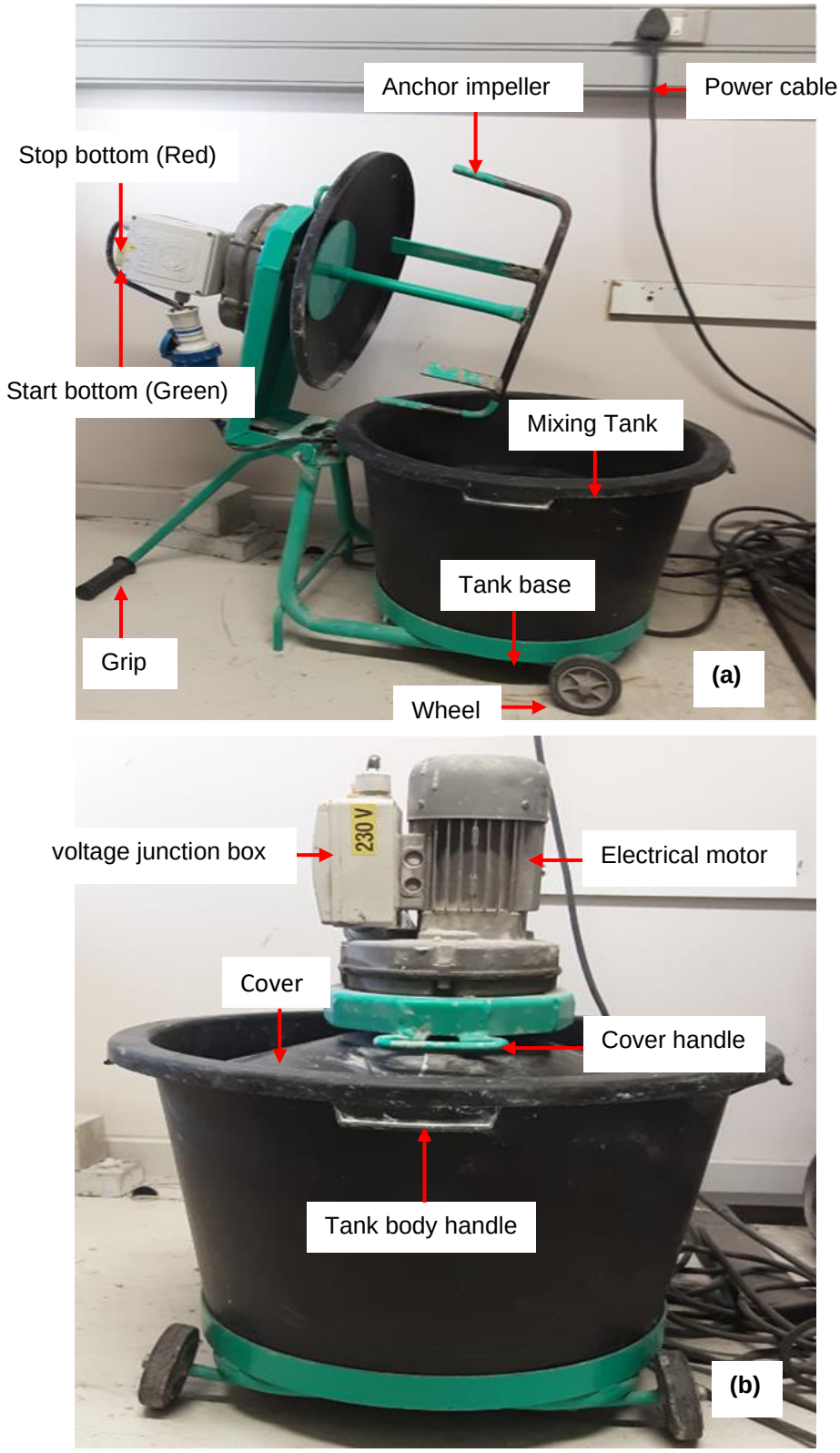

Figure 3-7: Detailing of mobile geopolymerization stirred tank used built with anchor impeller and the electrical motor of 2.1 kWh running at 55 rpm; at rest (a) and during mixing (b)

3.3.4 Residence time and homogenisation number

In this study, the residence time (RTD) of each raw material and the mixing time (quality of mixing) were considered as the main factors of the mixing as considered in Chen et al. (2005; Nagy et al., 2012; Ghanem et al., 2014; Dong et al., 2017). The resident time of each raw material in the mixer was determined from Equation 3.3 during the synthesis of CFA-based geopolymer using a 2.1 kWh mixer at a volume of 13 litres.

$$t_R = \frac{V}{Q} \qquad \text{Equation 3.3}$$

Where: - V volume of the reaction in cubic meters (m^3)

- Q is the volumetric flow rate of a specific reactant in cubic meters per second (m^3/s)
- t_R residence time in second (s)

After defining a mixing time from visual observation every 5 minutes with the mixer impeller running at 55 revolutions per minute (rpm), the homogeneity (degree of mixing) from the homogenisation number was calculated using Equation 3.4, considering the mixing time as blend time t_{bend} or t_{95} (mixing time required to create a homogeneous mixture in the mixer or time within 95% homogeneity is reached).

$$Ho = \frac{t_{blend}}{N} \qquad \text{Equation 3.4}$$

Where: -Ho is the homogenisation number (dimensionless number)

- N is the rotational rate (the number of impeller revolutions) in revolutions per minute (rpm).
- t_{blend} is the blending time in minutes (min)

3.3.5 Curing (strength growth)

Synthesised CFA-based geopolymer given mixing time by obtaining a homogeneous geopolymer mix, samples were cast in different shapes such as cubic shapes and cylindrical shapes. After the casting, curing regimes were defined, where some specimens were cured in an oven for 60 ^oC by sealing these samples with a plastic sheet to avoid scaping moisture. Another set of samples was sealed with plastic and stored at room temperature, while another set was neither sealed with plastic nor cured at an oven temperature. After 24 hours of curing, all specimens were de-moulded. Figure 3-8 represents different curing methods for CFA-based geopolymer products.

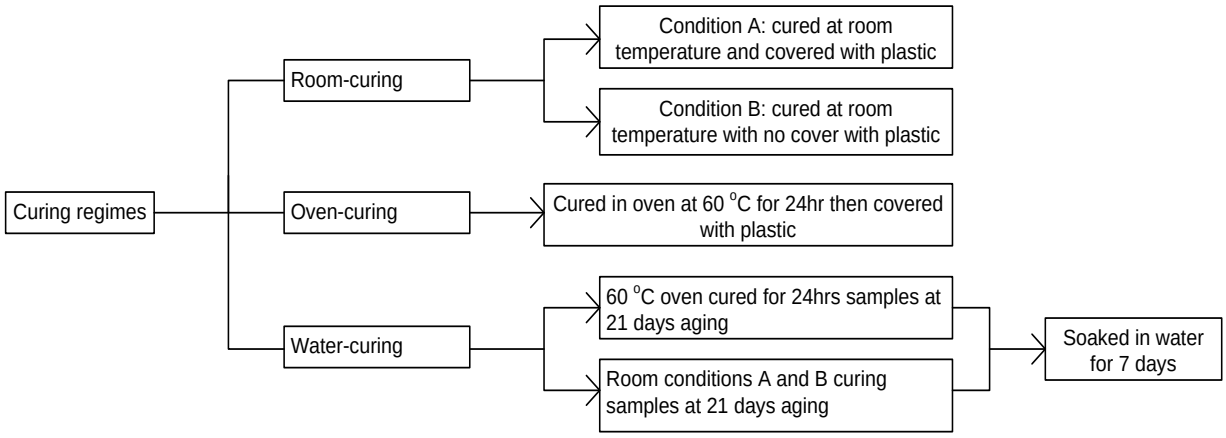

Figure 3-8: Different types of curing regimes applied in the study

As soon as the specimens were demoulded, they were cured under the following conditions: (1) Heat curing samples were placed in large plastic and well-sealed; (2) ambient-curing with sealed plastic samples were placed in plastic sheets and the other ambient curing samples with no plastic covered were kept open; (3) water-ponding were a set 3 samples collected from heat curing, ambient (room) curing with and without plastic sealing soaked in water at 21 days of ageing until they reached 28 days of ageing. Oven and room curing samples were monitored in the lab environment until the testing stage by recording the environmental temperature and humidity readings. Figure 3-9 illustrates the samples after casting and during the curing process.

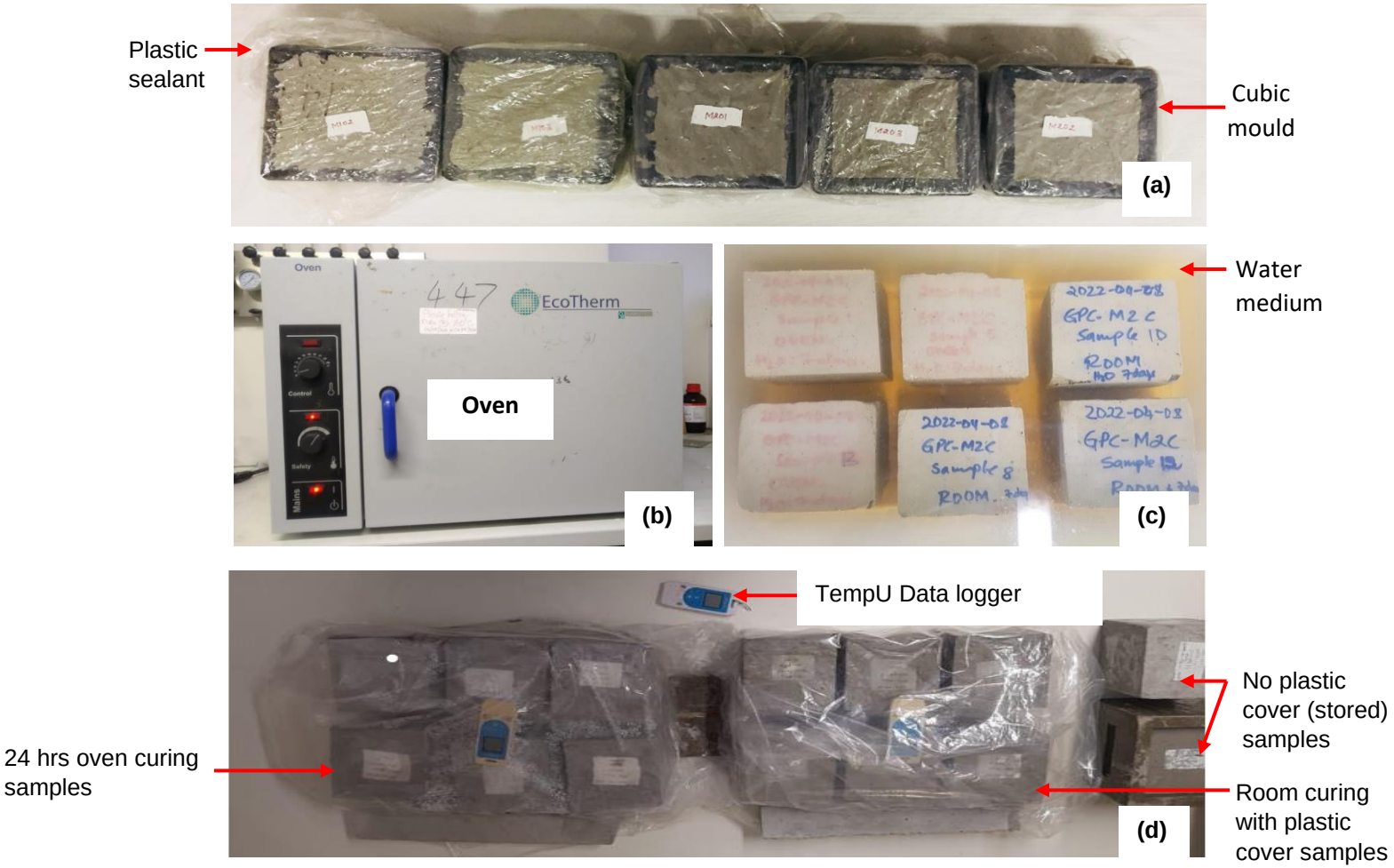

Figure 3-9: Illustration of different curing of CFA-based geopolymer samples; samples after casting sealed with plastic sheet ready for curing (a), samples at oven curing in progress at 60 ^{o}C (b), samples soaked in water at 21 days of ageing (c), oven and room curing sample after being demoulded at 24 hrs and stored in plastics sheets for continuous curing (d).

3.4 Materials and product characterisation

To deeply understand the structure performance of CFA-based geopolymer products relationship that influences its strength, deformation and thermal behaviours, which relatively impact its service life when exposed to environmental conditions, some characterisation techniques were used to determine the types of atoms present, types of bonds and crystalline structure of Lethabo CFA and formulations developed for the synthesis of geopolymer. Optimised formulation (mix) cured at different curing conditions were analysed for X-ray fluorescence (XRF) and Inductively Coupled Plasma Optical Emission Spectroscopy (ICP-OES), X-ray diffraction analysis (XRD), Scanning Electron Microscopy (SEM) and Fourier Transform Infrared Spectroscopy (FTIR) analyses where samples were crushed to a particle size of less than 100 µm using a Jaw crusher.

3.4.1 Particle size analysis

A particle size analysis was performed using the University of Cape Town (UCT) Malvern Panalytical Mastersizer 2000 for a small volume wet dispersion unit (Hydro 2000SM) run at a stirring speed of 1500 rpm (revolutions per minute) with about three scans per from the sample, to determine CFA particle sizes. The dispersant used was Propan-2-ol, also called Isopropyl-alcohol (IPA), with an assay of 99.5% and a particle refractive index of 1.73 mixed at a ratio of 1:3 in volume basis (using a spatula) with CFA (CFA: IPA) to create a well-coated slurry. The following Figure 3.10 represents the testing setup during the analysis.

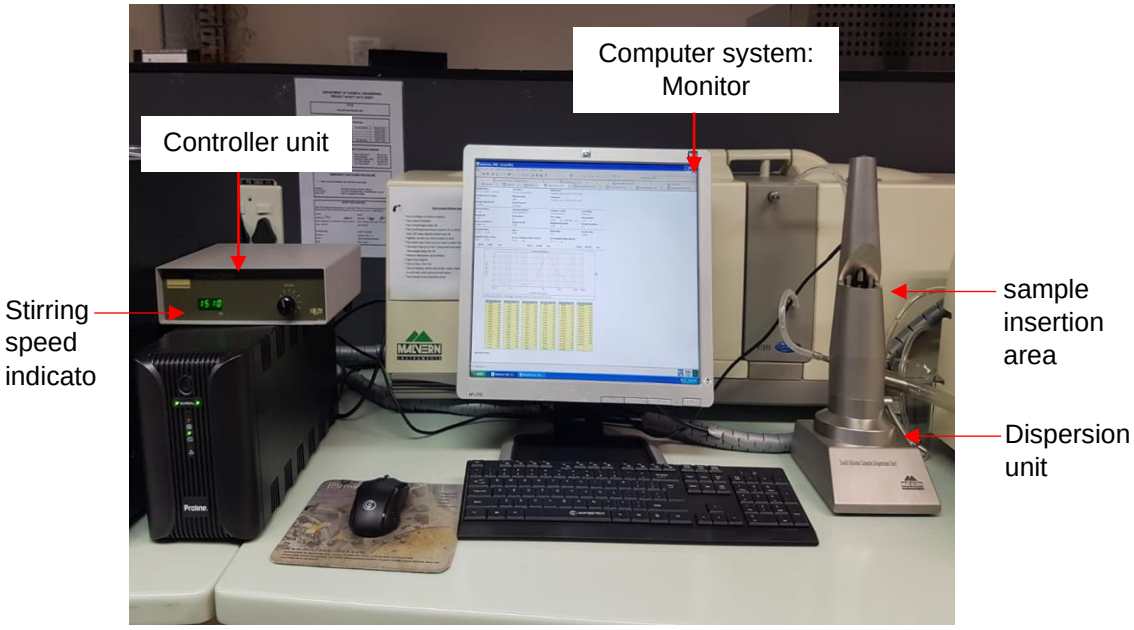

Figure 3-10: Lethabo low calcium CFA particle size analysis in progress using UCT's Hydro 2000SM Malvern Panatycal Mastersizer 2000.

3.4.2 Scanning electron microscope and energy-dispersive X-ray spectroscopy

SEM, the energy dispersive X-ray spectroscopy (EDS) characterisation analysis was performed in this study to identify the morphology (for imaging (shape), morphology and sizing detection) and the elements of Lethabo CFA and synthesised geopolymer products at optimised conditions, respectively. Furthermore, it determined the homogeneity and elemental distribution in the synthesised CFA-based geopolymer paste, mortar and concrete. The SEM and EDS analysis was carried out using the SE +EDS technique by considering Si, Al, Na and Fe elements in EDS analysis under a 1-2μm scale on a UWC scanning electron microscope. ImageJ was used to measure the size of SEM particles or any other physical observation on the image, and the analysed scale was taken as a reference.

3.4.3 X-ray diffraction

Qualitative XRD patterns characterisation analysis was performed to evaluate the mineral phases (crystalline or amorphous) of Lethabo CFA and synthesised geopolymer product at optimised conditions, respectively. PXRD data were recorded on a Bruker D2 Phaser Diffractometer using CuKα radiation ($\lambda = 1.5418$Å) generated at 30kV and 10mA. Each sample was scanned from 4-70° or 80° with 2θ steps of a 0.02° and 0.5 second exposure time per step; the total scanning time is about 30-40 minutes.

3.4.4 X-ray fluorescence and Inductive couple-plasma

XRF and Inductive couple-plasma (ICP) techniques were carried out to determine the presence of major oxides and trace elements using weight per cent (wt.% except for H2O- and LOI) measured from fused disks made from ignited powder and concentration (ppm) methods, respectively, on UCT- XRF spectrometer machine for CFA and synthesis geopolymer optimised product.

3.4.5 Fourier transform infrared spectroscopy

FT-IR spectra analysis was carried out using the universal attenuated total reflectance (UATR) technique on PerkinElmer UATR Two spectrophotometer (Llantrisant, U.K.) at force gauge (pressure) of 35 N for ATR crystal to sample and detector contact with 32 scans per sample and recorded over the range of 4000 and 400 cm− 1 at 4 cm− 1 resolution to analyse the functional groups present. Based on shifting FTIR bands, characteristic peaks of Al-O/ Si-O bond identification were investigated to determine the due effect of temperature on hydration reactions according to phase formation and extent from fingerprint region. A characteristic peak of the C

single bond O functional group was interpreted as an indication of carbonation in the geopolymer product in the synthesis from the functional group region.

3.4.6 Radon exhalation and emanation

Radon exhalation and emanation test measurements were performed at the SC7 laboratory at the University of the Western Cape to consider the potential radioactivity issue related to the use of South African Lethabo low CFA as a binder in building materials through a synthesis of geopolymer paste. A 100 mm cubic block of Lethabo low calcium CFA geopolymer paste was used for measurements. Two issues were considered.

i. The gamma radiation from the blocks. Gamma rays penetrate ionising electromagnetic radiation, which most materials emit from naturally occurring long-lived radionuclides (^{40}K and members of the ^{238}U and ^{232}Th decay series).

ii. The radon emanated from the bricks. Radon exhalation from materials depends on many factors, such as the grain size and pore space.

Lethabo CFA-based geopolymer paste 100 mm cubic block was placed in a lead castle gamma chamber for the gamma radiation. The radium content (and therefore uranium if the decay series is in secular equilibrium) and thorium concentrations were obtained with a NaI (Tl) detector in a very similar way to the methods described in Pilakouta et al. (2018) study. The detector's efficiency is needed for the geometry of the block that was tested. A sample of known activity is used to do this; a sample of soil from a mine dump measured at iThemba LABS was used for the measurements described in this report. The detector at the ERL at iThemba LABS was calibrated by the use of IAEA samples. This sample from the mine dump has a high activity of 226Ra (290 Bq/kg) and 40K (230 Bq/kg); hence, it can be used to calculate the 226Ra and 40K concentrations in the brick samples. A high thorium sample was used similarly to find the thorium concentrations, as shown in Figure 3.11.

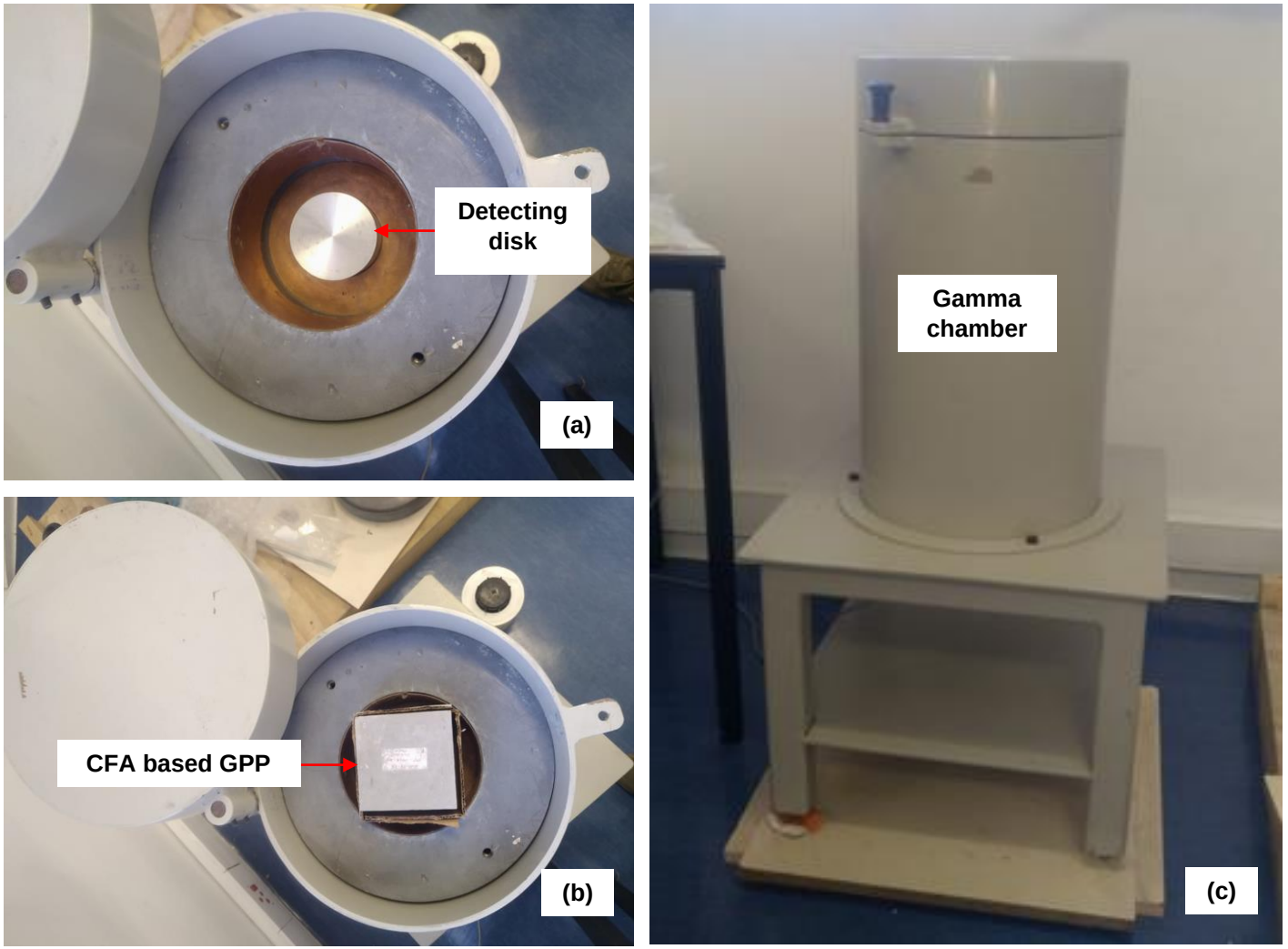

Figure 3-11: Process involved in thorium concentrations measurement at SC7 laboratory from the University of Western Cape; Chamber detector (a), CFA-based GPP specimen in the chamber (b) and chamber closed for testing (c).

For radon measurement, the 100 mm cubic low calcium CFA-based geopolymer paste block was placed in an air-tight chamber that is connected to a radon detector, namely a RAD7 radon detector (Available at https://durridge.com/products/rad7-radon-detector/, Accessed on 8 August 2022) as shown in the following Figure 3.12. The radon exhaled from the brick causes the radon concentration to increase in the chamber.

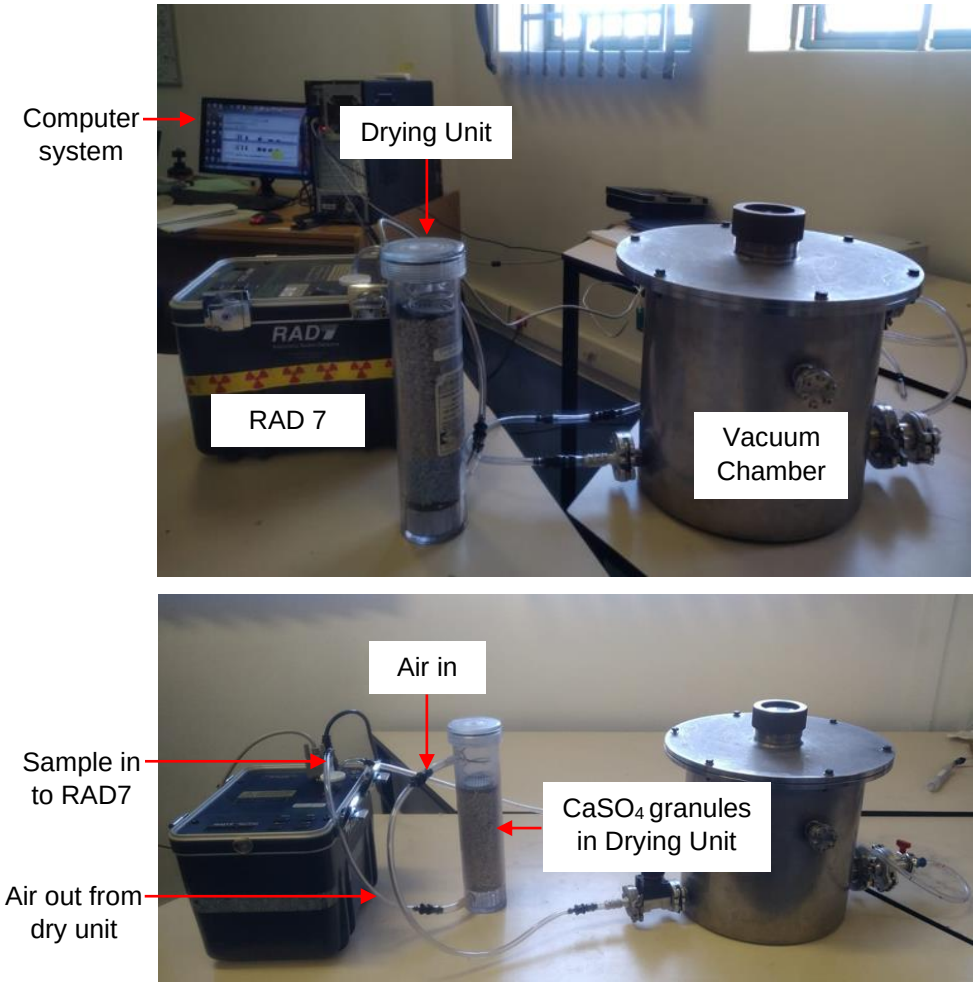

Figure 3-12: Radon monitor set up measurements using RAD7 at SC7 laboratory from the University of Western Cape.

According to Amin (2015), the radon exhaled from the block causes the radon concentration to increase in the chamber. This radon concentration increases in chamber C(t), as shown in Equation 3.5.

$$C(t) = \frac{C_{Ra}}{V}\left(1 - e^{-\lambda t}\right) \qquad \text{Equation 3.5}$$

Where: - V is the volume of the chamber and the detector = 14 litres in our case

-$C(t)$ is the radon concentration to increase in the chamber, in Becquerels per cubic meter $(\mathrm{Bq.m^{-3}})$

- C_{Ra} is the effective strength of the radium source in the brick that makes it into the chamber in Bq.

- t is the time in seconds (S)

- λ is the decay constant of radon 2.1×10^{-6}, in S^{-1}

It was assumed that for a particular sample, the radon increased in the Chamber (as read by the RAD7) at a rate of x Bq.m-3 per hour for the first few hours. In this period, Equation 3.5 can be approximated to Equation 3.6 since $e^{-\lambda t} \sim 1$ and it is very small. The slope x is then defined as shown in Equation 3.7.

$$C(t) = \frac{C_{Ra\lambda t}}{V} \qquad \text{Equation 3.6}$$

$$x = \frac{C_{Ra\lambda}}{V} \quad \text{or } C_{Ra} = \frac{Vx}{\lambda} \qquad \text{Equation 3.7}$$

More description of the op view of RAD 7 and the placement of CFA-based geopolymer paste in the gamma chamber is shown in Figure A-9.

3.5 Testing methods optimisation factors consideration

The engineering properties of geopolymer paste, mortar, and concrete investigated in this study were defined in the fresh and hardening states based on strength (mechanic of material) and durability aspects. These properties are important for construction materials, defined according to the testing standards. The fresh properties will define the behaviour of the geopolymer material when still moistened. The mechanical properties will define the structural behaviour of CFA-based geopolymer under loading, while durability properties will predict CFA-based geopolymer products' behaviour under environmental exposure, which may lead to product degradation. Once the optimised mix is in the required target value, an economic and environmental assessment of this mix will be a performance to analyse its impact on business decision-making. Table 3.6 illustrates the engineering properties of CFA-based geopolymer properties investigated at fresh and hardened states, including the decision-making parameter viewed.

Table 3-5: *CFA-based geopolymer as building materials fresh and hardened engineering properties target value expected after mix optimisation and decision-making parameters viewed.*

Material state properties		Characteristic	Target Value	References
Fresh	CFA-based GPP	Consistency (mm)	5-7 mm of penetration in 2 min the better	ASTM 191
		Initial setting time (min)	25 mm penetration from 120 min the better	
		Final setting time (hr)	40 mm penetration before 6 hrs the better	
		Fluidity time (min)	lower the better	
	CFA-based GPC	Slump test (mm)	75-100 mm the better	Mamlouk, 2011:257
		Slump flow (mm)	higher the better	
		Fresh density (Kg/m3)	lower the better	
	All	Curing regime (temperature)	no oven heat curing the better	
Hard	Mechanical	Compression strength for (MPa)	higher than 20 MPa better for structural application at 28 days or ref Table 2.10	Li, 2011:16
		Breaking pattern (satisfactory fracture)	A or B, the better	
		Flexural MPa (% of compression MPa)	from 10 % towards the better	Mamlouk, 2011, p257-293
		Tensile MPa (% of compression MPa)	from 10 % towards the better	
		Modulus of elasticity (GPa)	10.3-34.5 GPa is the better	
		Poisson ratio	higher the better	
	Durability	Water penetration (mm/min)	lower the better	
		Water absorption (%)	lower than 20% the better	ASTM C62:2017; Mamlouk, 2011, p322
		Water absorption rate (Kg/m2)	lower the better	
		Thickness swelling (%)	lower the better	
		Carbonation	The surface mostly covered with fuscia or pink colour the better	
		pH measurement	8 to 12 the better	
		Efflorescence	lower than moderate the better	NCTEL, 2013
		Hardened density (Kg/m3)	lower the better	
		Fire resistance (hr)	higher the better	
Decision making	Economic and Environmental	Embodied energy	lower the better	
		Cost of the mix	lower the better	
		LCA environmental impact	lower the better	

3.5.1 Fresh properties of geopolymer

3.5.1.1 Setting time

As discussed by Andrade et al. (2009), the initial setting time is the period when the concrete temperature increases after the dormant period (plastic state) when the mix starts to show stiffness. The initial setting time stiffness of the concrete is crucial to its ability to sustain the tensile force caused by plastic shrinkage in the case of concrete elements that have a physical restriction, such as crimping, which prohibits dimensional variation without cracks.

The setting times were performed in this study according to ASTM C 191: 2018 (Standard Test Methods for Time of Setting of Hydraulic Cement by Vicat Needle), which is the same as the national standard method SANS 50196-3:2006 part 6 (30% of water was used as w/b ratio) using the Vicat apparatus shown in Figure 3.13. This experiment was carried out at room temperature at a range of 25 – 27^{o}C. 400 g of CFA was collected as a binder and mixed with 120 alkaline activators containing additional water. A Vicat apparatus, as shown in Figure 3.13, was used to perform the test. A needle of 1 mm was used for an initial and final setting time, while the plunger (10 mm) and a cap load were used to determine the consistency (control of water demand ratio) of the paste mix.

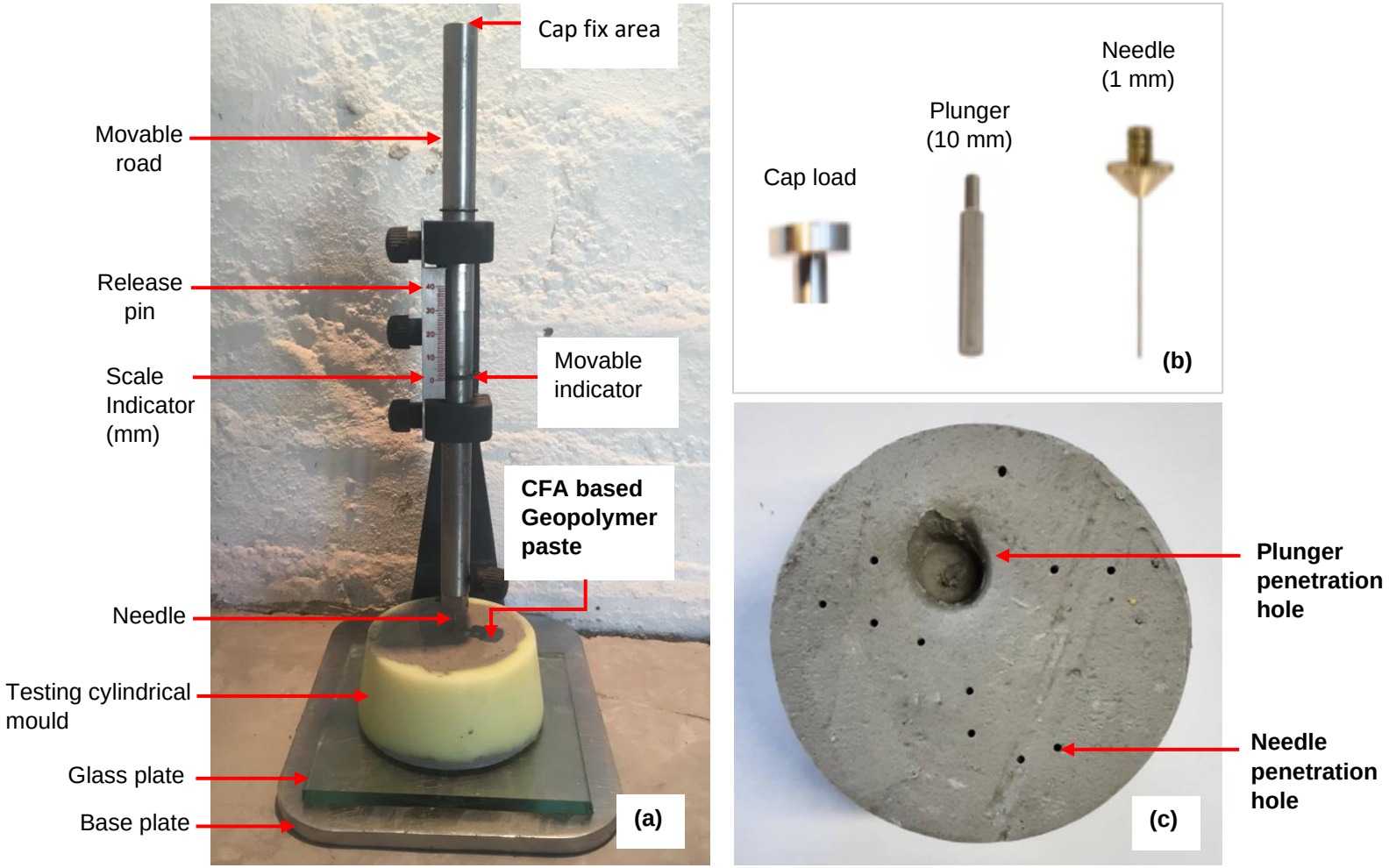

Figure 3-13: Vicat apparatus during CFA-based geopolymer paste setting time determination (a) Needle, Plunger, and Cap load used for initial and final setting time and consistency determination (b) CFA-based geopolymer paste sample being tested showing Plunger and Needle penetrations (c)

3.5.1.2 Flow cone test

The fluidity test was performed using a Marsh cone to determine the CFA-based geopolymer paste (GPP) flow timing properties. This was performed in accordance with ASTM C939-10. Water (1725 mL ±5) was used to calibrate the flow cone. The flow cone was steady and levelled. A temperature data logger was used to measure the temperature of CFA-based geopolymer paste. Figure 3.14 describes the experiment setup and the fluidity test of CFA-based geopolymer paste.

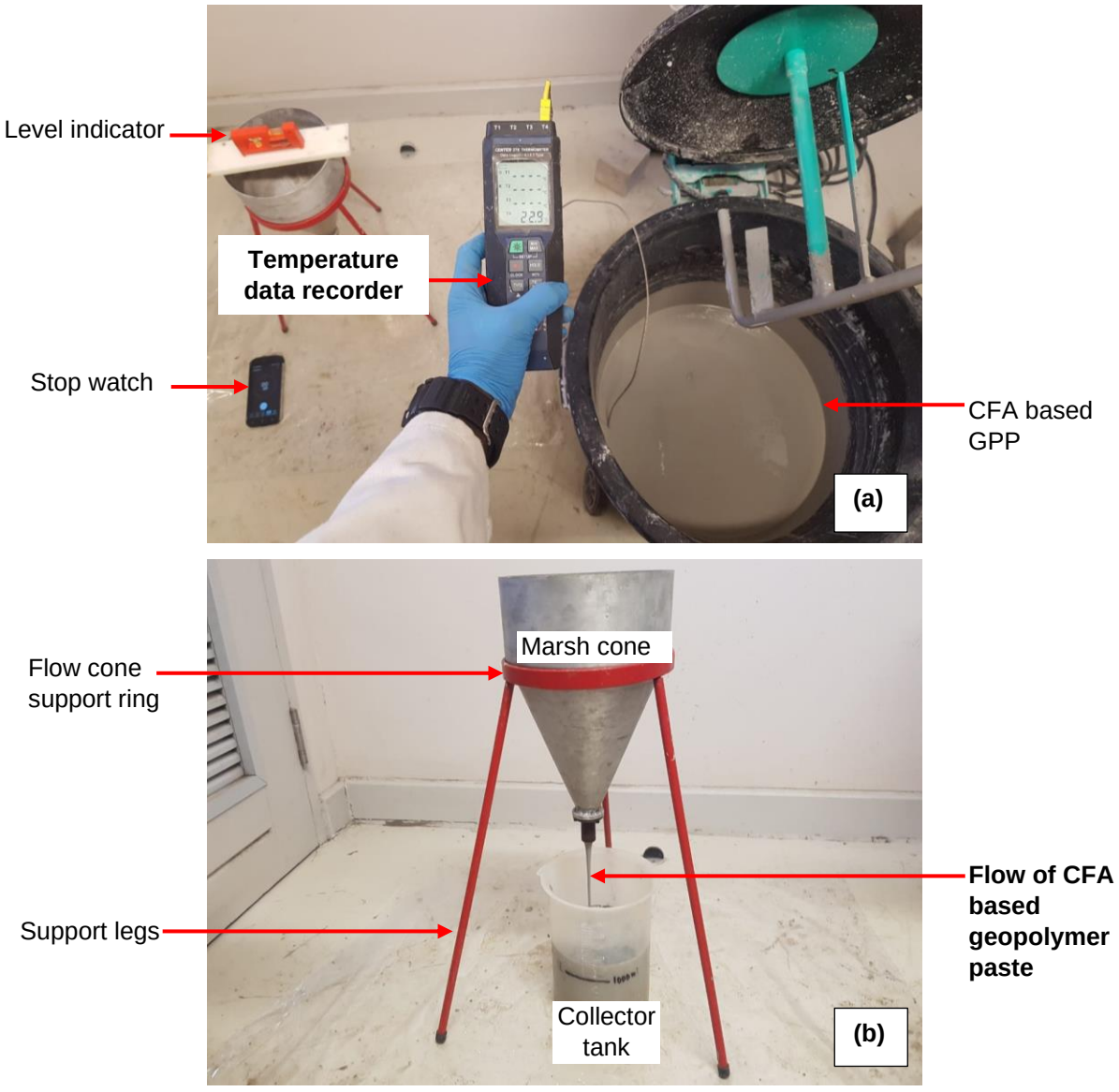

Figure 3-14: Fluidity test of CFA geopolymer paste; Experiment set up and mixing of the paste (a) and CFA-based geopolymer paste fluidity test in progress (b).

3.5.1.3 Slump test

A slump test was performed using a slump cone to determine the flow property of CFA-based geopolymer concrete. This was performed in accordance with SANS 5862-1:2006 (consistency of freshly mixed concrete-slump test). The following Figure 3.15 shows the experiment apparatus setup for slump test testing

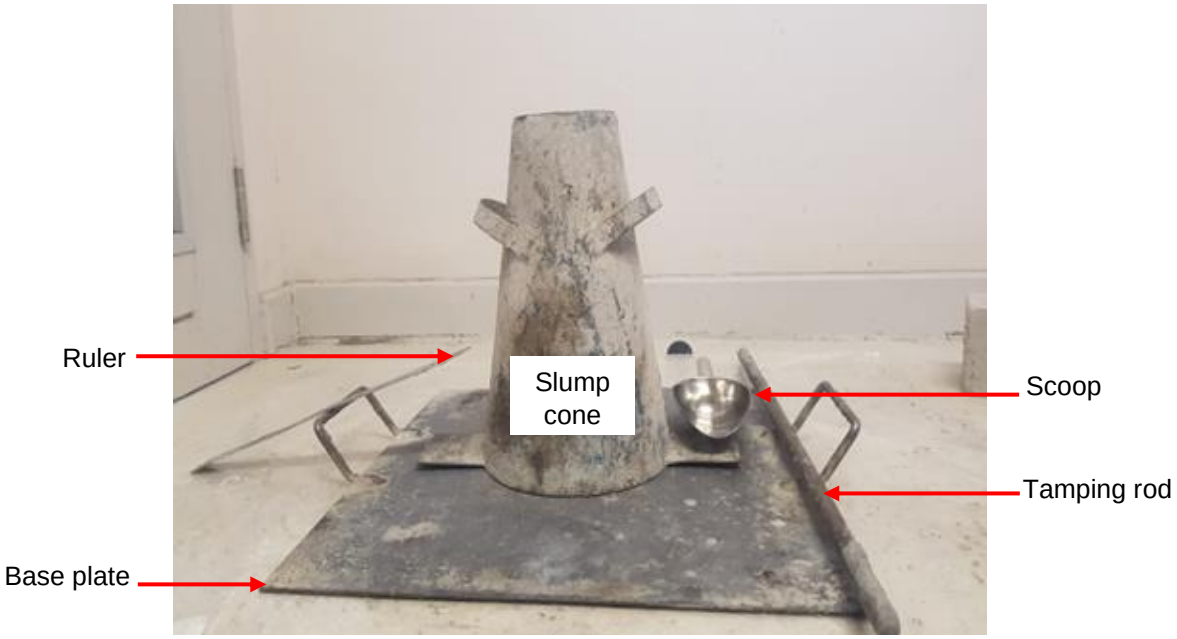

Figure 3-15: Slump test apparatus (a), CFA-based geopolymer concrete; optimised mix

3.5.1.4 Slump flow test

Similar to the slump test, slump flow was performed using a slump cone to determine the flow property of very wet CFA-based geopolymer concrete. This was conducted according to the experiment apparatus setup for slump flow testing.

Figure 3-16: Slump flow apparatus and wet CFA-based geopolymer concrete during slump flow test.

3.5.1.5 Density of fresh

The fresh density of CFA-based fresh geopolymer paste, mortar, and concrete was measured after the casting of these samples in 100 mm cubic moulds, as shown in Figure 3.11. The density was calculated according to the following Equation 3.8 as indicated in SANS 6250:2006 (Density of compacted freshly mixed concrete).

$$D_{wet} = \frac{m_s - m_{mol}}{V_{mol}} \qquad \text{Equation 3.8}$$

Where: -D_{wet} is the fresh density of geopolymer in Kilogram per cubic meter (Kg/m^3)

- m_{wet} and m_{mol} are the masses of wet geopolymer and cubic mould in Kg

- V_{mol} is the volume of cubic mould in cubic meters (m^3)

3.5.2 Mechanical properties

Mechanical properties consisted of the application of loads to CFA-based geopolymer products cast. This was done at the hardening state, where most of the tests were performed from the maturity age (28 days).

3.5.2.1 Compression strength

The compression strength was the most reputable hardening test in this study to ensure the formulations developed were strong enough to substantiate a given structural load. SANS method

5863:2006 (concrete tests - compressive strength of hardened concrete) was used as the standard to conduct this test. A fully automatic 1800 kN concrete cube press completed with a digital controller with a load capacity of 1800 kN and load rate of 18 kN/min, as shown in Figure 3.17, was utilised to compress the samples.

CFA-based geopolymer paste, mortar and concrete compression strength on average of three 100 mm cube specimens at a specific curing age were tested. The machine compression loading rate was set up at 180 kN/ mm. At the end of the crushing load, the compression strength of the specimen was calculated according to the formula in Equation 3.9.

$$f_c = \frac{P}{A} \qquad \text{Equation 3.9}$$

Where: -f_c is the characteristic strength of a specimen in mega-pascal (MPa)

- P is the crushing load obtained from the machine in Newton (N)
- A is the load applied surface area of the specimen in millimetre square (mm^2).

For testing purposes, once the specimen was inserted into the machine, the Test rate at which the sample was compressed was obtained based on the following Equation 3.10.

$$Test\ rate = \frac{A}{1000} \times Sp \qquad \text{Equation 3.10}$$

Where: -A is the specimen in millimetre square (mm^2)

- Sp is the machine compression speed which was built at 18 kN/min

The testing on the strength of CFA-based geopolymer concrete using the compression strength method was done at 3, 7, 14, 21, and 28 days, including 90 days (three months). A sample breaking pattern was identified, as shown in Figure 3.17c.

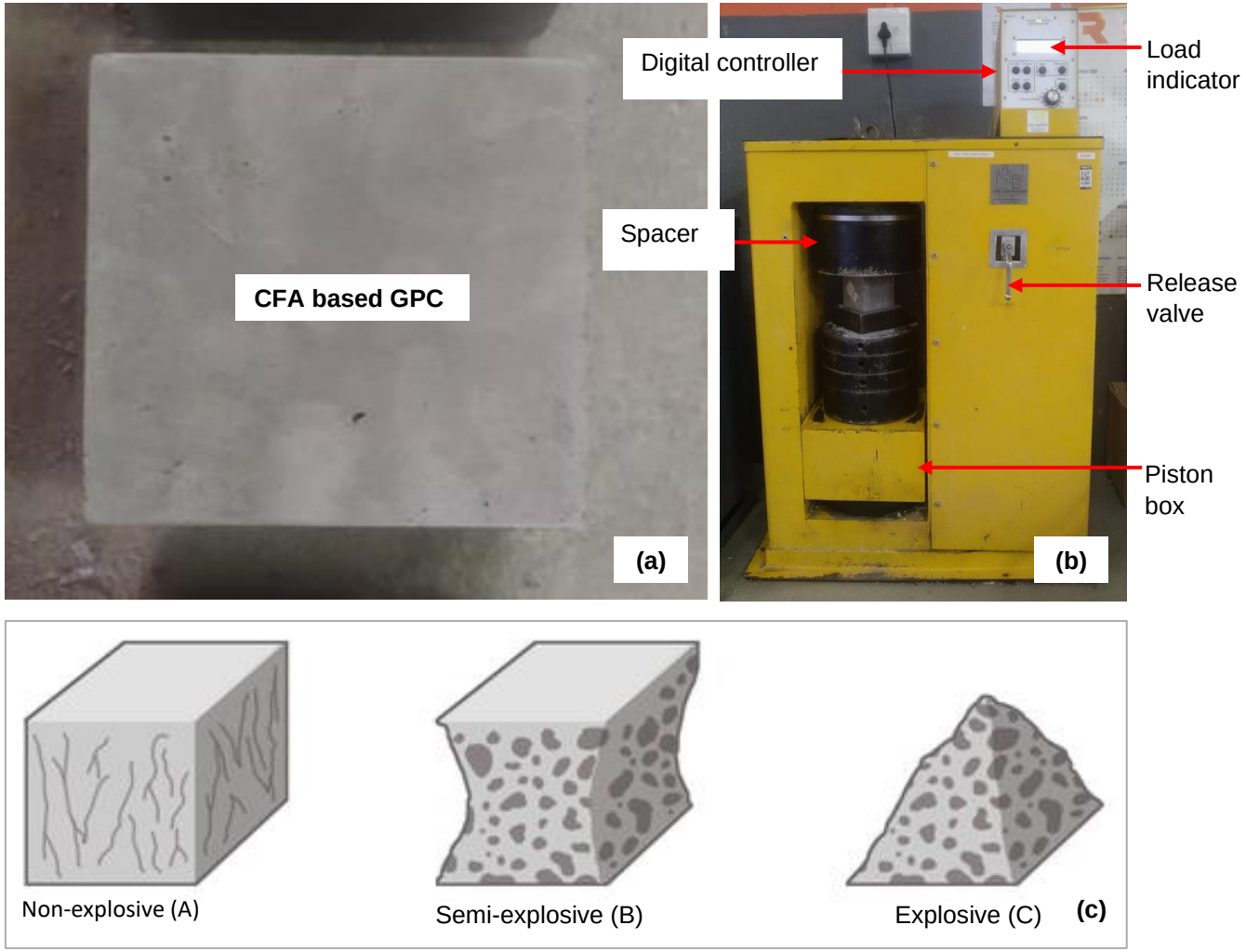

Figure 3-17: CFA-based geopolymer concrete before compression strength (a), fully automatic 1800kN concrete cube press machine in testing mode (b) and satisfactory fracture pattern observed in concrete cube specimen at the end of compression testing (Source: modified from source: Available at https://theory.labster.com/failure-concrete/, Accessed on 24 July 2022) (c).

3.5.2.2 Flexural strength

The flexural strength of CFA-based geopolymer paste (GPP) and concrete (GPC) were conducted to determine their bending behaviour under a certain moment. Results obtained will be important for better analysis of the structure constructed using low calcium CFA-based geopolymer concrete (better determination loads: moment, shear, axial or overturning forces acting on GPC structure). A Roadlab civil engineering laboratory centre-point load bending (single load at midspan) machine, shown in Figure 3.18 below, was utilised to test the specimens of 500 mm length, 100 mm width, and 100 mm thick. This test was not so reputable in this study as it was based on suitable formulations. The test was performed according to BS EN 12390-5:2009 (Concrete tests - Flexural strength of hardened concrete) standard, which is similar to SANS 5864:2006. Before inserting the sample into the machine, it was marked in the middle as the load cell application indication area for proper bending moment distribution.

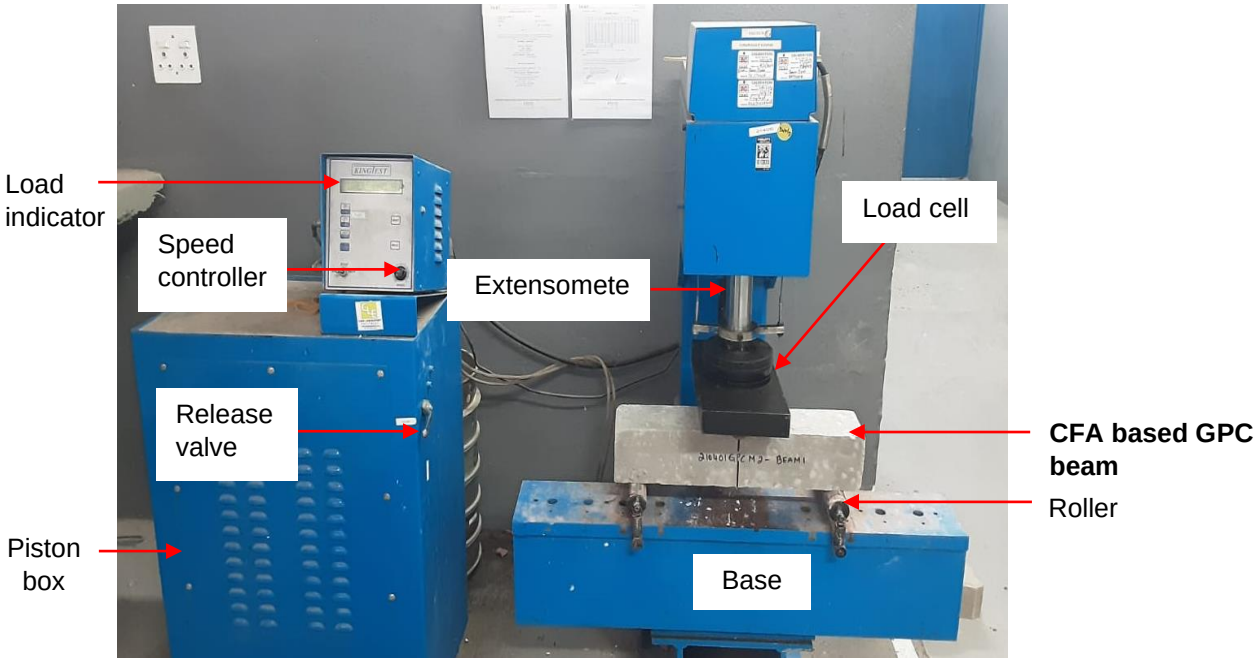

Figure 3-18: CFA-based geopolymer concrete beam under centre-point load bending testing using King Test machine.

None of the beam samples tested was reinforced with steel or any mesh. At the end of the test, Equation 3.11, for centre-point load bending, was used to determine the flexural strength of the geopolymer beam when

$$f_r = \frac{3PL}{2bd^2} \qquad \text{Equation 3.11}$$

Where: -f_r is the flexural strength of a specimen in mega-pascal (MPa)

- P is the total load evenly distributed over one loading point in Newton (N)

- L is the beam span (distance between rollers) in mm, taken as $L = 3 \times d$

- *b* and *d* are the width and depth of the beam in mm

3.5.2.3 Tensile splitting strength

The tensile splitting strength of CFA-based geopolymer paste, mortar, and concrete was conducted to examine the type of cracks developed from the tested geopolymer formulation with and without fine and coarse aggregates. The specimen was loaded, as shown in Figure 3.19. The test was performed according to the standard of the SANS method 6253:2006 (Concrete tests - Tensile splitting strength of concrete).

Figure 3-19: Tensile splitting machine used for the testing of CFA-based geopolymer formulations

A cubic CFA-based geopolymer concrete specimen of size $a = 100$ mm was used to perform the test. This was conducted on suitable formulations. Equation 3.12 was used to determine the tensile splitting strength of the specimen.

$$f_{ct} = \frac{2P}{a^2}$$ Equation 3.12

Where: -f_{ct} is the flexural strength of a specimen in mega-pascal (MPa)

- P is failure load tensile strength in Newton (N).

3.5.2.4 Modulus of elasticity and poison ratio

Modulus of elasticity was performed according to ASTM C469 (Standard Methods of Test for Static Modulus of Elasticity, and Poisson's Ratio of Concrete in Compression) to determine the stress-strain behaviour of CFA-based geopolymer concrete and mortar under loading using 104 mm diameter and 120 mm height cylinder. It determines the ability of a material to resist deformation. This test is helpful to provide the information for better analysis and design for flexure of structure that can be built using low calcium CFA-based geopolymer concrete (understanding the stress-strain performance of GPC). The low calcium CFA-based geopolymer concrete specimen was levelled by capping according to ASTM C617-10 (Standard Practice for Capping Cylindrical Concrete Specimens) to ensure proper testing. This experiment was carried out using a compressometer/ extensometer and a fully automated 1800kN concrete press machine complete with a digital controller. Figure 3.20 describes the steps involved in CFA-based geopolymer concrete stress-strain determination. Two CFA-based geopolymer concrete specimens per mix were used for this test, where the first specimen was fully compressed without inserting it into the compressometer. The second was compressed up to 40% of the first specimen's strength when inserted into a compressometer. A stress-strain curve will be plotted from the results obtained. The modulus of elasticity was determined according to the following equation: 3.13.

$$E = \frac{G_2 - G_1}{(\varepsilon_2 - 0.00005)}$$ Equation 3.13

Where: -E is the static chord modulus of elasticity in MPa

- G_1 is the applied load at a strain of 50×10^{-6} divided by the cross-sectional area of the unloaded specimen in MPa

-G_2 is the test load, divided by the cross-sectional area of the unloaded specimen in MPa.

-ε_2 is the deformation at test load, divided by the gauge length, in 10^{-6} mm

The Poisson ratio was calculated to the nearest 0.01 from the average strains from second and successive loadings following Equation 3.14.

$$\nu = \frac{(\varepsilon_4 - \varepsilon_3)}{\varepsilon_1 - 0.00005}$$ Equation 3.14

Where: -ν is the Poisson ration

- ε_4 is the average transverse strain at the test load

-ε_3 is the average transverse strain coincident with the average longitudinal strain of 50×10^{-6} m/m

-ε_1 is the average longitudinal strain at test load.

According to ASTM 469, as the strains are determined only on the nearest $10^{-6}\mathrm{m/m}$, the accuracy of the test results determined by this method will depend on the relative magnitude of the strains.

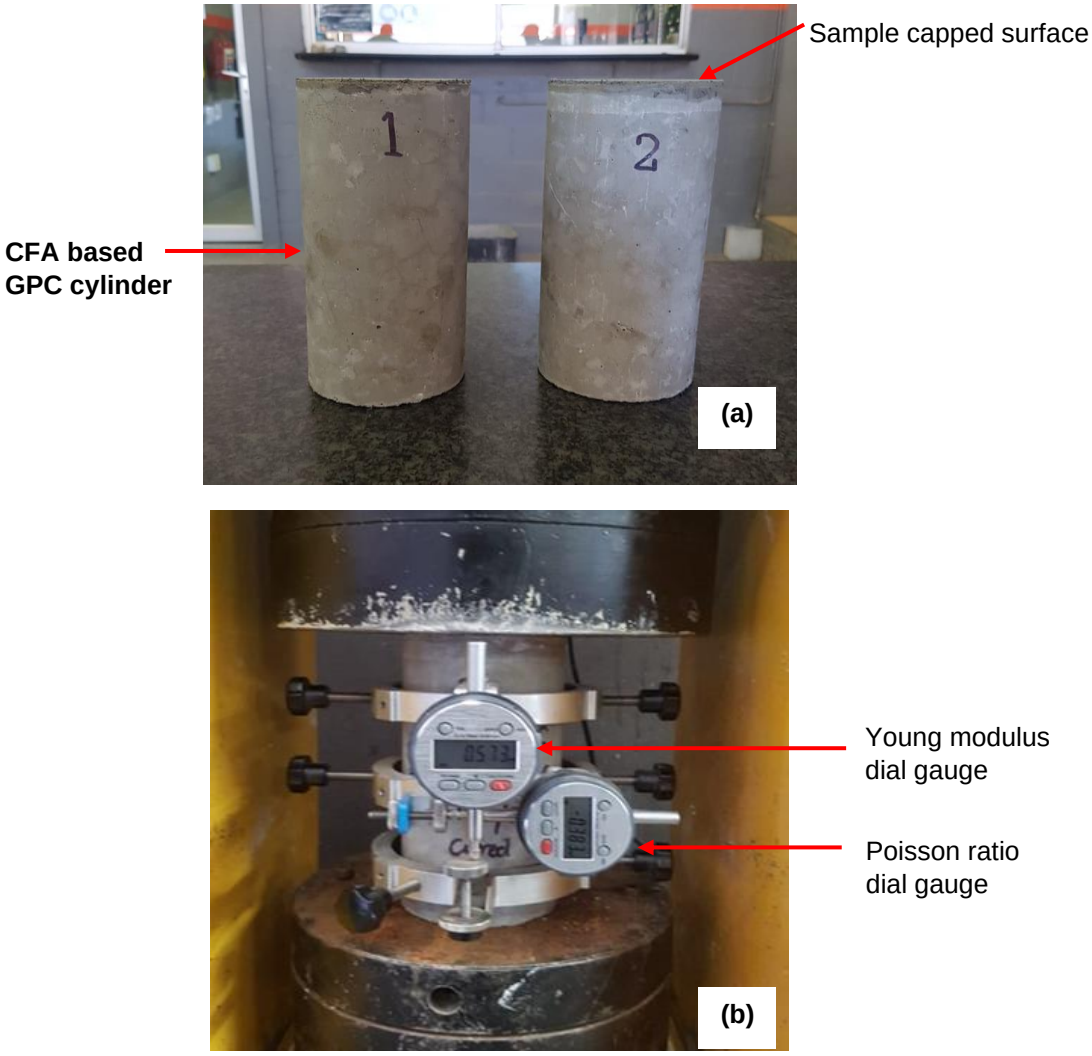

Figure 3-20: An illustration of steps involved for modulus of elasticity and Poisson ratio cylinder testing; samples capping (a) and the sample under testing (b).

3.5.3 Durability properties

Durability properties determine the ability of construction materials to withstand their service life when exposed to environmental conditions. The materials may be subject to weathering action, chemical attack, and deterioration due to carbon penetration or fire, which may also lead the reinforcement to corrode, as well as other deterioration processes, depending on the environment. This material serving process is therefore considered durability. In this study, the durability test of CFA-based geopolymer was investigated and considered a vital indication of estimating CFA-base geopolymer structure lifespan. Similar to normal concrete, this durability indication was invested based on the CFA-based geopolymer's ability to resist physical and chemical attacks. The aggressiveness of these attacks on the durability of CFA-based geopolymer originally may depend on factors of the geopolymer system. Figure 3.21 illustrates the geopolymer system factors and the aggressiveness of the exposure environment effects investigated in this study based on the optimised CFA-based geopolymer concrete on oven curing, room with plastic cover and room open air curing regimes.

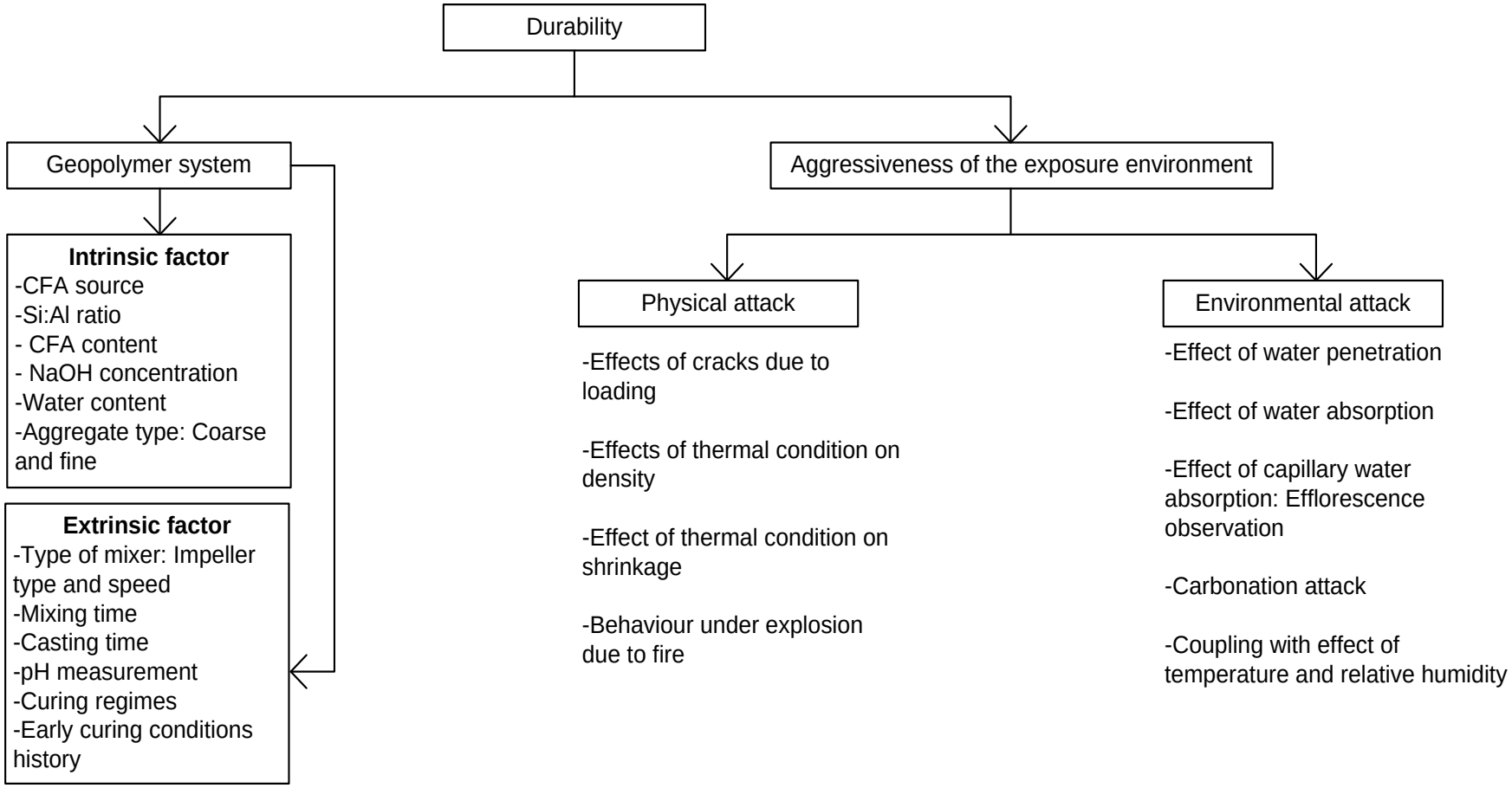

Figure 3-21: Illustration of Lethabo low CFA-based geopolymer system and environmental factors influencing its durability investigated during the study.

3.5.3.1 Water penetration

The TQC Karsten Tube Penetration Method DIN 1048 (same as Measurement of Water Absorption Under Low-Pressure RILEM Test Method – Test No. 11.4) was used to investigate the CFA-based geopolymer concrete as building material water ingress. A graduated glass tube (vertical tube in this study) was bonded to the CFA-based geopolymer concrete by plasticine and then filled with water. Water pressure was observed while exerted on the CFA-based geopolymer concrete surface. The amount of water penetrating the sample surface was recorded every minute by observation of its level decreasing on the graduated scale indication over time (20 minutes for each sample). Here, water penetration was compared based on an optimised mix of GPC samples cured at oven 60 ^{o}C for 24 hours in a room with plastic (condition A) and a room with open air (condition B). Figure 3.22 shows the experiment setup done on CFA-based geopolymer concrete Karsten tube water penetration.

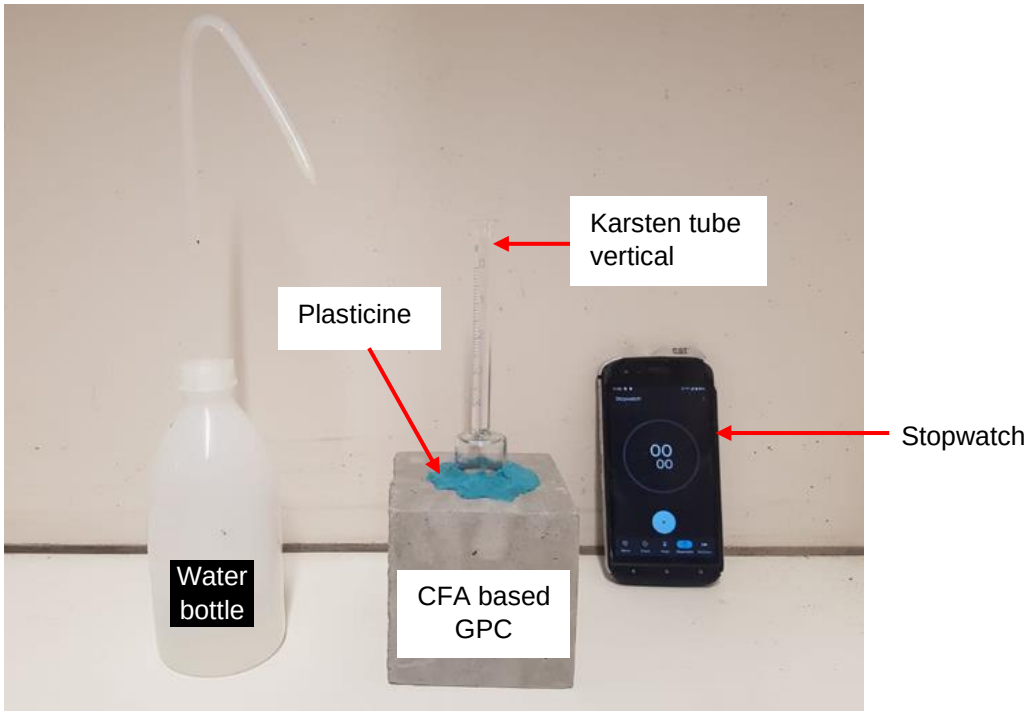

Figure 3-22: Water penetration testing of low calcium CFA-based geopolymer concrete as building materials under low tube water penetration test by TQC Karsten tube penetration test method.

3.5.3.2 Water absorption

A water absorption test was performed to determine the amount of water absorbed by a material under specified conditions. The test was conducted under SANS method 1215:2008 (Sampling

and Testing Concrete Masonry Units and Related Units), which is similar to ASTM C62:2017 (Standard Specification for Building Brick). The test aimed to compare optimised GPC formulation samples cured at oven 60 ^{o}C for 24 hours in a room with plastic (condition A) and a room with open air (condition B). In this method, samples are dried in an oven for 24 hours at 110 ^{o}C to freeze any initial moisture, then cooled at ambient temperature for 4 hours. A water bath at 23±2 °C for 24 hours was used, as shown in Figure 3.23, to immerse the cooled samples after they had been weighed. After removing the samples, they are wiped dry with a lint-free cloth and weighed.

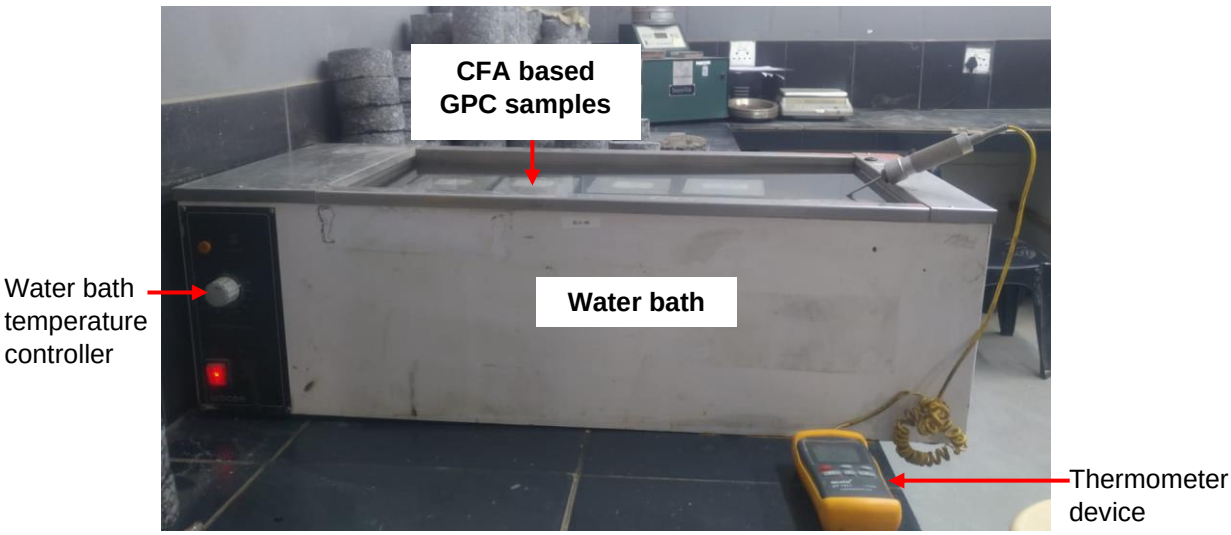

Figure 3-23: Lethabo low CFA-based geopolymer concrete samples water absorption test in progress at 23 ^{o}C using Roadlab water bath

CFA-based geopolymer concrete cubic samples dried were used. Equation 3.15 was used to calculate the percentage of the mass of water absorbed by each specimen.

$$X = \frac{m_{wet} - m_{dry}}{m_{dry}} \times 100 \qquad \text{Equation 3.15}$$

Where: - X is mass moisture absorption after 24 hrs in percentage (%)

- m_{dry} and m_{wet} are oven dry at 110^{o}C mass and 24 hours final water immersed mass of samples respectively in kilogram (Kg).

At the end of the 24-hour water absorption test, all samples were crushed for compression strength to absorb the effect of water absorption on the mechanical properties of CFA-based geopolymer products. Equation 3.16 was used to determine any strength again and a loss percentage of the specimens. A sample of water use was collected before immerging the specimens and after removing them to evaluate the possible leaching of chemical elements from

the specimens by using the Inductively Coupled Plasma Optical Emission Spectroscopy (ICP-OES) as an analytical technique.

$$F_{loss}\ or\ F_{gain}(\%) = \frac{|F_{wet} - F_{dry}|}{F_{dry}} \quad \textbf{Equation 3.16}$$

Where: -$F_{gain}(\%)$ is the compression strength loss if $F_{wet} - F_{dry}$ is positive, in (%)

- $F_{loss}(\%)$ is the compression strength gain if $F_{wet} - F_{dry}$ is negative, in (%)
- F_{dry} and F_{wet} are compression strength on dry geopolymer at the same ageing and 24 hours water immerged specimens' compression strength tested, in MPa

3.5.3.3 Capillary water absorption test and efflorescence test

The capillary water absorption test was conducted to determine CFA-based geopolymer concrete's absorption rate when in contact with water. The test method used was ASTM 1585-20 (Standard Test Method for Measurement of Rate of Absorption of Water by Hydraulic-Cement Concretes). CFA-based geopolymer concrete samples cured at different regimes were partially soaked at 12 mm height in a shallow water flat bottom tray, as shown in Figure 3.24. The testing water temperature measured was around 13±2 ^{o}C, and the environmental condition (temperature and relative humidity) was recorded using the TempU data logger. Samples were weighted and thickness measured for 2, 24, 48 and 72 hours of water soaking.

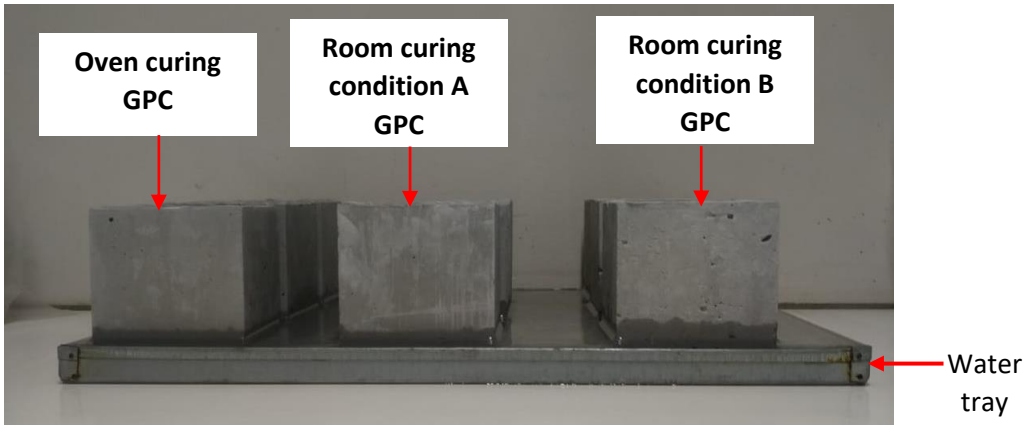

Figure 3-24: Lethabo low CFA-based geopolymer concrete cured at different regimes under capillary water absorption test and efflorescence observation.

Equations 3.17 and 3.18 were used, respectively, to determine the amount of water absorbed and the thickness swelling of the specimen at the specific soaking age.

$$m\ (\%) = \frac{m_t - m_i}{m_i}$$ Equation 3.17

Where: -$m\ (\%)$ is mass absorbed water in percentage

- m_i and m_t are the initial mass and mass at a specific time t of specimen respectively in Kg

$$TS\ (\%) = \frac{t_t - t_i}{h_i}$$ Equation 3.18

Where: -$TS\ (\%)$ is the thickness swelling percentage

- t_i and t_t are the initial thickness and thickness at a specific time t of specimen respectively in mm

Equation 3.19 was applied to estimate the specimen's water absorption rate over time (72 hrs.

$$\dot{m}_r = \frac{(m_t - m_i)}{A} \times 10^3$$ Equation 3.19

Where: - $\dot{m}_r$ is the weight of absorbed water per unit area (Kg/m^2)

- A is the area of the specimen mm^2

During the different ageing of the specimen in water, they were physically according to ASTM C1400-1 (Test Method for Determining the Efflorescence Potential of Masonry Materials Based on Soluble Salt Content) to determine the potential efflorescence appearance in CFA-based geopolymer materials based on the extent of deposits of sodium hydroxide (salt) observed on the specimen as illustrated in Table 3.6.

Table 3-6: Efflorescence extends deposit reporting by observation of building material for use in construction (source: NCTEL, 2013).

Description	Extent of deposits
Nil	No perceptible deposit of efflorescence
Slight	18% area, covered with thin salt deposits
Moderate	Up to 58% area, covered; heavy deposit, no powdering or flaking
Heavy	58% or more area covered; heavy deposit, no powdering or flaking
Serious	Heavy deposit powdering or flaking observed

At the end of 72 hours of water soaking, samples were kept unsoaked in the testing room condition for continuous efflorescence monitoring and then crashed after 28 days of exposure after the applied Equation 3.18 to determine the strength loss or again of specimens.

3.5.3.4 Carbonation depth and pH measurements

This test was performed on crashed specimens cured at different regimes under the RILEM CPC-18 method (measurement of hardened concrete carbonation depth). A 1% solution of phenolphthalein in ethanol was utilised as an indicator. The phenolphthalein solution was sprayed on the broken surfaces of the crashed GPC specimen, and the carbonated and non-carbonated portions observed on the specimen, as illustrated in Figure 3.25, were reported. A vernier calliper was then used to measure the carbonated depth (covering) from about four (4) different depths or directions (4 measurements per sample).

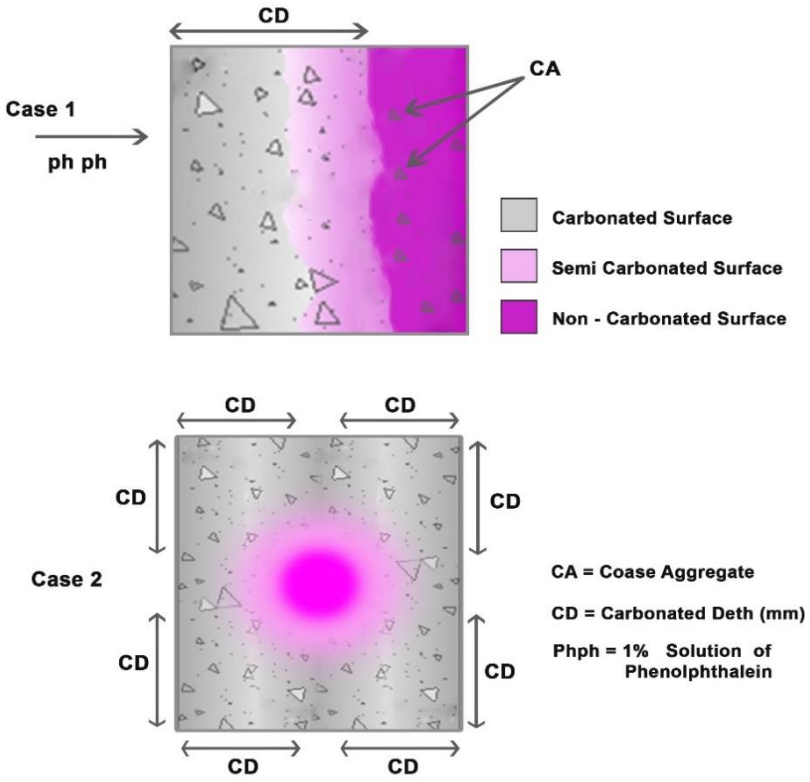

Figure 3-25: Illustration of visual observation of carbonation and non-carbonation zones in a concrete specimen using a 1% solution of phenolphthalein in ethanol as an indicator (modified from source: Possan, 2010; Possan et al.,2017)

To obtain the average carbonation, semi-carbonation and non-carbonation depth percentage of each specimen in this study, the following mathematical Equation 3.20 was used.

$$A_{req(\%)} = \frac{A_{req}}{A_T} \times 100 \qquad \text{Equation 3.20}$$

where: -$A_{req(\%)}$ is the carbonated, non-carbonated or semi-carbonated depth area percentage, in %.

-A_T is the specimen's total surface area, m^2

- A_{req} is the average carbonated, non-carbonated or semi-carbonated depth area calculated from average measured carbonated dimensions (CD) in m^2.

The pH of CFA-based geopolymer concrete in this study was first measured using a pH at its fresh state by collecting a small amount of the paste from the mixer using a plastic tube tested metre, as shown in Figure 3.26. Once the sample was crashed, it was ground into a fine powder mixed with a ratio (mass basis) of 1 to 5 distilled water and then retested.

Figure 3-26: Lethabo low calcium CFA-based geopolymer concrete at fresh state pH measurement in progress.

3.5.3.5 Hardened density variation and dry shrinkage measurements

The variation in density of hardened and dry shrinkage measurement of low calcium CFA-based geopolymer concrete was measured according to a similar method of SANS 6250:2006 (similar to ASTM C948) and ASTM C157 standards for density and shrinkage, respectively, at different curing ages. A calibrated scale was used to record the weight of the cubic specimen at corresponding ageing for mass purposes. Therefore, the final density obtained at maturity age (28 days) will define the classification (category) of the low calcium-based geopolymer concrete optimised mix developed, as shown in Table 3.7. Equation 3.21 illustrate the density calculation at different age over time (age).

Table 3-7: Classification of concrete in accordance with unit weight (Zongjin, 2011:16)

Classification	**Unit Weight,**	**kg/m3**
Ultra-lightweight concrete	<1200	
Lightweight concrete	1200 < UW < 1800	
Normal-weight concrete	~2400	
Heavyweight concrete	>3200	

$$D_s = \frac{m_s}{V_s} \qquad \text{Equation 3.21}$$

where: -D_s is the density of the hardened specimen at given ageing in, Kg/m^3

- m_s is the mass of the specimen at a specific age, in kg

- V_s is the volume of the specimen at a specific mass ageing, in m^3

As for the volume of the specimens at the different masses recorded, the three measurements of each specimen on width (mm), breadth (mm) and depth (mm) were measured using a vernier calliper. These measurements were also used for dry shrinkage variation and illustrated as shown in the following Figure 3.27.

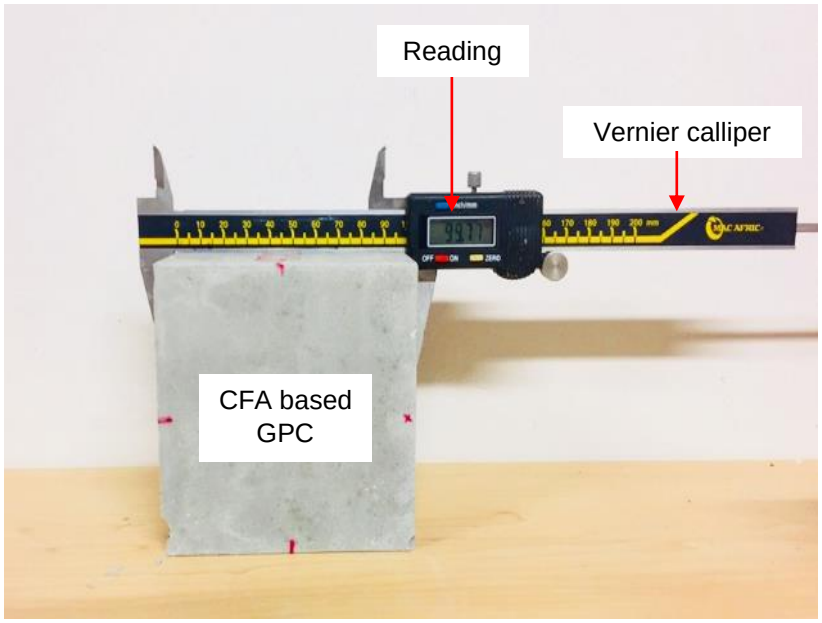

Figure 3-27: Lethabo CFA-based geopolymer concrete oven curing at 60 ° C during hardened density volume and dry shrinkage measurements using a digital vernier calliper method at seven days of ageing.

Equation 3.22 was used to calculate the dry shrinkage of each specimen at a given ageing density. As material deformation occurs on a micro-level, the strain will then be converted to Macrostrain by a factor of 10^{-6}.

$$Dry\ shrinkage\ = \frac{\Delta L}{L} \times 10^{-6} \qquad \text{Equation 3.22}$$

Where: -$Dry\ shrinkage$ of the specimen over time in microstrain

- ΔL is the change in length of the specimen in mm

- L is the original length of the specimen in mm

3.5.3.6 Fire-resistance rating

Lethabo coal fly-based geopolymer concrete was used to examine the devastating effects of the product made out of an optimised mix following the reaction of flame exposure. Here, the objective will be to investigate whether or not the optimised mix developed will pass the minimum of 30 minutes of fire rating requirement for building elements as specified in a relevant standard. SANS 10177-2 (Fire testing of Materials, Components and Elements Used in Buildings) guidelines were followed to conduct the fire-resistance ratio of the optimised mix with steel reinforcement 600 x 600x 65 mm cast and cured at room temperature GPC panel as shown in the following Figure 3.28. The ISO 834 Fire curve was used as a reference standard for time-temperature exposure.

The panel was reinforced with a 6 mm diameter hot rolled high-yield steel (Y6) using a cover of 25 mm centre to centre (25 mm from base to centre and 30 mm from centre to top). During the test, the following criteria illustrated in Table 3.8 failure time will be reported as indicated in SANS 10177-2 to determine the fire rating passing conditions of low calcium-based geopolymer concrete. Thermocouples were bonded on the reinforced steel and the fire unexposed (cold face) surface of the panel and then connected to a thermocouple data logger to record the temperatures of the steel and panel unexposed surface during testing.

Table 3-8: Building materials, fire-resistance rating, criteria failure conditions to be evaluated and reported during the testing time (Source: SANS 10177-2, 1997).

Criteria	**Failure conditions**
Stability	- The system is deemed to have failed if the specimen collapses in such a way that it no longer continues to perform the function for which it was constructed.
	-Deem a horizontal test specimen to fail when the maximum deflection exceeds L/30
	-The system is considered to fail structurally should the primary stud temperature reach 375 ^{o}C for a light-weight steel system
Integrity	The system is deemed to have failed if cracks (6 mm width and 150 mm long), holes, or other openings through which flames or hot gas can pass, or are formed in the test specimen
Insulation	The temperature on the unexposed surface may not exceed 140 ^{o}C plus ambient temperature on average or 180 oC plus ambient maximum at any of the measured surface positions
Additional observation	The chemical toxic effects observed during the test

L is a clear span between supports

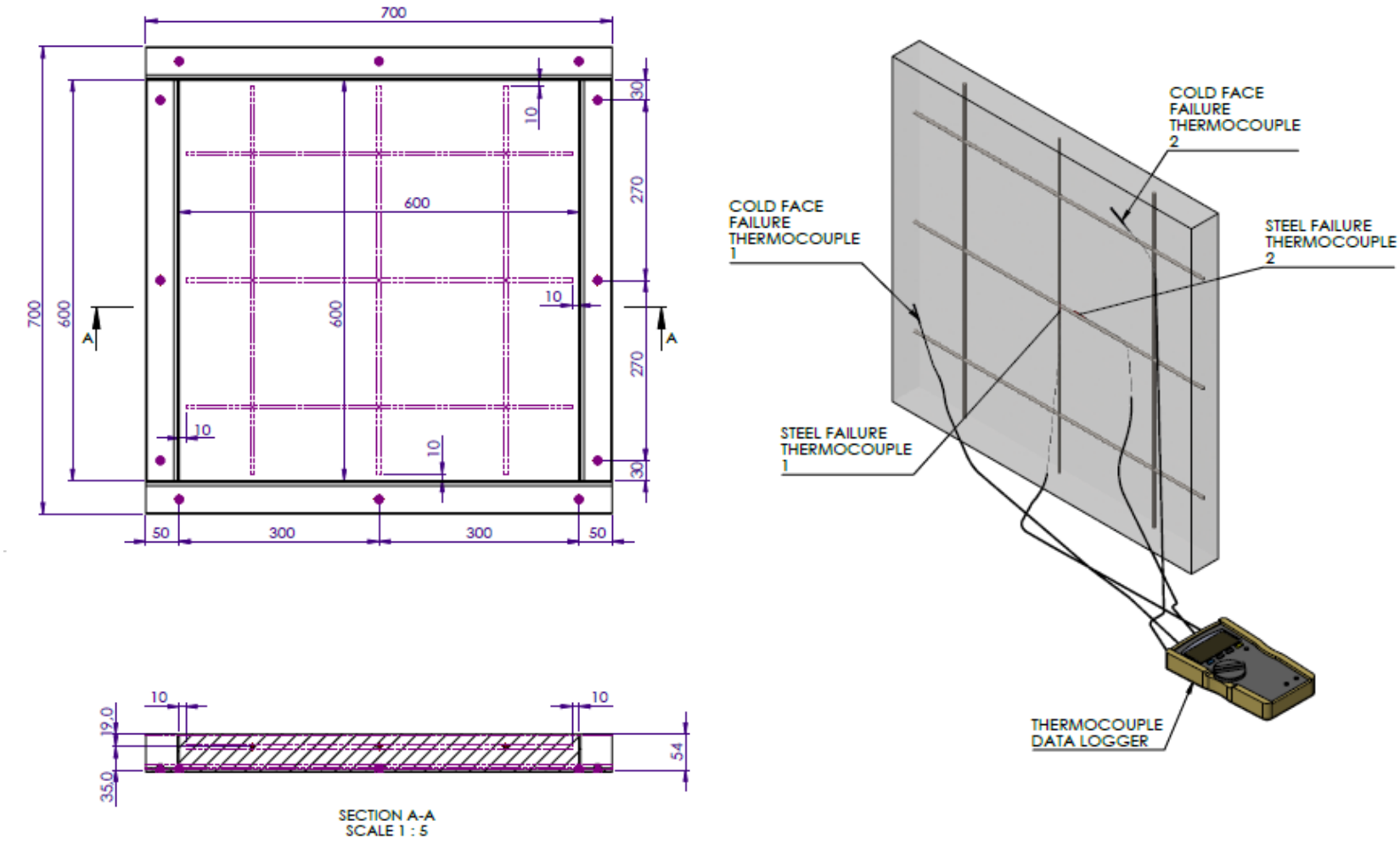

Figure 3-28: Engineering detailing drawing of low calcium CFA-based geopolymer concrete 600 x 600 x 50 mm fire testing panel, including the cast mould dimensions.

Lethabo CFA-based reinforced geopolymer concrete panel for fire test casting steps involves the end product for fire testing, which is shown in Figure 3.29. The 600 x 600 x 60 mm panel consisted of the fourth element of the chemical reaction of the fire triangle, which was composed of gas as fuel, oxygen as an oxidising agent and matches as the heat source. The fire was transferred from gas as a fuel through burners to the fire-exposed surface (hot face) of the panel by radiation, from the panel's hot face to the cold face by convection and from the cold face to the cold face failure thermocouple by conduction. The panel mould, reinforcement steel and finish product are illustrated in Figure A-8

Figure 3-29: Steps involved in casting to the testing of low calcium CFA-based geopolymer reinforced concrete; panel being cast and steel reinforcement after bottom the casting of the bottom cover (a), Panel at the end of casting (b), demoulded panel after three days of ageing (c), grinding and polishing of the panel in progress (d) and NES Consult 600x600x60 designed fire oven used for testing (e) and panel oven installation ready for fire testing (f)

3.6 Environmental impact analysis using life cycle assessment

Life Cycle Assessment (LCA) in this study on the synthesis of CFA-based geopolymer products was developed. It was intended to estimate the potential environmental impacts associated with its manufacturing process depending on the curing temperature and the addition of fine and coarse aggregates as case studies. Guidelines of ISO 14040 (2006) methodology were followed for the LCA analysis.

3.6.1 Life cycle evaluation steps

Four (4) steps: goal and scope of the study, life cycle inventory analysis, cycle impacts assessment and life cycle interpretation were considered to evaluate the processes developed, as shown in Figure 3.30.

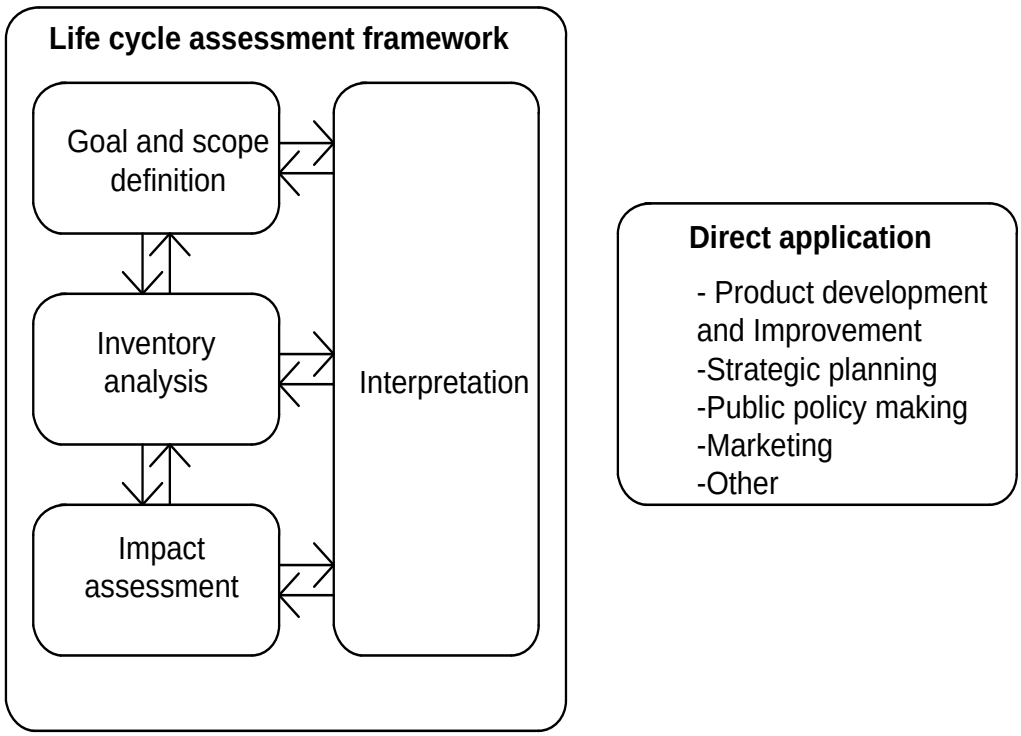

Figure 3-30: Stages of LCA (Source: ISO 14040:2006:8)

3.6.2 Inventory analysis and assessment method

A simulation program called SimaPro was used to conduct calculations. As there was a lack of South African data on the software related to all raw materials utilised, databases such as the Ecoinvent Database (Available at https://ecoinvent.org/, accessed on 8 August 2022) and U.S. Life Cycle Inventory (USLCI) Database (Available at https://www.nrel.gov/lci/, accessed on 8

August 2022) available in the software were used for simulation as applied in study of Salas et al (2018). The Environmental Product Declaration (EPD) method was applied to report the impact of each process,

3.6.3 Life cycle impacts assessment

The following environmental impact categories listed in Table 3.10 were considered from the SimaPro simulation. Table B-8 illustrates the equivalency of CO_2 to other greenhouse gases and their emissions sources. To calculate the amount of greenhouse emissions emitted by each product for a certain amount of product produced, Equation C.1 can be used.

Table 3-9: Environmental impact categories and their measurement units considered from SimaPro software simulations using EPD (2018) V1.02 / Character for a production of 1 kg from the synthesis of Lethabo low calcium CFA based geopolymer paste cured and oven vs room temperatures and geopolymer concrete cured at room temperature (Source: PRé, 2021).

Impact category	Indicator	Indicator Abbreviation	Unit	Reference
Climate change	Global warming potential over 100 years	GWP100a	kg CO_2 eq	A measure comparing the intensity of greenhouse gases' effect to that of CO_2. Some greenhouse gases have a stronger warming potential than others. The consequence of this is a Temperature increase on earth
Acidification	Acidification potential	AP	kg SO_2 eq	Measured the impact of the activity of the soil, groundwater, surface water, organisms, ecosystems and materials (buildings). Soil and water lose their neutral pH after altering their chemical composition. Polluting gases in the atmosphere cause acid rain to precipitate due to pollution. As a reference substance, SO2 is used to measure the severity of acidification.
Eutrophication or Nitrification	Nitrification potential	NP	kg PO_4 eq	Expression of the degree to which the emitted nutrients reach the freshwater end compartment (phosphorus is considered a limiting factor in freshwater).
Photochemical oxidation	Photochemical Ozone Creation Potential	POCP	kg NMVOC	Measured the impacts due to the formation product from reactive substances contribution to photochemical ozone formation (summer smog), which are injurious to human health and ecosystems and damage crops.

Impact category	Indicator	Indicator Abbreviation	Unit	Reference
Resource use, mineral and metals/ Abiotic depletion, elements	Abiotic depletion, element	ADP	kg Sb eq	Measured the impact of inputs in a system on mineral extraction. Each extraction of minerals is assessed by its Abiotic Depletion Factor (ADF)
Resource use, energy carriers /Abiotic depletion, fossil fuel	Abiotic depletion, fossil fuel	ADP	MJ	Measure the impact of fossil fuel extraction due to inputs into the system. For each fossil fuel extraction, the ADF is determined.
Water scarcity	Water Scarcity Footprint	WSF	m^3 eq	Assesses the effects of water deprivation on humans, ecosystems, and buildings. It is assumed that the less water available per area, the greater the likelihood that another user will be deprived.
Ozone layer depletion	Ozone depletion potential	TOP	kg.CFC-11	Measured the destructive effects (emissions) of different gases on the stratospheric ozone layer over an infinite time span as a result of a larger fraction of UV-B radiation on the earth's surface. Results in Increases in stratospheric ozone breakdown

NMVOC= non-methane volatile organic compounds
SO_2 = sulphur dioxide
m^3 eq= m^3 water eq. deprived
CFC-11=
PO_4 = Phosphate
Sb= Surplus energy per kg mineral or ore
MJ= Mega Joules
CFC-11= Chlorofluorocarbons; hydrocarbons containing combined bromine, fluorine and chlorine.

3.7 Material and energy balances and economic analysis

A brief description of the methods used for performing CFA-based geopolymer concrete mass and energy balances and its economic analysis in this study will be provided in this Section. All mixes and curing regimes may not be completely defined in the calculation. As shown in Table 3.6, the best-optimised mix with acceptable engineering characteristics' target values will be considered and discussed.

3.7.1 Material and energy balances

Material and energy balances in this study will be performed based on chemical engineering calculation rules of converting raw material into a specific product, looking at unit operations and energy utilised in the process. In this study, the CFA-based geopolymer products were synthesised in a batch process, and sodium hydroxide solution preparation was considered a semi-batch system.

3.7.1.1 Material balance

Material balance in this study simply applied Lavoisier's law of conservation of matter, which, according to the chemical principle, mass cannot be created or destroyed. Material balance was crucially considered as a first step in the design of this process. This was based on Felder's (1986) statement that material balances are always essential to solving process engineering problems. The molecular species balance method was used to determine the input and output chemical elementary composition of the feed and product according to Figure 3.31

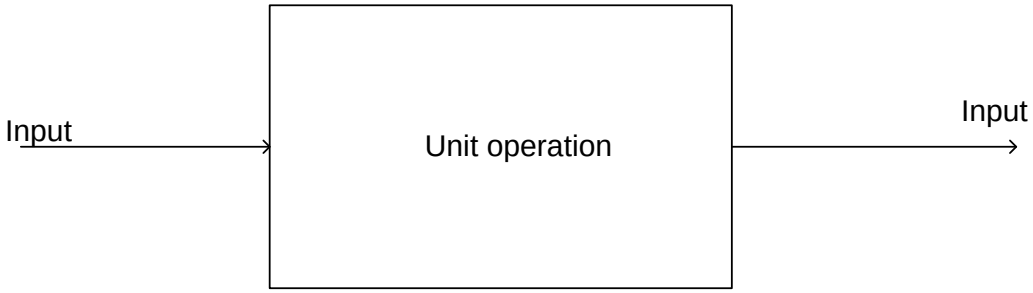

Figure 3-31: Illustration diagram for material balance.

Before conducting material balance calculations, the degree of freedom (DOF) for the molecular species method was performed according to Equation 3.23.

$$DOF = \begin{pmatrix} Number \\ of \\ unknown \\ variables \end{pmatrix} + \begin{pmatrix} Number \\ of \\ Chemical \\ reactions \end{pmatrix} - \begin{pmatrix} Number\ of \\ independent \\ molecular \\ species \end{pmatrix} - \begin{pmatrix} Number \\ of \\ other \\ equations \end{pmatrix}$$ Equation 3.23

i. Alkaline activator solution preparation and synthesis process

For these processes, the general material balance Equation 3.24 was taken into consideration

$$Accumulation = Input - Output + Generation - Consumption$$ Equation 3.24

where: -$Accumulation -$ material staying back in the system, considered as zero due to steady state assumption.

- $Input -$ material entering the system

- $Output -$ material leaving the system

- $Generation -$ a new material that is formed in the system

- $Consumption -$ material that is consumed in the system

ii. Drying of solids

In this study, a material balance around the drying process was performed, using the following Equations to remove water and other solvents by evaporation to obtain a bone-dry CFA-based geopolymer product.

a. Moisture loss

The moisture loss at any time X_t is calculated as shown in Equation 3.25

$$X = \frac{m_{wet} - m_{dry}}{m_{wet}} \times 100$$ Equation 3.25

where: - X is moisture loss in percentage (%)

- m_{dry} and m_{wet} are the moisture of dry and wet CFA-based geopolymers.

b. Amount of evaporated ($\dot{m}_{ev}$ in kg water per second) water for $t_d = 24$-hour curing is a function of the initial and final moisture of the specimen per curing time according to Equation 3.26

$$\dot{m}_{ev} = \frac{Mass\ loss}{t_d}$$ Equation 3.26

The mass air flow rate for oven curing for 24 hours was determined according to Equation 3.27.

$$\dot{m}_{air} = \frac{m_s}{t_d} \times \frac{(X_1 - X_2)}{(X_i - X_f)} \quad \text{Equation 3.27}$$

where: - $X_2 - X_1$ are the inlet and outlet humidity of the air, in%

-$X_i - X_f$ are the inlet and outlet moisture of the geopolymer, in%

- t_d is the oven drying time in seconds.

The rate of drying of the specimen from oven curing, room with plastic covered and room with open air were calculated using Equation 3.28 and compared for the first 24 hours of curing.

$$R = -\frac{\dot{m}_s}{A}\frac{dX}{dt} \quad \text{Equation 3.28}$$

Where: - R is the rate of drying the specimen over time in kg. $s^{-1}.m^{-2}$

- $\dot{m}_s$ is the rate of evaporation, will be taken as the dry mass of the specimen at a specific time, in kg.
- A is the drying area in m^2
- dX is a variation from initial to final free-moisture, in %
- dt is a variation from the initial to final time, in second.

3.7.1.2 Yield and product yield percentage

It is important to determine the yield (in general, the volume of concrete produced per batch) of each CFA-based geopolymer type, such as paste, mortar and concrete, and the product yield percentage (amount of product produced from the raw material used). The yield also helps to determine the number to be produced from each batch mix, while the yield percentage is useful when determining the desired product percentage from which the rest can be considered as waste on a 100% scale as this will also have an impact on the environment and economic analysis of the project. For construction materials, the yield is preferable on a volumetric basis as the cost of the product is often estimated in squared or cubic meters. The yield was determined according to ASTM C138/C138M and the calculation according to Equation 3.29. The product yield percentage is calculated according to Equation 3.30.

$$Y = \frac{M_{feedstock}}{D} \quad \text{Equation 3.29}$$

$$Y_p = \frac{M_{product}}{M_{feedstock}} \times 100 \quad \text{Equation 3.30}$$

where: - Y is the yield in m^{-3}

- $M_{feedstock}$ is the total mass of materials batched, kg
- D is the density of fresh CFA-based geopolymer in kg/m^3
- $M_{product}$ is the total mass of materials batched, kg
- Y_p is the yield percentage, in %

3.7.1.3 Energy balance

Like material balance, the energy balance was simply the application of the first law of thermodynamics, which states that energy cannot be created nor destroyed but only transformed. From one form to another (the amount of energy gained by a system must be exactly equal to the amount of energy lost by its surroundings). As there were no mass flows in or out in all processes, the fundamental energy balance Equation 3.33 below derived from Equation 3.31 to Equation 3.32 was applied. Compared to material balance, generation and consumption terms in the energy balance equation were not considered (only input, output and accumulation). This is fully illustrated in the Appendix Section from Equation C.2 to Equation C.7

$$\begin{pmatrix} Final\ system \\ energy \end{pmatrix} - \begin{pmatrix} Initial\ system \\ energy \end{pmatrix} = \begin{pmatrix} net\ energy\ transferred \\ to\ the\ system \end{pmatrix} \quad \text{Equation 3.31}$$

$$\left(U_f + E_{kf} + E_{pf}\right) - \left(U_i + E_{ki} + E_{pi}\right) = Q - W \quad \text{Equation 3.32}$$

$$\Delta U + \Delta E_k + \Delta E_P = Q - W \quad \text{Equation 3.33}$$

where: - ΔU is the change in internal energy in Joule (J)

- ΔE_k is the change in kinetic energy, in J
- ΔE_P is the change in potential energy, in J
- $Q\ and\ W$ is the energy transferred in the form of heat and work, respectively, in J

The unit operations used for material balance were also investigated for energy balances

i. Sodium hydroxide reaction process

Adding sodium hydroxide pellets gradually in the volumetric flask, the assumption is that this is an open system. Here, the heat of the solution (change in enthalpy) was considered

in the energy balance to account for the energy change because of the formation of sodium hydroxide solution. Equations 3.34 and 3.35 were used to determine the heat of solution and heat required to produce one sodium hydroxide using specific centration or mass, as shown in Table 3.4.

$$q_{sol} = \left(m_w + m_{NaOH(s)}\right) \times C_w \times \Delta T \qquad \text{Equation 3.34}$$

$$\Delta H^o{}_{sol} = \frac{q_{sol}}{number\ of\ mole} \qquad \text{Equation 3.35}$$

where: - q_{sol} is the heat of the solution at sodium hydroxide molar mass of 40 g/mole

- m_w and $m_{NaOH(s)}$ are the masses of water and sodium hydroxide pellet at 98% purity, Kg
- ΔT is the change in temperature, Kelvin (K)
- C_w is the specific heat capacity of water given taken as 4184 $J{\cdot}kg^{-1}.K^{-1}$
- $\Delta H^o{}_{sol}$ is the heat required to produce one mole of sodium hydroxide at a specific mass or concentration taken.

ii. Synthesis process

In this process, energy consumption was calculated with a focus on the power consumption of the impeller (mechanical power). Using an Anchor impeller, as shown in Figure 3.7, the following were considered.

- Measurements of the tank and impeller are shown in the following Figure 3.32

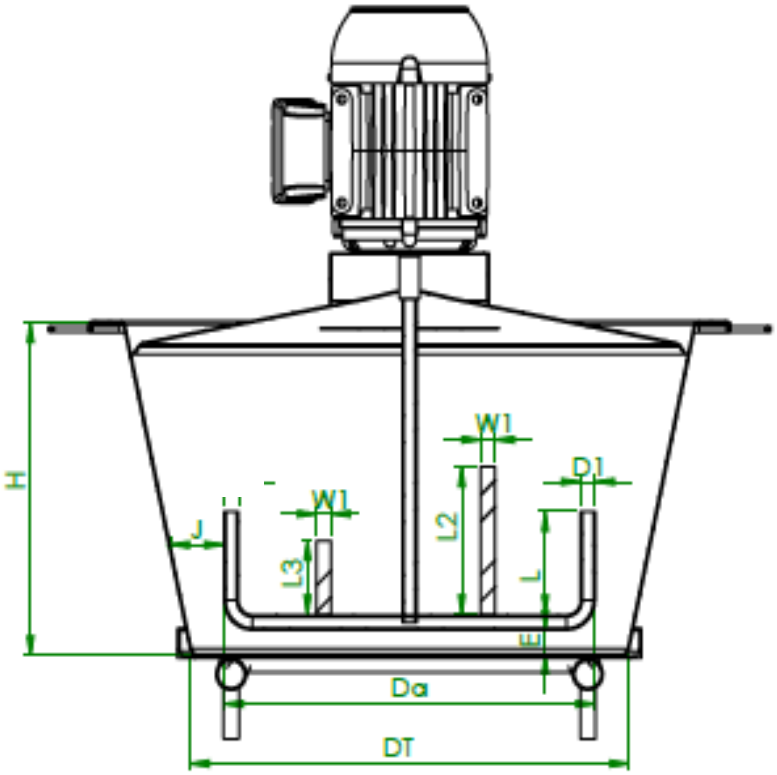

Figure 3-32: Technical drawing of the synthesis mixer dimensions; DT: diameter, H: height of the tank, Da: diameter of impeller, E: distance from the base to the impeller, J: width from tank to impeller, L1 to L3: length of impellers, D1: diameter of the impeller and W1: width of the impeller.

- Fluid properties: density and viscosity
- Speed of the impeller
- Gravitational acceleration.
- The blending time (mixing time)

The following dimensionless numbers were calculated using Equations 3.36, 3.37 and 3.38 for the Reynold number (N_{Re}), Power number (N_p) and Froude number(N_{Fr}) respectively. The Reynold was first calculated from which the power number was obtained using power characteristics of close clearance agitators' curve for anchor agitator (anchor impeller) from Figure A-4.

$$N_{Re} = \frac{\rho N {D_a}^2}{\mu} \qquad \text{Equation 3.36}$$

$$N_p = \frac{P}{{D_a}^5 N^3 \rho} \qquad \text{Equation 3.37}$$

$$N_{Fr} = \frac{N^2 D_a}{g}$$ Equation 3.38

where: - P is the mechanical power input to the mixer, in Watt (W)

- N is the speed of the rotation of the mixer, in rps (rps/60=s^{-1})
- D_a is the impeller diameter, in m
- ρ is the fluid density, in $kg.m^{-3}$
- μ is the viscosity of the fluid, Pascal second (Pa. s)
- g is the gravitational acceleration, in $m.s^{-2}$

Power (in kW) deduced from the power number in Equation 3.36 was multiplied by the blending time (in seconds) to obtain the energy consumption of the mixing process (Q) in kJ, as shown in Equation 3.39.

$$Q = P \times t_{blend}$$ Equation 3.39

iii. Drying process

Energy balance for the drying of CFA-based geopolymer product was highly investigated from the oven curing process with minimum consideration on the room curing process as the curing was through natural radiation; therefore, no energy was required. The mechanical energy input power of the air inlet fan of 1 kW (can be negligible) and heat loss were taken into account to perform the energy balance using the EcoTherm curing oven. In addition, the following were also considered:

- The curing set temperature used to cure the specimen
- The curing time the specimen spent in the oven
- The dimensions of the oven
- The heat insulation properties of the curing oven.

Equation 3.40 determines the heat transfer to geopolymer solids in watts based on the parameters considered.

$$\dot{q}_d = \dot{m}_{air} C_{P_{air}} (T_f - T_i)$$ Equation 3.40

where: - $\dot{m}_{air}$ air the mass flowrates air respectively, in kg/s

- T_f and T_i are the final and initial temperatures of the air, in K
- $\dot{m}_{air}$ is the mass flow rate of air, in kg. s^{-1}
- $C_{P_{air}}$ is the specific heat capacity of air taken as 1000 $J.kg^{-1}.K$

The energy required to evaporate water from geopolymer product from initial to final moisture was calculated according to Equation 3.41.

$$Q_{ep,water} = \dot{q}_d \times t_d \qquad \text{Equation 3.41}$$

The heat loss percentage was determined using Equation 3.42, considering the amount of heat loss from Equation 3.43 based on oven properties.

$$Q_{Loss} = (U\Delta T_m) \times A_{ev} \times t_d$$

$$Q_{Loss} = \left(\frac{T_{inside} - T_{outside}}{{}^{1}/_{h_1} + {}^{L}/_{k_1} + {}^{1}/_{h_2}}\right) \times A_{ev} \times t_d \qquad \text{Equation 3.42}$$

$$Q_{LR} = \frac{Q_{loss}}{Q_{ep,water}} \qquad \text{Equation 3.43}$$

where:
- $h_1 and\ h_2$ is the convection transfer coefficient of the materials in and out of the oven, in W.m^{-2}. K
- k is the insulated materials' thermal conductivity, in W.m^{-1}.K^{-1}
- A_{av} is the oven's average drying area, in m^2
- L is the thickness of the oven, in m
- t_d is the oven drying time, in s
- U is the overall heat transfer coefficient, in W.m^{-1}. K^{-1}
- Q_{loss} is the energy loss during the 24 hr of curing, in J
- Q_{LR} is the energy loss ratio, no unit

3.7.2 Economic analysis

An analysis of engineering economics of the process of synthesis geopolymer using a South African low calcium CFA obtained from Lethabo Power Station is provided in this Section. This economic analysis is intended only to be performed on the optimised mix with better target characteristic values than other formulations developed to easily launch the product cast with this formulation into the construction industry. The effect of fine and coarse aggregates will be evaluated, as well as the effect of curing regimes.

3.7.2.1 Large-scale raw materials

Under this Section, a yearly production capacity will be assumed for a batch process at certain annual operating hours with the operators working hours regulations set. The cost associated with raw materials will be reviewed per batch. This also required a scale-up of the equipment, including their cost estimation.

3.7.2.2 Equipment scaling-up, costing and power cost

Compared to the lab scale equipment used, the large-scale process for economic analysis will require a scale-up of certain equipment used. In most cases, the main equipment, the synthesis mixer, must be redesigned for the following points that need to be considered.

i. Geometric similarity

Here, all the tensions of ratios, for instance, impeller diameter to the tank diameter or impeller diameter to the tank height, must be conserved at a large scale. The large-scale mixer dimensions will then be obtained by multiplying the lab scale dimensions shown in Figure 3.32 by the scale-up ratio obtained from Equation 3.44

$$R = \left(\frac{V_{large}}{V_{lab}}\right)^{\frac{1}{3}} \quad \text{Equation 3.44}$$

where: - R is the scale-up ratio, no unit.

- V_{large} is the large-scale volume capacity, m^3
- V_{lab} is the volume of the mixer at a small scale, m^3

ii. Kinematic similarity

Mixing speed must be scaled up based on the laboratory scale used depending on Equation 3.45 and requirements in Table 7.1 of the Appendix.

$$\frac{N_{larg}}{N_{lab}} = \left(\frac{1}{R}\right)^{n} \quad \text{Equation 3.45}$$

where: - N_{larg} is the rotational speed at large scale, rpm

- N_{lab} is the lab rational speed used, given as 55 rpm.

iii. Dynamic similarity

This will be assumed to be maintained once Sections i and ii are correctly calculated, as this depends on the viscosity and gravitational force. This requires a physical experimental set-up of large-scale production.

Based on the above criteria, the power consumption of the mixer at a large scale will be obtained from its ratio to scale small, as shown in Equation 3.46

$$\frac{P_{larg}}{P_{lab}} = \frac{kD_{a_{larg}}{}^{5}N_{large}{}^{3}}{kD_{a_{lab}}{}^{5}N_{lab}{}^{3}} \quad \text{Equation 3.46}$$

where: - $D_{a_{larg}}$ and $D_{a_{lab}}$ are the diameter of the impellers at large and laboratory scales, respectively.

In comparison with the oven process, the energy consumption at a large scale will be defined from the ratio of the oven to synthesis process at a laboratory scale calculated according to the following Equation 3.47

$$P_{ratio} = \frac{\dot{q}_d}{P} \qquad \text{Equation 3.47}$$

where: - $\dot{q}_d$ and P are the powers consumed from the oven curing and synthesis process, respectively, in W.

3.7.2.3 Investment cost estimation

Manufacturing decisions are often influenced by product costs. According to Sinnott (2005:266), Table 3.10 shows components of the operating costs used to approximate and estimate production costs.

Table 3-10: Components used for the summarisation of production cost (Sinnott, 2005:267 and Silla, 2003).

Variable costs	
1. Raw materials	Amount of Incoming stream x cost
2. Miscellaneous materials	10% of the maintenance cost of the item (5)
3. Utilities	
Electricity	Power consumed x cost
Fuel	Power consumed x cost
Steam	Steam consumed x cost
Water	Water consumed x cost
Refrigeration	The heat removed x cost
4. Shipping and packaging	Usually, negligible
Sub-total A	.....
Fixed costs	
5. Maintenance	5-10 per cent of fixed capital from manning estimates
6. Operating labour	
7. Quality control laboratory cost	20-23 per cent of the item (6)
8. Operating supervision cost	20 per cent of the item (6)
9. Plant overhead cost	50 per cent of the item (6)
10. Capital charges	10 per cent of the item of the fixed capital
11. Insurance	1 per cent of the item of the fixed capital
12. Local taxes	2 per cent of the item of the fixed capital
13. Royalties	1 per cent of the item of the fixed capital

	Sub-total B	……..
Direct production costs	A+B	
14. Sales expense		20-30 per cent of the direct production cost
15. General overheads		
16. Research and development		
	Sub-total C	……
Annual production cost = A + B + C		

$$\boldsymbol{Production\ cost\ R/Kg} = \frac{\boldsymbol{Annual\ production\ cost}}{\boldsymbol{Annual\ production\ rate}}$$

Sales and expenses (0.045% for administration, 0.1535 for Marketing, 0.0575 research and development)

3.7.2.4 Element of investment cash flow

The most significant engineering economics criteria to be evaluated in this study to facilitate large-scale manufacturing decision-making and their main advantage are shown in Table 3.11 and will be calculated using the following Equations listed. The currency used in the calculation will be the South African Rand currency, abbreviated as R.

Table 3-11: Project investment parameters to be analysed.

Project criteria	Abbreviation	Unit	Description (main advantage)	Equation number	Reference
Production cost	COP	R/kg or m3	Defines the total cost incurred to produce 1 Kg of a product or 1 m3 in the case of concrete	Table 3.10	Sinnott, 2005
Bare module cost	CBM	R	Described the sum of costs associated with capital cost plus installation, shipping, insurance, taxes, engineering and some overhead expenses.	3.48	Turton et al., 2008
Total module cost or fixed capital investment	CBM	R	Some of the bare module costs plus unforeseen costs and contractor fees or price changes	3.49	Turton et al., 2008
Manufacturing cost or investment	-	R	Shows financial resources needed.	3.50	Turton et al., 2008
Profit	P	R	Measures the performance of capital.	3.51	Sinnott, 2005
Present Value or Net present value	PV or NPV	R	It will be used to analyse the profitability of this project investment. It should not be less than zero	3.52	Park, 2020
Net Future Value	NFV	R	Used to measure the value of current investment cost at a future time of the project life based on a specific growth rate.	3.53	Park, 2020

Project criteria	Abbreviation	Unit	Description (main advantage)	Equation number	Reference
Payback period	PP	years	Shows how soon investment will be recovered	3.54	Sinnott, 2005
Internal rate of return	IRR	%	It is used to estimate investment profitability. Found when NPV=0	3.55	Park, 2020
Profitability index	PI		Decision-making criteria. A ratio determining how much can be earned from every currency unit spent. Should not be less than zero.	3.56	Park, 2020
Break-even point	BEP	No unit	It is essentially the capacity of the project and under consideration at which all costs are equal to the revenue earned	3.57	Park, 2020
Break-even volume or Break-even capacity	-	m^3 or kg	Shows the number of sales needed to cover overall fixed costs. Should not be higher than the assumed or proposed capacity	3.58	Park, 2020

$$C_{BM} = Capital\ cost + \quad \text{Equation 3.48}$$

$$C_{BM} = 1.18C_{TM} \quad \text{Equation 3.49}$$

$$Investment = 0.18 \times Capital\ cost + 2.73 \times Labour\ cost + 1.23 \times (Utility + waste + Raw\ material) \quad \text{Equation 3.50}$$

$$PV = \frac{P_1}{(1+i)} + \frac{P_3}{(1+i)^2} + \frac{P_3}{(1+i)^3} + \cdots \frac{P_n}{(1+i)^n} \quad \text{Equation 3.52}$$

where: - In will be considered as yearly salaries

- n is the rate of return

$$Net\ Profit = Income - Expenses - Taxes - Investment \quad \text{Equation 3.44}$$

where: - $Income$ will be considered as yearly salaries

- $Expenses$ will be taken as utility

$$NFV = NPV\ (1+i)^n \quad \text{Equation 3.53}$$

where: - P is the profit

- $Expenses$ will be taken as utility

$$Payback\ period = \frac{100}{ROR} \quad \text{Equation 3.53}$$

where: - ROR is the Rate of return in %

$$NPV = 0 = \frac{P_1}{(1+i)} + \frac{P_3}{(1+i)^2} + \frac{P_3}{(1+i)^3} + \cdots \frac{P_n}{(1+i)^n} \quad \text{Equation 3.50}$$

$$PI = \frac{Present\ value\ of\ all\ future\ cash\ inflows}{Initial\ cash\ outflow} \quad \text{Equation 3.55}$$

$$BEF = \frac{Fixed\ expenses}{Unit\ contribution\ margin} \quad \text{Equation 3.51}$$

3.7.2.5 Sensitivity analysis

The sensitivity analysis will be performed as a quantitative risk analysis to economically assess the impact associated with the project's net present value due to inflexion in the cost of raw material used. Changes in the cost of input materials such as CFA, sodium hydroxide pellet, sodium silicate, water and fine and coarse aggregates may negatively or positively affect the cost of output CFA-based GPP, GPM or GPC. CFA used in this project at free cost will be highly considered for the sensitivity analysis at the lower and upper percentage of ± 50% of the based cost of taking.

Chapter 4

Development of geopolymer for construction application using coal fly ash: optimisation and characterisation

CFA-based geopolymer paste, mortar and concrete formulations were optimised and characterised to meet diverse construction application requirements. It was unnecessary to test all mixes designed for all tests. The best formulations of synthesised geopolymer paste, mortar, and concrete based on compression strength were explored further for other properties. These formulations were designed based on the optimised setting time formulation.

4.1 Raw materials and product characterisation

Raw materials and products were characterised to understand the properties that influenced the formulation mix design for specific raw materials and their impact on the final product. The investigated parameters were CFA particle size, volume and cumulative percentage, properties of coarse fine aggregates, SEM and energy-dispersive X-ray spectroscopy (EDS), ray diffraction, XRF and Inductive couple-plasma, FTIR radon exhalation and emanation.

4.1.1 CFA particle size volume and cumulative percentage.

CFA particle size and volume were performed to define its maximum and minimum sizes and the percentage of dominant particles. The technique was performed as described in Section 3.4.1. CFA particle size cumulative and volume distributions of CFA were analysed and shown in the following Figure 4.1

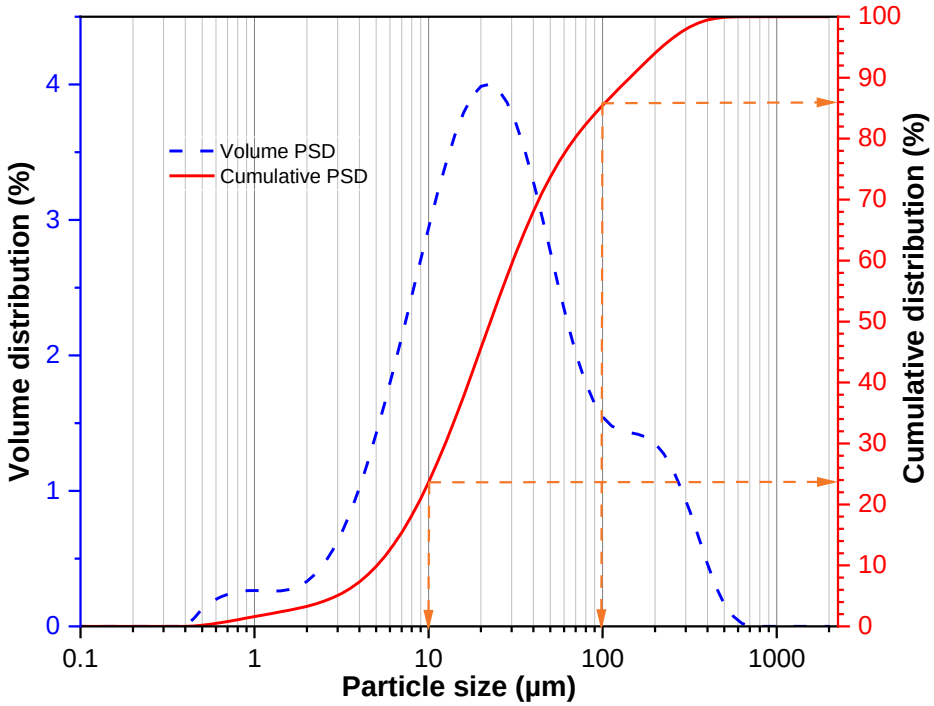

Figure 4-1: CFA -particle size cumulative and volume distribution.

From the results obtained, CFA was found to be fine particles, with about 24% of CFA found to be less than 10 micrometres and about 86% less than 100 µm.

4.1.2 Properties of coarse fine aggregates

Fine and coarse aggregates' particle size sieve analysis was performed to define their maximum and minimum sizes. The cumulative percentage of fine and coarse aggregates was analysed using the sieves by calculation with Equation 3.1 (Tables 7.5 and 7.6). The results obtained are shown in the following Figure 4.2

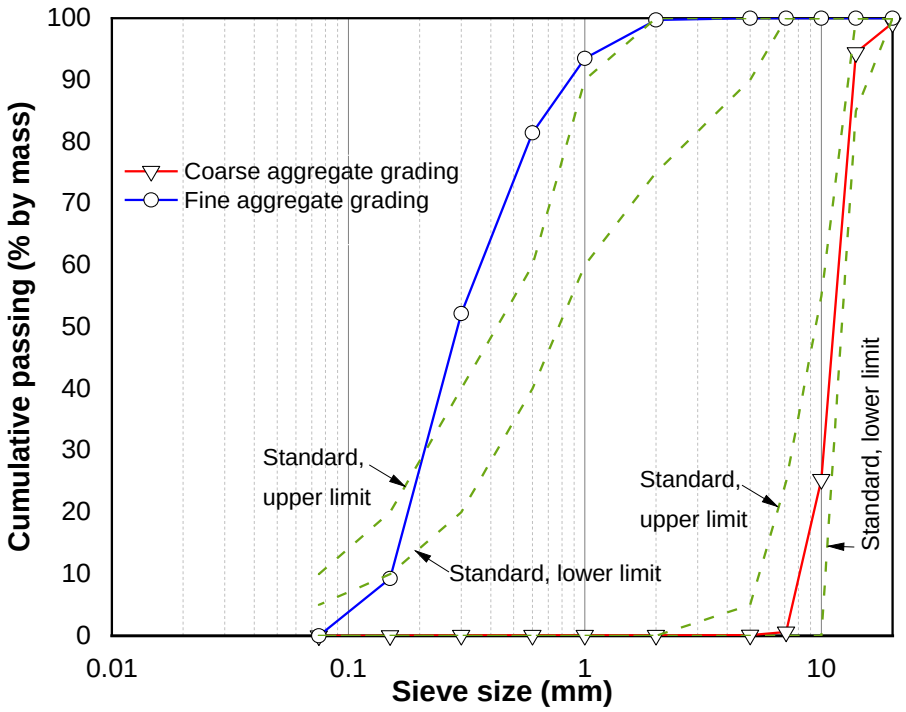

Figure 4-2: Particle size distribution of fine and coarse aggregates used for the synthesis of CFA-based geopolymer concrete and grading enveloped.

The coarse aggregate's cumulative passing percentage fitted the standards upper and lower limits of grading enveloped for the aggregates with a max size of 13 mm, while that of fine aggregates was out of the expected range, as shown in Figure 4.2. Determining the particle size is an important aspect as many studies have confirmed the impact of particle coarseness on concrete strength decreasing (Haque et al., 2012; Siregar et al.,2017; Wang et al., 2022). This may also affect the durability of concrete due to high porosity, as big-sized particles tend to create more voids than smaller particles. To determine the particle size range, the finesse modulus of both fine and coarse aggregates was determined according to SANS 3001 standards. The results are shown in Table 4.1.

Table 4-1: Fineness modulus of fine and coarse aggregates used as an additive in the synthesis of CFA-based geopolymer concrete.

Aggregates types	Fineness modulus	Standard Range
Fine aggregates	1.64	2.2-3.2
Coarse aggregates	6.00	3.5-8.0

Both fine and coarse aggregate fineness modulus obtained met the SANS 3001 standard requirement. The unacceptable fineness modulus had a significant effect on the formulation mix

as the presence of bigger particles in fine aggregate decreased the workability and smaller particles and promoted segregation. This can also lead to a lack of mix cohesion, affecting the compressive strength and durability properties. The fine modulus (FM) of 1.64 shows that most of the particles are in the 0.15 -0.20 mm sieve size range, which, according to the Wentworth grain-size scale for siliciclastic sediment (Figure A-7 in Appendix), is described as a mix of very fine and fine sand as the FM for fine particles ranges from 2.2. Depending on the formulation, the compression strength can change due to aggregate size change (Yu et al.,2019). Table B-4 and Table B-5 (Appendix) present the sieve analysis and particle size of both coarse and fine aggregates, respectively.

4.1.3 Scanning electron microscope and energy-dispersive X-ray spectroscopy

Scanning electron microscope (SEM) and energy-dispersive X-ray spectroscopy (EDS) were used to determine the morphology and the presence of chemical elements in CFA and synthesised CFA-based geopolymer formulations. This was conducted as described in Section 3.4.2. Figure 4.3 represents the SEM and EDS of CFA, CFA -GPP (GPP-M2A), CFA -GPM (GPM-M2A) and CFA -GPC (GPC-M2A) cured at room temperature as well as oven temperature.

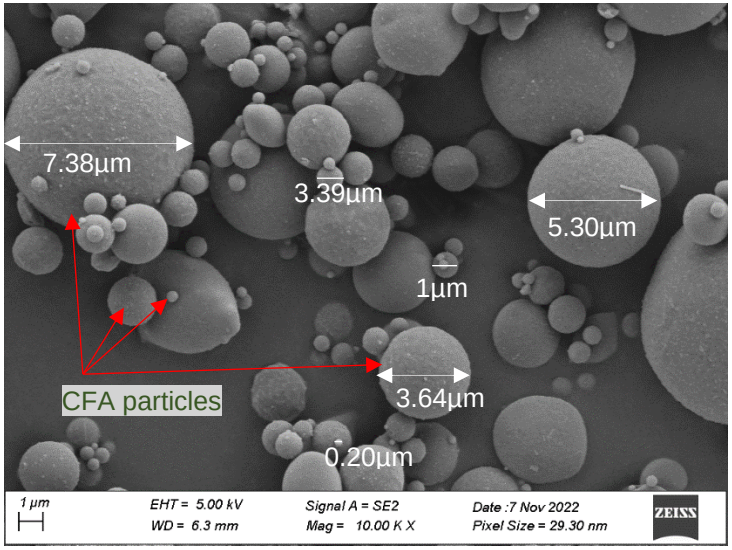

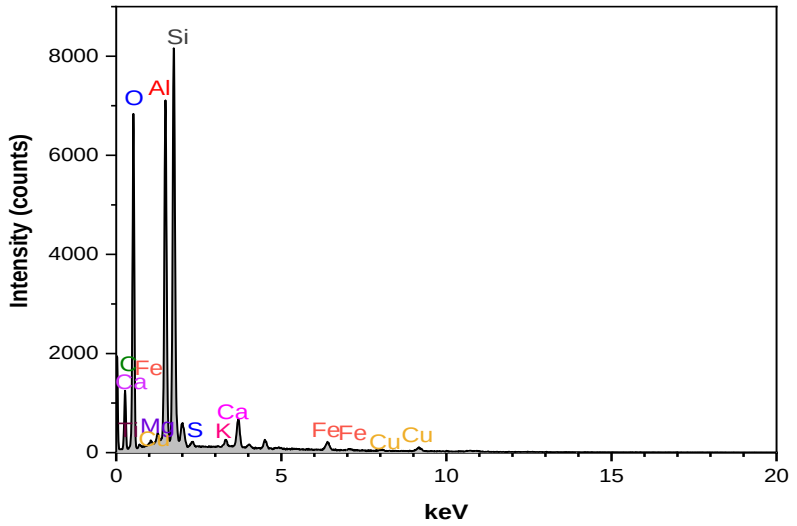

Coal fly ash (a)

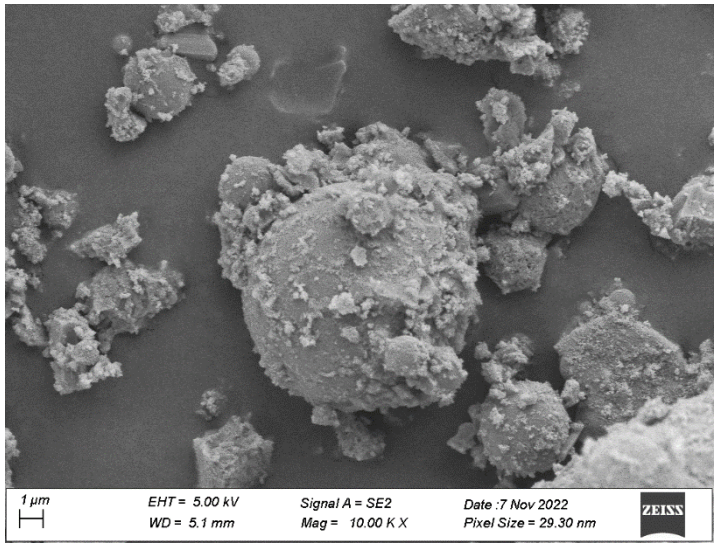

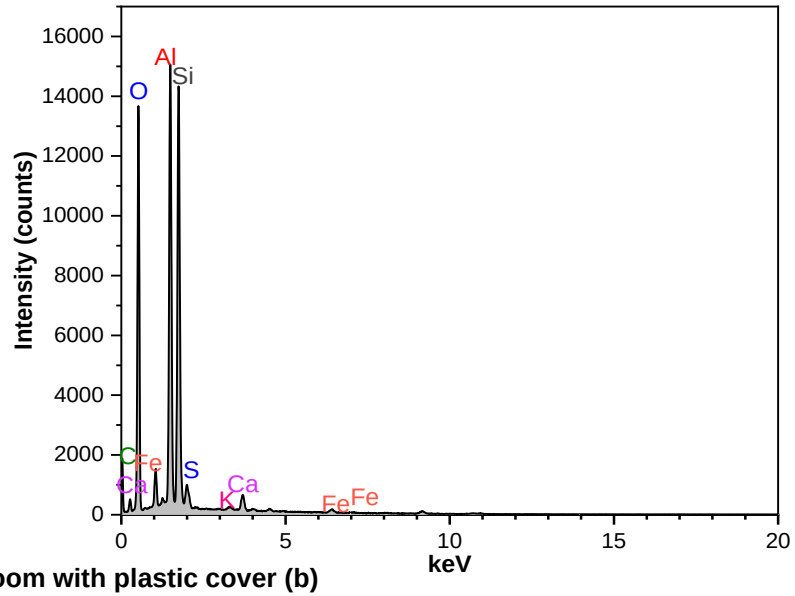

GPP-M2A, room with plastic cover (b)

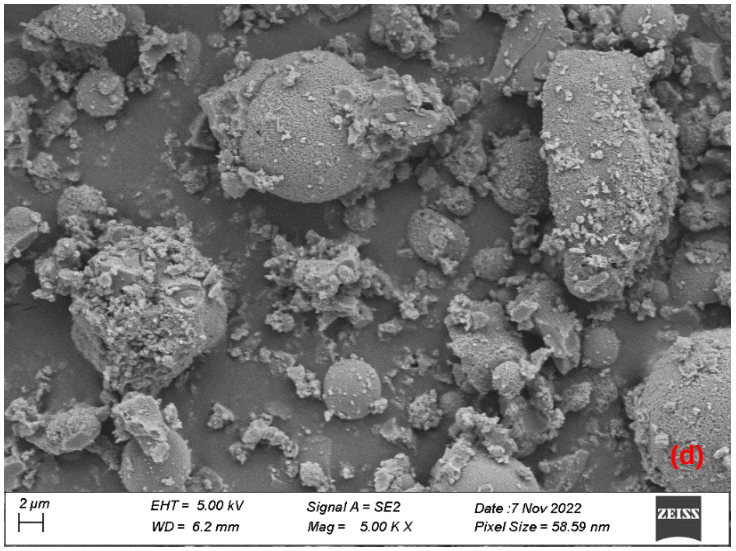

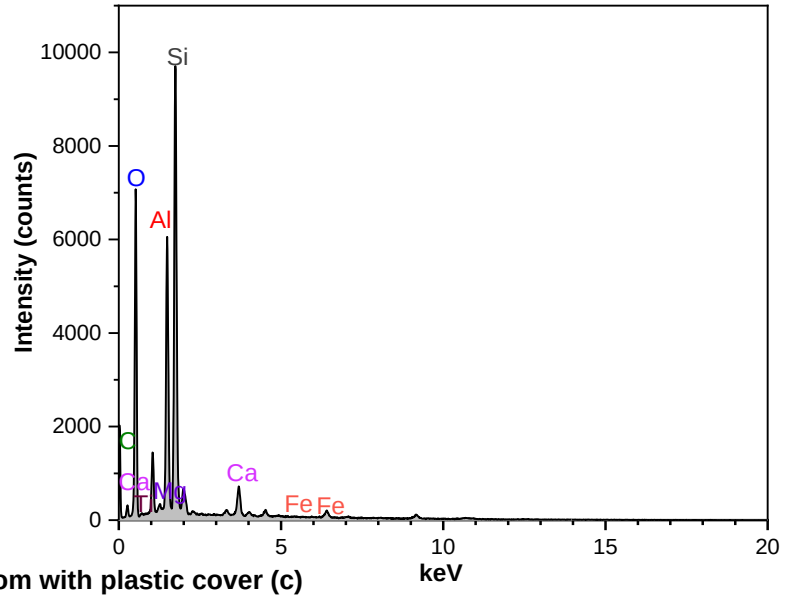

GPM-M2A, room with plastic cover (c)

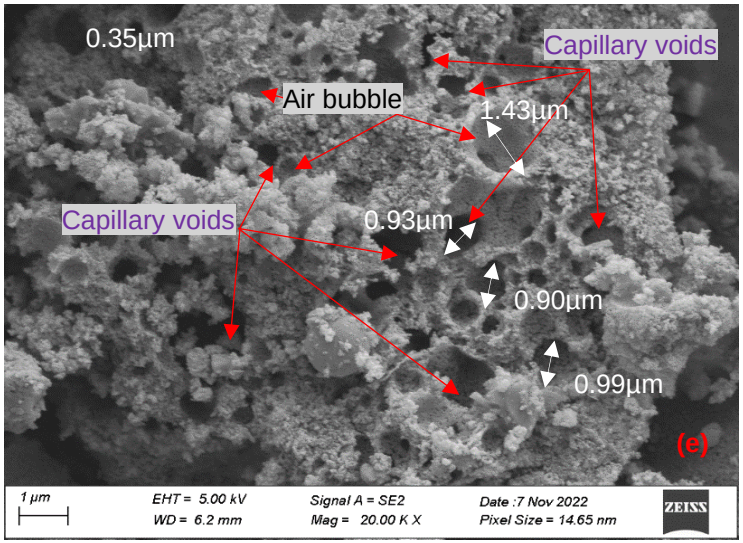

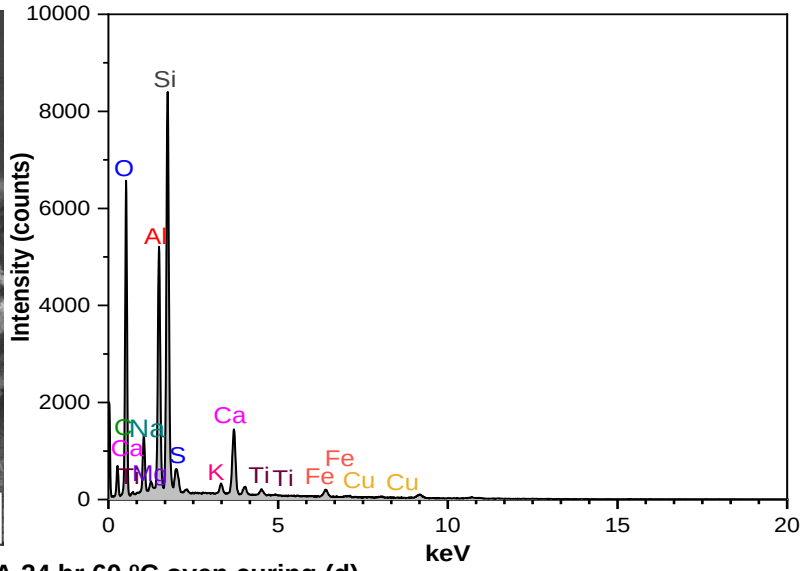

GPC-M2A 24 hr 60 ºC oven curing (d)

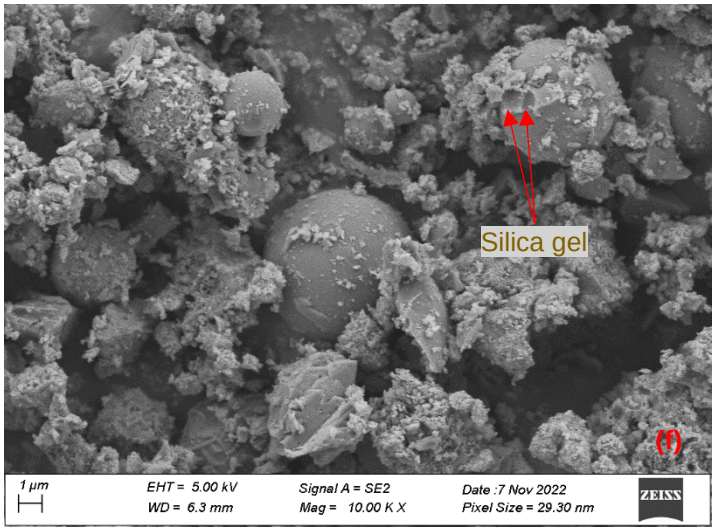

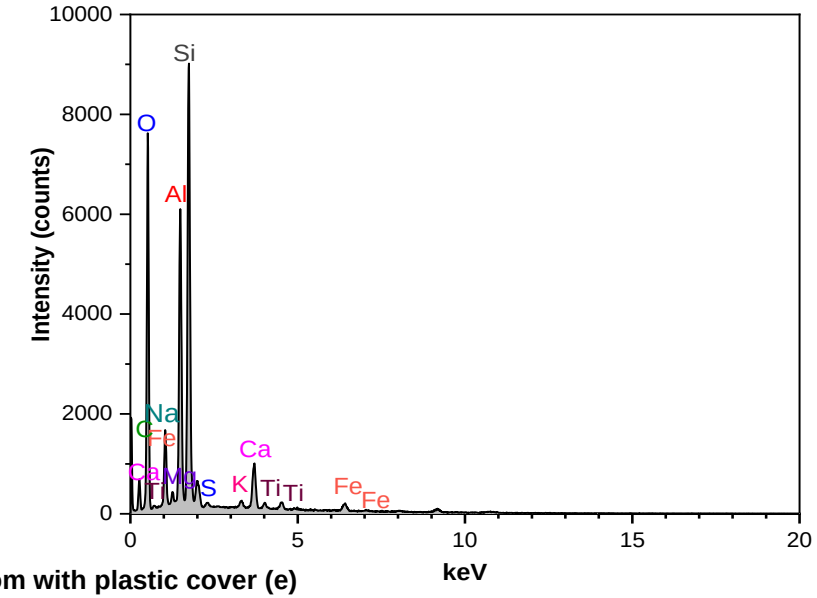

GPC-M2A, room with plastic cover (e)

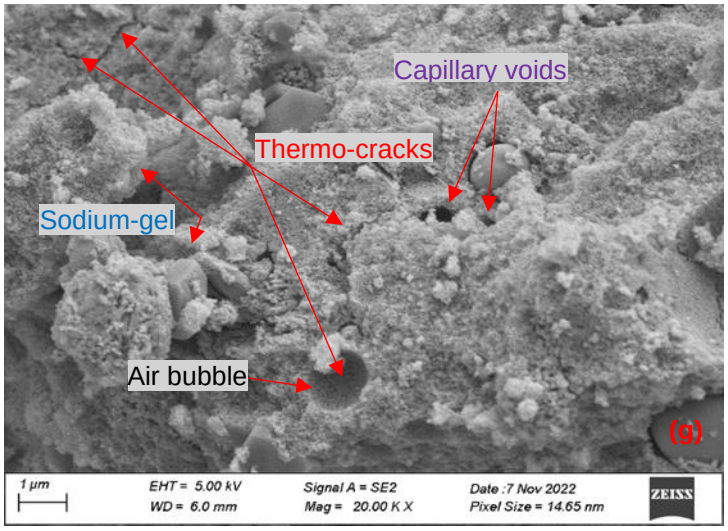

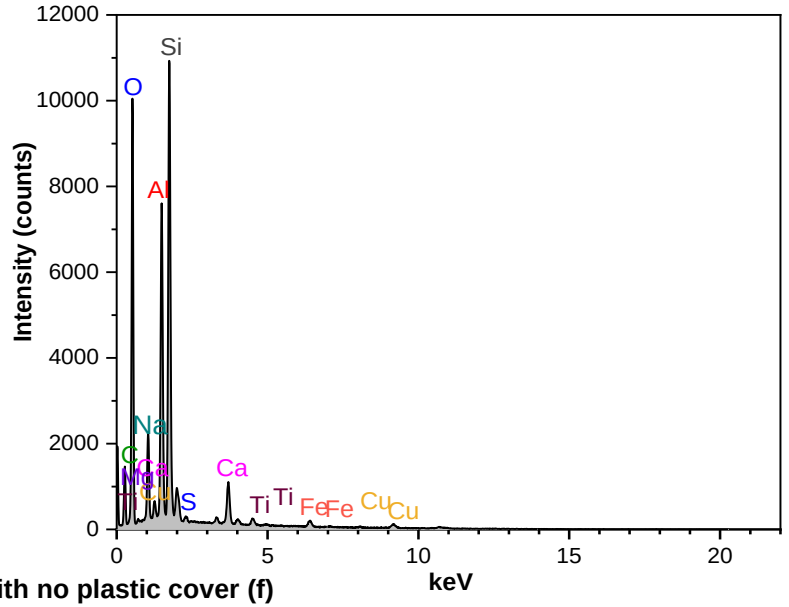

GPC-M2A, room with no plastic cover (f)

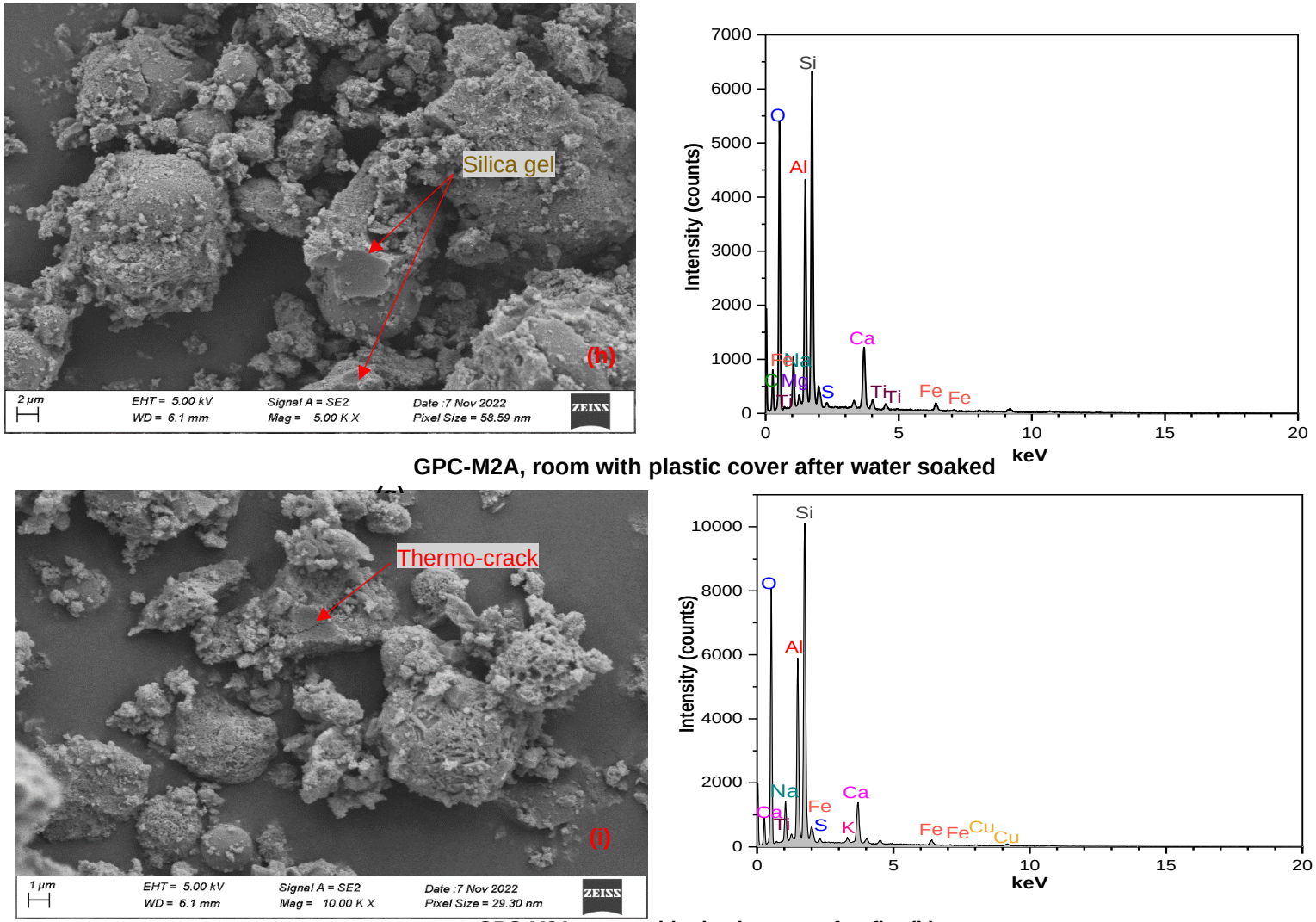

Figure 4-3: SEM imaging and EDS of CFA compared to synthesised CFA-based geopolymer product at different curing conditions and after certain durability exposures analysis.

SEM and EDS results of the morphology of as received CFA, as well as geopolymer products CFA-based GPP, GPM and GPC, which were cured respectively at 60 ^{o}C oven temperature for 24 hours or at room temperature with or without plastic covers. CFA-based GPC after water immersion and fire tests were also examined by SEM imaging.

During the EDS measurement, various areas of the samples were analysed for quantitative wt%, and the corresponding peaks are shown along with the SEM image in Figure 4.3 for pure CFA and synthesised CFA-based geopolymer paste, mortar and concrete made at different curing regimes and after some durability tests. Silica (Si) and aluminium (Al) are the main elements of the CFA and the geopolymers, as seen in pure CFA and synthesised CFA-based geopolymer products, as visible in the EDS spectra. Details of the EDS spectra of the element values measured in atomic and weight % are listed in Table B-9 of the appendix

To further investigate, the morphology of pure CFA demonstrated a variation in size distribution with a diameter ranging from 0.2 to 7.38 µm from SEM imaging set at a 1 µm scale. Figure 4.3 (a) shows that CFA particles were spheric in shape. Based on curing regimes, CFA-based GPC cured at an oven temperature of 60 ^{o}C for 24 hours demonstrated few air bubbles and a large presence of capillary voids ranging from 0.35 to 1.43 µm from SEM imaging at 1 µm scale. A higher temperature applied to the samples may cause water to evaporate, resulting in early hydration. CFA-based GPC cured at room temperature without a plastic cover was subjected to the same test; however, in this case, thermal cracking occurred because the samples were not covered with plastic, which allowed water to evaporate. In the case of oven samples wrapped in plastic, after 24 hours of curing, the water that evaporated from the samples was absorbed back into the samples over time. In this case, direct sun exposure may lead to delayed ettringite formation (DEF) since temperatures could rise above 70 ^{o}C during the first few days of curing, which could result in more cracking damage. (Taylor, 2013:39). These samples also showed the presence of Sodium gel, which proves the evidence of heavy efflorescence results obtained in Section 4.4.2 illustrated in Figure 4.3 (f). CFA-based GPC formulations in this study result only in opening thermal cracks, which were assumed to be initiated due to improper curing as described in Section 4.3.5, contrary to the open voids observed after the fire in Peng et al. (2020). In that study, the foaming formulation might have played a role.

4.1.4 X-ray diffraction

Mineral phases of geopolymer formulation in Section 4.1.3 were determined by X-ray diffraction. The technique was performed as described in Section 3.4.3. The results of the analysis are shown in Figure 4.4.

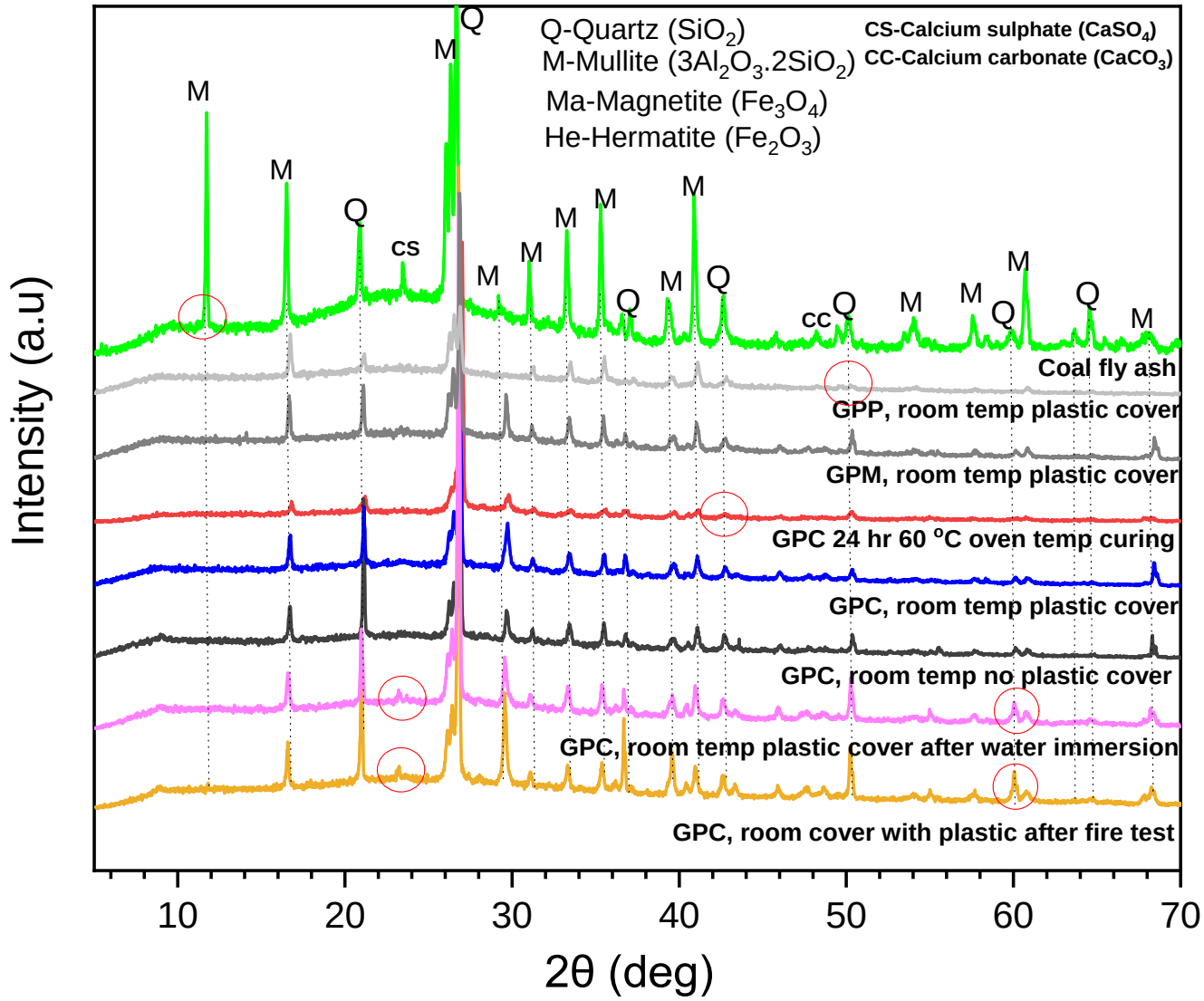

Figure 4-4: XRD Peaks results of pure CFA compared with synthesised CFA-based geopolymer products made under different curing conditions and after certain durability exposure tests.

Figure A-6, the Appendix, illustrates the X-ray patterns for amorphous and crystalline materials (Nunes et al., 2005). Figure 4-4 matches the standards data of the Joint Committee on Powder Diffraction Standards (JCPDS) used to identify. CFA and synthesised CFA-based geopolymer mineral phases that reflected the existence of quartz and mullite peaks as the major mineral phases (Valeevet al., 2018; Peng et al., 2020).In the pure CFA, calcium sulphate and calcium carbonate peaks were identified at 23.2theta and 50.5.2theta, respectively (Chindaprasirt et al., 2013). The disappearance of mullite peaks from pure CFA was observed in the case of all synthesised CFA-based geopolymer products at 12.2theta, 54.2theta and 58.2theta, respectively. The calcium sulphate peak at 23.2theta from pure CFA was only found in GPC after the fire and water immersion tests, while this phase was not present in other samples. The calcium carbonate peak at 50.5.2theta from pure CFA was again observed only in the GPC after the fire test sample. From the following results, no new peaks were observed in synthesised CFA-based GPP, GPM, or GPC, GPC after and fire and water-immersed products. It was also observed that the quartz peak at 60.2theta in pure CFA was again found to be present only from GPC after the fire test and water-immersed samples. This observed from CFA-based geopolymer is due to the presence of CFA in the formulation.

4.1.5 X-ray fluorescence and Inductive couple-plasma

XRF analysis of pure CFA and synthesised CFA-based GPP, GPM and GPC cured at room temperature with plastic cover as well CFA-based GPC cured at 60 ^{o}C oven temperature for 24 Hours, and room temperature with no plastic cover were analysed for major and trace elements using the method described in Section 3.4.4 using the same formation as in Section 4.1.3. Results of the analysis are shown in Table 4-2 and Table 4.3 for XRF and ICP, respectively.

Table 4-2: CFA and synthesised CFA-based geopolymer formulations major elements XRF results.

Metal oxide element content	CFA-based geopolymer formulations wt.% dry weight					
	Ash	Concrete			Paste	Mortar
	CFA	GPC-M2C, oven temp , 24hr 60 °C	GPC-M2AC room temp plastic cover	GPC-M2C, room temp, no plastic cover	GPP-M2C, room temp plastic cover	GPM-M2C, room temp plastic cover
SiO_2	54.81	53.20	54.12	53.96	54.66	54.58
TiO_2	1.69	0.83	0.82	0.84	0.82	0.81
Al_2O_3	32.76	16.97	16.53	17.00	16.66	16.42
Fe_2O_3	3.11	1.71	1.80	1.64	1.64	1.59
MnO	0.03	0.02	0.02	0.02	0.02	0.02
MgO	1.05	0.69	0.70	0.65	0.65	0.60
CaO	4.14	9.05	8.81	9.67	9.20	9.56
Na_2O	0.15	2.76	2.41	2.20	2.67	2.51
K_2O	0.70	0.49	0.59	0.44	0.45	0.42
P_2O_5	0.46	0.25	0.24	0.24	0.25	0.25
SO_3	0.23	0.23	0.20	0.14	0.22	0.24
Cr_2O_3	0.04	0.02	0.02	0.02	0.02	0.02
H_2O	0.10	4.17	5.39	3.31	3.43	3.94
LOI	0.72	9.15	8.64	9.39	9.14	9.36

Table 4-3: CFA and synthesised CFA-based geopolymer formulations trace elements ICP results

Trace elements content	CFA-based geopolymer formulations dry weight					
	Ash	Concrete			Paste	Mortar
	CFA	GPC-M2C, oven temp 24hr 60 oC	GPC-M2C, room temp plastic cover	GPC-M2C, room temp, no plastic cover	GPP-M2C, room temp plastic cover	GPM-M2C, room temp plastic cover
Zn	76	64	63	60	63	124
Cu	53	31	31	30	31	31
Ni	67	44	46	43	45	42
Mo	<5	<5	<5	<5	<5	<5
Nb	48	27	27	28	27	26
Zr	389	219	222	206	220	225
Y	64	34	34	32	32	32
Sr	905	762	722	816	740	745
Rb	40	29	29	27	27	26
U	9	<5	<5	5	<5	<5
Th	44	26	27	27	27	26
Pb	81	62	64	62	64	62
Co	10	<5	<5	<5	<5	5
Mn	261	223	224	204	227	207
Cr	290	229	229	227	239	237
V	194	161	147	130	153	155
S	1481	1714	1681	1173	1415	1625
Cl	36	105	49	69	59	93
Sc	25	21	19	21	19	20
Ba	934	574	547	547	568	562

The results are shown in Tables 4.2 and 4.3 for major and trace elements, respectively. When comparing all XRF results for GPP (GPP-M2C), GPM (GPM-M2C) and GPC (GPP-M2C), results based on GPP, GPM, and GPC, as well as the effect of curing, showed no significant difference. Synthesised geopolymer formulations were compared to pure CFA on major. The silica oxide content was similar, while about half of aluminium and iron oxides were reduced compared to that in CFA. Using Tables 2.5 and 2.6 to compare the pure CFA with a silica oxide content of 54.82 % and a calcium oxide content of 4.14% (less than 10%), the Lethabo CFA is classified as low calcium coal fly ash.

4.1.6 Fourier transform infrared spectroscopy

Fourier transform infrared spectroscopy (FT-IR) spectra of raw CFA powder and synthesised geopolymer in the following scenario were investigated: CFA-based geopolymer cured at oven temperature for 24 hours, room curing with plastic cover, room curing without plastic cover, fire exposed sample and water-immersed samples as shown in Figure 4.5 based on the method described in Section 3.4.5.

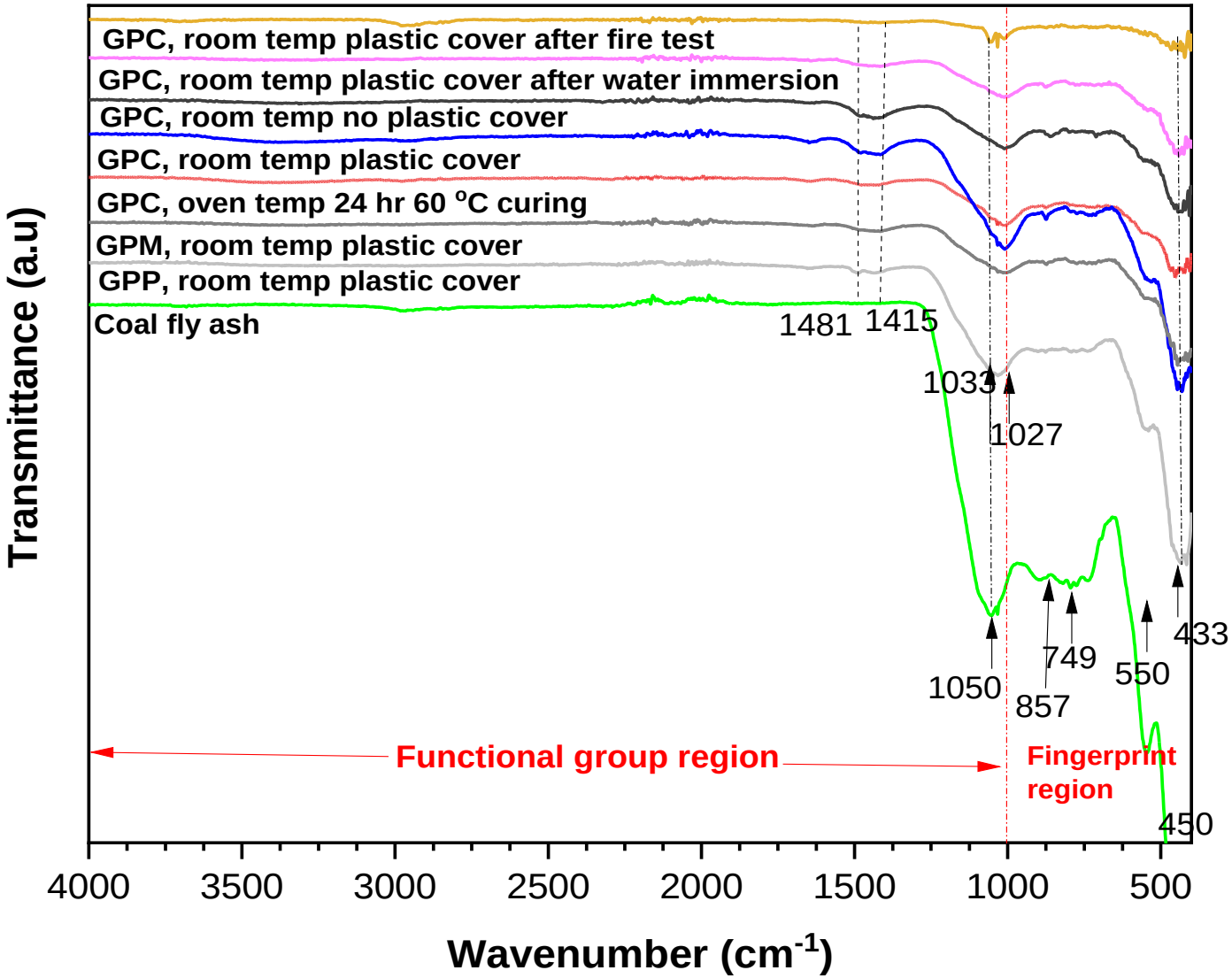

Figure 4-5: FTIR analysis results of CFA-based geopolymer paste, mortar and concrete at different curing regimes and after-durability test performance.

From the results obtained, no appearance of the C single bond O or -OH bonds was observed in the functional group region (usually associated with bands at approximately 3500 cm^{-1} and 1650 cm^{-1}) on CFA and synthesised geopolymer concrete exposed to fire (GPC-M2C room cover temp plastic after fire test) which were similar to Barbosa et al. (2000), Aguiar et al. (2009) and Vinai and Soutsos (2019). At about 1415 cm^{-1} and 1481 cm^{-1} the presence of sodium bicarbonate was indicated in synthesised geopolymer paste (GPP-M2C, room curing temp plastic cover), geopolymer mortar (GPM-M2C, room cured temp plastic cover), geopolymer concrete soaked in water (GPC-M2C, room cured temp plastic cover after water soaked) geopolymer concrete cured at room temperature with plastic cover (GPC-M2C, room temp cured with plastic cover), geopolymer concrete cured at room temp plastic cover (GPC, room with no plastic cover) and geopolymer concrete cured at the oven for 24 hours (GPC-M2C, 24 hr, 60 ^{o}C oven curing temp) by stretching vibrations of the O-C-O bond which were similar to Mužek et al. (2012) and Padmapriya et al.(2022). The main peak corresponds to the Si-O-Si stretching band in the raw CFA powder, and the synthesised geopolymer transmission spectrum was observed at about 1050 $cm^{-1,}$ which would occur for pure amorphous silica at 1100 cm-1 as found in Ferraro and Manghnani (1972), Simonsen et al. (2009) and Vinai and Soutsos (2019) studies. The bonds from coal raw CFA at 450 cm^{-1} and 555 cm^{-1} may be similar to AlO/SiO in the plane and bending modes and at about 1004 cm^{-1} with asymmetric AlO/SiO stretching. All synthesised geopolymers at different curing conditions, including water-soaked and fire-exposed samples except on CFA-based geopolymer paste where stretching vibrations of Si–O–Si and Al–O–Si, took place at 1027 cm^{-1} and 1033 $cm^{-1,}$ which may be seen as a new formation of geopolymeric reaction and for CFA based geopolymer paste (GPP-M2C); this was similar to Palomo and Glasser (1992), Phairet et al.(2000), Kumar et al. (2015), Nath et al. (2016), Yousuf (1993) and Padmapriya et al. (2022) studies. Peaks observed at 857cm^{-1} and 749 cm^{-1} for raw CFA bending vibrations of Si-O-Si and O-Si-O may indicate the presence of quartz (Bakharev, 2005; Padmapriya et al., 2022).

4.1.7 Radon exhalation and emanation.

The activity related to CFA and CFA-based GPP radon exhalation and emanation results are presented in the following sub-sections. The analysis was conducted as described in Section 3.4.6.

4.1.7.1 Radioactivity content and gamma radiation

The concentration of CFA and synthesised CFA-based GPP (GPP-M2A) uranium and thorium series and ^{40}K are shown in the following Table 4.4

Table 4-4: The activity of uranium and thorium decay series and the ^{40}K in different synthesised geopolymer samples.

Samples	Radioactivity concentration, Bq/Kg			
	U	Th	K	Average total activity
CFA	263	288	133	684
GPP SM 1A	159	200	79	438
GPP MR1	139	187	82	408
GPP MR2	209	181	69	459

The average total activity of CFA was higher than in the synthesised CFA-based GPP; the activity of uranium in CFA-based GPP (GPP MR1 and GPP MR2 formulations) ranged from around 139-209 Bq.kg^{-1} in the thorium concentration varied between 181- 250 Bq.kg^{-1} and the 40K was low at less than 100 Bq.kg^{-1}. The average total activity concentration of 408 to 459 was found in CFA-based GPP SM1A and CFA-based GPM MR2 and exceeded the world average value of 420 Bq/kg, while CFA-based GPP-MR1 was found to be less than this average world value. However, the study by Estokova et al. (2022) on radioactivity in a historical building in Slovakia resulted in a world average value of 594.0 Bq/kg. Since their obtained average value was above the world average, it was accepted to use for residential purposes as no significant health impact was expected due to the radioactivity of the building materials manufactured.

It is difficult to decide what the effect of gamma radiation in building materials will be on inhabitants of houses because it depends on whether the material is used for the walls only, walls and floor only or walls, floor and ceilings in an apartment. Another issue is that the occupation time of the dwelling is also unknown. The European Commission or EC (1999) gives an indicative rule that finds an activity concentration index (I) that gives an idea of the concentrations in building materials that would lead to a dose of 1 mSv per annum (millisievert per annum). This is the accepted maximum annual dose to which members of the public can be exposed. The equation to calculate the Concentration Index is:

$$I = \frac{C_{Ra}}{300\ Bq/kg} + \frac{C_{Th}}{200\ Bq/kg} + \frac{C_K}{3000\ Bq/kg} \qquad \text{Equation 4.1}$$

It is important to note that the weighting factors in the denominators relate to the number of gamma rays and their energies in the decay series. ^{232}Th has the most gamma rays, ^{238}U has less, and there is only one in the case of ^{40}K. An activity Concentration Index of 1 corresponds to an annual dose of 1 mSv. However, this does depend strongly on the structures in the building,

as explained in Table 2 in reference (EC, 1999). Note also from Table 1 (from the reference) that usual clay bricks do not contribute zero doses. On the contrary, the radioactivity values are about half of that of CFA for ^{232}Th.

4.1.7.2 Radon exhalation

Radon exhalation in synthesised CFA-based geopolymer concrete was calculated using Equation 3.7. For the GPP SM1A sample of 1.6 kg, the value C_{Ra}= 9.98 Bq.m^{-3} per hour. Figure 4. 6 shows an example of the measurement values of the radon concentration in the chamber as measured by the RAD7 detector.

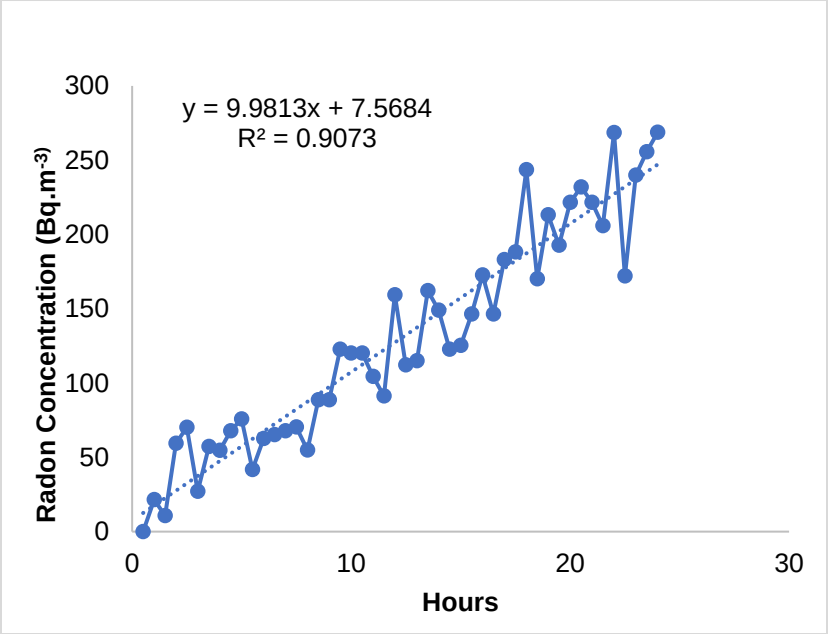

Figure 4-6: Radon builds up in 14 L chamber as measured with RAD7 detector for synthesised CFA-based GPP SM1A sample.

Using Equation 3.5, the effective strength C_{Ra} of the radium source in the block that exhales it into the chamber in Bq was determined as:

$$C_{Ra} = \frac{0.014\, m^3 \times \frac{10.0}{(3600)} . Bq . m^{-3} s^{-1}}{2.1 \times 10^{-6}} = 18\, Bq$$

This means that this CFA-based GPP SM1A block acts like a radium source that causes 18 radon atoms to enter the chamber every second. This can be used to calculate the radon exhalation rate from the block.

The exhalation of radon, or radon flux, is usually given in terms of the radon activity concentration that is released from 1 m^2 of the material per second or per hour. Taking this per hour as given in Amin (2015), the radon flux can be considered as E_A and determined according to Equation 4.2

$$E_A = \frac{\lambda C_{Ra}}{Area} \times 3600 \qquad \text{Equation 4.2}$$

where: - $C_{Ra}\lambda$ is the radon activity concentration released into the air.

-$Area$ is the area of the brick and 3600 converts from flux per second to flux per hour.

For CFA-based GPP SM1A, this leads to

$$E_A = \frac{2.1\times10^{-6} \times 18}{6\times(10\ cm \times 10\ cm)\times10^{-4}} \times 3600 = 2.4 \text{ Bq.m}^{-2}\text{.hr}^{-1}$$

It is important to understand that the answer obtained can also be written as 2 400 mBq. $m^{-2}.h^{-1}$ if this is the subject of comparison with results obtained from Amin's (2015) study. This value is higher than any of the values in that paper but is not an obvious cause for concern. The radon flux of the different CFA-based GPPs is presented in Table 4-5.

Table 4-5: Radon flux of different CFA-based geopolymer paste mix tested

Sample	Slope of radon build-up, Bq.m^{-3}. hr^{-1}	C_{Ra}	Radon flux, Bq.m^{-2}.h^{-1}
GPP SM1A	9.98	18	2.4
GPP MR1 S2	21.10	39	4.9
GPP MR2 S2	20.00	37	4.7

In general, radon escape values measured in Table 4-5 are fairly typical for building materials and do not seem to imply any specific radiation protection issue. Llope (2011) has reported that granite countertops may cause radiation damage, but realistic calculations suggest this is unlikely to be a serious concern.

4.2 Fresh property tests

Fresh properties tests were performed to determine the early behaviour of the geopolymer products such as paste, mortar and concrete. The techniques used are described in Section 3.5.1, such as setting time, flow cone test, slump test and fresh density.

4.2.1 Setting time and consistency

The setting of time and consistency techniques were used to investigate the curing behaviour of CFA-based geopolymer paste. The technique was used as described in Section 3.5.1.1. Two parameters were investigated: the effect of sodium hydroxide concentration and the mass addition of CFA in the formulation.

4.2.1.1 Effect of sodium hydroxide concentration

Five different trial formulations (mixes) were designed: GPP-M1A, GPP-M2A, GPP-M3A, GPP-M4A and GPP-M5A, as shown in Table 3-3 based on sodium hydroxide concentrations of 8, 10, 12, 14 and 16 molarities (M) respectively and mix for 5 minutes. Thus, Table 4.6 and Figure 4.7 show the setting time and consistency and the final setting time behaviour of each concentration.

Table 4-6: CFA-based geopolymer paste Vicat apparatus consistency, initial and final setting time results.

			Setting time (min)	
Mix code	Concentration (M)	Consistency (mm)	Initial	Final
GPP-M1A	8	40	5	65
GPP-M2A	10	35	120	180
GPP-M3A	12	7	170	230
GPP-M4A	16	5	200	360
GPP-M5A	16	5	230	290

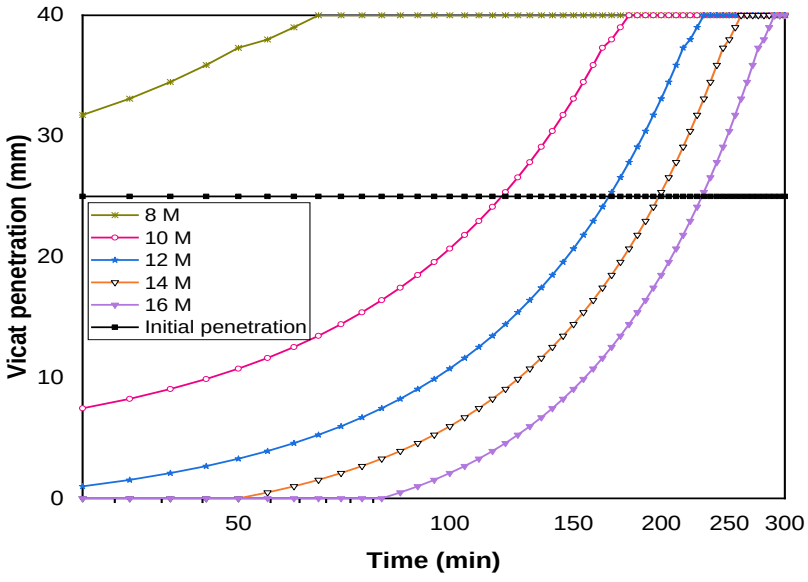

Figure 4-7: Effect of sodium hydroxide concentration on CFA-based geopolymer paste final setting time behaviour over time, using Vicat apparatus.

Formulations containing 8M and 10M of NaOH resulted in an immediate set, whereas those containing 14 M and 16 M mixes delayed the setting time according to the ASTM C191 standard requirement in Table 3-5. As shown in the following, GPP-M3A formulation at 12 molarity (12M) showed good signs of setting properties when all were tested at a room temperature range of 25-27 ^{o}C. The GPP-M3A sample at the end of the setting time test is shown in Figure A-10 in Appendix A.

4.2.1.2 Effect of CFA addition on setting time

CFA was gradually added to the GPP-M3A reference (considered as 0%) up to 20% to observe the effect of CFA on consistency and initial and final setting time. Figures 4.8 (b) and 4.8 (c) show the effect of the addition of CFA on GPP-M3A formulation, considering the control formulation (no extra CFA % added) being CFA 0%.

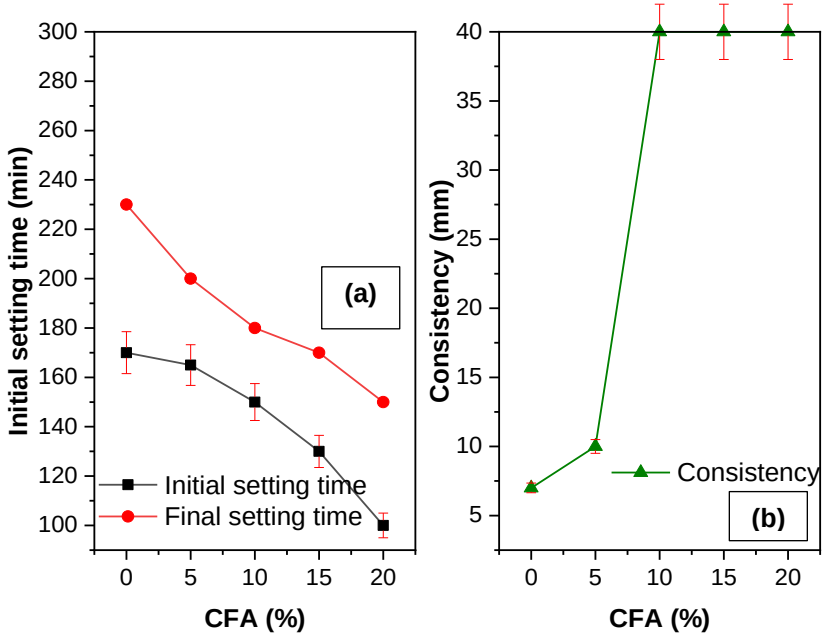

Figure 4-8: Effect of CFA mass addition on consistency, initial and final setting time of CFA-based paste.

From the results obtained, an increase in CFA showed a decrease in initial and final setting time; however, this affected the mix's consistency. The control formulation was still acceptable based on the testing standards from which other formulations containing fine and coarse aggregates were developed.

A delay in setting can reduce the durability - causing cracks to appear– of concrete that is subject to plastic shrinkage with physical restrictions. Therefore, it was important to understand the setting properties of CFA-based geopolymer formulation, such as consistency, which was related to the

amount of alkaline activator (sodium hydroxide concentration and sodium silicate content) and water content that consequently affects the initial setting time as well as the final setting time.

4.2.2 Fresh bulk density of synthesised geopolymer

Following SANS 6250:2006 guidelines, the density of CFA-based geopolymer paste (GPP), mortar (GPM), and concrete (GPC) were calculated using Equation 3.8. Figure 4.9 represents the average results of each CFA-based geopolymer type.

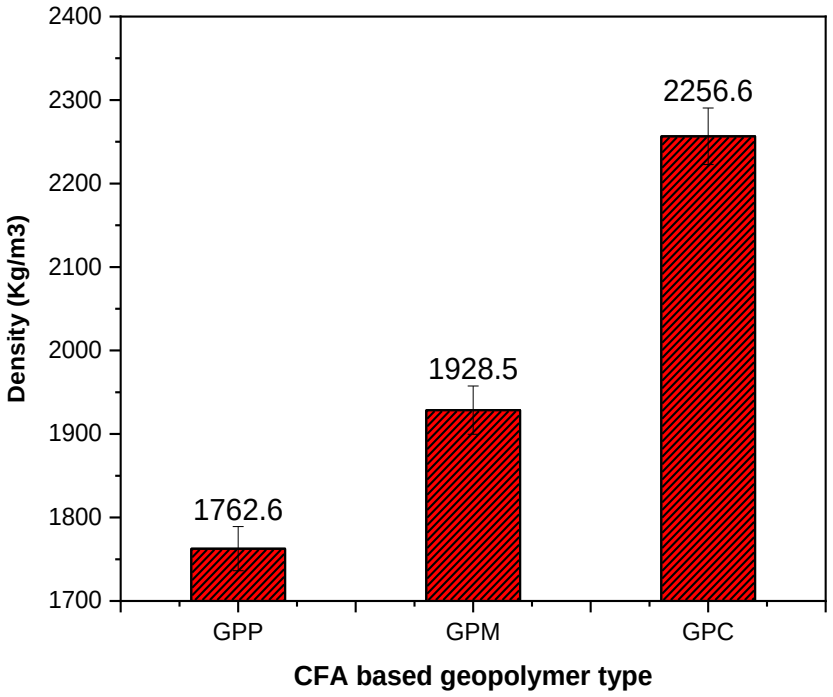

Figure 4-9:Density of CFA-based geopolymer paste, mortar and density

As illustrated in Figure 4.3 above, the density of synthesised fresh geopolymer paste increased by about 9% and 28 % when fine and coarse aggregates were added, respectively, to create mortar and concrete. In Table 3.7, CFA-based GPC is classified as normal-weight concrete.

4.2.3 Flow cone, slump test and slump flow

Slump cone and slump tests were performed to determine the flow of behaviour of CFA-based GPP and GPC, respectively. The technique was performed as described in Sections 3.5.1.2 and 3.5.1.2. The results of these tests are shown in Table 4.7 and Figure 4.10, representing the physical observation of the slump test and slump flow of the GPC-M2C formulation.

Table 4-7: Optimised CFA-based geopolymer concrete flow properties

Properties	Formulation code	value	Unit
Flow test	GPP-M2C	102	seconds
Slump test	GPC-M2C	180	mm
Slump flow	GPC-M2C	560	mm

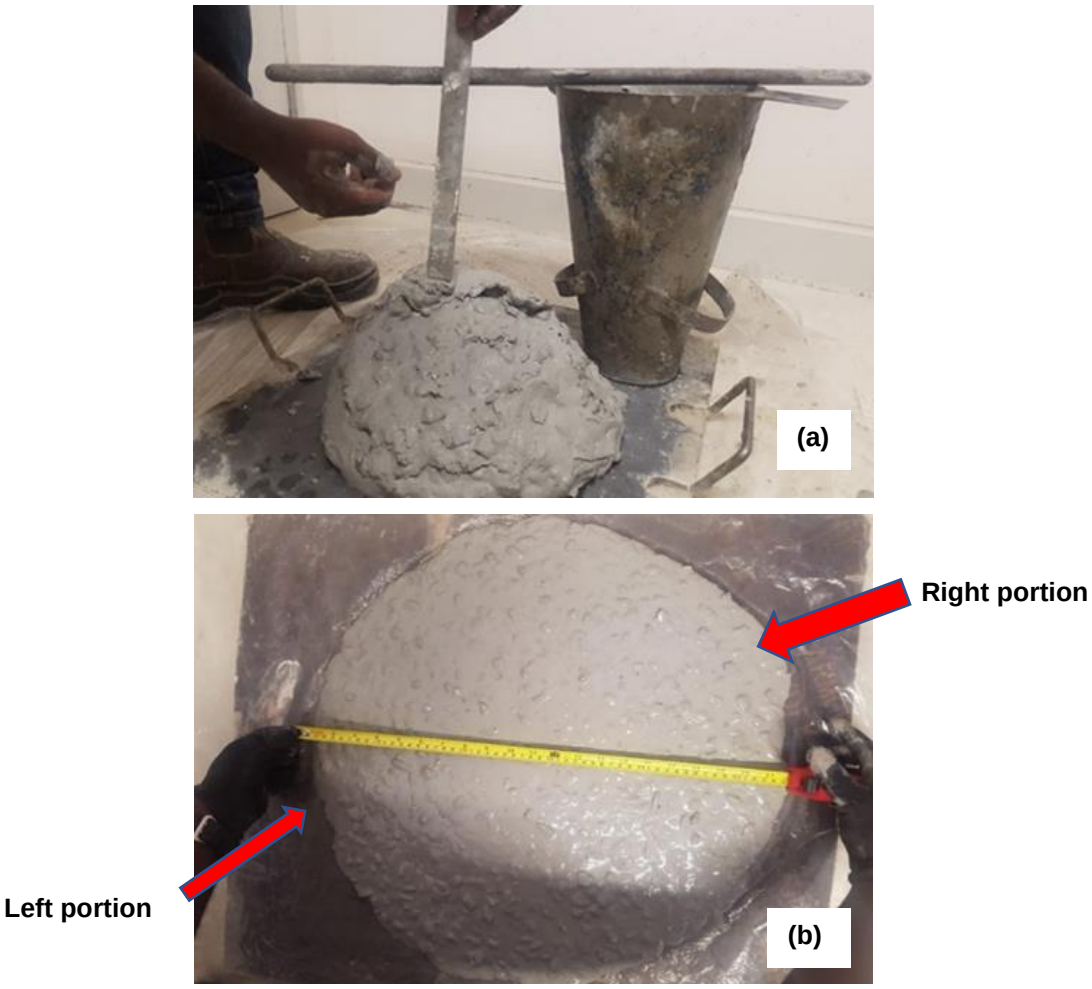

Figure 4-10: CFA-based geopolymer concrete Slump and slump test (a) and slump flow (b) and slump flow (c) appearances.

Figure 4-10 of the slump test and slump flow physical appearances represent a sign of sufficient slump, which is a highly acceptable slump by the SANS 5862-1:2006 standard. According to the testing standards, an acceptable slump test represents a sign of a better combination of both binder (CFA) and aggregates (fine and coarse aggerates) and binder. It appears that even though

a better slump was achieved, a closer look at slump flow results may reveal marginal inconsistencies in aggregates, where the left portion has slightly more aggregate content than the right portion, which consists primarily of CFA-based geopolymer mortar. There might be a sign of the lowest fine modulus in fine aggregates (the majority of fine aggregates being very fine particles), which is the subject of a demonstration by sieve analysis.

Table 4-7 flow test results compared to Jayasree and Gettu (2008) represent a sign of low flowable formulation. This shows that CFA-based geopolymer paste is less flowable than normal cement-made paste.

4.3 Mechanical properties

This Section describes material strength and deformation properties when applied loads. The following tests were conducted: compression strength, flexural strength, tensile strength, and modulus of elasticity.

4.3.1 Compression strength

The compression strength of CFA-based geopolymer formulations can be affected by many parameters. Various parameters such as sodium hydroxide concentration addition of CFA, oxide content, fine and coarse aggregate content in the formulation, curing regime and water exposure were carefully investigated to obtain an optimal formulation.

4.3.1.1 Effect of sodium hydroxide concentration

Coal fly-based geopolymer paste GPP-M1A, GPP-M2A, GPP-M3A, GPP-M4A and GPP-M5A formulations developed were tested for compression strength after 28 days of room curing with plastic curing. The results are shown in the following Figure 4.11.

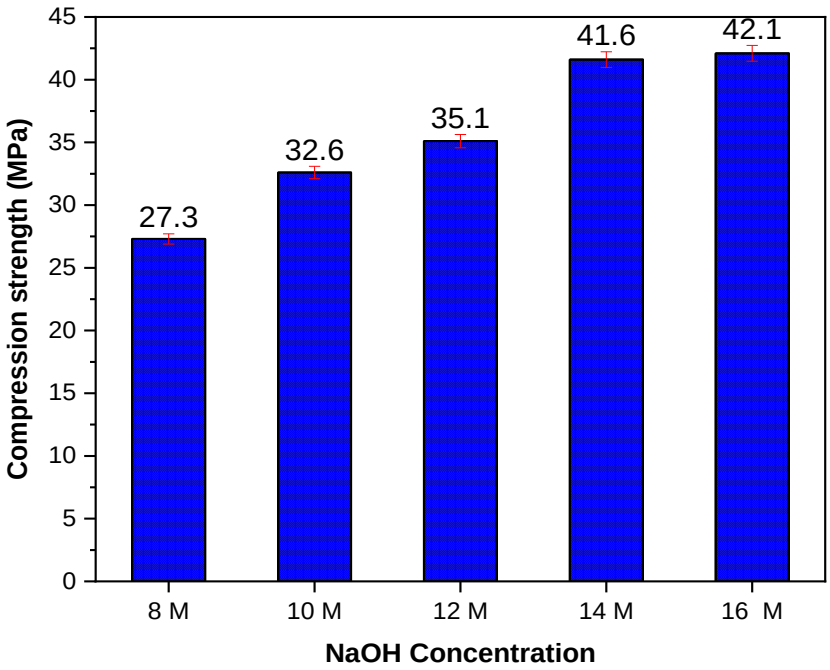

Figure 4-11: Effect of sodium hydroxide concentration on CFA-based geopolymer paste compression strength.

Similar to Adewumi et al. (2010), the results showed that compression strength increased as sodium hydroxide concentration increased and stabilised from 14 M to 16 M instead of decreasing. These formulations also became very brittle during the compression strength as sodium hydroxide concentration was increased from 14 M to 16 M.

As a result, 12M NaOH were selected for its better setting properties and lower brittleness behaviour compared to 14 and 16M.

4.3.1.2 Effect of CFA addition on compression strength

Formulations developed with mass addition of CFA of 5, 10,15 and 20% as in Section 4.1.1.2 were tested for compression strength at the same curing age to observe the effect of CFA on compression strength from a controlled 12 M of NaOH at 35.1 MPa. Figure 4.12 represents the results of the compressive strength obtained.

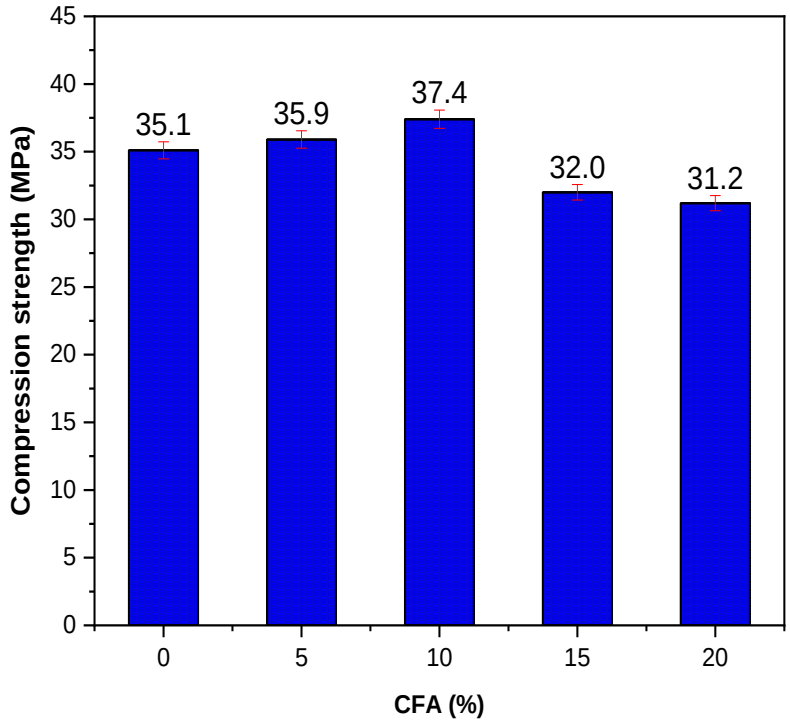

Figure 4-12: Effect of CFA mass addition on compression strength of CFA-based geopolymer paste

The results obtained showed that an increase in CFA by up to 10% can increase the compression strength of CFA-based geopolymer paste from 35.1 MPa to 37.4 MPa (about 7%), and more than 10% of CFA addition resulted in lowering the compression strength from 35.1 to 32.0 (about 9% of the initial strength) based on the GPP-M3A formulation. The lower strength obtained can be related to the formation of capillary voids due to an incomplete reaction between CFA and alkaline activator solution because of the overfeed in CFA.

GPP-M3A was reformulated to improve the formulation brittleness behaviour, resulting in GPP-SMR1 and GPP-SM1A, shown in Table 3-3. The compression strength and other parameters results for GPP-SMR1 and GPP-SM1A compared to GPP-M3A are shown in Table 4-8.

Table 4-8: Properties of CFA-based geopolymer paste pattern improvement.

Mix code	Compression strength	STD	Density	Consistency	Initial setting time	Final setting time
	MPa	MPa	kg/m3	mm	min	min
GPP-M3A	35.1	2.3	1689.6	7	170	230
GPP-MR1	38.7	2.1	1621.5	5	160	210
GPP-SM1A	45.0	2.2	1683.3	7	175	250

GPP-SM1A resulted in high compression strength, and it was observed to have a lower brittleness effect than GPP-M3A and GPP-MR1. From Table 4-8, other GPP-SM1A parameters, such as density, consistency, and initial and final setting time, were similar to the value obtained from GPP-M3.

4.3.1.3 Effect of dry mix coloured dye on compression strength

Dye oxide pigment was added to CFA-based geopolymer paste for colouring purposes. Its effect on compression strength was investigated on GPP-MR1 with results in Figure 4-13.

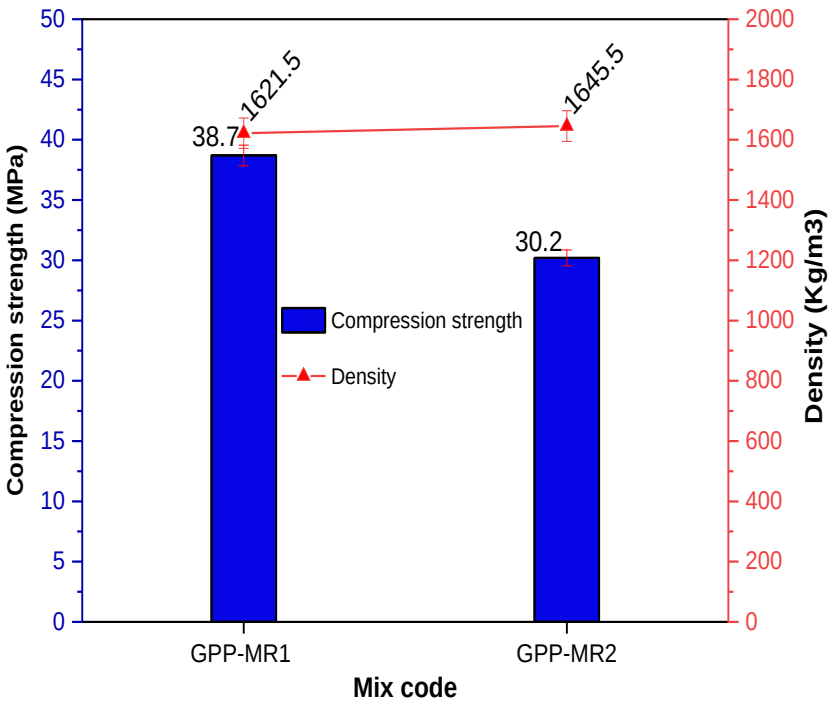

Figure 4-13: Effect of dye oxide on CFA-based geopolymer paste formulation compression strength

Adding 2.5% of CFA content in the formulation by oxide pigment considering GPP-MR1 to make GPP-MR2, it was observed that the compression strength decreased from 38.7 to 30.2 (about 22% less than the original compression strength). On the other hand, the density was slightly increased from 1621.5 to 1645.5 kg/m^3 (about 1.5 %).

4.3.1.4 Effect of fine and coarse aggregates

Similar to OPC concrete, fine and coarse aggregates were added to CFA-based geopolymer paste to form geopolymer mortar (GPM) and geopolymer concrete (GPC), as illustrated in Figure 2.13. The effect of both fine and coarse aggregates on compression strength was investigated, as shown in Figure 4-14.

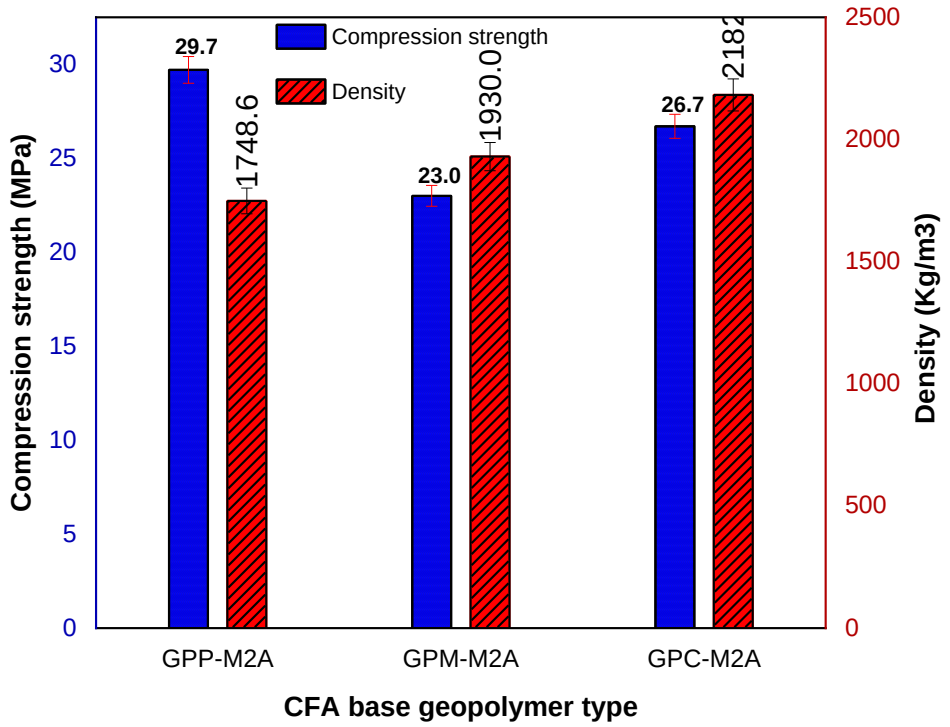

Figure 4-14: Effect of fine and coarse aggregates on the synthesis of CFA-based geopolymer mortar (GPM) and geopolymer concrete (GPC).

From the above results, the addition of fine aggregate to GPP-M2A to form a GPM-M2A decreased the compression strength from 29.7 MPa to 23 MPa. Adding fine and coarse aggregates from GPP-M2A to form GPC-M2C also decreased the compression strength from 29.7 to 26.7 MPa.

The brittleness effect of the GPP-M2A, GPM-M2A and GPC-M2A was physically observed during the compression strength. The compression breaking patterns obtained are shown in the following Figure 4-15

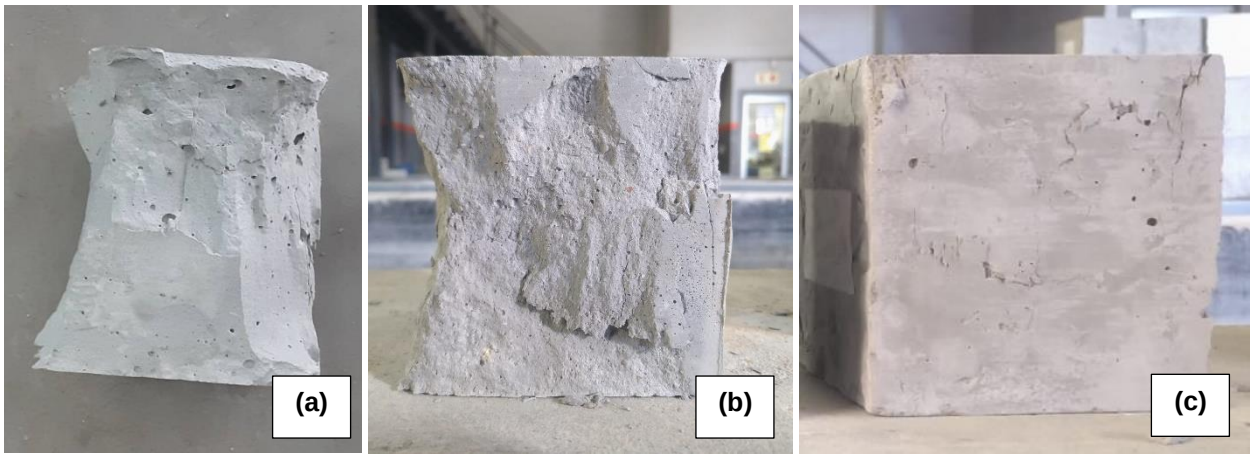

Figure 4-15: Effect of fine and coarse aggregates on CFA-based geopolymer breaking pattern; CFA-based GPP (a), CFA-based GPM (b) and CFA-based GPC (c).

The addition of fine aggregate to GPP resulted in a semi-explosive pattern type B. Adding both fine and coarse aggregates to GPP to form GPC resulted in non-explosive materials with pattern A, which is a sign of material ductility.

4.3.1.5 Effect of curing regimes

CFA-based geopolymer concrete was cured at different curing conditions described in Figure 3.8. The effect of room curing conditions A and B and oven curing at 60 ^{o}C was investigated on compression strength. The compression strength development was determined at different ageing: 3 days, seven days, 14 days, 21 and 28 days and three months. The variation in compression strength from each curing condition is shown in Figure 4.16

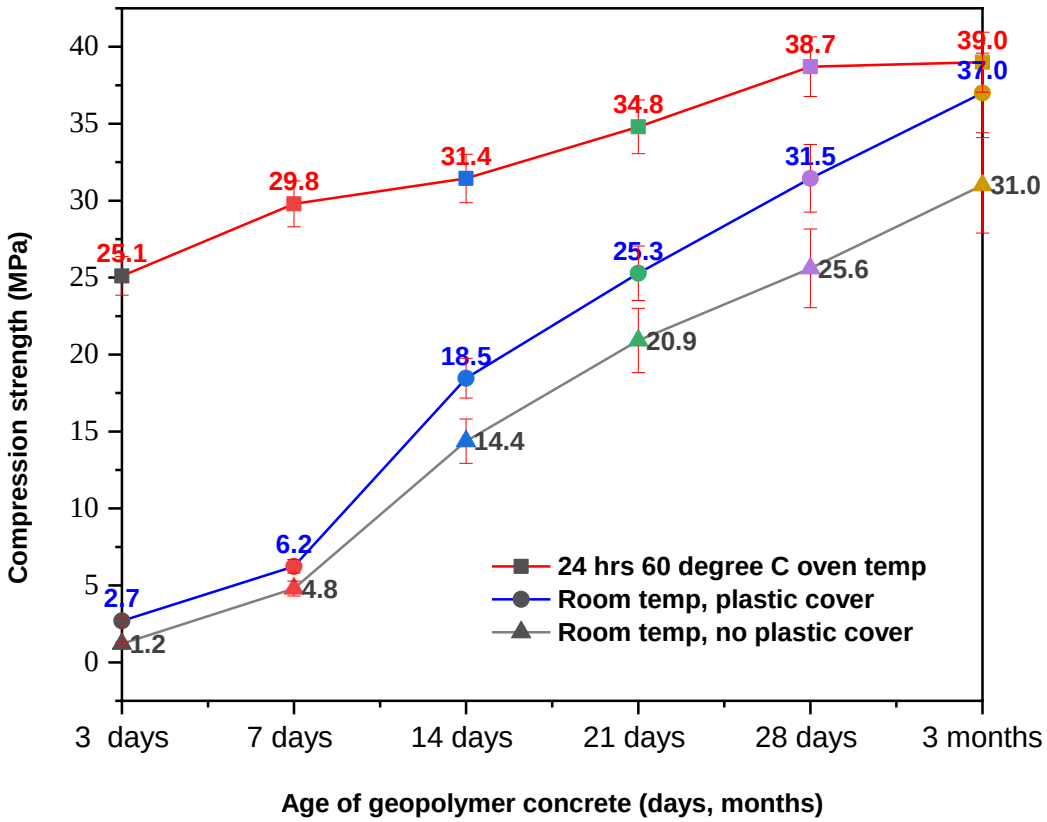

Figure 4-16: Effect of curing regime on CFA-based geopolymer concrete compression strength variation from 3 days to 3 months of monitoring.

Using GPC-M2A formulation, it was observed that at three days, specimens cured at oven temperatures for 24 hours were already 89 to 93% stronger than those cured at room temperature with and without plastic cover, respectively. At this stage, lower temperatures cured specimens did not have breaking points during compressive strength tests and were considered soft. At 14 days, the room-cured samples covered with a plastic sheet specimen improved by achieving 18.5 MPa of compressive strength. At three months of ageing the samples that had been cured in the room, compressive strength was still improving and found to be similar to that of samples cured in the oven, which had been stabilised.

Based on curing regimes, sample-breaking cracks were physically observed at the end of compression strength. This physical appearance is shown in Figure 4-17.

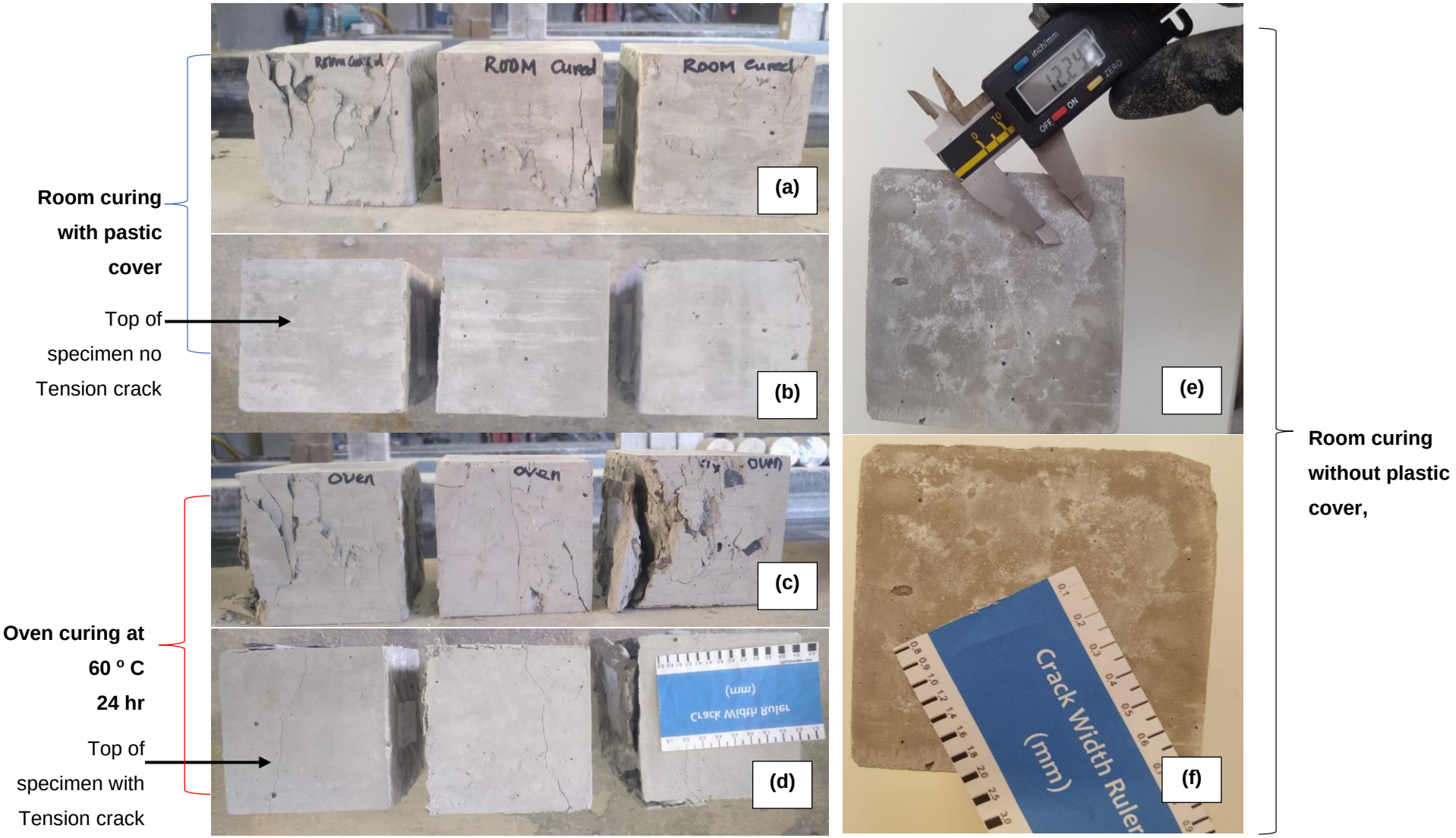

Figure 4-17:Effect of curing regimes of CFA-based geopolymer concrete on compressive strength breaking patterns after room curing with plastic cover and oven curing, and effect of thermal curing on room curing without a plastic cove

Specimens cured at room temperature that had been covered with a plastic sheet at the normal pattern, are shown in Figure 4-17 (a and b). The oven temperature specimens, as shown in Figure 4.17 (c and d), resulted in a tension crack of 0.2 mm in width and 100 mm long. Specimens cured at room temperature that had not been covered with a plastic sheet resulted in thermal cracking, from 7 days up to 3 months, of 0.15 mm and 12.24 mm width and long, respectively, shown in Figure 17 (e and f).

4.3.1.6 Effect of water absorption

CFA-based geopolymer concrete soaked in water, as described in Section 3.5.3.2, was tested for compression strength at the end of the water absorption test. Thus, Figure 4.18 shows the compression strength and density of the non-soaked and soaked specimens at different curing regimes.

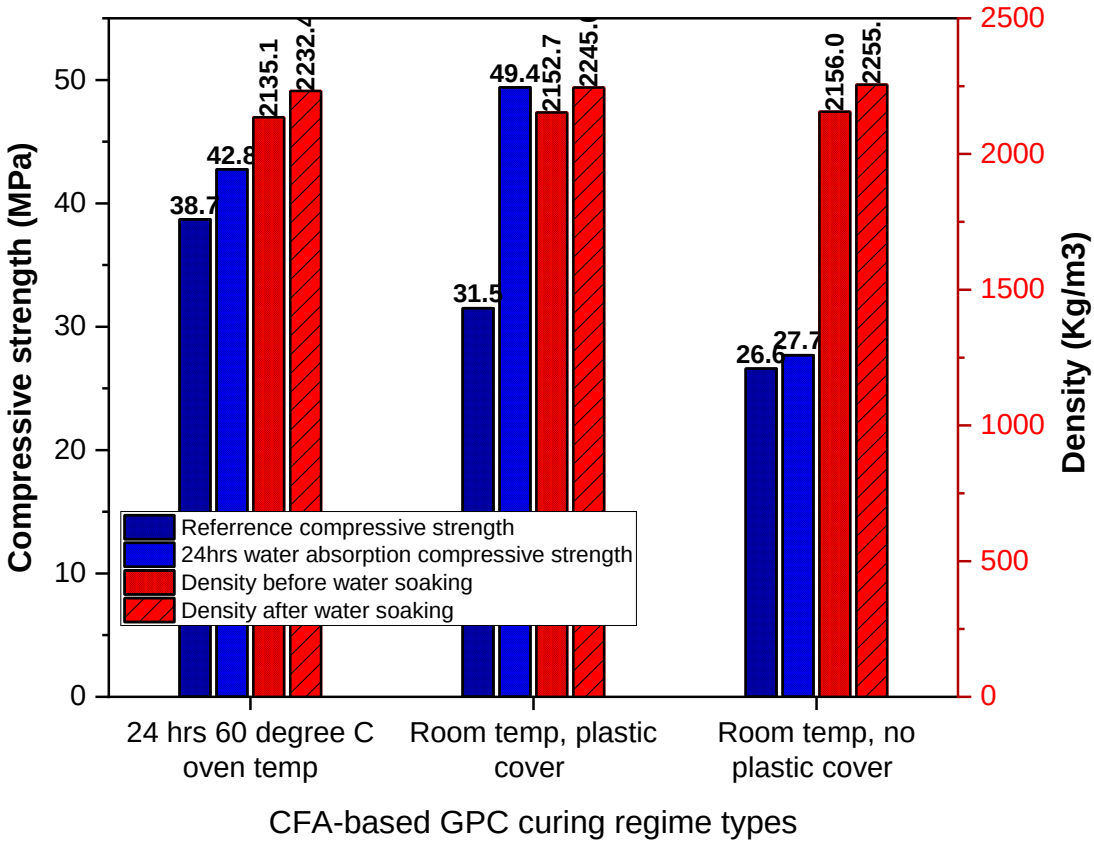

Figure 4-18: Effect of 24 soaked on CFA-based geopolymer concrete compression strength based on curing regimes

As a result of the effect of water absorption on GPC-M2C formulation, the compressive strength of CFA-based geopolymer concrete at 28 days of ageing was increased. Strength gains of 10,

36, and 4% were observed from oven curing for 24 hours at 60 °C, room-covered sample with plastic and room with non-plastic covered, respectively, from their original 28 days. In addition, CFA-based geopolymers cured at room temperature with plastic covers were 13% and 44% stronger than those cured at oven temperature and room temperature without plastic cover, respectively.

4.3.2 Effect of fine and coarse aggregate on flexural strength

The bending behaviour of CFA-based geopolymer paste and geopolymer concrete were investigated under a certain loading using the flexural strength technique. As described in Section 3.5.2.2, this was performed. Figure 4-19 illustrates the flexural strength results, including the flexural-to-compression strength ratio on GPC-M2C and GPP-M2C formulations.

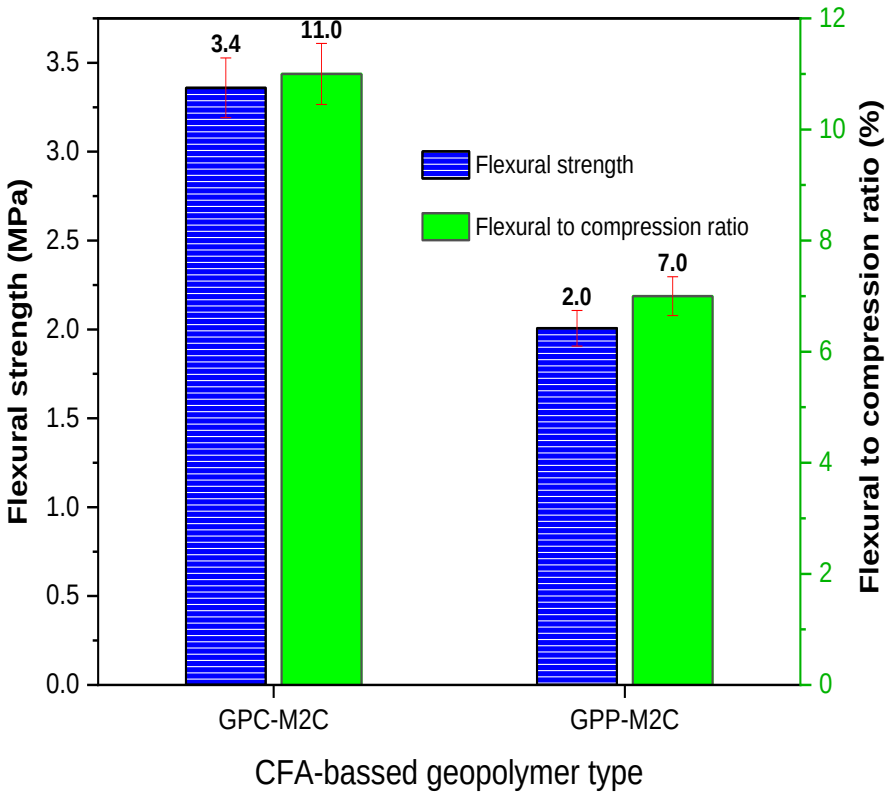

Figure 4-19: Effect of fine and coarse aggregates on flexural strength of CFA-based geopolymer paste and concrete.

The results show that adding both fine and coarse aggregates on CFA-based geopolymer paste to form CFA-based geopolymer can increase its flexural strength from 2.0 to 3.4 MPa.

During the flexural test load application, sample crack development was physically observed. This physical appearance is shown in the following Figure 4-20.

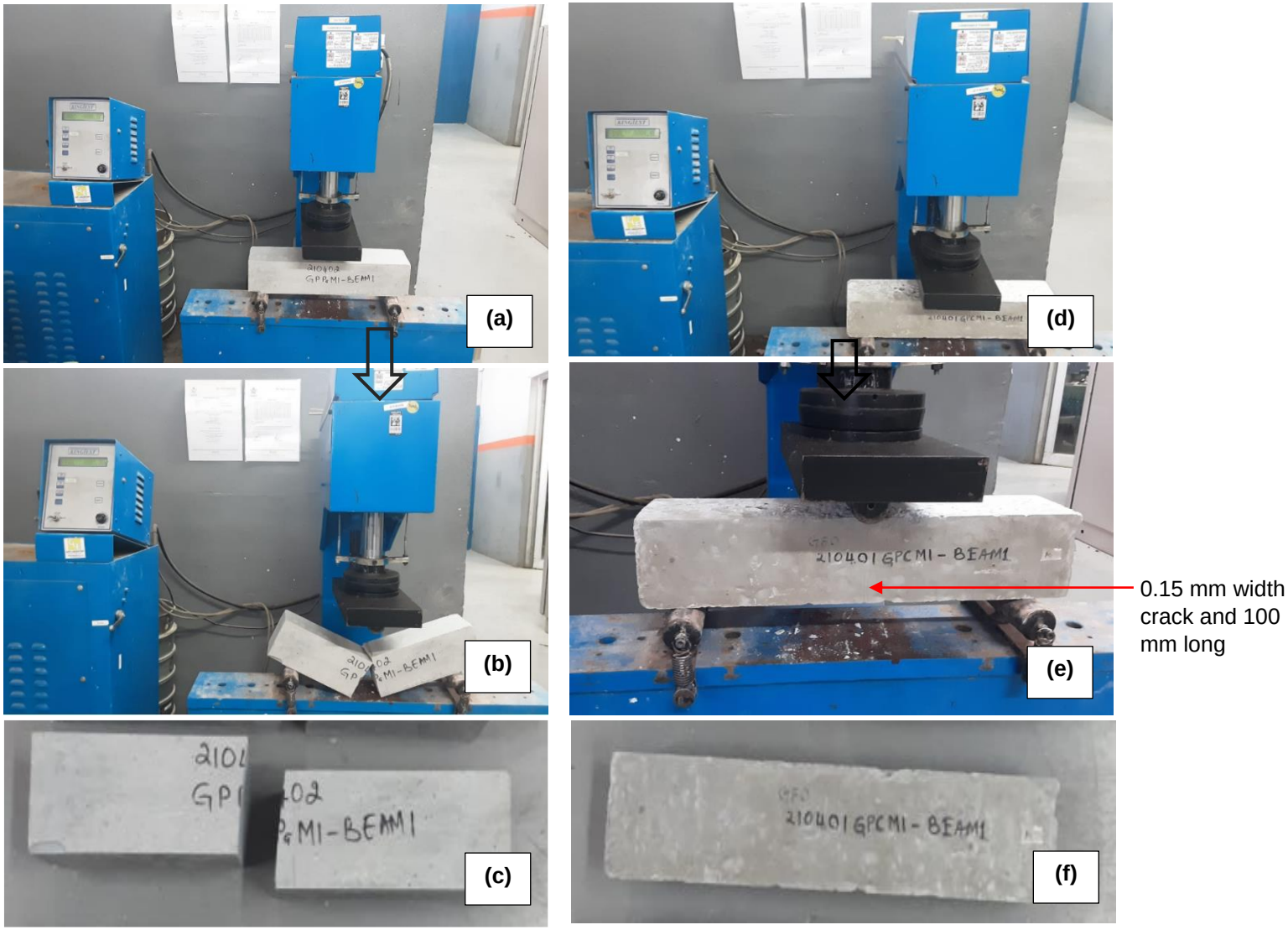

Figure 4-20: Bending behaviour on CFA-based geopolymer paste and concrete under centre-point bending test

As shown in Figure 4-20(b) and Figure 4-20 (c), the CFA-based GPP resulted in brittle tension failure when reaching a final load of 4.5 ± 0.35 kN (2.0 ± 0.16 MPa), while the addition of fine and coarse aggregates in GPC only resulted in plastic failure with shear tension failure as shown in these Figure 4-20 (e) and Figure 4-20 (f) when reaching a flexural strength of 2.2 ± 0.61 MPa (a load of 5.9 ± 1.34 kN) with a crack of 0.15 mm width and 50 mm long before reaching the final flexural strength of 3.4 ±0.29 MPa (load of 7.5 ±0.64 kN) with a crack length of 100 mm. Based on calculations, the flexural strength to compression strength ratio of 6.7 and 10-12.8 % was obtained from CFA-based GPP-M2C and GPC-M2C, respectively, as shown in Table B-7. Further investigations may take place under the tensile splitting test.

4.3.3 Tensile splitting strength

The splitting behaviour of CFA-based geopolymer paste and geopolymer concrete were investigated under a certain loading using the tensile splitting technique. The test was conducted as described in Section 4.2.3. Figure 4-21 (a) illustrates CFA-based geopolymer paste and concrete cured at different regimes based on GPP-M2C and GPC-M2C formulations.

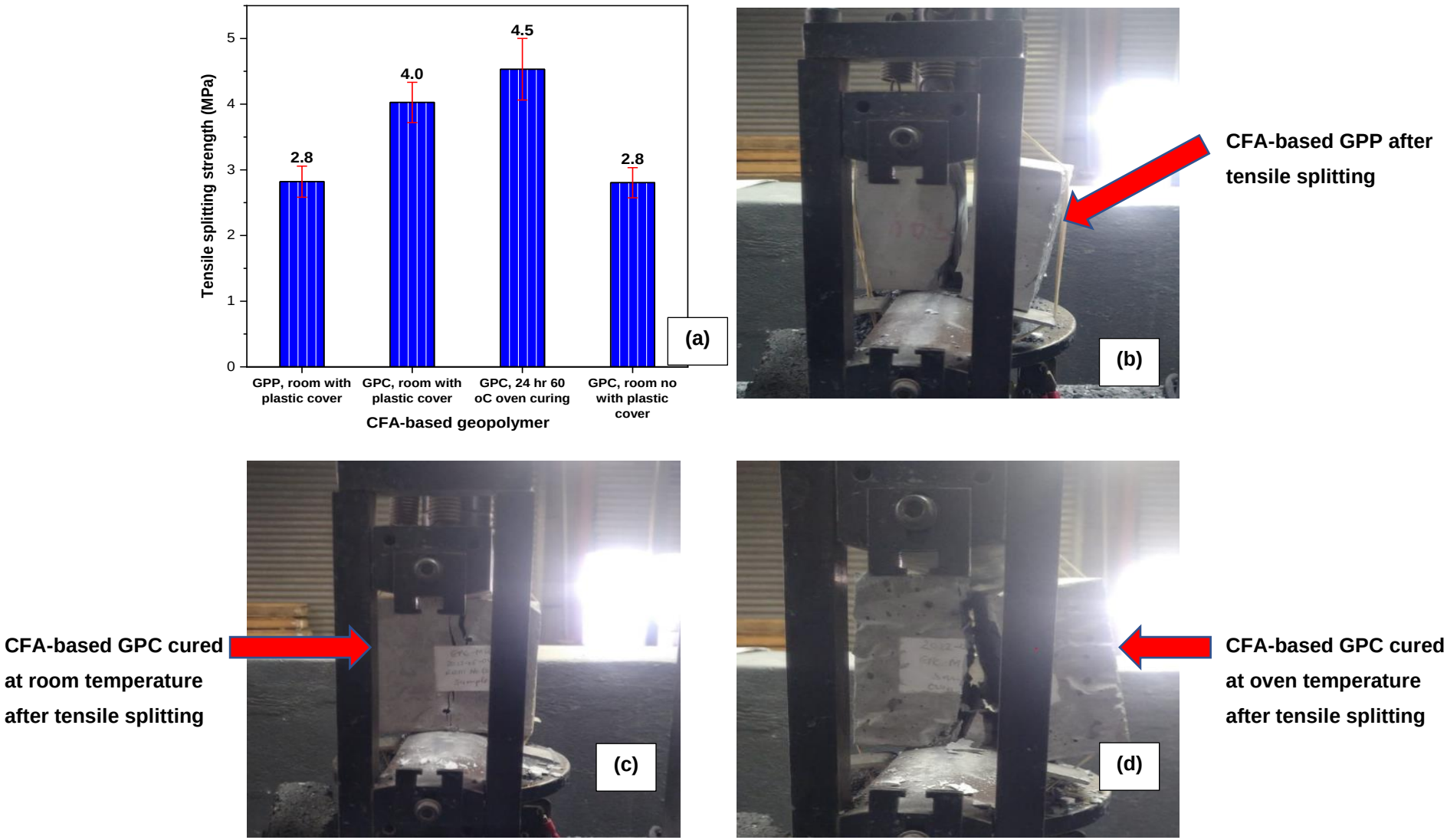

Figure 4-21: CFA-based geopolymer concrete paste and concrete cured at a room and oven tensile splitting strength; results ((a) and behaviour after the test.

Figure 4-21 shows the results. Figure 4-21 (a) represents the tensile strength required to fracture the tested CFA-based geopolymer paste and concrete at different curing regimes. The results show that CFA-based geopolymer paste had lower tensile strength than CFA-based geopolymer concrete. Figure 4-21 (b) - represents the splitting fracture behaviour of CFA-based GPP, which was very destructive and resulted in a very brittle creating point with loud sound effects during the testing compared to CFA-based GPC. The fracture in CFA-based GPC cured at 60 ^{o}C temperature is greater than that of CFA-based GPC cured at room temperature, as shown in Figure 4-21 (c and d). The magnitude of the fracture may be related to the low moisture content of these samples since the oven evaporated an excessive amount of water.

4.3.4 Modulus of elasticity and Poisson ratio

The ability of CFA-based GPP and GPC to resist deformation and fracture behaviour was performed by the modulus of elasticity and Poisson ratio technique. The test was performed as described in Section 3.5.2.4. Figure 4-22 (a) illustrates CFA-based geopolymer paste and concrete cured at room temperature modulus of elasticity and Poisson ratio.

.

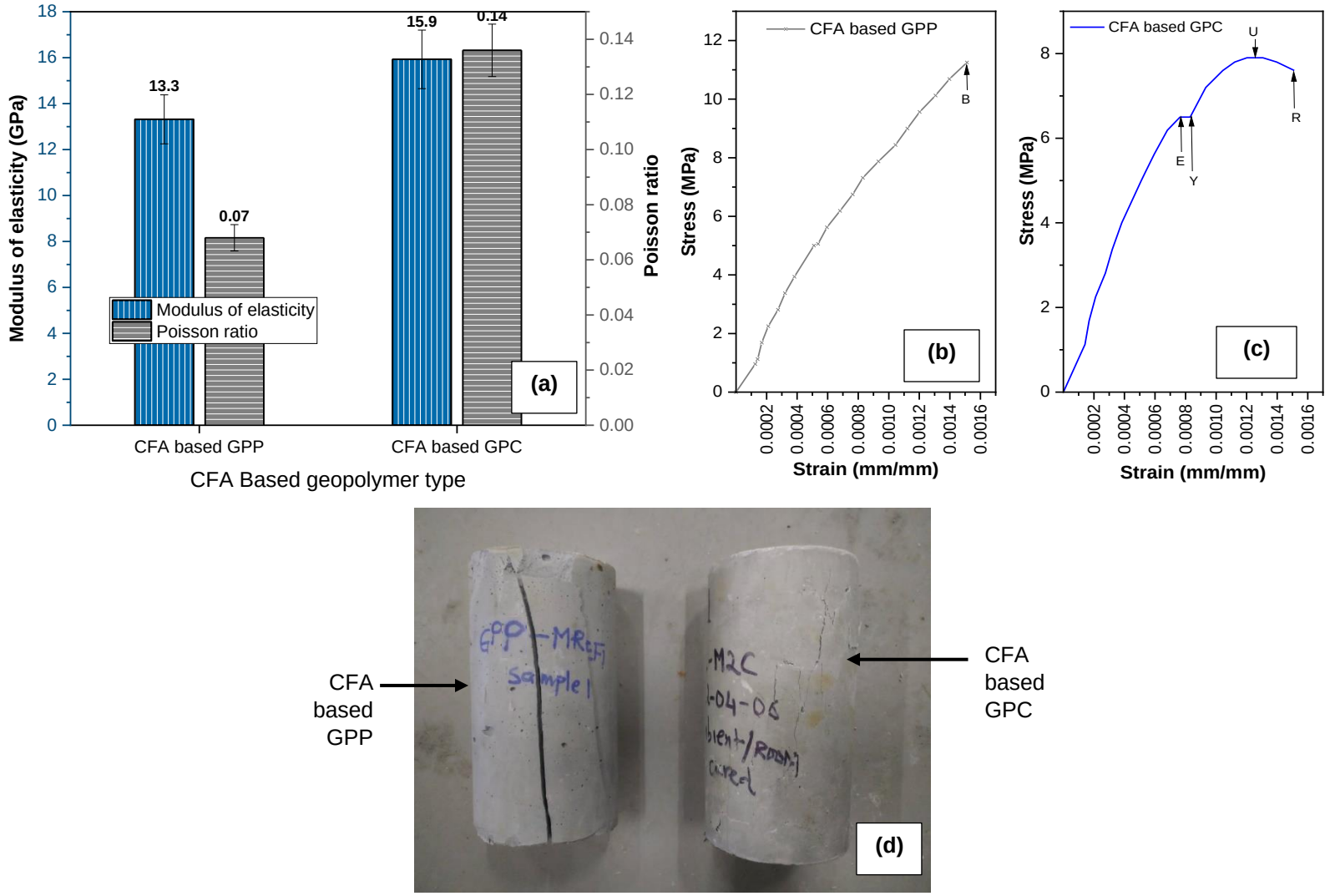

Figure 4-22: Stress-stain curves for CFA-based geopolymer paste and concrete; B=brittle, E=elastic limit, Y=yield point, U=Ultimate strength reaching point, R=Actual rupture strength (a), modulus of elasticity and Poisson ratio (a) and at the end of test (d).

As shown in Figure 4-22 (a), adding fine and coarse aggregate to CFA-based GPP-M2C to form GPC-M2C improves the modulus of elasticity from 13.3 to 15.9 GPa (13300 to 15900 MPa) and the Poisson ratio. The data shows that GPP can more easily fracture compared to GPC.

By comparing the stress-strain behaviour of CFA-based GPP to that of CFA-based GPC, Figure 4-22 (b) illustrates the stress-strain curve behaviour of CFA-based GPP, which is similar to that of brittle material while that of CFA-based GPC in Figure 4-22 (c) corresponds to that of ductile polymer (Sadiku et al., 2016). Figure 4-22 (d) shows the sample at the end of the test. The CFA-based GPC sample showed an acceptable standard failure type 3 in contrast to the CFA-based GPP, which may not be acceptable for elements such as columns and beam slabs, as illustrated in Figure A-1 of in the appendix

4.4 Durability properties

As described in Section 3.5.3, durability tests were conducted on CFA-based geopolymer paste, mortar, and concrete to determine their long-term performance. The following were investigated: the effect of water penetration and absorption, capillary water absorption and efflorescence tests, carbonation depths and pH measurements, curing regimes and fine and coarse aggregates on density change and drying shrinkage and fire resistance test.

4.4.1 Effect of water penetration and water absorption

A CFA-based geopolymer paste, mortar and concrete's ability to resist water ingress and absorption was tested using both water penetration and water absorption techniques. The techniques were described in Sections 3.5.3.1 and 3.5.3.2. Figure 4-23 (a) illustrates Karsten water penetration and penetration results on CFA-based GPM and GPC cured at different curing regimes.

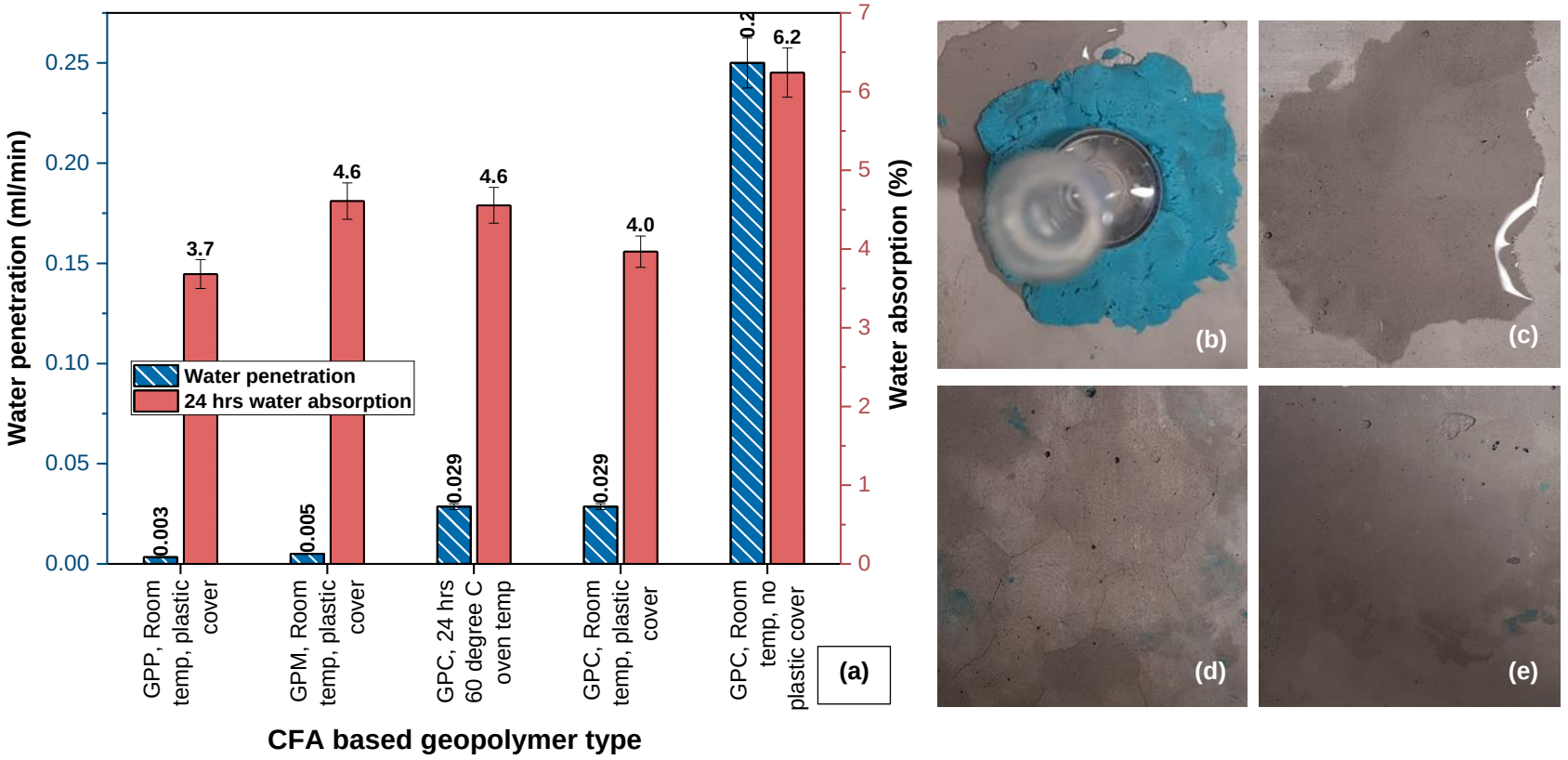

Figure 4-23: CFA-based geopolymer products: Karsten-tube water penetration and 24-hour water bath water absorption test results in (a), samples behaviour during water penetration at around 20 minutes (b), samples after Kartesn tube removable (c), GPC room temp with no plastic cover surface after water whipped (d) other specimens surface finish after water wiped (e).

As a result of a better surface finish with a lower presence of voids in CFA-based geopolymer products, the measuring may exceed up to 30 minutes of penetration per sample. The results showed low water ingress and absorption of CFA-based GPP, GPM, and GPC cured in an oven and room with a plastic cover. Thermal cracks, mentioned in Section 4.2.1.3, were present in samples cured at room temperature that had not been covered. These cracks were responsible for water absorption in CFA-based GPC-M2A with the appearance of cracks of about 0.15 mm width and 10-12.5 mm length on the surface after water ingress. From the exact marginal penetration, it was observed that water penetrated the plasticine sealing and caused the Karsten tube to be unsealed from the specimen, and no cracks were observed on the surface, as in Figure 4-23 (a and b). These results are similar to the test results discussed by Weisheit et al. (2016).

4.4.2 Capillary water absorption test and efflorescence test

Capillary water absorption and efflorescence techniques determine the rate of water absorption and possible efflorescence appearance on CFA-based geopolymer paste, mortar and concrete's ability. The techniques are described in Sections 3.5.3. The efflorescence types, as described in Table 3-6 (Chapter 3), are shown in the following Table 4-9 and Figure 4-24 (a) illustrate the capillary water absorption, Figure 4-24 (b) the capillary rate of water absorption, Figure 4-24 (c) shows the specimens dimensional change when in contact with water and Figure 4-24 (d,e and f) are specimens at the end of the test.

Table 4-9: CFA-based geopolymer types and curing regimes efflorescence extend type observed after capillary water absorption

CFA-based Geopolymer type	Curing regimes	Efflorescence description
GPC-M2A	Oven, 24 hours	Slight
GPC-M2A	Room, plastic cover	Nil
GPC-M2A	Room, No plastic cover	Heavy
GPM-M2A	Room, plastic cover	Nil
GPP-M2A	Room, plastic cover	Nil

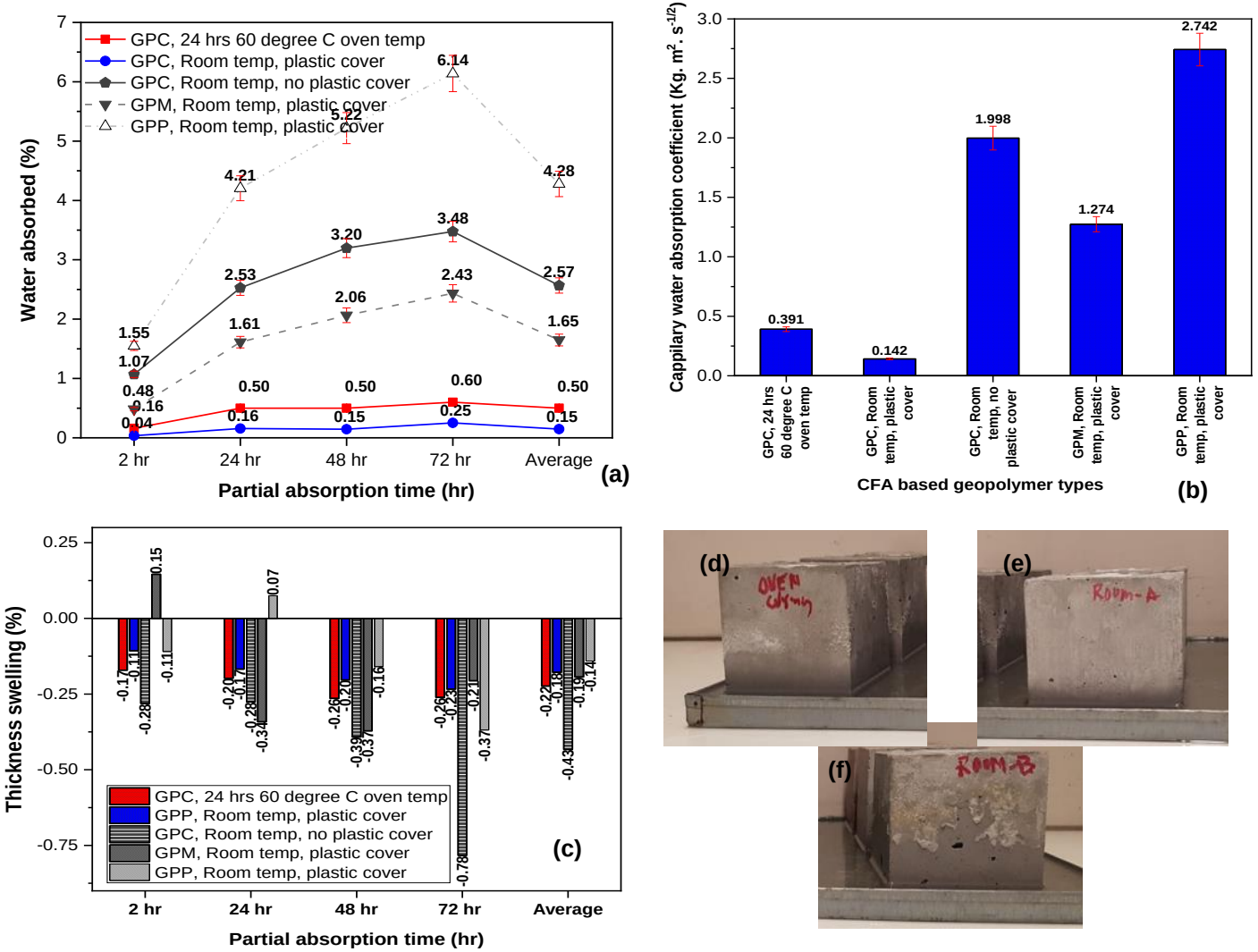

Figure 4-24: CFA-based geopolymer capillary water absorption results; water absorbed (a), capillary water absorption coefficients (b), thickness swelling (c) and types of curing regimes samples surface finish after capillary water absorption; oven curing samples (d), room with plastic cover (e) and room without plastic cover (f).

The addition of fine and coarse aggregates and curing regimes were investigated on a CFA-based geopolymer in a water sink medium containing water at 13.6 ±1 ^{o}C temperature and 60 ± 7.6 % relative humidity, as shown in Figure 4-24 (d to f). It was observed that the GPP-M2A (GPP) was absorbing more water under the capillary water absorption test, as illustrated in Figure 4-24 (a). The results obtained are similar to Sengun et al. (2014). The capillary water absorption coefficient, as shown in Figure 4-24 (b), was again high with GPP-M2A formulations. In Figure 4-24 (c), the swelling took place at 2 hr of absorption in the case of CFA-based GPM-M2A and after 24 hrs for CFA-based GPP. At the end of 72 hours of being partially immersed in water, efflorescence was observed, as shown in Figures 4-24 (d, e and f).

4.4.3 Carbonation depths and pH measurements

The carbonation depth and pH measurements were conducted to investigate the effect of carbon ingress in CFA-based geopolymer formulations. The technique was described in Section 3.5.3.4, and the non-carbonated area was CFA-based GPM, GPM, and GPC cured at toom with plastic, and GPC cured at an oven temperature of 60 ^{o}C and the room without the plastic cover. The results of this experiment are shown in Figure 4-25.

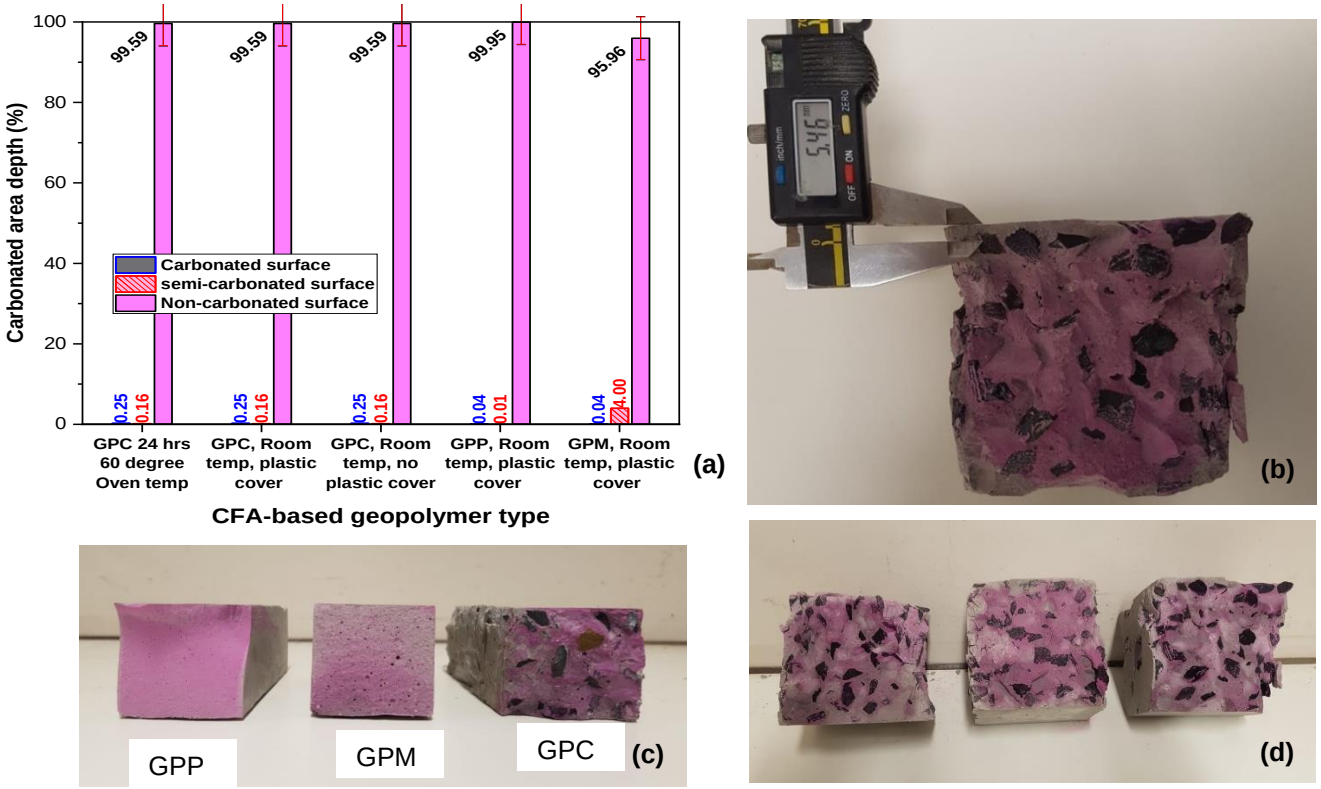

Figure 4-25: CFA-based geopolymer types carbonation and pH results; carbonation depth measurement (a) and effect of phenolphthalein carbonation CFA-based GPC sample during measurement (b), GPP, GPM and GPC cured at the room with plastic cover (c), curing regimes; oven curing sample, room with plastic cover and room without plastic cover (d).

A strong relationship between concrete carbonation depths that are exposed in natural and accelerated environments has been reported (Khunthongkeaw et al., 2006). Carbonation naturally occurs throughout the ageing process of concrete, causing reinforcement corrosion. Calcium carbonate (CaCO3) is formed during carbonation, and pH (around 13) decreases to 9. Due to the reduction in pH, the passive layer of reinforcement can be destroyed. Due to this, construction material with carbonation penetration has emerged as a significant durability issue in the urban environment (Yoon et al., 2007).

All the samples resulted in a non-carbonation depth of about 95.96 to 99.59 %, as shown in Figure 4-25 (a). The pH reading on the pH meter shown in Figure 3.26 of the paste was found to vary from 13.83 to 14. Figures 4-25 (b and d) illustrate the carbonation depth by visual observation after the spraying of phenolphthalein indicator to identify the carbonated, semi-carbonated and non-carbonated depths on CFA-based GPP-M2A, GPM-M2A, GPC-M2A cured at room temperature with plastic cover and GPC cured at oven temperature, room with plastic cover, no plastic cover curing temperatures.

4.4.4 Effect of curing regimes and fine and coarse aggregates on density change and drying shrinkage.

Shrinkage and density change of CFA-based geopolymer paste, mortar and concrete were determined as described in Section 3.53.5 under certain environmental temperatures and relative humidity shown in Figure 4-26 (b and d). The shrinkage and density variating over product ageing are shown in Figure 4-26 (a) and Figure 4-26 (c), respectively.

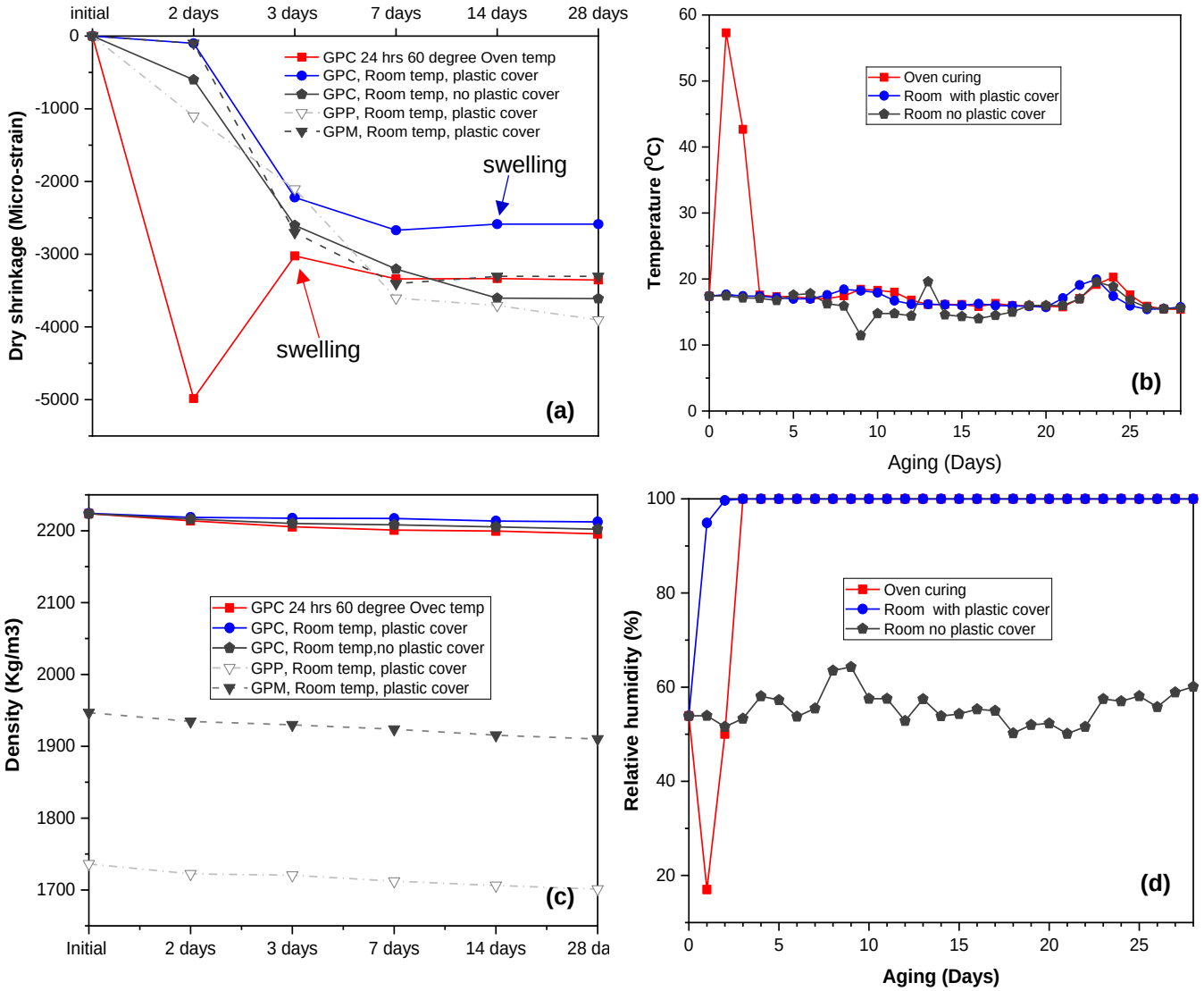

Figure 4-26: Effect of fine and coarse aggregate and curing regime on CFA-based geopolymer types; dry shrinkage (a), density change (c), medium temperature (b) and relative humidity (c).

A high shrinkage value was observed from GPC-M2A cured in an oven at two days (24 hours) of oven removable, after which the block's shrinkage value is reduced by swelling due to its cooling at room temperature as shown in Figure 4-26 (a). Room curing samples mostly swelled at 14 days, after which they stabilised. Compared to Waldmann et al. (2017), the shrinkage results in concrete are better with blocks cured at room temperature with a plastic cover.

All specimens' densities decreased slightly, as shown in Figure 4-26 (c).

4.4.5 Fire resistance test

A fire test was performed to predict the fire behaviour of material made from CFA-based geopolymer reinforced concrete panel cast with GPC-M2C formulation. The technique used was described in Section 3.5.3.6. Table 4-10 lists a description of physical observation during the test from the unexposed (U) and exposed (E) product fire explosion side.

Table 4-10: Panel testing description of visual observation at specific timing

Time, min	Description	Observation face or side	Figure 4-21
1	Test started	U	a
10	Evaporation of water via the initial thermal curing racks (water egress)	U	b
25	Observation of sealant lines on the panel	U	c
42	0.84 mm centre deflection measured	U	d
50	Reinforced steel reaches an average temperature of 232.6 ^{o}C and 2.80 mm centre deflection measured	U	-
53	The disappearance of sealant lines	U	-
59	About 130 mm crack long measured when reinforced steel reached 341.95 ^{o}C	U	f
65	Steel reinforcement was assumed to reach a failing temperature of 375 ^{o}C as 378.8 ^{o}C was obtained at 65 minutes	E	-
65	Data logger stopped	E	h

U=unexposed; E=exposed

The testing observation results are summarised in Table 4-10. Figure 4-27 (a) represents the fire-burning behaviour of CFA-based geopolymer concrete compared with the ISO standard burning curves. Figure 4-27 (a to o) lists the material's physical deterioration behaviour illustrated in Table 4-10.

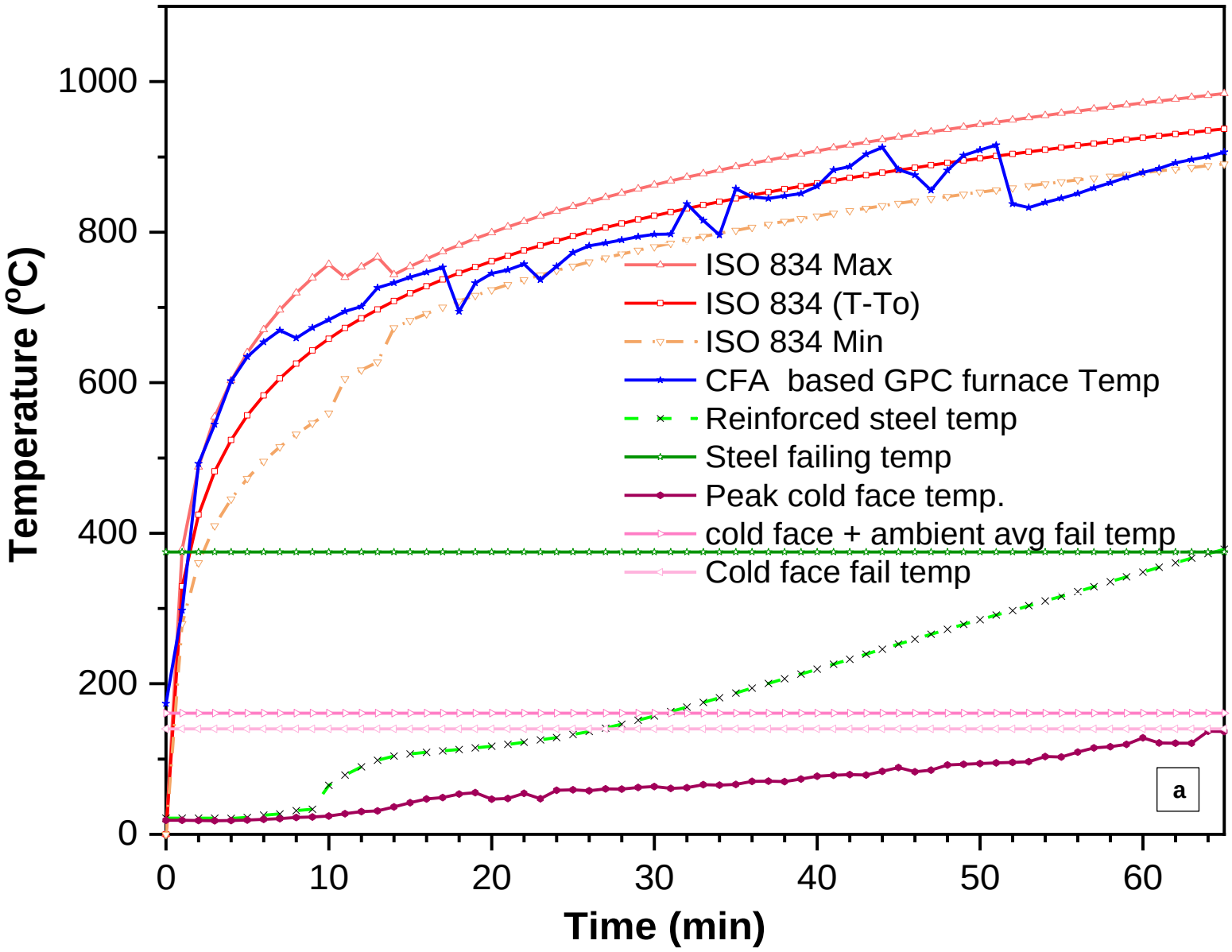
Temperature (°C)
Time (min)
0
200
400
600
800
1000
0
10
20
30
40
50
60
ISO 834 Max
ISO 834 (T-To)
ISO 834 Min
CFA based GPC furnace Temp
Reinforced steel temp
Steel failing temp
Peak cold face temp.
cold face + ambient avg fail temp
Cold face fail temp
a

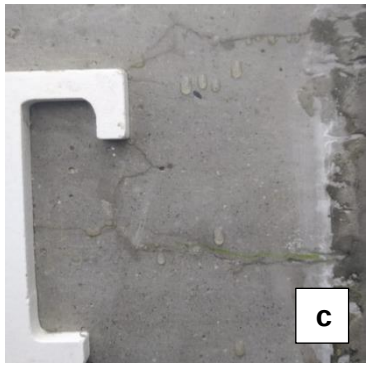

Panel during fire at 10 min (U)

Liquid sealant appearance (U)

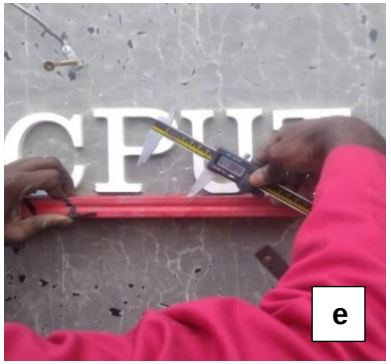

Deflection measurement (U)

Flame behaviour Inside fire oven observation (E)

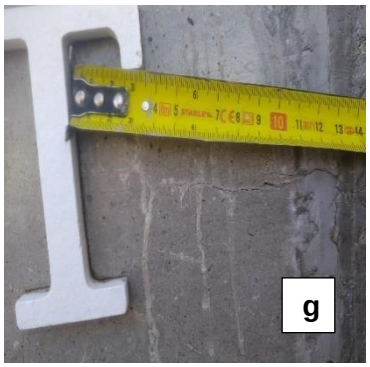

Crack measurement at 59 min (U)

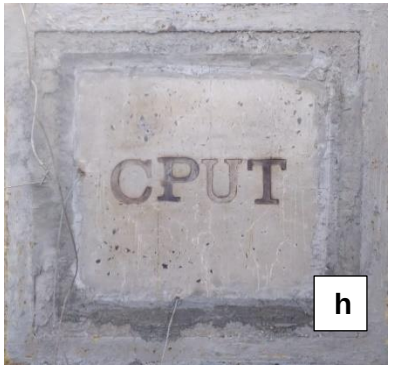

Panel at the end of the test (U)

Wooden board fixed on panel at the end of test.

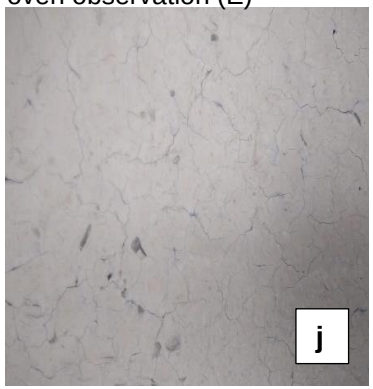

Panel fire exposed surface at the end of the test (E)

Cracks of 0.2 mm observed exposed surface (E)

A crack with width of 0.5 mm from unexposed surface (U)

Unexposed surface of the panel after being demoulded from fire oven (U)

Steel measurement from the demolished panel (U)

Steel observation after destroying the panel with hammer.

Figure 4-27: CFA-based reinforced geopolymer concrete Testing temperature profile in comparison with ISO 834 temperature (a), test set up (b) and the behaviour of the material during and after fire testing (c).

Due to improper plastic cover during the first 24 hours of curing, thermal curing cracks were absorbed on the panels, from which, during the fire, water egress was observed at about 10 minutes of explosive on the unexposed surface. A hammer was used to destroy the panels at the end of the test to observe the behaviour of the steel, which showed no signs of degradation. The panel partially failed on stability at around 64 minutes (1hr04min), and at 65 minutes, the average light-weight steel temperature reached 378.8 ^{o}C, which is more than the required 375 ^{o}C without 50% deflection of wall thickness. This failure may be understandable for the 50 mm panel thickness design, whereas, for a 100 mm thickness, this could not happen. The failure criteria time was reported as shown in Table 4.11.

Table 4-11:CFA-based geopolymer reinforced concrete panel fire failure evaluation criteria.

Criteria	Failure description	Time of failure, min
Stability	Reinforced steel reached 375 ^{O}C	64
Integrity	No cracks of 6 mm with a 150 mm length were observed	65+
Insulation	No 140 ^{o}C or 180 ^{o}C plus the ambient temperature was reached	65+
Pollution observation	No pollutant gases were observed	65+

4.5 Demonstration products

Demonstration products manufactured using CFA-based GPC (GPC-M2A formulation), such as a 600 x 600 x 60 mm precast panel tested for fire test, are shown in Figure 3.29. Furthermore, paving blocks and small pipes were cast in this study, as shown in Figure 4.28 and Figure 4.29, using GPP-M2A and GPC-M2A formulations, respectively.

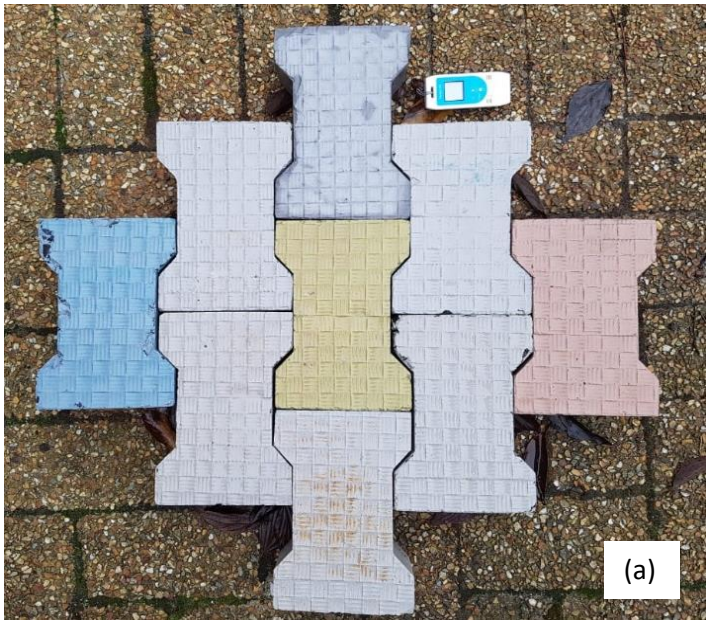

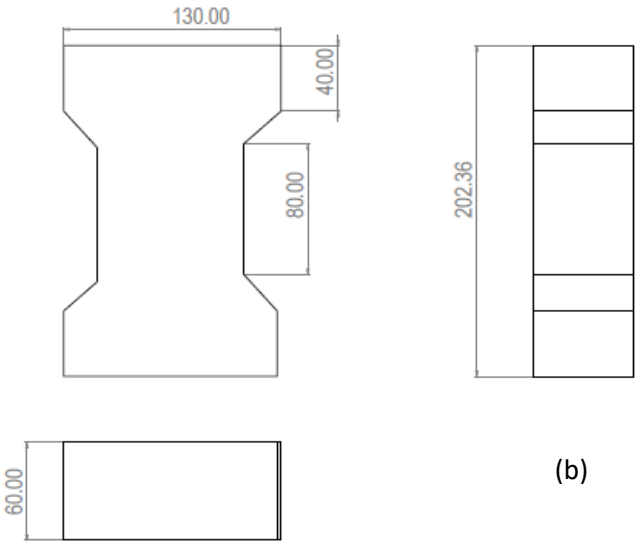

Figure 4-28: CFA-based geopolymer concrete paving blocks (a) as demonstration product and its dimensions design in mm (b).

Figure 4-29: CFA-based geopolymer paste demonstration pipe cast

4.6 Chapter Summary

The paste GPP-M3A and GPP-M2A formulations resulted in an acceptable set setting time and flow properties complying with the standards values, as shown in Table 3.5. Mechanical properties showed improvement in strength with an increase in sodium hydroxide. However, this also delays the setting time. A high concentration may also affect the cost and CO2 emissions of the product depending on the concentration used. Additional fine and coarse aggregates added to CFA-based GPP (GPP-M2A) to form CFA-based GPC (GPC-M2C) enhance the ductility despite the high-density increase. The oven curing at 60 ^{o}C process resulted in early high-compressive strength materials compared to both room curing regimes of room curing with a plastic cover and room curing without a plastic cover.

On the other hand, the durability properties such as water absorption, penetration, and carbonation complied with the testing standards value listed in Table 3-5, except that heavy efflorescence was observed with room temperature curing without a plastic cover process which was related to thermal cracking during hydration as illustrated by SEM analysis. High early shrinkage and slight efflorescence were observed in samples cured at 60 ^{o}C of oven curing temperature. One hour after exposure to fire, CFA-based geopolymer concrete showed better fire resistance properties, as described in Section 4.4.5. The results of fineness on CFA demonstrated that most of the particles are less than 100 µm. From XRF analysis, the CFA used is classified as low-class F, with a crystalline structure containing quartz and mullite minerals, as revealed by XRD. CFA-based geopolymer formulations also presented a crystalline structure with the presence of quartz and mullite identified from CFA. In most formulations, unreacted CFA was observed, but this may not be a concern since it is marginal, and no complete homogeneity exists. The next chapter may compare the effects of room-curing regimes with oven-curing regimes for environmental analysis and impact assessment.

Chapter 5

Development of geopolymer for construction application using coal fly ash: Life Cycle Assessment

An overview of the methods used to environmentally assess the impacts of Lethabo low CFA-based geopolymer products in construction applications and the sustainability aspect of the product or its production considering the impacts of climate change was assessed through the life cycle analysis method. The goal and scope and other evaluation steps are defined in this Section as they depend on the material properties, such as strength obtained in Chapter 4.

5.1 Goal and scope of the study:

5.1.1 Goal

The goal of LCA in this study was to perform an environmental impact assessment comparison in terms of Global warming potential, land emissions and water scarcity on the synthesis of CFA-based GPP formulations cured at an oven temperature of 60 ^{o}C for 24 hours compared to room curing process including an evaluation of the effect of aggregate addition on CFA-based GPC

5.1.2 Scope

The scope of LCA in this study was considered gate-to-gate (limited at the laboratory scale) as no industrialisation has yet occurred.

5.1.3 Functional Unit

1 Kg as a functional unit of each CFA-based GPP either cured at 60 ^{o}C in an oven for 24 hours, on GPP cured at room temperature and CFA-based GPC cured at room temperature product of a specific compression strength of 35 - 40 MPa with better durability properties are discussed.

5.1.4 System boundary

The system boundary involves transporting CFA and alkali chemicals, including fine and coarse aggregates, at specific distances from the suppliers to the laboratory. Figure 5.1 illustrates the system boundary conditions.

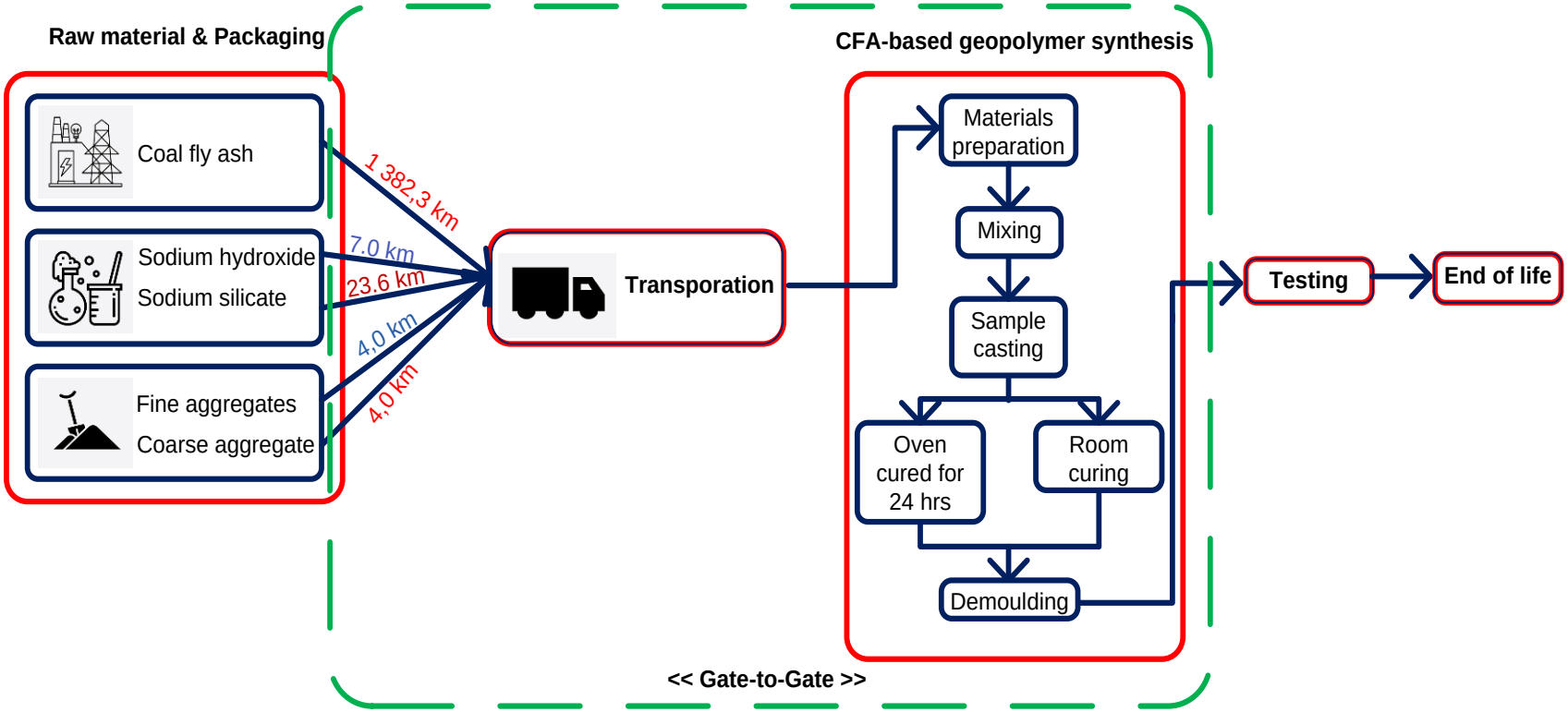

Figure 5-1: Synthesised CFA-based geopolymer paste and concrete gate-to-gate system boundaries

The system boundary condition represented in Figure 5-1 includes the preparation of the necessary reagents for the manufacture of GPP and GPC. Emissions associated with the extraction and packaging of raw materials were not taken into account since this requires further investigation from suppliers

5.1.5 Allocation

No allocation to waste has been considered from the geopolymer synthesis in this project since the system contains no by-products.

5.2 Life cycle inventory analysis and assessment method

5.2.1 Inventory analysis

The inventory analysis was described in Section 3.6.2, from which materials and energy required as inputs from each boundary phase are illustrated in the following diagram in Figure 5-2.

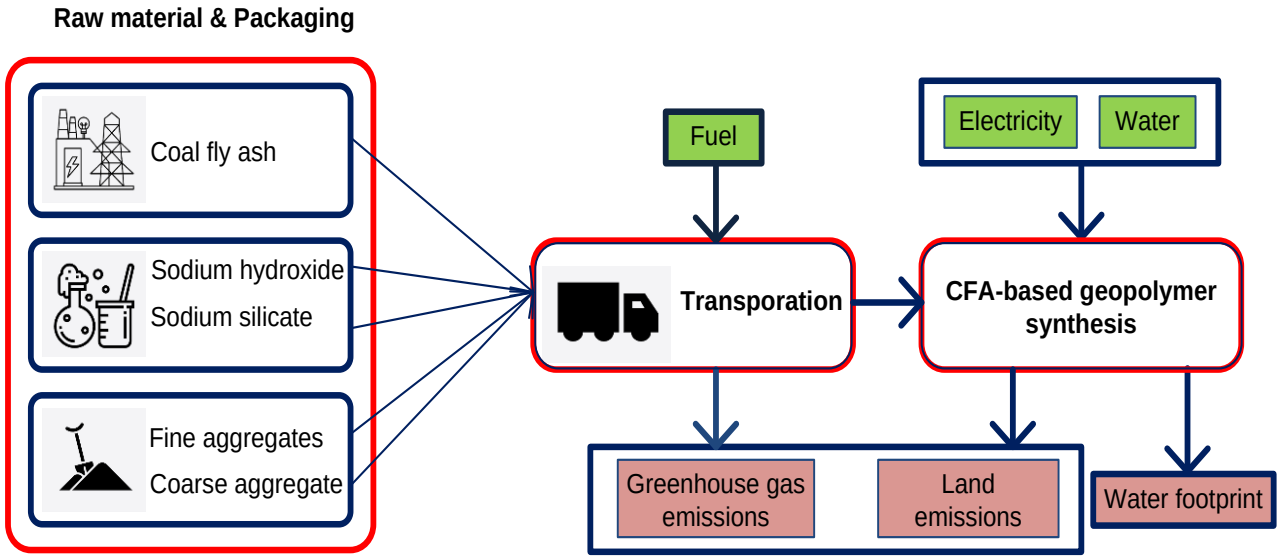

Figure 5-2: CFA-based geopolymer paste and concrete material and energy types used at different stages of the process.

The energy or materials used at each phase were responsible for certain emissions, as illustrated in the diagram, which was similar to Colangelo et al. (2018).

5.2.2 Assessment method

As discussed in Section 3.6.2, the environmental product declaration in SimaPro was listed as EPD (2018) V1.02/ Character.

5.3 Life cycle impacts assessment

The different impact categories assessed in this Section were illustrated in Table 3.9 under Section 3.6.3. However, global warming potential (CO_2 emissions) is mainly compared between different curing regimes and includes the effect of adding fine and coarse aggregates on synthesised CFA-based GPC.

5.4 Life cycle interpretation

The environmental impacts generated by the life cycle analysis of the 1 Kg of each CFA-based product (GPP-M3A formulation cured at 60 ^oC oven for 24 hours; GPP cured at room; GPC-M2C formulation cured at room temperature) at a specific compression strength of 35 to 40 MPa, were simulated using SimaPro. The results obtained are described as two case studies as follows:

5.4.1 comparative analysis

The emissions factor obtained from SimaPro based on a specific impact category for CFA-based geopolymer formulations developed and cured at 60 ^oC in an oven for 24 hours, GPP cured at room, and CFA-based GPC cured at room temperature and with the addition of fine and coarse aggregates are shown in Table 5.1.

Table 5-1: Summary of comparative LCA results from CFA-based GPP oven cured at 60 ^oC for 24 hours versus GPP or GPC cured at room temperature.

Impact category	Unit	CFA-based		
		GPP 24 hrs, 60 degree C oven curing	GPP room curing	GPC room curing
Acidification (fate not incl.)	kg SO_2 eq	0.10100	0.00375	0.00202
Eutrophication	kg PO_4 eq	0.0256	0.0011	0.000605
Global warming (GWP100a)	kg CO_2 eq	0.8940	0.0537	0.029
Photochemical oxidation	kg NMVOC	0.04710	0.00276	0.00135
Abiotic depletion, elements	kg Sb eq	1.02E-05	1.00E+00	1.02E-05
Abiotic depletion, fossil fuels	MJ	249	140	47.1
Water scarcity	m^3 eq	0.684	0.163	0.094
Ozone layer depletion (ODP) (optional)	kg CFC-11 eq	9.49E-08	1.00E+00	9.49E-08

Based on the curing regimes, it was observed that GPP cured at 60 ^oC for 24 hours had higher environmental pollution from global warming (CO_2), water scarcity (water footprint) and Abiotic depletion, fossil fuels and other impact categories compared to GPP cured at room temperature. These results are a sign of correct simulation as the oven-curing process in the case of South African energy production is related to the emissions of coal burning and more water being required from electricity production at the turbine stage. The energy required to produce oven

curing should also be higher since it takes into consideration the mixing and drying process of 24 hours. The addition of fine and coarse aggregates was furthermore responsible for reducing the emissions of the room curing process when producing GPC. This is understandable as raw materials such as fine aggregates (sand) and coarse aggregates (stone) are naturally available and absorb less water as well as require less energy to obtain compared to CFA. A comparison of CO_2 emissions of the geopolymer factor in Table 5.1 with that of OPC concrete of 0.132 kg CO_2 eq (132 kg CO_2 eq per tonne) obtained from the UK Government GHG Conversion Factors for Company Reporting (Conversion factors 2022: full set (for advanced users) (Available at: https://www.gov.uk/government/publications/greenhouse-gas-reporting-conversion-factors-2022, Accessed on the 25th October 2022) or that of 0.15 kg CO_2 eq (Available at: https://www.winnipeg.ca/finance/findata/matmgt/documents/2012/682-2012/682-2012_Appendix_H-WSTP_South_End_Plant_Process_Selection_Report/Appendix%207.pdf, Accessed on the 25th October 2022). Furthermore, Table B-1 shows the CO_2 emission factor of different construction materials. This shows that CFA-based-GPP cured at 60 ^{o}C in an oven for 24 hours is about 6.8-7.7 times higher in the CO_2 emitted than normal concrete made with OPC cement and fine and coarse aggregates (assuming no transportation emissions). When curing at room temperature and adding fine and coarse aggregates, OPC concrete turns out to be 2.4-2.7- and 4.5-5.1-times higher CO_2 emitted than CFA-based GPP cured at room temperature and CFA-based GPC cured at room temperature, respectively. Taking GPP cured at 60 oC in an oven for 24 hours as a reference product, these emissions from different curing regimes and the addition of fine and coarse aggregates were compared and illustrated in Figure 5.3.

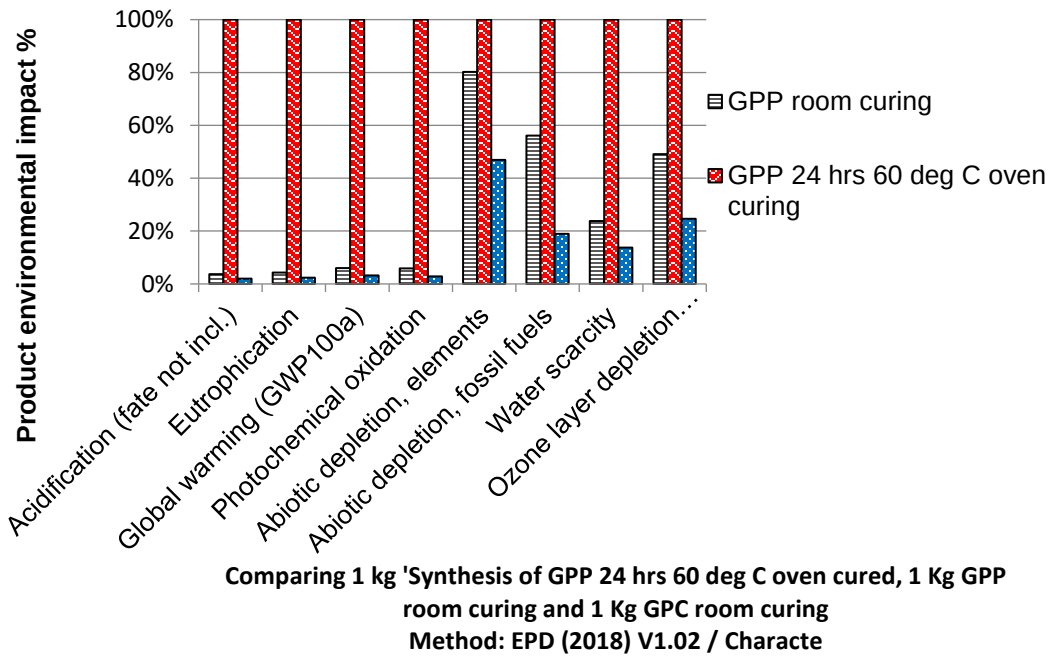

Figure 5-3: Comparison of different environmental impacts at 1 kg production CFA-based GPP oven cured at 60 ^{o}C for 24 hours versus GPP or GPC cured at room temperature.

5.4.2 Contribution analysis

Contributions analysis on global warming (CO_2) was further investigated to understand the effect of curing regimes and adding fine and coarse aggregates on CFA-based geopolymer CO_2 emissions. This was simulated to identify the most environmentally emitted CO_2 Section from the study boundary.

5.4.2.1 Effect of curing regimes

The effect of curing regimes was investigated from the synthesis of CFA-based GPP, which was oven-cured at 60 ^{o}C for 24 hours and room curing process (covered and non-plastic covered assumed to be the same).

i. Oven curing temperature

The synthesis of 1 kg CFA-based GPP when oven-cured at 60 ^{o}C was observed to be high carbon emitting, with results shown in Table 5.1. A deeper investigation is illustrated in the following Figure 5.4.

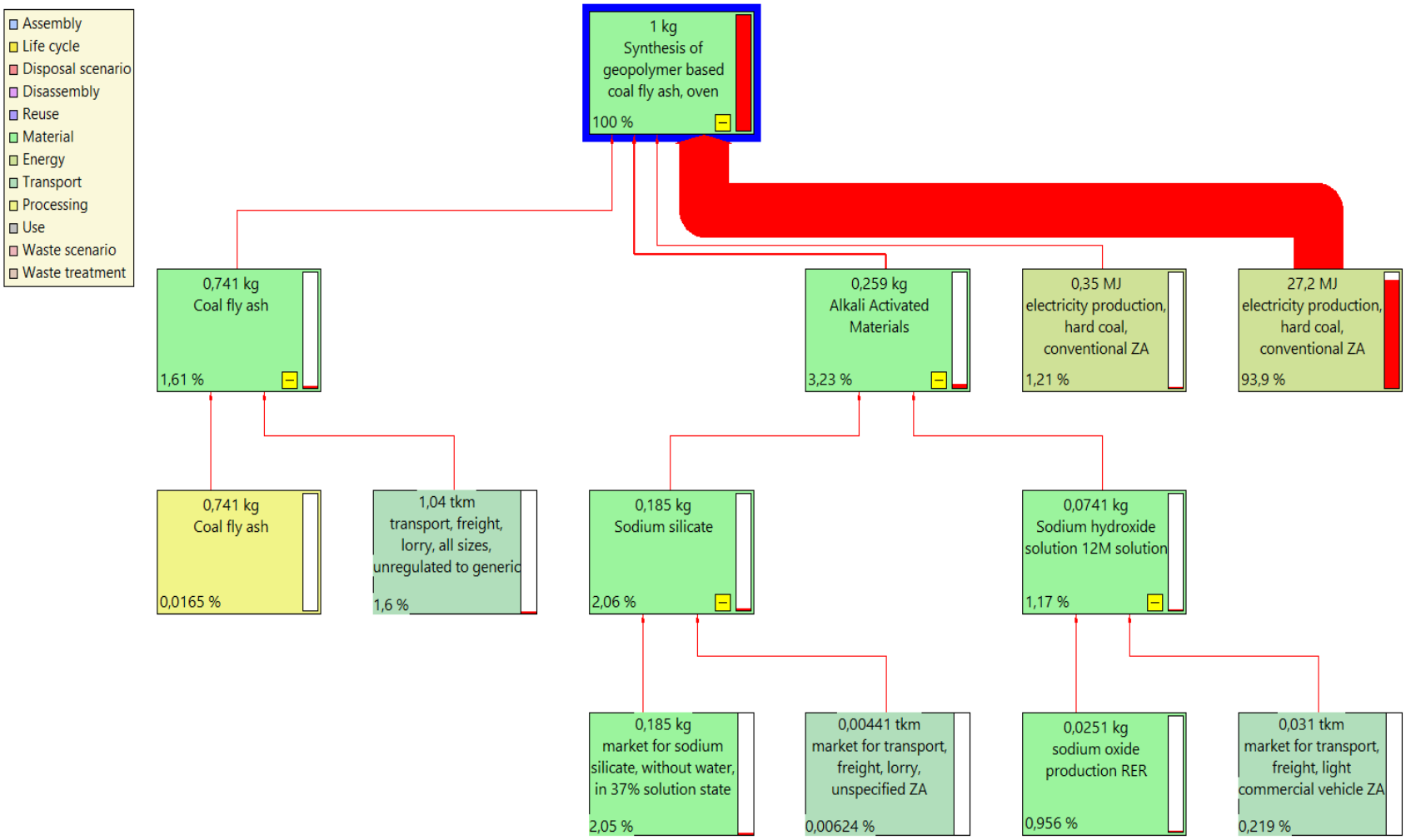

Figure 5-4: Process tree illustrating relative contributions to CO_2 emissions in the life cycle for a production of 1kg CFA-based GPP oven cured at 60 ^oC 24 hours.

In Figure 5-4, it is demonstrated from the simulation that 93.9% of CO_2 emissions associated with the oven curing process have resulted when coal power energy is used as a source of electricity for the performance of the oven as a dryer. About 3.23%, which is a nominated number, of results from alkaline activators were used.

ii. Room curing temperature

When cured at room temperature, the synthesis of 1 kg CFA-based GPP formulation was found to be environmentally acceptable. However, a deeper investigation of CO_2 emissions without the oven-curing process is illustrated in the process tree in Figure 5.5.

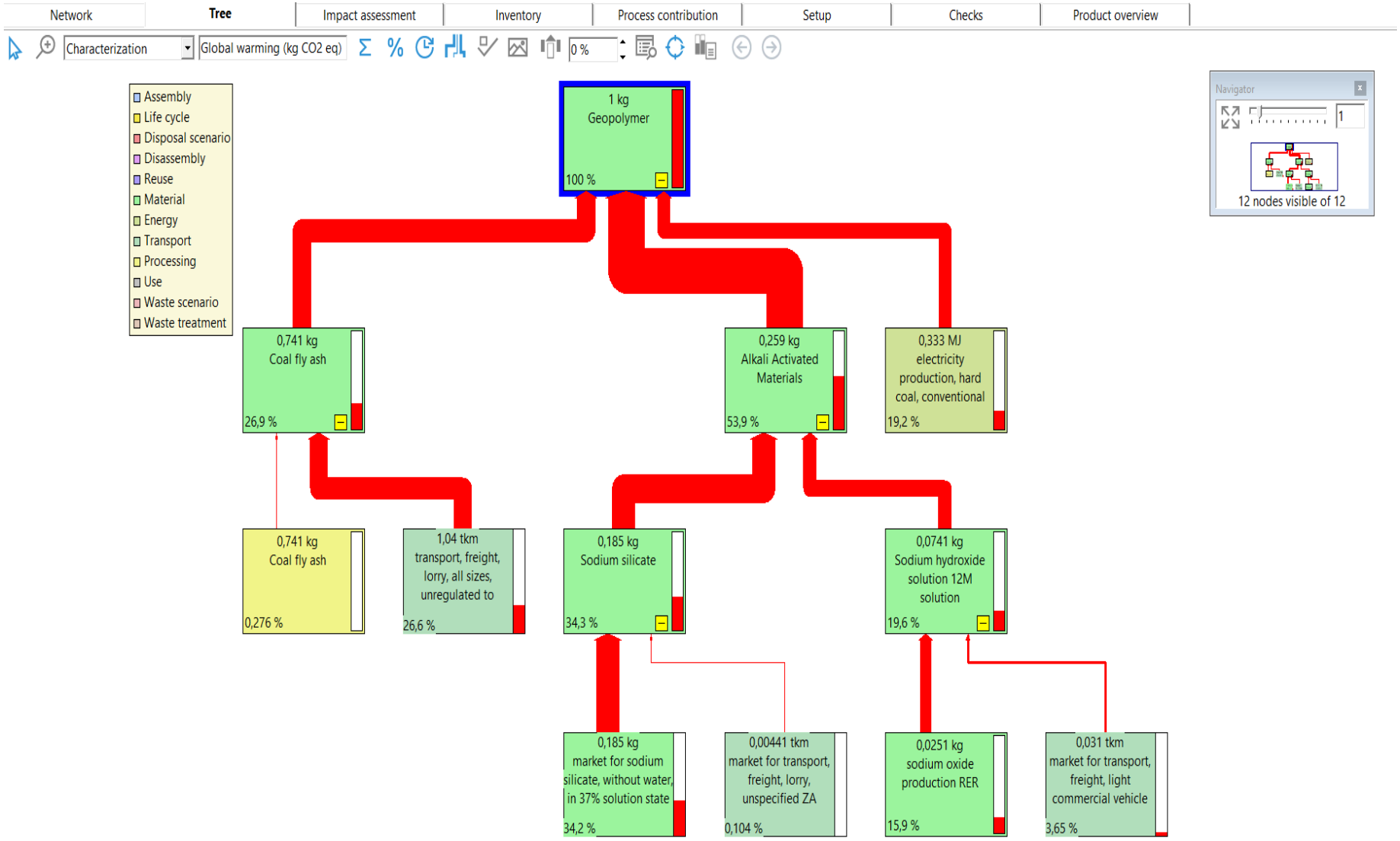

Figure 5-5: Process tree illustrating relative contributions to CO_2 emissions in the life cycle for producing 1kg CFA-based GPP cured at room temperature.

The room-curing process is more stable than when the oven-curing process is applied. The high CO_2 emission contribution is observed from an alkaline chemical, which is a combination of sodium silicate and sodium hydroxide, taking about 53.9% of the total process emissions, followed by 26.9% as illustrated in Figure 5.1, which is related to the transportation of CFA from long collection distance. The 19.2% of power consumption from electricity was due to the mixing process mixing and drying taking place. A future investigation was on the effect of adding fine and coarse aggregates on the curing process

5.4.2.2 Effect of fine and coarse aggregates

Adding fine and coarse aggregates to CFA-based GPP to synthesise 1 kg CFA-based GPC when cured at room temperature resulted in a similar CO_2 emissions percentage contribution in the process compared to that observed from CFA-based GPP. Figure 5-6 illustrates the process tree.

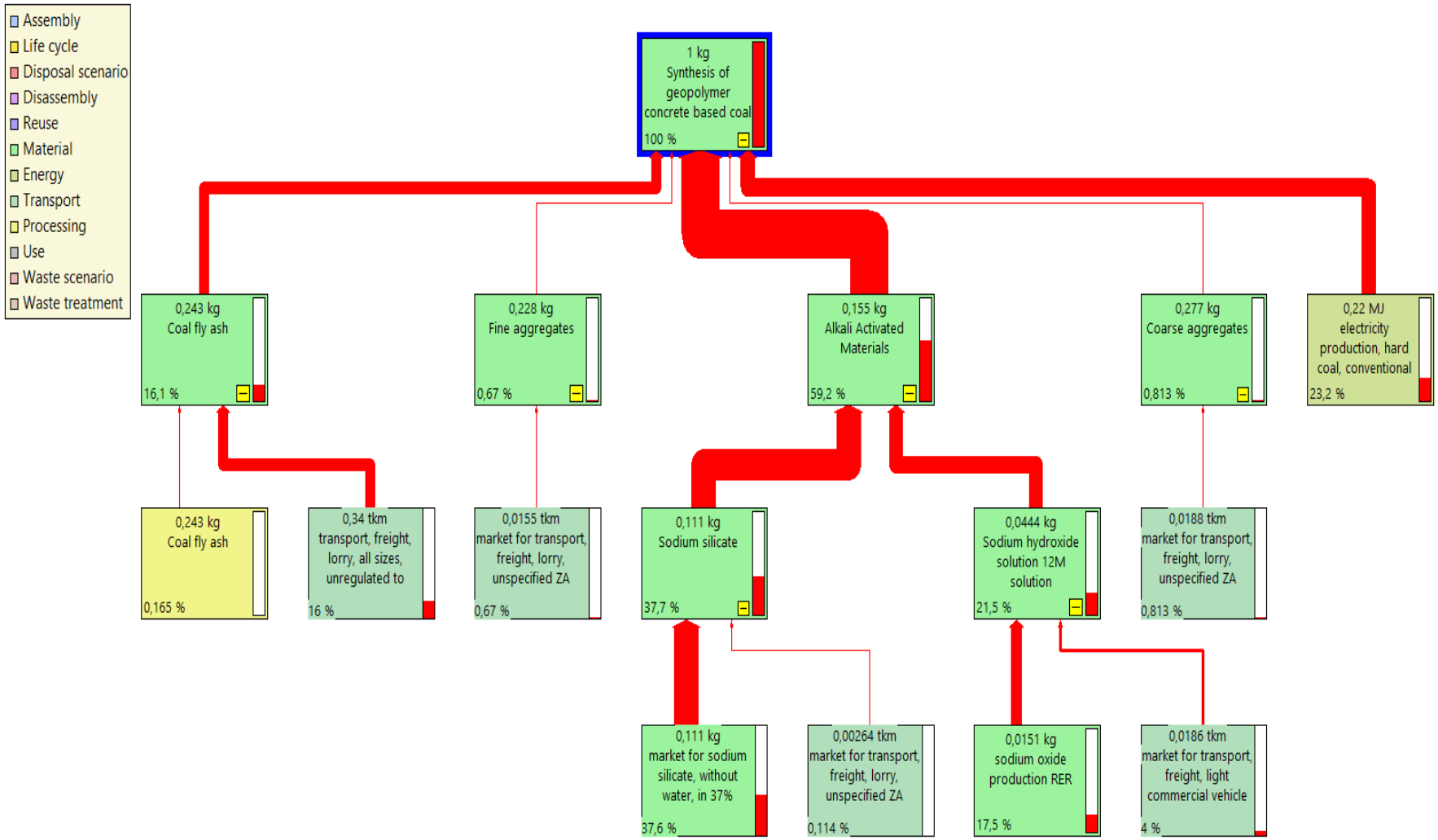

Figure 5-6: Process tree illustrating relative contributions to CO_2 emissions in the life cycle for the production of 1 kg of CFA-based GPC cured at room temperature.

It can be observed from Figure 5-6 that Alkaline activator chemicals are still the cause of the majority of CO_2 emissions emitted during the process at about 59.2%. Here, the electricity stream with 23.2% used becomes the second dominant stream compared to the transportation of CFA observed in Section 5.4.2.1ii. This is because, generally, when the fine and coarse aggregates are added to a paste (GPP), the mix becomes heterogeneous with high viscosity. Therefore, additional mixing time is required to obtain a homogeneous mix with a low viscosity.

5.5 Chapter Summary

Even though CFA-based geopolymer cured at an oven temperature of 60 ^{o}C for 24 hours results in a very good early compressive strength, greenhouse emissions simulations analysis demonstrated that the process is not sustainable in comparison to the conventional existing process of making construction materials with the use of OPC cement. On the other hand, the room-curing process is far more sustainable than oven curing and better than the conventional process of using OPC cement as a binder. However, this process may also be affected if raw materials such as CFA and others are collected from a long distance from the manufacturing plant. The emission associated with the alkaline activator materials must be controlled by setting a close collection from the manufacturing area or by substituting materials with similar properties. Again, the impact associated with the oven-curing process may be verified through the energy consumption and economic analysis from the next chapter.

Chapter 6

Development of geopolymer for construction using coal fly ash: Materials and Energy balances and Economics

Apart from mechanical, durability and environmental properties obtained from previous chapters, a better understanding of fundamental material chemistry composition, a relation between heat due to the temperature used, work and energy, as well as the cost associated with the manufacturing process of synthesised CFA-based geopolymer was subject to investigation.

6.1 Material balance

Material balance was performed to determine the composition of each stream. Considering the molecular species balance method, the main molecule species variation reviewed during calculations for the synthesis and drying processes were silicate oxide (SiO2), aluminium oxide (Al2O3), sodium oxide (H_2O) and water (H_2O) from raw material (RM) content to the streaming product (output) content. At the same time, full compositions, including other components, are shown in Table 6.1. Figure 6.1 illustrates the system boundary considered for the calculation.

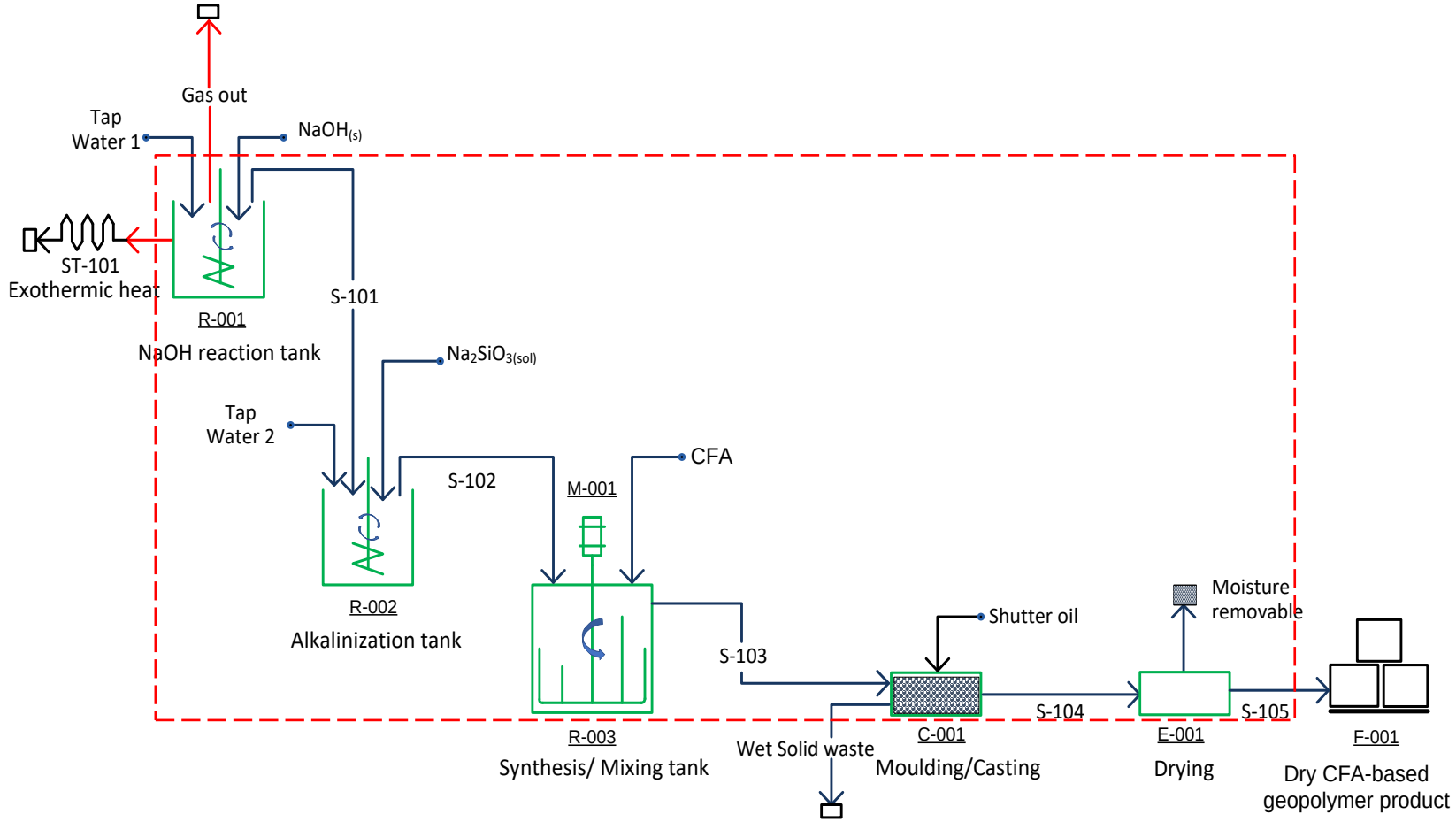

Figure 6-1: CFA-based geopolymer paste overall material balance block flow diagram system boundary.

Table 6-1: CFA-based geopolymer paste material balance stream composition on a mass basis.

Time Ref: Batch		**Water 1**	**Sodium hydroxide flakes**	**12M Sodium hydroxide solution**	**Sodium silicate solution**	**Water 2**	**FA**	**Gas out**	**S-101**	**S-102**	**S-103**	**S-105**
Type	Unit	RM	RM	RM	RM	RM	RM		RM	Ouput2	Ouput3	Ouput5
Total flow	g	975.43	480.00	1420.00	466.67	120.00	2000.00	35.43	253.33	840.00	2840.00	2817.44
Temperature	°C	17.00	17.00	90.00	17.00	17.00	17.00	40.00	17.00	27.00	25.00	25.00
Pressure	bar	1.013	1.013	1.013	1.013	1.013	1.013	1.013	1.013	1.013	1.013	1.013
Moisture content	%	100.00	1.00	67.35	60.80	100.00	0.00	-	67.35	68.38	20.29	4.05
Total contents	**g**	**975.43**	**480.00**	**1420.00**	**466.67**	**120.00**	**2000.00**	**35.43**	**253.33**	**840.00**	**2840.00**	**2817.44**
SiO_2		0.00	0.00	0.00	140.00	0.00	1096.20	0.00	0.00	140.00	1236.20	1524.24
Na_2O		0.00	475.20	463.63	42.93	0.00	3.06	0.00	82.71	125.65	128.65	70.72
Al_2O_3		0.00	0.00	0.00	0.00	0.00	655.2	0.00	0.00	0.00	655.20	471.08
CaO		0.00	0.00	0.00	0.00	0.00	82.80	0.00	0.00	0.00	82.80	260.90
Fe_2O_3		0.00	0.00	0.00	0.00	0.00	62.20	0.00	0.00	0.00	62.20	47.33
TiO_2		0.00	0.00	0.00	0.00	0.00	33.80	0.00	0.00	0.00	33.80	23.38
MgO		0.00	0.00	0.00	0.00	0.00	21.00	0.00	0.00	0.00	21.00	18.60
K_2O		0.00	0.00	0.00	0.00	0.00	14.00	0.00	0.00	0.00	14.00	13.52
P_2O_5		0.00	0.00	0.00	0.00	0.00	9.15	0.00	0.00	0.00	9.20	7.04
Cr_2O_3		0.00	0.00	0.00	0.00	0.00	0.80	0.00	0.00	0.00	0.80	0.56
MnO		0.00	0.00	0.00	0.00	0.00	0.62	0.00	0.00	0.00	0.60	0.56
V_2O_5		0.00	0.00	0.00	0.00	0.00	0.00	0.00	0.00	0.00	4.60	5.63
LOI		0.00	0.00	0.00	0.00	0.00	14.40	0.00	0.00	0.00	14.40	257.51
Gas out		0.00	0.00	0.00	0.00	0.00	0.00	35.43	0.00	0.00	0.00	0.00
H2O		975.43	4.80	956.37	283.73	120.00	0.10	0.00	170.62	574.35	576.35	114.11

RM represents Raw materials, while S-101, S-102, S-103, and S-105 are raw materials and product streams, as shown in Figure 6.1.

The final stream oxide results from the calculation were compared to the XRF analysis result. The calculation was performed on CFA-based geopolymer paste (GPP), as fine and coarse aggregate additives were considered inert materials. Equation 3.23 was initially used to determine the degree of freedom analysis, which indicated the possibility of performing the calculations based on each unit operation.

6.1.1 Alkaline activator and synthesis processes

Process units' calculations were fully demonstrated regarding fundamental material balance using Equation 3.24.

6.1.1.1 Alkaline activator solution preparation

The activator was prepared using 1 litre of a sodium hydroxide solution of 12M (see Table 3.4 for material requirement) in the reaction tank unit R-001 to obtain output 1 (shown as S-101 from the block flow diagram). The elements of the reaction were sodium hydroxide flakes (98% dehydrated, 2% assumed as water) and tap water 1. After cooling the prepared 12 M sodium hydroxide solution, sodium silicate (with composition illustrated in Table 3.1) was added to prepare the alkaline activator in the alkalinisation tank (unit R-002) to obtain the product composition from output 2 (S-102) in the process block flow diagram. A sample calculation in this process for the alkaline activator was done to obtain the molecular output composition for each stream input, as shown in Figure 6.2.

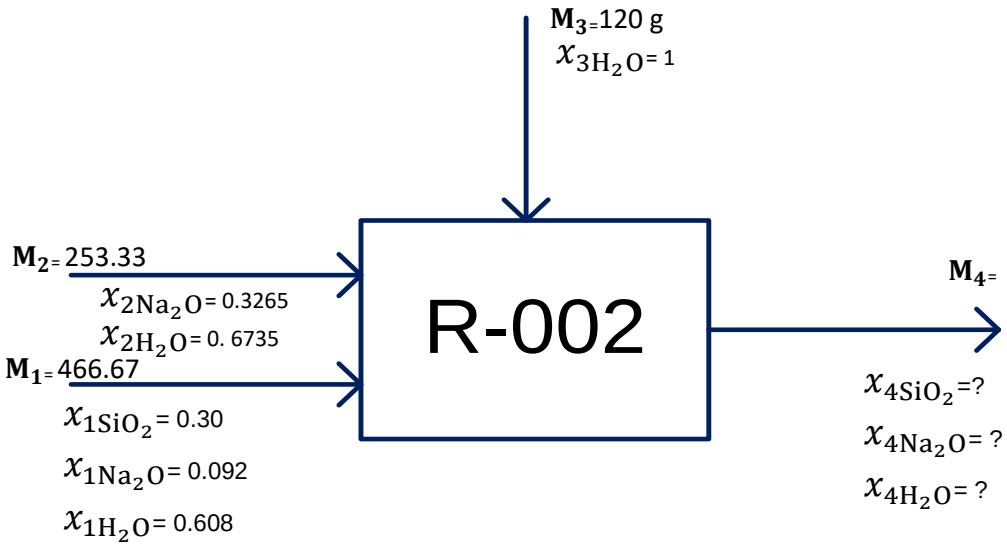

Figure 6-2: Alkaline activator preparation mass balance system boundary

From the above Figure 6.2 using Equation 3.23, the degree of freedom analysis was determined as follows.

+ 3 Unknown variables were labelled ($x_{SiO_2}, x_{Na_2O}, x_{H_2O}$)

0 independent chemical reaction assumed (no unique chemical compound formed)

- 3 independent molecular species balances (SiO_2, Na_2O, H_2O)

- 0 other equations relating unknown variables

DOF = 0

With these zero (0) degrees of freedom (DOF) obtained, it is, therefore, possible to perform material balance calculations around this alkalisation process following Equation 3.24, where the following assumptions were applied; therefore, the equation becomes simplified as Equation 6.1

a. Generation and consumption = 0 as no chemical reaction took place.
b. Assumption = 0 as the system is at a steady state, and in terms of diffusion, the concentration of the alkaline activator remains constant; as a result, the rate of diffusion remains constant.

$$Input = Output \qquad \text{Equation 6.1}$$

$$M_1 + M_2 + M_3 = M_4$$

Where: - M_1, M_2 , M_3 and M_4 are the masses of 12 M sodium hydroxide solution, sodium silicate, tap water 2 and alkali activator, respectively.

- $x_{SiO_2}, x_{Na_2O}, x_{H_2O}$ are the mass fraction of silicate oxide, sodium oxide and water, respectively.

$$M_4 = 253.33 + 466.67 + 120 = 840\ g$$

- For silicate oxide mass fraction, the final product.

$$x_{2SiO_2} \times M_2 = x_{4SiO_2} \times M_4$$

$$x_{4SiO_2} = \frac{0.3 \times 466.67}{840} = 0.1667 = 16.67\%$$

- For sodium oxide

$$x_{1Na_2O} \times M_1 + x_{2Na_2O} \times M_2 = x_{d4O} \times M_4$$

$$x_{4Na_2O} = \frac{(0.092 \times 466.67) + (0.3265 \times 253.33}{840} = 0.1496 = 14.96\%$$

- Water fraction

$$x_{1H_2O} \times M_1 + x_{2H_2O} \times M_2 + x_{3H_2O} \times M_3 = x_{4H_2O} \times M_4$$

$$x_{4H_2O} = \frac{(0.6838 \times 466.67 + 0.6735 \times 253.33 + 1 \times 120)}{840} = 0.6838$$

These mass fractions are then multiplied by the mass of the total content to obtain the mass of each oxide present in each stream, as shown in Table 6.1. In this case, the oxide mass is shown as follows.

$$\begin{cases} m_{4\mathrm{SiO_2}} = 0.1667 \times 840 = 140\ g \\ m_{4\mathrm{Na_2O}} = 0.1496 \times 840 = 126\ g \\ m_{4\mathrm{H_2O}} = 0.6838 \times 840 = 574\ g \end{cases}$$

6.1.1.2 From synthesis to dry product

In this synthesis process, the geopolymerization reaction was taken into consideration as the alkaline activator was responsible to break $Si-O-Si-O$ bonds. The mechanism forms $Si-O-Al-O-Si-O$ (aluminosilicate gels), which, by the addition of an alkaline activator, hardened into geopolymer paste similar to cement as shown in Equation 2.4. The overall material balance boundary was taken at this stage, as shown in Figure 6.3.

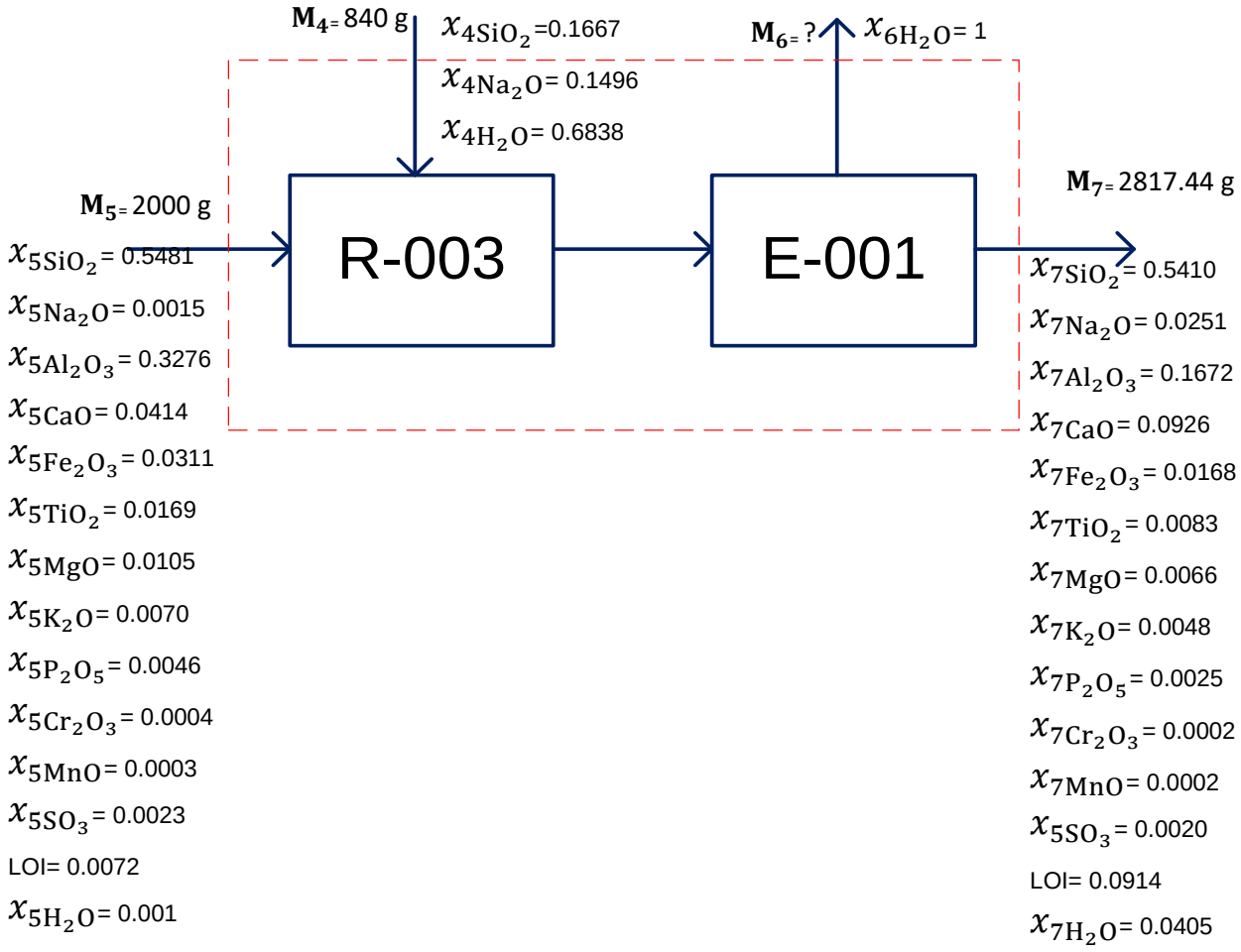

Figure 6-3: CFA-based geopolymer paste synthesis to final product material balance system boundary.

The stages from a wet material to a dry product were considered. The number of wet solids was negligible as the output streams S-103 and S-104 had the same oxide mass composition; therefore, only one stream is represented in Table 6.1.

Based on the XRF results obtained on the final product given in Table 6.2 and Figure 6.3 on M_7 output 5, the material balance at this stage was used to determine the consumed amounts of each oxide during the geopolymerization reaction. It is important to notice that oxides with a low mass fraction composition, such as SO_3, Cr_2O_3 and MnO, are considered in Table 6.2 as the values are much less and did not change from the raw material to the final product. The material balance sample calculation was not performed on those molecules; however, the results are fully shown in Table 6.1.

Table 6-2: Average CFA-based geopolymer product final product average XRF fractional mass composition results.

Oxide types	**SiO_2**	**TiO_2**	**Al_2O_3**	**Fe_2O_3**	**MgO**	**CaO**	**Na_2O**	**K_2O**	**P_2O_5**	**H_2O**
Mass fractional composition	54.10	0.83	16.72	1.68	0.66	9.26	2.51	0.48	0.25	4.05
Standards deviation	0.59	0.01	0.26	0.08	0.04	0.36	0.22	0.07	0.01	0.83

Here, Equation 3.24 was simplified into Equation 6.2 by taking into consideration the following assumption.

a. Generation was considered as zero (0) in most cases based on an oxide basis. As shown in Table 6.2 above, no additional oxide or molecule formation was observed compared to the initial raw material composition in Figure 6.3; however, some components were found to be consumed rather than generated. Any other product generated during the geopolymerization reaction may contain certain similar oxides based on the chemical structure. A negative consumption value from the material balance using Equation 6.2 will generally represent a generation term instead of consumption.

b. Assumption = 0 as the system is at a steady state.

$$Input = Output + Consumption \qquad \text{Equation 6.2}$$

$$M_4 + M_5 = M_6 + M_7 + Consumption$$

Where: - M_4, M_5 , M_6 and M_7 are the masses of alkaline activator, CFA, water and dry CFA-based geopolymer paste, respectively.

- $x_{SiO_2}, x_{Na_2O}, x_{H_2O}$ .....are the mass fraction of silicate oxide, sodium oxide and water, respectively.

- **Determination of M_6**

M_6, was related to the amount of water evaporated during the drying of CFA-based GPP. No generation term was considered at this stage.

$$M_4 + M_5 = M_6 + M_7$$

$$M_6 + consumption = (2000 + 840) - 2817.44 = 22.56g$$

- **For silicate oxide mass consumed.**

$$x_{4SiO_2} \times M_4 + x_{5SiO_2} \times M_5 = x_{5SiO_7} \times M_7 + consumption$$

$$consumption = 0.1667 \times 840 + 2000 \times 0.5481 - 2817.44 = -288.04\ g$$

This shows that the product of geopolymerization was mostly composed of silicate, as more silicate was generated than consumed.

- **For sodium oxide consumed**

$$x_{4Na_2O} \times M_4 + x_{5Na_2O} \times M_5 = x_{7Na_2O} \times M_7 + Consumption$$

$$Consumption = 0.1496 \times 840 + 0.0015 \times 2000 - 0.0251 \times 2817.44 = 57.93\ g$$

- **Aluminium oxide consumed**

$$x_{5H_2O} \times M_5 = x_{7H_2O} \times M_7 + Consumption$$

$$Consumption = 0.3276 \times 2000 - 0.1672 \times 2817.44 = 184.12\ g$$

- **Water mass consumed**

$$x_{4H_2O} \times M_4 + x_{5H_2O} \times M_5 = x_{6H_2O} \times M_6 + x_{7H_2O} \times M_7 + Consumption$$

$$Consumption = 0.6838 \times 840 + 0.001 \times 2000 - 0.0405 \times 2817.44 - 1 \times 184.43$$
$$= 439.69\ g$$

- **Calcium oxide mass consumed**

$$x_{5CaO} \times M_5 = x_{7CaO} \times M_7 + Consumption$$

$$Consumption = 0.0414 \times 2000 - 0.0926 \times 2817.44 = -178.10\ g$$

- **Iron oxide mass consumed**

$$x_{5Fe_2O_3} \times M_5 = x_{7Fe_2O_3} \times M_7 + Consumption$$

$$Consumption = 0.0311 \times 2000 - 0.0168 \times 2817.44 = 14.87\ g$$

- **Potassium oxide mass consumed**

$$x_{5\mathrm{K_2O}} \times M_5 = x_{7\mathrm{K_2O}} \times M_7 + Consumption$$

$$Consumption = 0.007 \times 2000 - 0.0048 \times 2817.44 = 0.48\ g$$

- **Loss of ignition variation**

$$x_{5\mathrm{LOI}} \times M_5 = x_{7\mathrm{LOI}} \times M_7 + variation$$

$$Consumption = 0.0072 \times 2000 - 0.0914 \times 2817.44 = \ -243.11\ g$$

Based on the calculated values obtained, compared with Chindaprasirt et al. (2013), the calcium oxide increase may be justified by the formation of secondary ettringite (delay ettringite) when a 12 M sodium hydroxide concentration was used. Regarding the XRD results shown in Section 4.1.4, a high increase of calcium oxide observed was due to the dissociation of calcium sulphate at peak position 22-2θ (degree), which generated the formation of calcium hydroxide. However, primary ettringite could be observed with a fresh paste and was considered as a product of hydration resulting from the reaction between aluminium oxide and sodium hydroxide or potassium hydroxide, resulting in the high heat of hydration. The analysed CFA-based geopolymer paste showed a pH value of 13 at that state. From the material balance, calculated masses of the consumed and generated oxides are allocated in the following Table 6.3

Table 6-3: Illustration of some oxides massed consumed or generated during the geopolymerization reaction.

Oxide types	SiO_2	TiO_2	Al_2O_3	Fe_2O_3	CaO	Na_2O	P_2O_5	H_2O	LOI
Mass consumed (g)	-	10.42	184.12	14.87	-	57.93	2.16	439.69	-
Mass generated (g)	288.04	-	-	-	178.10	-	-	-	243.11

The presence of high loss of ignition observed in the final product may be justified by the presence of plastic fibres in the product created during the synthesis process due to the friction caused by aggregate material on the plastic reactor tank at the end of the compression test when grinding samples for analysis, the presence of plastic fibres was observed. During the XRF analysis, the samples were heated at a temperature of 800 ^{o}C as described in Section 3.4.4, which may convert the plastic fibres into a carbon group.

6.1.2 Drying process

As described in Section 3.7.1.1 and based on the above in Figure 6.3, the following parameters were calculated.

6.1.2.1 Moisture loss

The moisture loss at 24 hours and 28 days of curing was calculated according to equation 3.25 based on different curing regimes of CFA-based GPP. The summarised results are shown in Table 6.4 at 24 hours and 28 days of curing. A sample calculation on a CFA-based GPP dry cubic block cured in a room with a plastic cover follows:

$$X = \frac{1762.6-1749.6}{1762.6} \times 100 = 0.0079 = 0.73\%$$

Table 6-4: Moisture loss at 24 hours and 28 days ageing of CFA-based geopolymer paste and concrete at different curing regimes.

CFA-based geopolymer type	Curing regime	Average moisture loss (%)	
		24hrs	28 days
GPP	Room	0.29	0.73
	Room open	0.39	0.98
	Oven	0.50	1.24
GPC	Room	0.17	0.41
	Room open	0.37	0.56
	Oven	0.42	0.70

6.1.2.2 Amount of water evaporated and air mass flow rate

The amount of water evaporated per hour after 24 hours was calculated for CFA-based geopolymer paste cured at room temperature with a plastic cover according to Equation 3.26, and the summarised results for each curing regime are shown in Table 6.5.

$$\dot{m}_{ev} = \frac{1762.6-1755.1}{(24)} = 0.31\ g/hr\ = 3.13 \times 10^{-4}\ Kg/hr = 8.68 \times 10^{-8} Kg/s$$

Table 6-5: CFA-based geopolymer paste and geopolymer concrete water evaporation rate from different curing regimes.

CFA-based geopolymer type	Curing regime	24 hrs water evaporated rate, Kg/s
GPP	Room	8.68×10^{-8}
	Room open	1.56×10^{-7}
	Oven	2.26×10^{-7}
GPC	Room	4.40×10^{-8}
	Room open	7.60×10^{-8}
	Oven	1.08×10^{-7}

The oven air mass flow was calculated according to Equation 3.27. The X_2 and X_1 moisture content was 75.9 and 16.5% at 60 and 17 °C, respectively. CFA-based GPP moisture content before and after oven drying was taken as 20.29% and 11.83%, respectively. Room-curing moisture content at 24 hours of curing was assumed to decrease from 20.29 to 18.67% based on average moisture loss in Table 6.4 or water evaporation rate in Table 6.5 based on a CFA-based GPP moisture content of 4.05 % shown in Table 6.1.

$$\dot{m}_{air} = \frac{1762.6}{24\times3600} \times \frac{(75.90-16.50)}{(20.29-11.83)} = 1.42 \times 10^{-2} Kg/s$$

6.1.2.3 Rate of drying

The drying rate of CFA-based geopolymer paste and geopolymer concrete was calculated according to Equation 3.28. The material was cast in a 100 mm x100 mm cubic mould with a surface area of 0.01 m^2. The drying rate from the casting time to 24 hours and 28 days of curing using different curing regimes are summarised in Table 6.6. A sample calculation was done at 24 hours based on an oven-curing regime.

$$R = -\frac{1745.40}{0.01} \times \frac{(11.83-20.29)}{24\times3600} = 17.10\ g.m^{-2}.s^{-1} = 1.71 \times 10^{-2} Kg.m^{-2}.s^{-1}$$

Table 6-6: CFA-based geopolymer paste and concrete after 24 hours rate of drying using different curing regimes.

CFA-based geopolymer type	Curing regime	Initial moisture content (%)	24 hrs moisture content (%)	Rate of drying, $Kg.m^{-2}.s^{-1}$
GPP	Room	20.29	18.67	3.28×10^{-3}
	Room open	20.29	15.25	1.02×10^{-3}
	Oven	20.29	11.83	1.71×10^{-2}
GPC	Room	20.29	19.87	1.08×10^{-3}
	Room open	20.29	17.25	1.01×10^{-3}
	Oven	20.29	14.33	1.53×10^{-3}

6.1.3 Yield and product yield percentage

The effect of fine and coarse aggregate and CFA-based GPP on yield and product yield percentage was investigated. The results obtained with the application of Equation 3.29 are shown in Table 6.7 with a sample calculation based on CFA-based GPP demonstrated as follows using a mix of GPC-M3C, GPM-M3C and GPC-M3C. The % yield was also calculated according to Equation 3.30, with results shown in Table 6.7. Adding fine and coarse aggregates to CFA-based geopolymer results in a higher yield than CFA-based geopolymer with no aggregates (GPP). This illustrates why more products (samples) were cast with CFA-based GPC than CFA-based GPP. In all cases, CFA-based GPP, GPM, and GPC result in a high yield of about 98%. This is experimentally acceptable as the synthesised material produced was fully used for the casting of samples, and the balance of about 2% was not considered waste material. Instead, these were residues that stuck to the mixer or fell on the ground during the casting (pouring) process, which can still be recycled at a large scale.

$$Y = -\frac{3+0.7+0.380+0.180}{1762.6} = \frac{4.26}{1762.6}0.0024\ m^3$$

$$Y_p = \frac{4.18}{4.26} = 0.9818 = 98.18\%$$

Table 6-7:Effect of fine and coarse aggregate addition on the yield and yield percentage of CFA-based geopolymer paste.

CFA-based geopolymer type	Mix yield and sample		Yield percentage, (%)
	Yield, m3	Number of cubes	
GPP	0.0024	2.42	98.18
GPM	0.0035	3.49	99.26
GPC	0.0048	4.82	98.16

Each cube sample size is 100 mm x100 mmx100 mm with V=0.001 m3

6.2 Energy balance

According to the application of the first law of thermodynamics, the energy consumed during the production of CFA-based geopolymer was investigated based on the effect of curing conditions. The effect of fine and coarse aggregate addition was assumed to be negligible even though when a high content is applied, it affects the viscosity of the product, which may require a mixer with a high-power number compared to the paste that contained no fine and coarse aggregates. The effect of fine and coarse aggregate was not taken into consideration during the energy balance. The energy consumed due to the addition of coarse aggregates was found to be very close to that of CFA-based paste as only an extra 3 to 5 minutes was added to the paste blending time. CFA-based GP formulation cured at room temperature was compared to that cured at 60 ^{o}C for 24 hours. The following calculations were done.

6.2.1 Sodium hydroxide reaction process

Equations 3.34 and 3.35 were used to determine the amount of heat associated with the preparation of a 12-molar sodium hydroxide solution and one mole of that solution. 975.43 g (1 litre) of water and 480 g of sodium hydroxide at a starting temperature of 17 ^{o}C were used, and the final reaction temperature was recorded to be 86 ^{o}C due to the exothermic nature of the reaction.

$$q_{sol} = (0.97543 + 0.480) \times 4184 \times (17 - 86) = -353192.1\, J$$

The number of moles (using 12 M or 480 g of sodium hydroxide as this was the optimised concentration from which the suitable setting time was obtained) was obtained as follows;

$$Number\ of\ moles\ = \frac{480}{40} = 12 \text{ moles; therefore the}$$

$$\Delta H^{o}{}_{sol} = -\frac{353192.1}{12} = -29432.68\,J = -2.94 \times 10^{4} J$$

From the results of the above calculation, it was evident that preparing a sodium hydroxide solution causes an exothermic reaction, as this was physically observed during the experiment. This shows that preparing CFA-based geopolymer with this solution will possibly lead to the formation of delay ettringite, as the internal temperature of the geopolymer could rise above the maximum of 65 - 70^{0}C as described in Scrivener and Young (1997) and Taylor et al. (2001) investigations. This will result in thermal cracking, as it also explains why the samples cured without plastic covering resulted in thermal cracking. On a large scale, this process may require proper insulation around the reaction tank so as to prevent the exothermic causing overheating. Based on Table 3.4, the heat released at different molar concentrations (NaOH) was calculated and summarised in Table 6.8.

Table 6-8: Heat released during the production of different sodium hydroxide concentrations.

Sodium hydroxide concentration, M	**Temperature rise, ^{o}C**	$\Delta H^{o}{}_{sol}$, **J**
8	75	-3.93 × 10^{4}
10	80	-3.34 × 10^{4}
12	86	-2.94 × 10^{4}
14	93	-2.66 × 10^{4}
16	95	-2.45 × 10^{4}

6.2.2 Synthesis process

The following parameters were defined for the synthesis process energy balance calculations, including mixer dimensions, mixing speed, blending time and homogeneity, density and viscosity, as detailed in the following subsections.

6.2.2.1 Mixer dimensions

Measurements of the mixer described in Figure 3.32 are shown in Table 6.9.

Table 6-9: Dimension of the mixer and impeller used to blend CFA-based geopolymer paste.

Parameters	Symbol	size, m
Impeller diameter	Da	0.435
Diameter of the tank	D_T	0.440
Height of the tank	H	0.360
Width of the impeller	W_1	0.013
	T	0.005
Diameter of the impeller	D_1	0.007
Width of baffle	J	0.005
Length of impeller	L	0.180
	L_2	0.232
	L_3	0.123
Distance from the base to the impeller	E	0.003

6.2.2.2 Mixing speed, blending time, and homogeneity

The synthesised mixer had a consistent speed of 55 rev/min (0.917 revs per second). The blending time was defined experimentally by observation, as shown in Figure 6.4, where the mix was assumed to be homogenised at around 30 minutes of mixing, from which time the homogenisation number was calculated using Equation 3.4. This is important as the synthesised mixing time depends on the rotational speed of the mixer as well as the type of impeller, which may also affect paste viscosity.

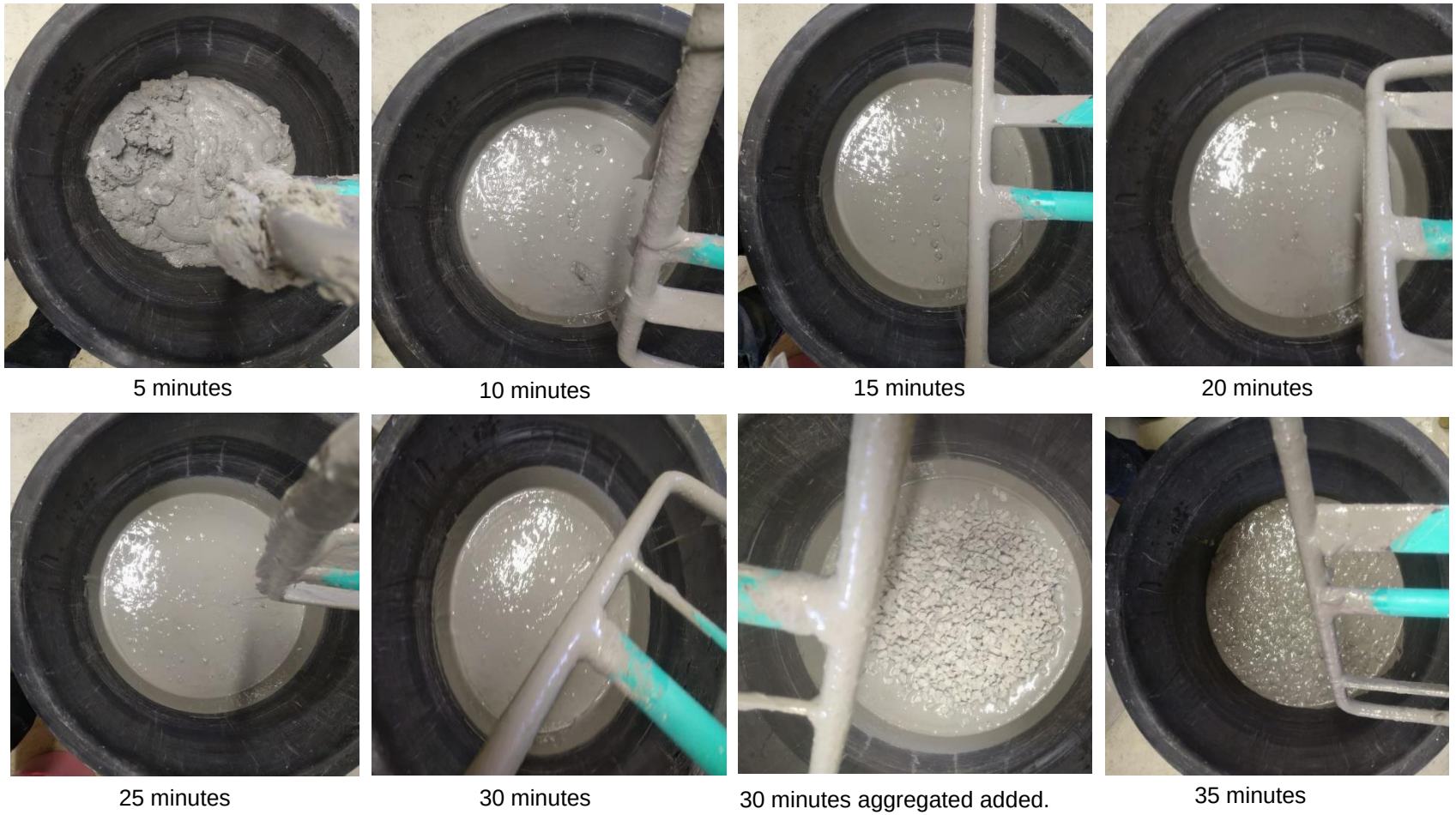

Figure 6-4: Visual observation of the blending of CFA-based geopolymer paste at different mixing times and the addition of coarse aggregates after 30 minutes of mixing

$$H_o = \frac{30}{55} = 0.55$$

On a large scale, this homogenisation number could be multiplied by the rotational speed of the mixer to define the blending or mixing time. For a continuous process design after defining the blending time and knowing the volume of the mixer, the volumetric flow rate of CFA as input material could be calculated using Equation 3.3. No coarse aggregate was used to avoid equipment damage

6.2.2.3 Density and Viscosity

The bulk density of the fresh CFA-based geopolymer paste was calculated according to Equation 3.8 and was found to be 1762.6 kg/m^3. This was taken as the desired bulk density for energy balance calculations in this study to determine the Reynold and power numbers of the paste as required. To determine the viscosity, the viscosity and rotational speed test was performed on the sodium hydroxide solution of 12 M and the sodium silicate as an alkaline activator and CFA-based geopolymer paste and mortar at a temperature of 25 ^{o}C. The results of this experiment are shown in Figure 6.5.

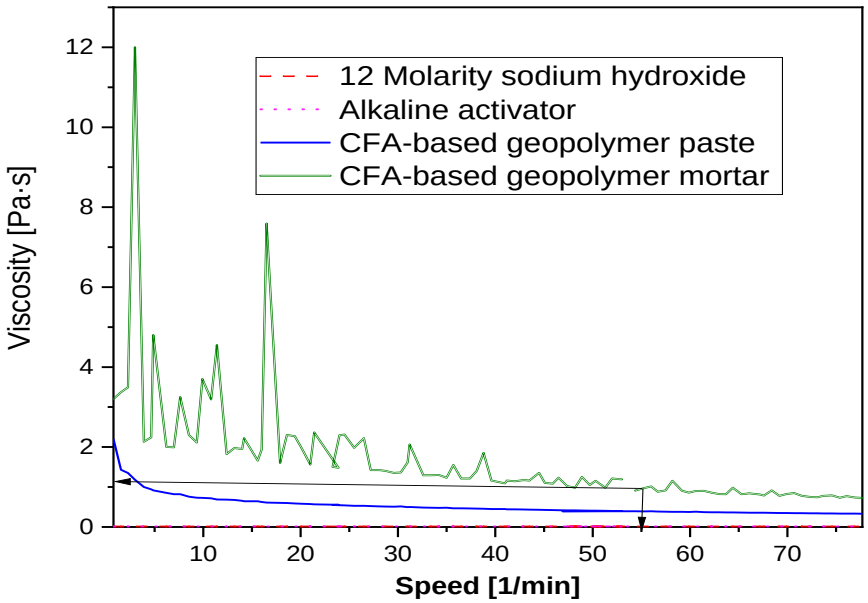

Figure 6-5: Viscosity test profile of a 12-molar sodium hydroxide solution, alkaline activator, CFA-based geopolymer paste and mortar at a set temperature of 25 ^{o}C.

It can be observed that adding CFA to the alkaline activator to form the paste resulted in a high viscosity. In the above graph, the viscosity of the paste was considered at a speed of 55 rev/min, corresponding to the synthesis mixer running speed. In the past, this was taken as 0.39 Pa.s. The

sodium silicate alkaline activator and the 12 molar sodium hydroxide solution had a low viscosity, similar to that of normal water, with a behaviour similar to that of a Newtonian fluid.

6.2.2.4 Dimensionless numbers and energy consumption

To determine the power required for synthesising CFA-based geopolymer paste, the power number (N_p) was calculated using Equation 3.37. It was important to determine the Reynold number to understand the flow behaviour of the paste and the Froud number, as this is useful when scaling up to determine the speed or diameter of the large-scale impeller. Sample calculations were as follows;

i. For Reynolds number

$$N_{Re} = \frac{1762.6 \times 0.917 \times 0.435^2}{0.39} = 1.05 \times 10^3 = 1054.26 < 2300$$

The Reynolds number obtained is less than 2300, which shows that the paste behaves in the laminar flow regime during the synthesis process. This confirms the assumption made in Green and Perry (2008), which states that for a paste, the Reynolds number is assumed to be less than 100.

ii. For power number

From Figure 7.1 of the appendix for power characteristics of close clearance agitators' curve for an anchor agitator (curve 1) using the Reynolds number obtained, the power number was found to be close to 10. Equation 3.36 is then defined as follows.

$$N_p = \frac{P}{{D_a}^5 N^3 \rho} = 5$$

iii. Froude number

Using the above power number obtained and the blending time of 30 minutes, the following synthesised energy consumption was calculated according to Equation 3.38

$$N_{Fr} = \frac{0.917^2 \times 0.435}{9.81} = 0.0373$$

From the power number obtained, the power consumption was determined from which the energy consumed was calculated according to Equation 3.38 by taking a blending time of 30 minutes (1800 seconds).

$$N_p = \frac{P}{{D_a}^5 N^3 \rho} = 5$$

$$P = 10 \times \mathrm{D_a}^5 \mathrm{N}^3 \rho = 5 \times 0.435^5 \times 0.917^3 \times 1762.6 = 105.76\ \mathrm{W} = 0.10673\ \mathrm{kW}$$

$$Q = 105.76 \times 1800 = 1.90 \times 10^5 J = 190.32\ KJ$$

6.2.3 Drying

The energy consumption in this stage was only related to synthesised geopolymer cured at an oven temperature of 60 °C for 24 hours. Figure 6.6 illustrates the overall mass and energy conditions during the oven curing process.

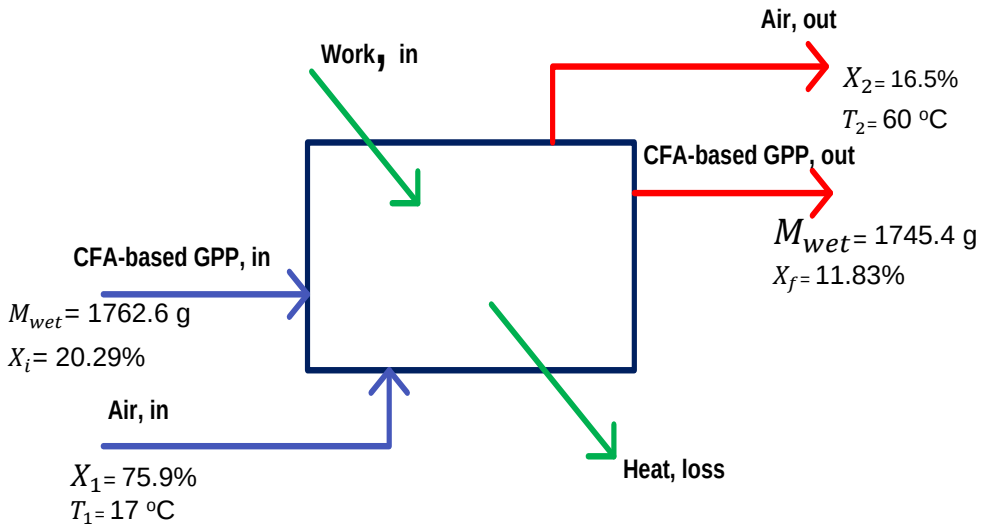

Figure 6-6: Overall mass and energy balance based on operating conditions for CFA-based geopolymer paste for 24 hours oven curing at 60 °C.

Equations 3.39 and 3.40 were used to calculate the power and energy required to evaporate $2.26 \times 10^{-7} Kg/s$ of water in the oven obtained from Section 6.1.2.2 and shown in Table 6.5 for different curing regimes calculations under drying at the material balance stage.

$$\dot{q}_d = 1.43 \times 10^{-2} \times 1000 \times (60 - 17) = 615.92 \text{ W} = 0.6192 \text{ kW}$$

$$Q_{ep,water} = 615.92 \times (24 \times 3600) = 5.32 \times 10^7 \text{J} = 5.32 \times 10^4 \text{ KJ}.$$

No heat loss value was provided by the oven supplier, including the properties of insulated material; therefore, this was estimated. Dimensions of the oven are illustrated in the technical drawing in Figure 6.7. Equations 4.42 and 4.43 were used to calculate the heat loss and the ratio of heat loss to that oven heat consumed to decrease the moisture content in CFA-based GPP from initial moisture of 20.9 to 11.8% during the oven curing, as shown in Figure 6.6. The oven inside temperature was taken as 60 °C while the outlet was measured to be 30 °C at 24 hours of curing (initially 17 °C). The properties related to the insulation materials, inside and outside steel, are shown in Table 6.10.

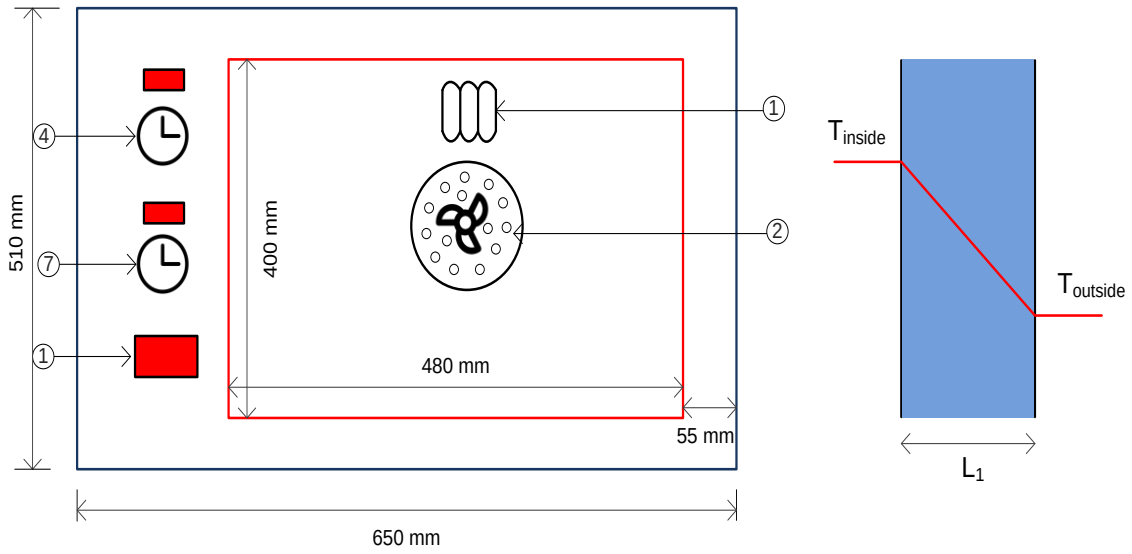

Figure 6-7: Technical drawing and dimensions of the oven used during the 24-hour heat curing process.

Table 6-0-10: Properties of oven steel material and insulation material.

Heat conductivity, W.m. K		Thickness, m
Steel	16	0.005
Insulation material	0.07	0.05

$$Q_{Loss} = \left(\frac{60-40}{{}^{1}/_{16}+{}^{0.055}/_{0.07}+{}^{1}/_{16}}\right) \times 0.2371 \times 24 \times 3600 = 4.50 \times 10^{5} J = 4.50 \times 10^{2}\ KJ$$

$$Q_{LR} = \frac{4.50 \times 10^{5}}{5.32 \times 10^{7}} = 0.008 = 0.85\% \ < 1\%$$

The results of energy consumption for both room curing and oven at 60 °C for 24 hours are summarised in Table 6.11. These results align with the hypothesis mentioned in Section 1.2 as it is observed that the curing process is energy intensive as it requires about 141 times more energy input than the room curing process. It also affected carbon emissions, as demonstrated in Section 5.4.1.

Table 6-11: Total energy consumed from 60 °C oven curing at 24 hours compared to the room curing process.

Process	Energy consumption, J	
	Oven curing	Room curing
Oven, 24hr at 60 °C	5.32×10^{7}	0
Synthesis	1.90×10^{5}	1.90×10^{5}
Total energy consumed, J	5.34×10^{7}	1.90×10^{5}

6.3 Economic analysis

The results obtained from previous chapters (chapters 4 and 5) demonstrated that it is possible to synthesise geopolymer from South African low calcium CFA for construction applications with a product resulting in good mechanical and durability properties and low environmental impact associated with the testing standards. These properties are similar in some cases and higher than those of standard construction materials made using ordinary Portland cement. A room curing was also investigated; therefore, performing an engineering economic analysis and evaluating both curing processes is important. As demonstrated in Sections 5.4.1 and 6.2.3, oven curing was less environmentally friendly and had a high energy consumption process compared to the room curing process. This will also be more expensive than the room-curing process. Therefore, the feasibility analysis at large-scale production will be highly investigated during the room curing process.

Coal CFA-based geopolymer concrete cured at room temperature with a plastic cover resulted in excellent engineering properties, whereas GPC-M2C formulation using room curing with no plastic cover and oven curing processes resulted in deterioration, high emissions, and high energy consumption, respectively. Production of a durable CFA-based GPC with a maturity strength of 35 MPa within 50 km 15 the CFA collection point was assumed for the manufacturing of such high-strength construction materials such as pavers. A project analysis and the evolution of a large-scale plant with a production capacity of 4 033 202.82 kg/year or 1 787.29 m^3/year of CFA-based GPC is further considered assumed.

6.3.1 Raw materials required and cost

A large-scale plant consisting of seven (7) daily production batches of 2812.5 Kg (about 971.65 litres) at 98% yield is assumed. Figure 6.8 shows the overall basic input raw materials required for a scale-up of a batch with associated costs shown in Table 6.12 to produce large quantities.

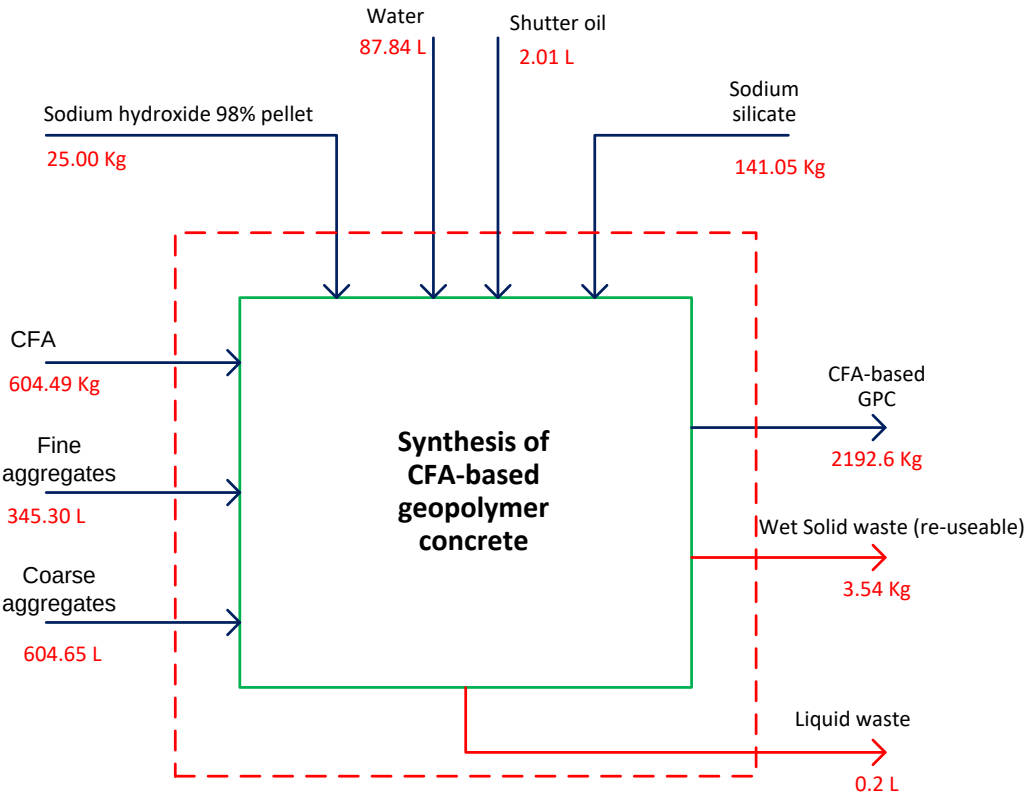

Figure 6-8: Overall large-scale batch raw materials input to produce CFA-based geopolymer concrete.

Table 6-12: CFA-based geopolymer concrete large-scale batch raw materials cost

Raw materials	Price, R/Unit	Batch materials quantity & cost				Source
		Quantity		Cost,	Unit	
Classified siliceous class F coal fly ash	R 0.80	604.49	R	483.60	Kg	Assumed from Lafarge, Ash resources
NaOH hydroxide (NaOH) 98% pellet	R 24.00	25.00	R	600.00	Kg	Protea Chemicals - Chemical Supplier
Sodium silicate	R 8.90	141.05	R	1 255.33	Kg	Protea Chemicals - Chemical Supplier
Water	R 0.04	87.84	R	3.15	L	Johannesburg, amendment of tariff charges for water services and sewage and sanitation services:2021/2022; Industrial/ Commercial
Fine aggregates (Building sand)	R 340.00	0.35	R	117.40	m^3	leroymerlin.co.za
Coarse aggregates (13 mm blue stone)	R 360.00	0.60	R	217.67	m^3	sand-stone.co.za
Powafix dry oxide	R 56.00	10.07	R	564.20	Kg	builders.co.za//Paint-Adhesives/Cement-oxides
Shutter release oil	R 29.98	2.01	R	60.40	L	joluka.co.za/construction/shutter-oil/
Total batch raw materials cost (excluding dry mix coloured dye)			**R**	**2 737.56**		
Total batch raw materials cost (including dry mix coloured dye)			**R**	**3 301.75**		
Total yearly raw material cost (excluding dry mix coloured dye)			**R**	**5 059 008.38**		
Total yearly raw material cost (including dry mix coloured dye)			**R**	**6 101 640.99**		

6.3.2 Equipment scale-up and costing

6.3.2.1 Scale-up for geometric similarity

The laboratory-to-industrial scale ratio was calculated for the equipment scale-up as described in Equation 3.44. The lab-scale batch product's total volume was 0.004822 m^3 (obtained from a total mass of 10.88 Kg with a density of 2256.6 Kg/m^3). The large-scale batch total mass produced is described in Section 6.3.1, which is about 0.9716 m^3 (463 litres) as total volume.

$$R = \left(\frac{0.9716}{0.0482}\right)^{\frac{1}{3}} = 5.86$$

From the scale-up ratio factor of 5.86 obtained, the lab mixer dimensions shown in Table 6.9 are multiplied, which changed as shown in Table 6.13 for the large-scale mixer dimensions. As the mixer was only about 1/3 utilised during the mixing, the size of the mixer and impeller may be assumed to be double the original lab scale dimensions.

Table 6-13: Dimensions of the mixer and impeller at the large-scale bath of 971.65 L for the synthesis of CFA geopolymer concrete.

Parameters	Symbol	Size calculated, m	Design assumption size, m
Impeller diameter	Da	2.550	0.870
Diameter of the tank	D_T	2.580	0.880
Height of the tank	H	2.111	0.720
Width of the impeller	W_1	0.076	0.026
	T	0.029	0.010
Thickness diameter of the impeller	D_1	0.041	0.014
Width of baffle	J	0.029	0.010
Length of impeller	L	1.055	0.360
	L_2	1.360	0.464
	L_3	0.721	0.246
Distance from the base to the impeller	E	0.015	0.005

6.3.2.2 Scale-up design for kinematic

Equation 3.45 determined the rotation speed of the assumed large-scale batch production. Based on Table B-2, the blending of solids was considered as the rate of mass transfer, which depended

on particle sizes, which are difficult to keep constant as the results of both CFA and aggregates show a variation in size as shown in Figures 4.20 and 4.21, confirmed with SEM analysis results of the raw CFA in Figure 4.22. Coarse aggregates need to be equally suspended in the paste for better consistency in the mix (formulation).

$$5.86 = \left(\frac{V_{large}}{55}\right)^{\frac{3}{4}}$$

$$V_{large} = 55 \times (4.58)^{\frac{4}{3}} = 581.41 \approx 581\, rpm$$

A 500-1600 Litre batch concrete mixer (Available at https://www.alibaba.com/product-detail/JS-1000-concrete-mixer-batch-concrete_1219644419.html, Accessed on 13th November 2022) with half revolutions speed 291 rpm (design with 25 kWh) and similar design dimensions assumed at high shear rotor with one dispersion blade shown in Figure A-5 as described in Ghanem et al (2014) may be ideal for the large scale production. The power consumption at large-scale production was assumed, as shown in Equation 3.46. The full cost associated with purchasing the above-mentioned mixer may be seen in Table B-3.

$$\frac{P_{larg}}{P_{lab}} = \frac{k{\times}0.870^5 291^3}{k{\times}0.435^5 55^3} = \frac{5307185.96}{2591.40} = 2048.00$$

This shows that the power consumption at a large scale may be assumed to be 2048 times that of the lab scale when room curing with the plastic cover process is considered. This is then calculated as follows.

$$P_{large} = 105.73 \times 2048 = 2165.38\, W = 21.65\ \text{KW}$$

6.3.2.3 Equipment costing

Costing of the equipment required to operate a plant is shown in Figure 6.9, and costs from different suppliers in South Africa are listed in Table 6.14, from which the capital cost, bare module and total module costs are calculated as shown in Equations 3.48 and 3.49, respectively. Assuming the production of CFA-based GPC paving blocks.

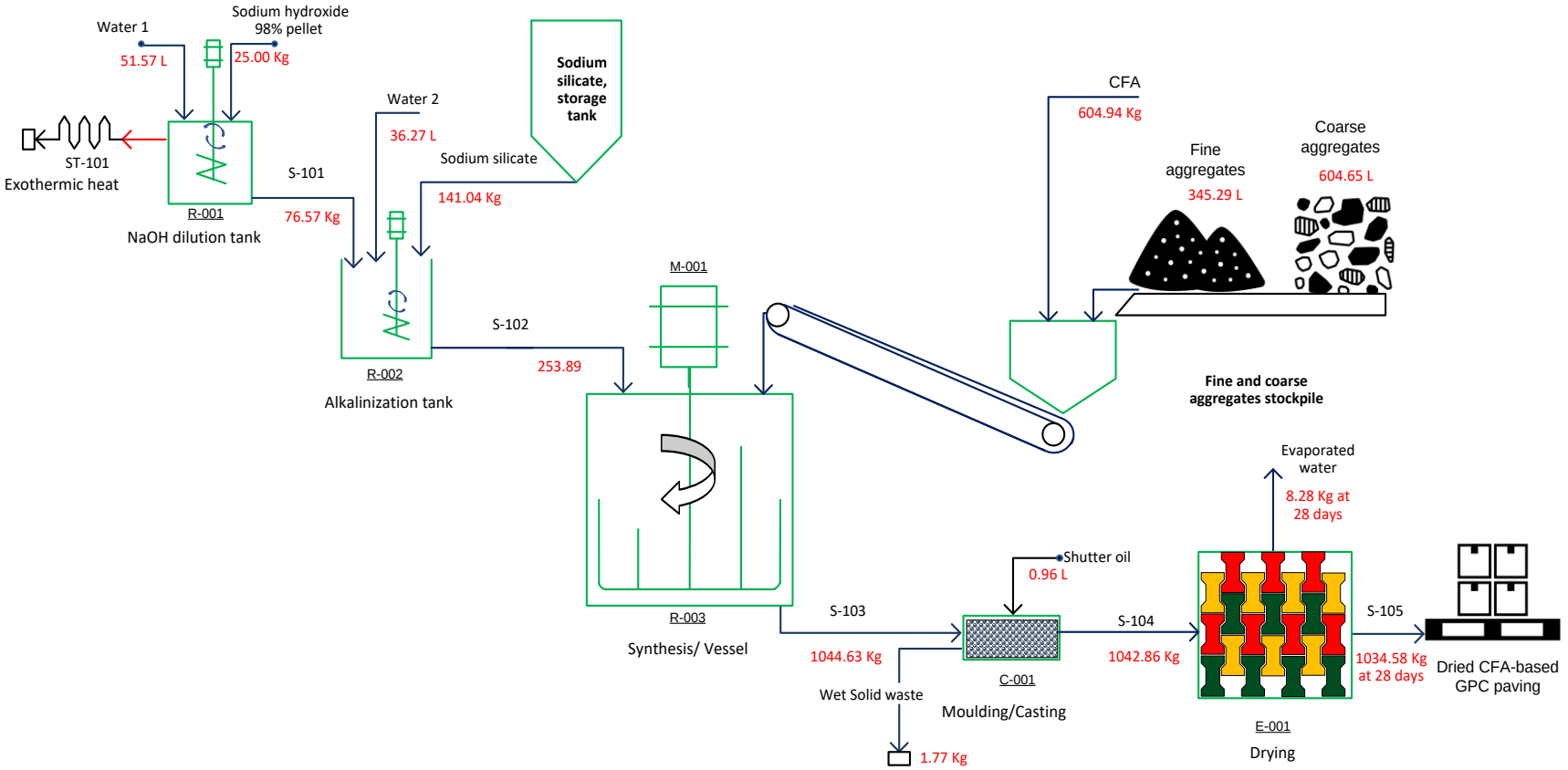

Figure 6-9: CFA-based geopolymer concrete production large-scale batch raw materials input and equipment

Table 6-14: Equipment required for the manufacturing of 1000L CFA-based geopolymer concrete for paving materials

Activity Section	Equipment name	Capacity	Quantity and Total price				Supplier
			Quantity	Unit price		Total price	
Production line	JS 1000 concrete batch mixer set	1000 L	1	R	103 654.20	R 103 654.20	Fangyuan Group concrete mixer
	Paving moulds	0.02 m2	343	R	70.00	R 24 034.50	diywesterncape.co.za
	Water measurement bucket	25L	2	R	39.99	R 79.98	sanitizetoday.co.za
	Sodium hydroxide preparation tank	250L	1	R	985.00	R 985.00	neltanks.co.za
	Sodium hydroxide solution measuring bucket	25L	2	R	39.99	R 79.98	sanitizetoday.co.za
	Sodium silicate measuring drum	100L	2	R	229.00	R 458.00	game.co.za
	Alkaline storage drum	100 L	7	R	469.00	R 3 283.00	sanitizetoday.co.za
	120 R Spiral Stirrer		1	R	1 655.00	R 1 655.00	Festool
	Industrial weighing scale	500 Kg	1	R	2 999.00	R 2 999.00	Makro.co.za
	Plastic sheeting,	60 m2	6	R	599.00	R 3 594.00	Builders.co.za
Quality control	Set of sieves for fine and coarse aggregates	19 mm to 0.075 mm	11	R	450.00	R 4 950.00	Cape Laboratory Equipment
	Cube moulds, plastic and nylon	100 mm3	18	R	75.00	R 1 350.00	Turner Morris
	Slump Test Set	6 Kg	1	R	3 250.00	R 3 250.00	Cape Laboratory Equipment
	Digital thermometer probe	50-300 ^{o}C	2	R	1 536.81	R 3 073.62	instruments.co.za
Capital cost						**R 153 446.28**	
Shipping		-	-			R 74 009.10	
Installation		-	-			R 38 144.75	
Insurance		-	-			R 4 871.75	
Taxes		-	-			R 15 548.13	
Engineering		-	-			R 14 096.97	
Some overhead expenses		-	-			R 53 706.20	
Bare module cost						**R 353 823.17**	
Total module cost (Fixed capital investment, excluded land)						**R 417 511.34**	

6.3.3 Project investment cost estimation and cash flow analysis

To determine the investment cost profitability and other criteria listed in Table 3.10 using Equation 3.48 to 3.51, Other costs associated with utility and raw material were determined to calculate the production cost as shown in Table 3.9. The sub-total Sections A, B and C listed in Table 3.9 are illustrated.

6.3.3.1 Utility cost

The utility cost was that of electricity used during the synthesis process. The oven-curing and room-curing processes were compared based on utility cost. It was observed that the curing process for 24 hours with a temperature starting from 60 ^{o}C during a full-year operation will be very expensive, as shown in the following Table 7.15. An electricity cost of R1.42 per kWh was considered (Available, www.joburg.org.za/documents_/Documents/Tariffs%202022-2023/Electricity%20Tariff.pdf, Accessed on 16th November 2022).

Table 6-15: CFA-based geopolymer concrete yearly utility cost associated with room curing vs oven curing at 60 ^{o}C for 24-hour processes.

Process	**Process power kWh cost estimation**					
	Room curing			Oven curing		
	R /Batch	R/ day	R /year	R /Batch	R/ day	R /year
Oven, 24hr 60 ^{o}C	R -	R -	R -	R5 033.28	R 5 033.28	R1 328 786.57
Synthesis	R 17.94	R 125.56	R33 146.79	R 17.94	R 125.56	R 33 146.79
Total power cost	R 17.94	R 125.56	**R33 146.79**	R5 051.22	R 5 158.84	**R1 361 933.35**

R1.42 kWh was considered in the country

6.3.3.2 Variable costs

The annual variable cost was the sum of the cost associated with purchasing raw materials, utility and miscellaneous materials, as shown in Table 7.15.

Table 6-16: CFA-based geopolymer concrete yearly variable cost estimated

Type of cost	**Cost, R**	
Raw material cost	R	5 059 008.38
Utility cost	R	33 146.79
Miscellaneous materials	R	2 087.56
Sub-total A	**R**	**5 094 242.73**

6.3.3.3 Labour and operating costs

A small plant with production at a benchmark of 2400 hours (264 days) and 9 hours (based on national governmental basic conditions of employment act regulations of 45 hours a week) (Available at https://www.westerncape.gov.za/general-publication/basic-conditions-employment-act#:~:text=You%20must%20not%20work%20more,than%205%20days%20a%20week., Accessed on 18th November 2022). The following manufacturing activity conditions in Table 6.17 were considered for a batch process (Sinnott, 2005).

Table 6-17:CFA-based geopolymer concrete batch production hours and activity requirement

Manufacturing activity	Duration
Daily working time (hr)	9.00
Cleaning and material preparation (hr)	2.00
Production time (hr)	7.00
Mixing time (min)	35.00
Casting time (min)	25.00
Number of batches	7.00
Monthly working time (days)	22.00
Project lifetime (year)	12.00
Number of working days per year (days)	264.00

From the above assumptions and percentage given in Table 3.10, operating labour cost is calculated considering the national process operating rate of R45.70 per hour (Available at www.payscale.com/research/ZA/Skill=Machine_Operation/Hourly_Rate, Accessed on 18th November 2022), where the results are shown in Table 6.18

Table 6-18: CFA-based geopolymer concrete room curing process yearly operating labour cost

Labour operating cost	Human resources	annual salary, R	Contract duration, months	Total annual salary, R
Process operator labour	4	R 96 518.40	12	R 386 073.60
Process operator assistance labour	3	R 81 610.39	12	R 244 831.16
Total direct operating labour cost				R 630 904.76
Quality control technician	2	R 126 180.95	12	R 252 361.91
Process operator supervision	1	R 126 180.95	12	R 126 180.95
Maintenance cost	-	-	-	R 20 875.57
Plant overheads cost	-	-	-	R 193 036.80
Capital charges	-	-	-	R 41 751.13
Insurance	-	-	-	R 4 175.11
Local taxes	-	-	-	R 8 350.23
Royalty	-	-	-	R 4 175.11
Total fixed costs (sub-total B)				**R 1 281 811.58**
Administration	2	R 143 461.22	12	R 286 922.44
Marketing	-	R 860 767.33	12	R 860 767.33
Research and development	-	R 366 623.12	12	R 366 623.12
General production cost (Sub-total C)				**R 1 514 312.90**
Total cost B+C, R				**R 2 796 124.48**

6.3.3.4 Fixed cost and production cost

To obtain the production cost, the fixed or annual production cost was determined as the sum of sub-total Sections, which was then divided by the production capacity or volume illustrated in Section 6.3, as shown in Table 3.10. The production cost in R/kg or R/m^3 for CFA-based geopolymer cured at room temperature process, which was considered for investment, is shown in Table 6.19.

Table 6-19:CFA-based geopolymer concrete cured at room temperature yearly fixed cost and production cost in R/kg and R/m^3

Sub-total Section		**Cost, associated**
Sub-total A	R	5 094 242.73
Sub-total B	R	1 281 811.58
Sub-total C	R	1 514 312.90
Fixed cost	**R**	**7 890 367.20**
Production cost, Kg	**R**	**1.96**
Production cost, m^3	**R**	**4 414.71**

6.3.3.5 Investment cash flow analysis and profitability.

At this stage, it was important to focus on the production on a volume basis (R/m^3) rather than a mass basis (R/Kg) as the price of concrete materials is usually listed on a volumetric basis (dimensions) online. A kerb concrete block of 1000 mm x 205mm x 150 mm (equivalent to 0.03075 m^3) was found to cost R205.00 at about 30 MPa of strength (Available at www.buildersmerchant.co.za/products/barrier-kerb-bk1-supplier-cape-town-johannesburg-pretoria-durban, Accessed on 18th November 2022) which is equivalent to R6 666.67/ m^3. This was found to be 33.78% higher than when this product was made with CFA-based geopolymer concrete at R4 414.71/m^3 with 35 MPa strength. An investment analysis was performed from which the profitability and other investment-associated criteria were determined after calculating the manufacturing or investment cost using Equation 3.50 based on the results in Table 6.20. The cost associated with concrete waste management is negligible as less geopolymer concrete waste was produced and could be recycled in the next batch before reaching the final setting time.

Table 6-20: Manufacturing cost of CFA-based geopolymer concrete cured at room temperature

Parameter of manufacturing cost	Cost, R	
Raw material cost	R	5 059 008.38
Utility cost	R	33 146.79
Waste management cost	R	-
Labour cost	R	2 796 124.48
Capital cost	R	417 511.34
Investment cost	**R**	**13 971 922.72**

An investment cost shown in Table 6.20 was considered. In order to determine the yearly profit of the process, which helps analyse the process, the revenue was first at a percentage breakage (breakage due to various factors such as improper demoulding or curing or other production issues) of 4% of the 1 787.29 m^3 of product. Thus, the output would be 96% or about 1 715.80 m^3 (obtained from a conversation with the concrete manufacturing company). The yearly revenue is then listed in Table 6.21 (which is based on 96.00% of the overall product (1787.29 m^3) as production capacity and R6 341.46 as selling unit cost per volume) from which the annual production cost was deducted to obtain the yearly profit.

Table 6-21: CFA-based geopolymer concrete yearly revenue and profit assumption

Yearly cost		**Cost, R**	
Yearly revenue (assuming a 4% percentage breakage)		R	10 880 684.13
Annual production cost	Labour and	-R	2 796 124.48
	Raw material	-R	5 059 008.38
	Utility	-R	33 146.79
	Miscellaneous material	-R	2 087.56
Profit per year		**R**	**2 990 316.93**
Assumed 85% of profit reached/ year		**R**	**2 541 769.39**

From Table 6.21, it was assumed that a minimum of 85% of the yearly profit should be reached. Analysis based on an equal annuity basis was performed assuming a minimum attractive rate of return (MARR) of 10% to determine the criteria listed in Table 3.11, such as net present value, profitability index, or payback period, based on the given equations. The results of the calculations are shown in Table 6.22. The break-even point and payback period are illustrated in Figure 6.1

Table 6-22: CFA-based geopolymer concrete investment profitability analysis results in rand value

MARR	10.00%
Project life	12.00

Period, years		Cash flow	Discount factor		Cash balance		Interest earned		Discount cash flow
0.00	-R	13 971 922.72	1.00	-R	13 971 922.72	-R	13 971 922.72	-R	13 971 922.72
1.00	R	2 541 769.39	0.91	R	2 310 699.44	-R	1 397 192.27	-R	12 827 345.60
2.00	R	2 541 769.39	0.83	R	2 100 635.86	-R	1 282 734.56	-R	11 568 310.78
3.00	R	2 541 769.39	0.75	R	1 909 668.96	-R	1 156 831.08	-R	10 183 372.47
4.00	R	2 541 769.39	0.68	R	1 736 062.69	-R	1 018 337.25	-R	8 659 940.33
5.00	R	2 541 769.39	0.62	R	1 578 238.81	-R	865 994.03	-R	6 984 164.97
6.00	R	2 541 769.39	0.56	R	1 434 762.56	-R	698 416.50	-R	5 140 812.08
7.00	R	2 541 769.39	0.51	R	1 304 329.60	-R	514 081.21	-R	3 113 123.91
8.00	R	2 541 769.39	0.47	R	1 185 754.18	-R	311 312.39	-R	882 666.91
9.00	R	2 541 769.39	0.42	R	1 077 958.34	-R	88 266.69	R	1 570 835.79
10.00	R	2 541 769.39	0.39	R	979 962.13	R	157 083.58	R	4 269 688.75
11.00	R	2 541 769.39	0.35	R	890 874.66	R	426 968.88	R	7 238 427.02
12.00	R	2 541 769.39	0.32	R	809 886.06	R	723 842.70		10 504 039.10
			NFV	R	10 504 039.10			R	10 504 039.10
			NPV	R	3 346 910.57			R	3 346 910.57
			PI	R	2.18			R	2.18
			IRR		14.67%				
	Payback period								8.35 years

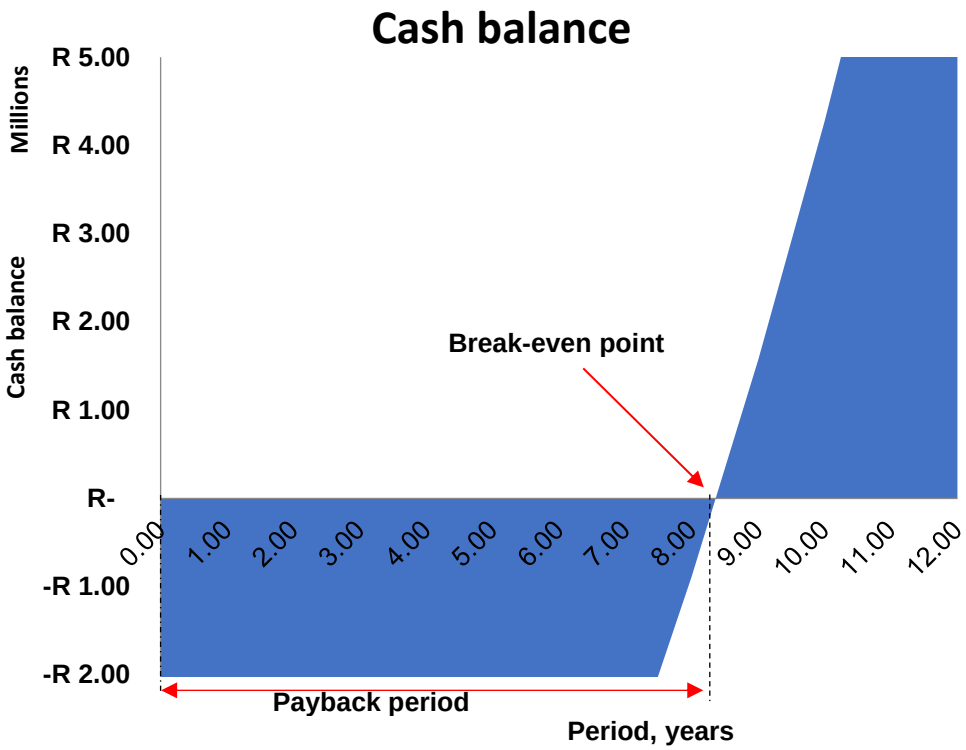

Figure 6-10: CFA-based geopolymer concrete investment break-even point and payback period from assumed investment.

From Table 6.22, the investment results in a positive profit with a profitability index greater than zero; therefore, this investment is subject to consideration. The payback period was determined as 8.35 years (8 years, four months and six days). An internal rate of return on investment was calculated to be approximately 14.67%.

To meet all these requirements, it was important to determine the minimum quantity of CFA-based geopolymer concrete volume to be sold yearly, described as a break-even volume to sustain the project. This was found to be 801 m^3 yearly based on the 1787.29 m^3 total product produced. This is illustrated in Figure 6.11, where the production break-even point is shown (in this case, the stage at which the business is not losing or making profits).

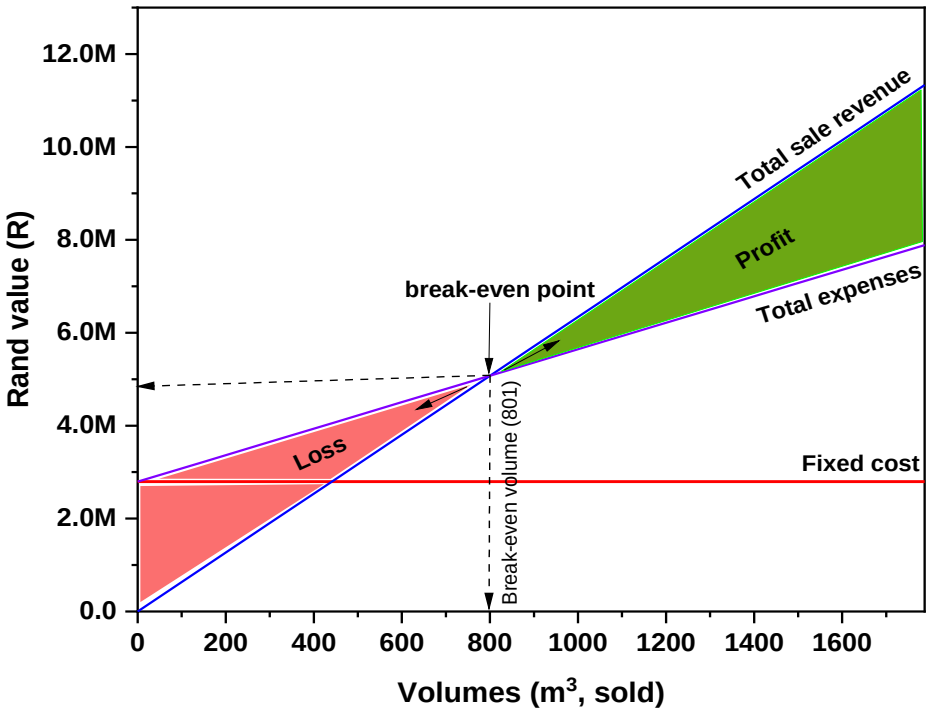

Figure 6-11: CFA-based geopolymer concrete annual break-even volume required from assumed capital investment.

6.3.4 Sensitivity analysis

The effect of low calcium class F CFA and other raw materials on investment was analysed through a sensitivity analysis. Figure 6.12 shows the upper and lower impact on base price with the investment net present value. It is scientifically evident that lowering the price of any raw material from base cost will not negatively impact the investment but rather improve it. As an increase in cost may be challenging, based on the results obtained, up to 60% variation in the price of raw materials such as fine and coarse aggregates, as well as utility cost when using the room curing method, did not negatively impact the net present value. On the other hand, variations of CFA, sodium silicate and sodium hydroxide negatively have affected the present value, starting from 30% for sodium silicate and 45% for sodium hydroxide and CFA.

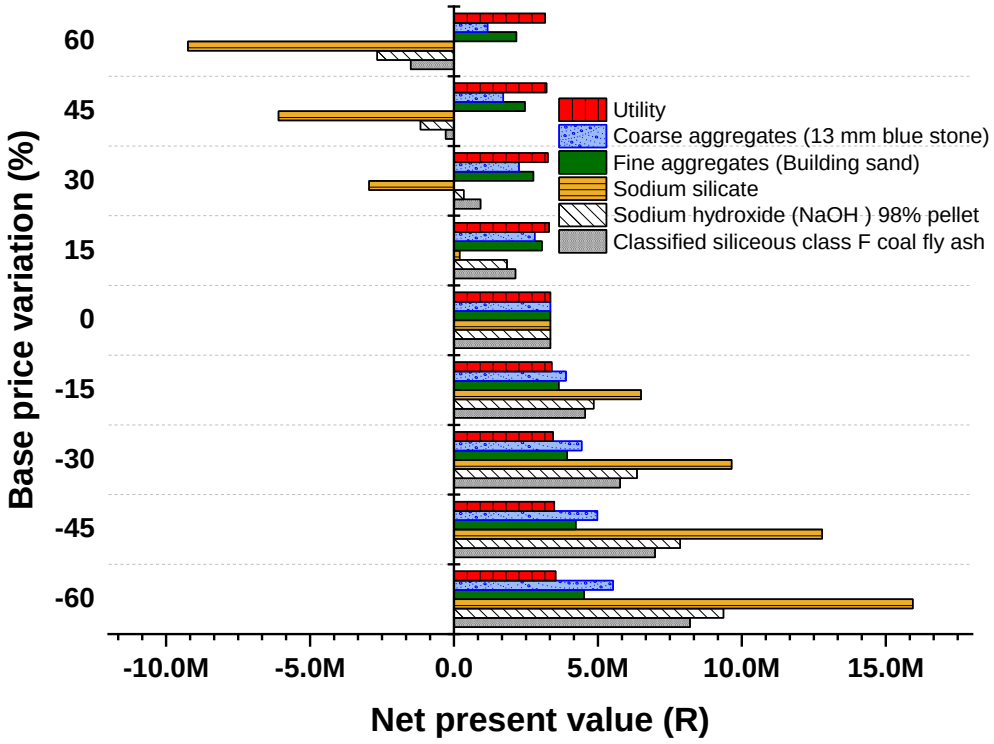

Figure 6-12: CFA-based geopolymer concrete, a sensitivity analysis impact of raw materials used and utility on the net present value.

CFA as waste raw material and the most used in this study was analysed, including other parameters such as production cost, payback period, break-even volumes and net present value. As observed from Figure 6.12, an increase in cost was demonstrated to have a negative impact on other parameters listed. Figure 6.13 illustrates investment parameters' variation due to an increase in base cost (from CFA, where a similar analysis for other raw materials is shown from Table 7.3 to Table 7.9 of the appendix).

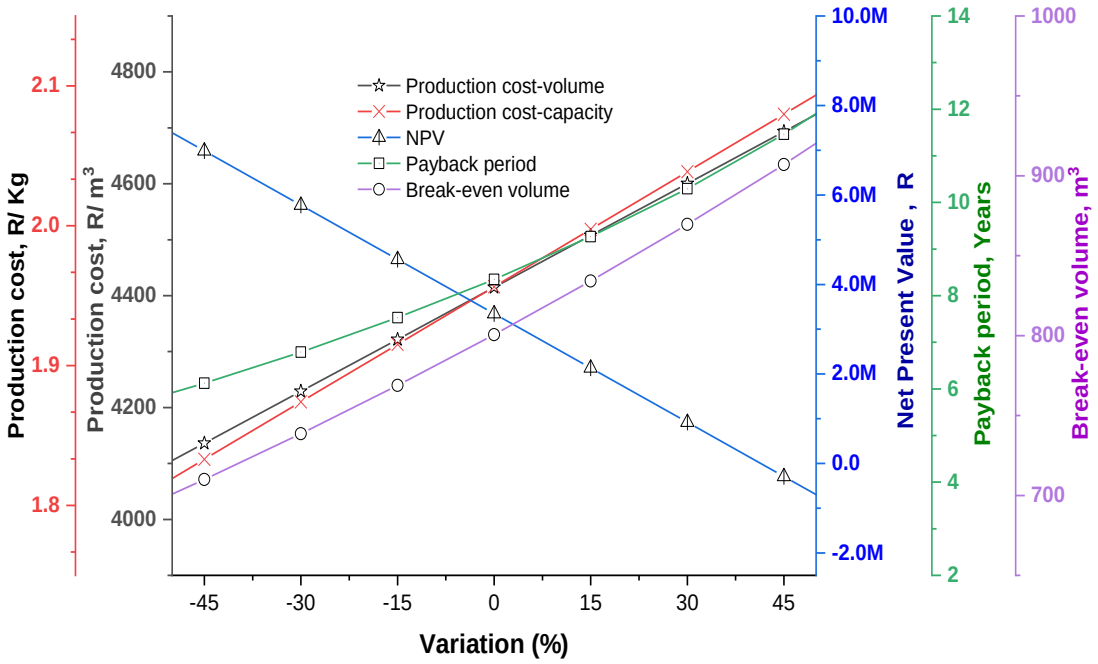

Figure 6-13: Impact of CFA base cost variation on investment parameters.

6.4 Chapter Summary

The oven process was found to be a very energy-intensive process on the utility basis from which the addition of its capital cost, bare module cost, as well as the cost associated with its maintenance will largely affect the production cost, which is directly related to investment cost. For 12 years of operation, as assumed from the room curing process, the oven curing will result in a negative net profit with a profitability index lower than zero. The investment resulted in a very economical process based on a net present value obtained. This also shows that for every R1 invested, a profit of R2.18 is obtained as a profitability index. This would not be possible using the oven-curing process due to the total module and utility cost associated with the oven, which will directly require higher investment funds and negatively impact the production cost as it may also affect the feasibility of the process over 12 years of plant life on an equal annuity basis. A previous calculation result in Kalombe's (2018) resulted in a production cost of R5/Kg at a plant capacity of 152 880 Kg/year when the oven curing process was used for 24 hours at 60 to 80 ^{O}C, which is higher than R1.96/Kg. A sensitivity analysis shows that variation in the cost of CFA can negatively and positively impact the profitability of this project; however, CFA as waste should be procured at a lower cost to facilitate its reuse.

Chapter 7

Conclusions, precautions and recommendations for future work

This study consisted of synthesising CFA-based geopolymer formulations optimised for different construction applications by avoiding heat-curing regimes compared to previous studies. This chapter provides a conclusion, recommendations, and suggestions for future work. To conclude this study, the research questions in Section 1.4 related to major findings, along with recommendations, were answered. Challenges found to be beyond the scope of this study were considered for future research.

7.1 Overview of findings

This study focused on developing an environmentally friendly method for converting power plant waste (CFA) into durable and strong value-added construction materials with high energy efficiency and cost-effectiveness by utilising versatile formulations with good structural properties. Considering the research questions, it is important to understand that pure CFA is characterised using XRF, FTIR, XRD, and SEM-EDXS imaging techniques, including a particle size analyser that illustrates the cumulative and volume distribution percentages. A chemical analysis of the fly ash by XRF revealed high silica and aluminium oxides, respectively, with less than 10% calcium, classified as low calcium CFA according to ASTM 618. The XRD analysis of CFA indicates a crystalline structure with quartz and mullite phases identified. The particle size of CFA analysed with SEM imaging shows about 86% cumulative distribution percentage for particles less than 100 µm ranging from 0.2 to 7.38 µm. SEM imaging also showed the presence of marginal unreacted CFA in all formulations. The presence of capillary voids was high in the CFA-based geopolymer concrete cured at 60 ^{o}C oven temperature and room temperature with no plastic or open-air curing method.

The acceptable sodium hydroxide concentration of 12 M was considered, resulting in a consistency of 7 mm, with initial and final setting times of 170 and 230 minutes, respectively. Using a NaOH molar concentration lower than 12 M could result in a formulation with a flash setting and rejectable consistency of lower than 5-7 mm. On the other hand, using a NaOH molar concentration higher than 12 M can lead to a delay in setting times and higher consistency. CFA-

based geopolymer cement-free formulations were found to set at both oven and room temperatures in accordance with standardised setting times for concrete materials of less than 12 hours. A homogeneous number (dimensionless) of 0.55 was obtained using a mixing time of 30 minutes, while all formulations were cast within 5 minutes for a volume of 0.003 m^3 for a demoulding time of 24 hours after casting.

The strength properties related to the formulations developed were investigated based on the effect of sodium hydroxide concentration and fine and coarse aggregates in addition to the CFA-based paste, as well as the effect of different curing regimes. A sodium hydroxide concentration ranging from 8 to 16 M shows compressive strength increases from 27.3 to 42.1 MPa on CFA-based geopolymer paste. An increase of 10% CFA from the controlled 12 M formulations at 35.1 MPa can increase the compressive strength up to 37.4 MPa. Concrete pigment oxide added at a rate of up to 10% of CFA weight can lower strength by up to 21% and increase density by about 1.5%. Fine and coarse aggregates significantly impacted the mechanical properties of CFA-based geopolymer paste. The addition of fine and coarse aggregates could marginally decrease the compressive strength of GPP-M2A in GPC-M2A with about and largely increasing the density for the formulations of CFA-based concrete. The results obtained from compression strength, flexural strength, tensile splitting and modulus of elasticity showed that the addition of fine and coarse aggregates improved the breaking pattern of the geopolymer formulation from unsatisfactory to satisfactory as well as could reduce the robustness of the material to be developed. The three curing methods examined (which were oven curing at 60 ^oC for 24 hours, room curing with a plastic cover or without a plastic cover) showed that room curing without a plastic cover was the most unsatisfactory curing regime that can be used for the curing of geopolymer formulations. Early thermal cracks were observed; therefore, this method promotes high heat of hydration. It was also observed that the oven curing method results in early strength development, meeting the standard concrete requirement after three days of curing, while this is not the case with room curing methods. Both these methods reach similar compressive strengths at ultimate ageing of 21 to 25.6 days. The room curing with a plastic cover was comparable to the oven curing method at three months of ageing, but this was not the case with room curing without a plastic cover. This shows that there is an alternative to curing CFA-based geopolymer formulations at room temperature as long as moisture is not lost.

The strength properties of geopolymer formulations are related to their durability properties. High water penetration was found in products that were room-cured without plastic cover, including a higher water absorption rate. Room curing without a plastic cover is a less desired method as it

not only results in high water penetration and absorption, but also showed a sign of heavy efflorescence, whereas oven curing and room curing with a plastic cover resulted in slight or nil efflorescence, respectively. All formulations at different curing regimes resulted in a better percentage of non-carbonation penetration depth of more than 95% because of the high pH level of 13.85-14 in these formulations. As part of shrinkage, the oven curing method is responsible for high early shrinkage of up to -5000 micro-strains compared to other curing methods, which were found to be less than -500 and -100 micro-strains for room curing without and with plastic cover, respectively. A fire testing according to ISO 834 or SANS 10177-2 for room curing with plastic cover panels passed the fire rating of 1 hour in all stability, integrity and insulation requirements, as well as no pollutant gases, were observed during the testing.

The environmental assessment impact of formulations shows that oven curing is a highly polluting process in comparison to both room curing methods and normal OPC concrete technology, with an emission factor of about 0.894 Kg CO_2 eq and about 93.9% CO_2 emissions associated with the curing at 60 ^oC for 24 hours when collecting CFA at about a transport distance of 1382.3 Km. Water scarcity and other greenhouse gases were found to be a major issue with this curing method compared to room curing methods. The addition of fine and coarse aggregates plays a significant role in reducing the emissions associated with CFA-based geopolymer paste formulation.

CFA-based geopolymer concrete cured at 60 ^oC oven temperature for 24 hours is a highly energy-intensive process of about 218 times greater than room curing processes. The results of economic analysis on a yearly basis show that the room curing process utility costs were about R33 146.79 while the oven curing process costs were about R1 361 933.35. The process scale-up is favourable with the room curing process, resulting in a production cost of R1.96 /Kg or R4 444.71/$m^{3,}$ which is very low compared to that of R5/Kg obtained from the previous study where the oven curing process was considered (Kalombe, 2018). The sensibility analysis shows that the oven-curing process can still be feasible with an increase of 15 to 60% of the current utility cost. With an increase of 30 and 45% in sodium silicate and sodium hydroxide, respectively, from the cost market cost, the net present value will be negatively affected, resulting in a non-profitable process.

Radioactivity measurements show that CFA has an average total radon activity of 680 Bq/kg. This is in contrast to the accepted 420 Bq/Kg value, while synthesised products have a radon activity ranging from 408 to 459 Bq/Kg, which is higher than the accepted limits

Overall, it can be said that the properties tested on CFA-based geopolymer formulations cured at room temperature met the standards required for construction applications, as shown in Table 3.5. The environmental impact and the energy consumption, including the manufacturing cost, made it the most suitable geopolymerization and curing process. This study investigated the properties of materials, the cost and the materials' environmental impact. The optimised product formulation considered was affordable and environmentally friendly as no heat was required during the curing process.

7.2 Recommendations

This study has proven that CFA-based geopolymer formulations can be cured at room temperature and covered with a plastic sheet to obtain similar and improved compared to oven curing methods to manufacture with lower environmental impacts and produce an affordable CFA-based geopolymer construction material. Considering the following precautions and future studies to improve coal ash waste management is important.

- Both sodium hydroxide and silicate should not be stored in an open container as this will start to evaporate water and form gel, changing the composition of the solution and then affecting that of the formulation.
- Proper container vessel material must be selected to prepare the hydroxide and alkaline solutions to avoid side reactions between hydroxide ions and the metal constituting the container material. It is more suitable to prepare the solution in a plastic drum. Never use drum made of metals such as aluminium because it results in a chemical reaction and cause more environmental issue
- When scaling up this process at an industrial level and for safety purposes, the dissociation of sodium hydroxide on a big scale must be done in a closed system to avoid high gas emissions to the atmosphere. The system may also be insulated for proper safety precautions due to the exothermic energy being released.
- It is important to know the class or chemical composition of any fly ash being used in any process to plan a proper production or avoid further unexpected effects on the strength and durability of the final product.
- The moisture content of this binder (FA) must not exceed 14. Higher moisture influences the designed mix ratio with an additional undefined water content, which reduces the initial and final setting time and leads to higher shrinkage.

- Once samples are made, they must be covered or sealed with a plastic sheet or soaked in water for 3- 7 days or more to prevent their surface from rapid evaporation of the moisture content, leading to cracks and deterioration of the geopolymer concrete.
- The brittle tension failure in GPP showed that when using CFA-based Geopolymer paste for structural application, more steel reinforcement is required for both the tension and compression zone, while CFA-based geopolymer concrete might only require reinforcement on the tension zone.
- Even though the oven curing results in an early strength, concrete is normally judged on 28 days' strength.
- More than a 2-hour fire rating can be obtained if the thickness of the testing product is increased to 100 mm.

7.3 Suggestions for future works

- The curing of geopolymer period of 24 hours oven curing temperatures will lead to the burden-shifting as impacts are increased in the curing process (impacts are reduced at one stage of the value chain but are then felt elsewhere). A full life analysis or a value chain of the product is required at an industrial scale to determine a cradle to the grave of the synthesis of geopolymer-based coal fly ash.
- CFA-based geopolymer products can largely be used for open structures such as bridges, road barriers, paving blocks, concrete kerbs, coastal protection, and fireproof walls for housing purposes. Initially, the CFA average total activity needs to be monitored and then taken into consideration when less than 684 Bq/Kg is achieved. Furthermore, to validate these results, a further study should investigate radiation on a full building envelope consisting of walls, floors, and ceilings made of CFA-based geopolymer formulations, as the results will give a clear indication based on radiation protection guidelines.
- Future work should investigate the effect of 60 ^{o}C oven curing for not more than 6 hours for early curing materials.
- The effect of the Si: Al ratio on compressive strength needs to be investigated on South African CFA-based geopolymer as the current ratio of 3:1 obtained shows a higher compressive strength than the 2.65 ratios investigated in Timakul et al. (2015) studies, as shown in Figure 3.16.

- Based on the durability results obtained, normalising the cost per year of service life (this can be predicted based on durability results but requires other study parameters), it may be scientifically evident that products cast by synthesis of CFA-based geopolymer concrete can again be a very attractive option.
- Perform a study on service life prediction of materials made from CFA-based geopolymer concrete. This can also be compared to normal concrete materials.
- Thermal methods such as differential scanning calorimetry (DSC), Thermogravimetry (GTA) and differential thermal analysis (DTA) are needed for a better understanding of phase change or reaction by mean of heat flow (hydration during the curing), mean of mass change and temperature difference in the curing process. Decomposition may be investigated when CFA-based geopolymer formulations are exposed to fire.
- Investigate the effect of different lightweight aggregates on CFA-based geopolymer concrete for light concrete making on their ductility and strength properties.

7.4 Chapter Summary

It may not be advisable to cure CFA-based geopolymer formulations at oven temperature for longer than 24 hours as this process is highly expensive and causes high CO_2 emissions and embodied energy compared to normal OPC concrete. Additional fine and coarse aggregates are critical in CFA-based geopolymer formulations when designing for ductile materials to avoid brittle failure. The study can also use low-cost lightweight aggregates as a substitute for fine and coarse aggregates to keep the density low for non-structural construction applicants from similar formulations.

References

Abdel-Ghani, N.T., Elsayed, H.A. and AbdelMoied, S., 2018. Geopolymer synthesis by the alkali-activation of blast furnace steel slag and its fire-resistance. Hbrc Journal, 14(2), pp.159-164.

Abdullah, M.M.A., Hussin, K., Bnhussain, M., Ismail, K.N. and Ibrahim, W.M.W., 2011. Mechanism and chemical reaction of fly ash geopolymer cement-a review. Int. J. Pure Appl. Sci. Technol, 6(1), pp.35-44.

ACAA, 2014. Coal Combustion Products Production & Use Statistics: 2000–2013 American Coal Ash Association, Farmington Hills, MI (2014) Google Scholar

Adewumi, A.A., Ariffin, M.A.M., Yusuf, M.O., Maslehuddin, M. and Ismail, M., 2021. Effect of sodium hydroxide concentration on strength and microstructure of alkali-activated natural pozzolan and limestone powder mortar. Construction and Building Materials, 271:121530.

Aguiar, H., Serra, J., González: and León, B., 2009. Structural study ofsol–gel silicate glasses by IR and Raman spectroscopies. Journal of Non-Crystalline Solids, 355(8), pp.475-480.

Akers, D.J., Gruber, R.D., Ramme, B.W., Boyle, M.J., Grygar, J.G., Rowe, S.K., Bremner, T.W., Kluckowski, E.S., Sheetz, S.R., Burg, R.G. and Kowalsky, M.J., 2003. Guide for structural lightweight-aggregate concrete. ACI 213R-03. American Concrete Institute (ACI), Michigan.

Alehyen, S., Achouri, M.E.L. and Taibi, M., 2017. Characterization, microstructure and properties of fly ash-based geopolymer. J. Mater. Environ. Sci, 8(5), pp.1783-1796.

Amin, R. M.,2015. A study of radon emitted from building materials using solid state nuclear track detectors. Journal of Radiation Research and Applied Sciences, 8(4), 516–522. https://doi.org/10.1016/j.jrras.2015.06.001

Andrade, L.B., Rocha, J.C. and Cheriaf, M., 2009. Influence of coal bottom ash as fine aggregate on fresh properties of concrete. Construction and Building Materials, 23(2), pp.609-614.

ASTM C1400-1., 2010. Test method for determining the efflorescence potential of masonry materials based on soluble salt content. In Masonry. ASTM International.

ASTM C1585-13., 2013. Standard test method for measurement of rate of absorption of water by hydraulic-cement concretes. ASTM Int., 41, pp.1-6.

ASTM C191, 2008. Standard Test Methods for Time of Setting of Hydraulic Cement by Vicat Needle; ASTM C191-08, Am. Soc. Test. Mater. 1–8. doi:10.1520/C0191-08.2

ASTM C33, A., 2004. Standard specification for concrete aggregates. American Society for Testing and Material, pp.1-11.

ASTM C39. Standard Test Method for Compressive Strength of Cylindrical Concrete Specimens1, no. C. pp. 1–7, 2015, doi: 10.1520/C0039.

ASTM C469 A., 2014. Standard Test Method for Static Modulus of Elasticity and Poisson's Ratio of Concrete in Compression, West Conshohoken, Pa, USA.

ASTM C-618., 2019. "Standard Specification for CFA and Raw or Calcined Natural Pozzolan for Use in Concrete", American Society for Testing and Materials, United States.

ASTM C939-10., 2016. "Standard Test Method for Flow of Grout for Preplaced-Aggregate Concrete", American Society for Testing and Materials, United States.

ASTM, A., 2016. C948-81: Standard test method for dry and wet bulk density, water absorption, and apparent porosity of thin Sections of glass-fiber reinforced concrete. West Conshohocken: ASTM International.

ASTM, A., 2016. C948-81: Standard test method for dry and wet bulk density, water absorption, and apparent porosity of thin Sections of glass-fiber reinforced concrete. West Conshohocken: ASTM International.

ASTM, A., 2017. C157: Standard Test Method for Length Change of Hardened Hydraulic-Cement Mortar and Concrete. West Conshohocken: ASTM International.

ASTM. 2019. "ASTM C618-19, Standard Specification for CFA and Raw or Calcined Natural Pozzolan for Use in Concrete." Annual Book of ASTM Standards (C):5. doi: 10.1520/C0618-19.

Bakharev, T., 2005. Resistance of geopolymer materials to acid attack. Cement and concrete research, 35(4), pp.658-670.

Barbosa, V.F., MacKenzie, K.J. and Thaumaturgo, C., 2000. Synthesis and characterisation of materials based on inorganic polymers of alumina and silica: sodium polysialate polymers. International Journal of inorganic materials, 2(4), pp.309-317.

Basu, M., Pande, M., Bhadoria:B.S. and Mahapatra, S.C., 2009. Potential fly-ash utilization in agriculture: a global review. Progress in natural science, 19(10), pp.1173-1186.

Beskopylny, A.N., Stel'makh, S.A., Shcherban', E.M., Mailyan, L.R., Meskhi, B., El'shaeva, D. and Varavka, V., 2021. Developing Environmentally Sustainable and Cost-Effective Geopolymer Concrete with Improved Characteristics. Sustainability, 13(24):13607.

Bhandari, R.B., Pathak, A. and Jha, V.K., 2012. A Laboratory Scale Synthesis of Geopolymer from Locally Available CFA from Brick Industry. Journal of Nepal Chemical Society, 29, pp.18-23.

Bhatt, A., Priyadarshini, S., Mohanakrishnan, A.A., Abri, A., Sattler, M. and Techapaphawit, S., 2019. Physical, chemical, and geotechnical properties of coal fly ash: A global review. Case Studies in Construction Materials, 11:e00263.

Biondi, L., Perry, M., Vlachakis, C., Wu, Z., Hamilton, A. and McAlorum, J., 2019. Ambient cured fly ash geopolymer coatings for concrete. Materials, 12(6):923.

Bisarya, A., Chouhan, R.K., Mudgal, M. and Amritphale, S.S., 2015. Fly ash based geopolymer concrete a new technology towards the greener environment: A review. Int. J. Innovative Res. Sci. Eng. Technol, 4(12), pp.12178-12186.

Blissett, R.S. and Rowson, N.A., 2012. A review of the multi-component utilisation of coal fly ash. Fuel, 97, pp.1-23.

Bogas, J.A. and Cunha, D., 2017. Non-structural lightweight concrete with volcanic scoria aggregates for lightweight fill-in building's floors. Construction and Building Materials, 135, pp.151-163.

Browning, E., 1969. Molybdenum. Toxicity of Industrial Metals, 2nd ed. Butterworths, London, pp.243-248.

Chatterjee, A.K., 2000. X-ray diffraction. Handbook of analytical techniques in concrete science and technology, pp.275-332.

Chen, G.G., Luo, G.S., Li, S.W., Xu, J.H. and Wang, J.D., 2005. Experimental approaches for understanding the mixing performance of a mini reactor. AIChE journal, 51(11), pp.2923-2929.

Chindaprasirt: and Chalee, W., 2014. Effect of sodium hydroxide concentration on chloride penetration and steel corrosion of fly ash-based geopolymer concrete under marine site. Construction and Building Materials, 63, pp.303-310.

Chindaprasirt:, Thaiwitcharoen, S., Kaewpirom, S. and Rattanasak, U., 2013. Controlling ettringite formation in FBC fly ash geopolymer concrete. Cement and Concrete Composites, 41, pp.24-28.

Chindaprasirt:, Thaiwitcharoen, S., Kaewpirom, S. and Rattanasak, U., 2013. Controlling ettringite formation in FBC fly ash geopolymer concrete. Cement and Concrete Composites, 41, pp.24-28.

Chowdhury, S., Mohapatra, S., Gaur, A., Dwivedi, G. and Soni, A., 2021. Study of various properties of geopolymer concrete–A review. Materials Today: Proceedings, 46, pp.5687-5695.

Colangelo, F., Forcina, A., Farina, I. and Petrillo, A., 2018. Life cycle assessment (LCA) of different kinds of concrete containing waste for sustainable construction. Buildings, 8(5):70.

Crawford, R., 2011. Life cycle assessment in the built environment, first edition, Spon Press, London, pp.15-38.

Curran, M.A. (1993) Broad-based environmental life cycle assessment, Environmental Science and Technology, 27(3): 430-6.

Davidovits, J. and Resins, G., 1980. Geopolymer chemistry and sustainable Development. The Poly (sialate) terminology : a very useful and simple model for the promotion and understanding of green-chemistry.'

Davidovits, J., 1989. Geopolymers and geopolymeric materials. Journal of thermal analysis, 35(2), pp.429-441.

Davidovits, J., 1999. Chemistry of Geopolymeric Systems, Terminology In: Proceedings of 99 International Conference. eds. Joseph Davidovits, R. Davidovits & C. James, France

Davidovits, J., 2008. Geopolymer Chemistry and Applications, Second Edition, Institut Geopolymère, Paris, pp.277-279.

Davidovits, J., 2008. Geopolymer Chemistry and Applications, Second Edition, Institut Geopolymère, Paris, pp.277-279.

Davidovits, J., 2008. Geopolymer Chemistry and Applications, Second Edition, Institut Geopolymère, Paris, pp.284.

Davidovits, J., 2017. State of the geopolymer 2017. [Online] Youtube. Available at: https://www.youtube.com/watch?v=ZkfYLtNkeo4&t=264s [Accessed 3 July 2022].

Davidovits, J., 2020. Geopolymer Chemistry and Applications. 2nd ed. Quentin, France: Institut Geopolymer. pp. 278.

Davidovits, J., 2021. State of the Geopolymer R&D 2021 (Keynote at the 13th Geopolymer Camp). Available at: https://www.youtube.com/watch?v=qjm3i3s0Yiw.

Davidovits, J.J.J.C.S.T., 2017. Geopolymers: Ceramic-like inorganic polymers. J. Ceram. Sci. Technol, 8(3), pp.335-350.

de Brito, J. and Kurda, R., 2021. The past and future of sustainable concrete: A critical review and new strategies on cement-based materials. Journal of Cleaner Production, 281:123558.

DE LA RILEM., 1988. CPC-18 Measurement of hardened concrete carbonation depth.

Department of Environmental Affairs., 2017. QUESTION NO. 3383 FOR WRITTEN REPLY: NATIONAL ASSEMBLY. Republic of South Africa, Available at https://www.environment.gov.za/sites/default/files/parliamentary_updates/pq3383_tonsinash_producedbyEskomandSasol.pdf.[Accessed 28 June 2021].

DOE., 2018. Department of Mineral Resources and Energy. Coal resources. Available at https://www.energy.gov.za/files/coal_frame.html [Accessed 10 September 2021].

Domone: and Illson, J., 2010. Construction Materials: Their nature and behaviour. 4th ed. Edited by Spon Press. London and New York.

Dong, Z., Zhao, S., Zhang, Y., Yao, C., Yuan, Q. and Chen, G., 2017. Mixing and residence time distribution in ultrasonic microreactors. AIChE Journal, 63(4), pp.1404-1418.

Duxson:, Fernández-Jiménez, A., Provis, J.L., Lukey, G.C., Palomo, A. and van Deventer, J.S., 2007. Geopolymer technology: the current state of the art. Journal of materials science, 42(9), pp.2917-2933.

Duxson:, Fernández-Jiménez, A., Provis, J.L., Lukey, G.C., Palomo, A. and van Deventer, J.S., 2007. Geopolymer technology: the current state of the art. *Journal of materials science*, *42*, pp.2917-2933.

Ebewele, R.O., 2000. Polymer science and technology. CRC press.

EC-European Commission, 1999. Radiological protection principles concerning the natural radioactivity of building materials. Radiation Protection, 112. (Available at www.sustainable-design.ie/arch/NORM_BuildingMaterials112.pdf , Accessed on 28th of September 2022).

Eichhorn, G.L., Berger, N.A., Butzow, J.J., Clark:, Heim, J., Pitha, J., Richardson, C., Rifkind, J.M., Shin, Y. and Tarien, E., 1973. Some effects of metal ions on the structure and function of nucleic acids. Metal Ions in Biological Systems: Studies of Some Biochemical and Environmental Problems, pp.43-66..

En, B.S., 2009. 12390-5: 2009–Testing hardened concrete. Flexural strength of test specimens.

Eskom ., 2015. Coal is used in the generation of electricity. Available at: https://www.youtube.com/watch?v=rQrK2sO6j5E.

Eskom.,2020. Lethabo power station. Available at: (Available at http://www.eskom.co.za/sites/heritage/Pages/LETHABOPOWERSTATION.aspx, Accessed 28 June 2021)

Eskom.,2021. Coal in South Africa. Available at: (Available at https://www.eskom.co.za/wp-content/uploads/2021/08/CO-0007-Coal-in-SA-Rev-16.pdf, Accessed 21th December 2021).

Estokova, A., Singovszka, E. and Vertal, M., 2022. Investigation of Building Materials' Radioactivity in a Historical Building—A Case Study. Materials, 15(19):6876.

Fatoba, O.J.O.O., 2007 'Chemical compositions and leaching behaviour of some South African fly ashes'. MSC thesis: Chemistry, Unpublished thesis, University of the Western Cape.

Fernández-Jiménez, A., Palomo, A., Sobrados, I. and Sanz, J., 2006. The role played by the reactive alumina content in the alkaline activation of fly ashes. Microporous and Mesoporous materials, 91(1-3), pp.111-119.

Fernández-Jiménez, A., Palomo, A., Sobrados, I., & Sanz, J., 2006. The role played by the reactive alumina content in the alkaline activation of fly ashes. Microporous and Mesoporous Materials, 91(1–3): 111–119.

Ferraro, J.R. and Manghnani, M.H., 1972. Infrared absorption spectra of sodium silicate glasses at high pressures. Journal of Applied Physics, 43(11), pp.4595-4599.

Fucic, A., Fucic, L., Katic, J., Stojković, R., Gamulin, M. and Seferović, E., 2011. Radiochemical indoor environment and possible health risks in current building technology. Building and Environment, 46(12), pp.2609-2614.

Gao, B., Jang, S., Son, H., Lee, H.J., Lee, H.J., Yang, J.J. and Bae, C.J., 2020. Study on mechanical properties of kaolin-based geopolymer with various Si/Al ratios and ageing time. Journal of the Korean Ceramic Society, 57(6), pp.709-715.

Ghanem, A., Lemenand, T., Della Valle, D. and Peerhossaini, H., 2014. Static mixers: Mechanisms, applications, and characterization methods–A review. *Chemical engineering research and design*, *92*(2), pp.205-228.

Gitari, M.W., Petrik, L.F., Etchebers, O., Key, D.L., Iwuoha, E. and Okujeni, C., 2006. Treatment of acid mine drainage with fly ash: removal of major contaminants and trace elements. Journal of Environmental Science and Health Part A, 41(8), pp.1729-1747.

Gollakota, A.R., Volli, V. and Shu, C.M., 2019. Progressive utilisation prospects of coal fly ash: A review. Science of the Total Environment, 672, pp.951-989.

Gollakota, A.R., Volli, V. and Shu, C.M., 2019. Progressive utilisation prospects of coal fly ash: A review. Science of the Total Environment, 672, pp.951-989.

Green, D.W., and Perry, H., 2008. Perry's Chemical Engineers' Handbook, Eighth Edition. McGraw-Hill: New York.

Grzywa-Celińska, A., Krusiński, A., Mazur, J., Szewczyk, K. and Kozak, K., 2020. Radon—the element of risk. The impact of radon exposure on human health. Toxics, 8(4):120.

Guinée, J.B. and Lindeijer, E. eds., 2002. Handbook on life cycle assessment: operational guide to the ISO standards (Vol. 7). Springer Science & Business Media.

Gursel, A.P., Maryman, H. and Ostertag, C., 2016. A life-cycle approach to environmental, mechanical, and durability properties of “green” concrete mixes with rice husk ash. Journal of Cleaner Production, 112, pp.823-836.

Hanle, L.J., Jayaraman, K.R. and Smith, J.S., 2004. CO2 emissions profile of the US cement industry. Washington DC: Environmental Protection Agency.

Haque, M.B., Tuhin, I.A. and Farid, M.S.S., 2012. Effect of aggregate size distribution on concrete compressive strength. SUST journal of science and technology, 19(5), pp.35-39.

Hardjito, D. and Rangan, B.V., 2005. Development and properties of low-calcium fly ash-based geopolymer concrete

Hardjito, D., 2005. Studies of fly ash-based geopolymer concrete (Doctoral dissertation, Curtin University).

Hartung, R., 1973. Biological effects of heavy metal pollutants in water. Metal Ions in Biological Systems: Studies of Some Biochemical and Environmental Problems, pp.161-172.

Heah, C.Y., Kamarudin, H., Al Bakri, A.M., Binhussain, M., Luqman, M., Nizar, I.K., Ruzaidi, C.M. and Liew, Y.M., 2011. Effect of curing profile on kaolin-based geopolymers. Physics Procedia, 22, pp.305-311.

International Organization for Standardization, 2000. Fire-resistance Tests: Elements of Building Construction. Specific Requirements for Loadbearing Horizontal Separating Elements. ISO.

ISO, I., 2006. 14044—Environmental Management—Life Cycle Assessment—Principles and Framework. International Organization for Standardization. Switzerland: Ginevra.

ISO, I., 2020. 14044: 2006 Environmental management—life cycle assessment—requirements and guidelines; 2006. International Organization for Standardization.

Jaworowski, Z. and Grzybowska, D., 1977. Natural radionuclides in industrial and rural soils. Science of the Total Environment, 7(1), pp.45-52.

Jayasree, C. and Gettu, R., 2008. Experimental study of the flow behaviour of superplasticized cement paste. Materials and structures, 41(9), pp.1581-1593.

Kalombe, M. R. (2018) 'Synthesis of geopolymer using South African Coal fly ash', (MEng thesis, Cape Peninsula University of Technology).p. 66.

Kalombe, R.M., Ojumu, T.V., Katambwe, V.N., Nzadi, M., Bent, D., Nieuwouldt, G., Madzivire, G., Kevern, J. and Petrik, L.F., 2020. Treatment of acid mine drainage with CFA in a jet loop reactor pilot plant. Minerals Engineering, 159:106611.

Kalombe, R.M., Ojumu, V.T., Eze, C.P., Nyale, S.M., Kevern, J. and Petrik, L.F., 2020. Fly ash-based geopolymer building materials for green and sustainable development. Materials, 13(24):5699.

Keyte, L. M., 2009. "Fly ash glass chemistry and inorganic polymer cements," Geopolymers: Structures, Processing, Properties and Industrial Applications, pp. 15–36. doi: 10.1533/9781845696382.1.15

Khale, D. and Chaudhary, R., 2007. Mechanism of geopolymerization and factors influencing its development: a review. Journal of materials science, 42(3), pp.729-746.

Khunthongkeaw, J., Tangtermsirikul, S. and Leelawat, T., 2006. A study on carbonation depth prediction for fly ash concrete. Construction and building materials, 20(9), pp.744-753.

Kumar, S., Kristály, F. and Mucsi, G., 2015. Geopolymerisation behaviour of size fractioned fly ash. Advanced Powder Technology, 26(1), pp.24-30.

Li, Z., 2011. Advanced concrete technology. John Wiley & Sons. First edition,…….

Llope, W. J., 2011. Activity concentrations and dose rates from decorative granite countertops. Journal of Environmental Radioactivity, 102(6), 620–629. https://doi.org/10.1016/j.jenvrad.2011.03.012

Lorenzo-Gonzalez, M., Torres-Duran, M., Barbosa-Lorenzo, R., Provencio-Pulla, M., Barros-Dios, J.M. and Ruano-Ravina, A., 2019. Radon exposure: a major cause of lung cancer. Expert review of respiratory medicine, 13(9), pp.839-850.

Luo, J., Emelogu, O., Morosuk, T. and Tsatsaronis, G., 2019. Exergy-based investigation of a coal-fired allam cycle. E3S Web of Conferences 137, 01018.

Madzivire, G., Maleka:P., Vadapalli, V.R., Gitari, W.M., Lindsay, R. and Petrik, L.F., 2014. Fate of the naturally occurring radioactive materials during treatment of acid mine drainage with coal fly ash and aluminium hydroxide. Journal of environmental management, 133, pp.12-17.

Mahmood, Z.S.M., 2019. Strength and durability characteristics of pumice-based geopolymer paste. Doctoral dissertation, published thesis, Institute of Natural Science and Applied sciences department of civil engineering. pp. 12

Maleka, R.M., 2015. Acid mine drainage treatment with CFA lime and aluminium hydroxide: Potential CO2 sequestration, Master degree, Unpublished thesis, Univesity of Western Cape. pp. 53

Marsh, H. and Rodríguez-Reinoso, F., 2006. Production and reference material. Activated carbon, 454.

Mužek, M.N., Zelić, J. and Jozić, D., 2012. Microstructural characteristics of geopolymers based on alkali-activated fly ash. Chemical and Biochemical Engineering Quarterly, 26(2),

Nagaratnam, S., Carthigesu, T.G., Rabin, T. and Kanna, M.B., 2016. Civil Engineering Materials, International Edition, Gengage Learning, Canada, pp.121-274.

Nagy, K.D., Shen, B., Jamison, T.F. and Jensen, K.F., 2012. Mixing and dispersion in small-scale flow systems. Organic Process Research & Development, 16(5), pp.976-981.

Naqi, A. and Jang, J.G., 2019. Recent progress in green cement technology utilizing low-carbon emission fuels and raw materials: A review. Sustainability, 11(2):537.

Nath, S.K., Maitra, S., Mukherjee, S. and Kumar, S., 2016. Microstructural and morphological evolution of fly ash based geopolymers. Construction and Building Materials, 111, pp.758-765.

NCTEL., 2019. Efflorescence in bricks. Available at https://www.youtube.com/watch?v=2pu2SxAK-Q8 , Accessed on 30th of July 2022).

Nematollahi, B. and Sanjayan, J., 2014. Effect of different superplasticizers and activator combinations on workability and strength of fly ash based geopolymer. Materials & Design, 57, pp.667-672.

Nguyen, K.T., Ahn, N., Le, T.A. and Lee, K., 2016. Theoretical and experimental study on mechanical properties and flexural strength of fly ash-geopolymer concrete. Construction and Building Materials, 106, pp.65-77.

North, M. R., & Swaddle, T. W. (2000). Kinetics of silicate exchange in alkaline aluminosilicate

solutions. Inorganic chemistry, 39(12), 2661-2665.

NRC., 2006. National Research Council BEIR VII: Health Risks From Exposure to Low Levels of Ionizing Radiation.

Nunes, C., Mahendrasingam, A. and Suryanarayanan, R., 2005. Quantification of crystallinity in substantially amorphous materials by synchrotron X-ray powder diffractometry. Pharmaceutical research, 22(11), pp.1942-1953.

Nyale, S., 2014. Geopolymers from South African Fly Ash: Synthesis and Characteristics Doctoral dissertation, Unpublished thesis, Univesity of Western Cape. pp. 79-106.

Omer, A.M., 2008. Energy, environment and sustainable development. Renewable and sustainable energy reviews, 12(9), pp.2265-2300.

Omer, A.M., 2018. Renewable energy technologies, sustainable development, and environment. Sustainable Development: Concepts, Methodologies, Tools, and Applications, pp.971-1008.

Padmapriya, M., Ramesh, S.T. and Biju, V.M., 2022. Synthesis of seawater based geopolymer: characterization and adsorption capacity of methylene blue from wastewater. Materials Today: Proceedings, 51, pp.1770-1776.

Palomo, A. and Glasser, F.P., 1992. Chemically-bonded cementitious materials based on metakaolin. British ceramic. Transactions and journal, 91(4), pp.107-112.

Papadakis, V., Vayenas, C. and Fardis, M., 1991. Physical and chemical characteristics affecting the durability of concrete. ACI materials journal, 88(2), pp.186-196.

Park, C.S., 2020. Fundamentals of engineering economics. Fourth Edition. Chan S. Park. Pearson Education.

Patankar, S. V., Ghugal, Y. M., & Jamkar, S. S., 2014. Effect of concentration of sodium hydroxide and degree of heat curing on fly ash-based geopolymer mortar. Indian Journal of Materials Science, 2014.

Peng, X., Shuai, Q., Li, H., Ding, Q., Gu, Y., Cheng, C. and Xu, Z., 2020. Fabrication and fireproofing performance of the CFA-metakaolin-based geopolymer foams. Materials, 13(7):1750.

Phair, J.W., Van Deventer, J.S.J. and Smith, J.D., 2000. Mechanism of polysialation in the incorporation of zirconia into fly ash-based geopolymers. Industrial & engineering chemistry research, 39(8), pp.2925-2934.

Pilakouta, M.I.R.O.F.O.R.A., Pappa, F.K., Patiris, D.L., Tsabaris, C. and Kalfas, C.A., 2018. A methodology for expanding the use of NaI (Tl) based spectrometry in environmental radioactivity measurements. Applied Radiation and Isotopes, 139, pp.159-168.

Possan, E., 2010. Modelling of Carbonation and the Service Life Prediction of Concrete Structures at an Urban Environment (Doctoral dissertation, Doctorate Thesis in Civil Engineering, Federal University of Rio Grande do Sul, Porto Alegre, 2010 (in

Portuguese)).

Possan, E., Thomaz, W.A., Aleandri, G.A., Felix, E.F. and dos Santos, A.C., 2017. CO2 uptake potential due to concrete carbonation: A case study. Case Studies in Construction Materials, 6, pp.147-161.

Pouhet, R., 2015. Formulation and durability of metakaolin-based geopolymers (Doctoral dissertation, Université Paul Sabatier-Toulouse III).

PRé, C., 2021. SimaPro Database Manual Methods Library. Available at https://simapro.com/wp-content/uploads/2021/07/DatabaseManualMethods920.pdf , Accessed on 9th August 2022. PRé Consultants.

PRé, C., 2021. SimaPro software version 9.2.0.2. Single user. Available at https://simapro.com/ , Accessed on 8th August 2022. PRé Consultants.

Priyanka, M., Karthikeyan, M. and Chand, M.S.R., 2020. Development of mix proportions of geopolymer lightweight aggregate concrete with LECA. Materials Today: Proceedings, 27, pp.958-962.

Provis, J.L. and Van Deventer, J.S.J. eds., 2009. Geopolymers: structures, processing, properties and industrial applications. Elsevier, pp.6

Rashidian-Dezfouli, H., Rangaraju:R. and Kothala, V.S.K., 2018. Influence of selected parameters on compressive strength of geopolymer produced from ground glass fiber. Construction and Building Materials, 162, pp.393-405.

Reynolds-Clausen, K. and Singh, N., 2019. South Africa's power producer's revised coal ash strategy and implementation progress. Coal Combustion and Gasification Products, 11(1), pp.10-17.

Romero-Gámez, M., Suárez-Rey, E.M., Antón, A., Castilla, N. and Soriano, T., 2012. Environmental impact of greenhouse and open-field cultivation using a life cycle analysis: the case study of green bean production. Journal of Cleaner Production, 28, pp.63-69.

RoofLock., 2013. What is Concrete Carbonation and how is it treated?. Available at https://www.rooflock.com/what-is-concrete-carbonation-and-how-is-it-treated/ , Accessed on 1st August 2022).

Rovnaník:, 2010. Effect of curing temperature on the development of hard structure of metakaolin-based geopolymer. Construction and building materials, 24(7), pp.1176-1183.

Roy, W.R., Thiery, R.G., Schuller, R.M. and Suloway, J.J., 1981. Coal fly ash: a review of the literature and proposed classification system with emphasis on environmental impacts. Environmental geology no. 096.

Sadiku, E.R., Phiri, G., Jayaramudu, T., Sudhakar, K., Moropeng, L., Khoathane, M.C., Adegbola, T.A. and Kupolati, W.K., 2016. Mechanisms of toughening in nanostructured polymer blends. In Design and Applications of Nanostructured

Polymer Blends and Nanocomposite Systems (pp. 365-384). William Andrew Publishing.

Salas, D.A., Ramirez, A.D., Ulloa, N., Baykara, H. and Boero, A.J., 2018. Life cycle assessment of geopolymer concrete. Construction and Building Materials, 190, pp.170-177.

SANS 3001 Standards., 2011. South African National Standards: Civil Engineering Test Methods. Parts GR1, GR2, GR3, GR5, GR10, GR11, GR12. Pretoria: South African Bureau of Standards.

SANS 5862-1, 2006. Concrete tests – Consistence of freshly mixed concrete - Slump test, Pretoria: South African Bureau of Standards, 2006.

SANS 5862-2, 2006. Concrete tests – Consistence of freshly mixed concrete - Flow test, Pretoria: South African Bureau of Standards, 2006.

SANS 5863:2006. Concrete tests – compressive strength of hardened concrete, Pretoria: South African Bureau of Standards, 2006.

SANS 5864:2006. Concrete tests – flexural strength of hardened concrete. Pretoria: South African Bureau of Standards, 2006.

SANS 6250:2006. Concrete tests - Density of compacted freshly mixed concrete, Pretoria: South African Bureau of Standards, 2006.

SANS 6253, 2006. Concrete tests - tensile splitting strength of concrete. Pretoria: South African Bureau of Standards, 2006.

SANS Standard 10400, 1990. The application of the National Building Regulations, The Council of South African Bureau of Standard, Gr 22:73.

SANS Standards Division.,1997. South Afrian National Standards 10177-2 Fire Testing of Materials, Components and Elements Used in Buildings. Pretoria: South African Bureau of Standards (SABS).

SANS Standards Division.,2006. South Afrian National Standards 6250:2006 concrete density test (1.1 ed.). Pretoria: South African Bureau of Standards (SABS).

Scrivener, K.L. and Young, J.F., 1997. Mechanisms of chemical degradation of cement-based systems. CRC Press, pp.222.

Scrivener, K.L., 2014. Options for the future of cement. Indian Concr. J, 88(7), pp.11-21.

Selih, J. and de Sousa, A.C., 2006. Use of LCA As a Decision Method in the Optimization of Use of LCA As a Decision Method in the Optimization of Construction Processes.

Sengun, N., Demirdag, S., Akbay, D., Ugur, I., Altindag, R. and Akbulut, A., 2014, October. Investigation of the relationships between capillary water absorption coefficients and other rock properties of some natural stones, V. In Global stone congress (pp. 22-25).

Shannag, M.J. and Shaia, H.A., 2003. Sulphate resistance of high-performance concrete. Cement and Concrete Composites, 25(3), pp.363-369.

Shi, C., Roy, D., & Krivenko: (2003). Alkali-activated cements and concretes. CRC press.

Silla, H., 2003. Chemical process engineering: design and economics. 1 st Edition CRC Press. Boca Raton. https://doi.org/10.1201/9780203912454

Silverstrim, T., Rostami, H., Larralde, J. and Samadi, A., Drexel University and Products Development Co, 1997. Fly ash cementitious material and method of making a product. U.S. Patent 5,601,643.

Simonsen, M.E., Sønderby, C., Li, Z. and Søgaard, E.G., 2009. XPS and FT-IR investigation of silicate polymers. Journal of materials science, 44(8), pp.2079-2088.

Sindhunata,, Van Deventer, J.S.J., Lukey, G.C. and Xu, H., 2006. Effect of curing temperature and silicate concentration on fly-ash-based geopolymerization. Industrial & Engineering Chemistry Research, 45(10), pp.3559-3568.

Sinnott, R., 2005. Chemical Engineering Design: Chemical Engineering Volume 6. Elsevier.pp.266.

Siregar, A.P.N., Rafiq, M.I. and Mulheron, M., 2017. Experimental investigation of the effects of aggregate size distribution on the fracture behaviour of high-strength concrete. Construction and Building Materials, 150, pp.252-259.

Somna, K., Jaturapitakkul, C., Kajitvichyanukul: and Chindaprasirt:, 2011. NaOH-activated ground fly ash geopolymer cured at ambient temperature. Fuel, 90(6), pp.2118-2124.

Soroka, I.,1979. Portland Cement Paste and Concrete. The Macmillan Press Ltd, London, UK, pp. 28.

Soroka, I.,1993. Concrete in a hot environment. E& FN Spon, London, UK, pp. 22.

Soutsos, M., Boyle, A.P., Vinai, R., Hadjierakleous, A. and Barnett, S.J., 2016. Factors influencing the compressive strength of fly ash-based geopolymers. Construction and Building Materials, 110, pp.355-368.

Speight, J. G., 2008. Synthetic fuels handbook: properties, process, and performance. McGraw-Hill Education, New York, pp.135-142.

Stanković, M., Pavlović, S., Marinković, D., Tišma, M., Gabrovska, M. and Nikolova, D., 2020. Solid green biodiesel catalysts derived from coal fly ash. Resources, Challenges and Applications:185.pp.89-95.

Sultana, S., Ahsan, S., Tanvir, S., Haque, N., Alam, F. and Yellishetty, M., 2021. CFA Utilisation and Environmental Impact. In Clean Coal Technologies (pp. 381-402). Springer, Cham.

Susilawati, R., 2015. Mineral matter in coal. Buletin Sumber Daya Geologi, 10(1), pp.14-27.

Taylor, H.F.W., Famy, C. and Scrivener, K.L., 2001. Delayed ettringite formation. Cement and concrete research, 31(5), pp.683-693.

Taylor:C., 2013. “Benefits of curing on concrete performance”. Curing concrete. 1st Edition CRC press. London. P.39. https://doi.org/10.1201/b15519

Timakul:, Thanaphatwetphisit, K. and Aungkavattana:, 2015. Effect of silica to alumina ratio on the compressive strength of class C fly ash-based geopolymers. In Key engineering materials (Vol. 659, pp. 80-84). Trans Tech Publications Ltd.

Tokyay, M., 2016. Cement and concrete mineral admixtures. CRC Press.

Turton, R., Bailie, R.C., Whiting, W.B. and Shaeiwitz, J.A., 2008. Analysis, synthesis and design of chemical processes. Pearson Education.

USEIA., 2014. Statistics on global coal production, consumption [WWW Document]. 2014. URL https://www.eia.gov/coal/data.php#production Google Scholar

Usha, S., Nair, D.G. and Vishnudas, S., 2014. Geopolymer binder from industrial wastes: A review. Int. J. Civ. Eng. Technol, 5(12), pp.219-225.

Valeev, D., Mikhailova, A. and Atmadzhidi, A., 2018. Kinetics of iron extraction from CFA by hydrochloric acid leaching. Metals, 8(7):533.

Van Chanh, N., Trung, B.D. and Van Tuan, D., 2008, November. Recent research geopolymer concrete. In The 3rd ACF international conference-ACF/VCA, Vietnam (Vol. 18, pp. 235-241).

Van Chanh, N., Trung, B.D. and Van Tuan, D., 2008, November. Recent research geopolymer concrete. In The 3rd ACF international conference-ACF/VCA, Vietnam (Vol. 18, pp. 235-241).

Van Deventer, J.S., Provis, J.L., Duxson: and Brice, D.G., 2010. Chemical research and climate change as drivers in the commercial adoption of alkali-activated materials. Waste and Biomass Valorization, 1(1), pp.145-155.

Velasquez, C., Rojas, F., Lara, V.H. and Campero, A., 2004. On the textural and morphological properties of crystalline and amorphous α-tin phosphate. Physical Chemistry Chemical Physics, 6(19), pp.4714-4721.

Vinai, R. and Soutsos, M., 2019. Production of sodium silicate powder from waste glass cullet for alkali activation of alternative binders. Cement and Concrete Research, 116, pp.45-56.

Waldmann, D., May, A. and Thapa, V.B., 2017. Influence of the sheet profile design on the composite action of slabs made of lightweight woodchip concrete. Construction and building materials, 148, pp.887-899.

Wallah, S., & Rangan, B. V., 2006. Low-calcium fly ash-based geopolymer concrete: long-term properties. Research Report GC2, Curtin University of Technology.

Wang, C., Xu, G., Gu, X., Gao, Y. and Zhao:, 2021. High value-added applications of CFA in the form of porous materials: a review. Ceramics International, 47(16), pp.22302-22315.

Wang, S., 2008. Application of solid ash-based catalysts in heterogeneous catalysis. Environmental science & technology, 42(19), pp.7055-7063.

Wang, Y., Wu, J., Ma, D., Yang, S., Yin, Q. and Feng, Y., 2022. Effect of aggregate size distribution and confining pressure on mechanical property and microstructure of cemented gangue backfill materials. Advanced Powder Technology, 33(8):103686.

Waters, M.D., Gardner, D.E., Aranyi, C. and Coffin, D.L., 1975. Metal toxicity for rabbit alveolar macrophages in vitro. Environmental research, 9(1), pp.32-47.

Wee, T.H., Suryavanshi, A.K., Wong, S.F. and Rahman, A.A., 2000. Sulphate resistance of concrete containing mineral admixtures. Materials Journal, 97(5), pp.536-549.

Weidema, B.P., Bauer, C., Hischier, R., Mutel, C., Nemecek, T., Reinhard, J., Vadenbo, C.O. and Wernet, G., 2013. Overview and methodology: Data quality guideline for the ecoinvent database version 3.

Weiland, N.T. and White, C.W., 2018. Techno-economic analysis of an integrated gasification direct-fired supercritical CO2 power cycle. Fuel, 212, pp.613-625.

Weisheit, S., Unterberger, S.H., Bader, T. and Lackner, R., 2016. Assessment of test methods for characterizing the hydrophobic nature of surface-treated High-Performance Concrete. Construction and Building Materials, 110, pp.145-153.

Wernet, G., Bauer, C., Steubing, B., Reinhard, J., Moreno-Ruiz, E. and Weidema, B., 2016. The ecoinvent database version 3 (part I): overview and methodology. The International Journal of Life Cycle Assessment, 21(9), pp.1218-1230.

Xie, T. and Ozbakkaloglu, T., 2015. Behavior of low-calcium fly and bottom ash-based geopolymer concrete cured at ambient temperature. Ceramics International, 41(4), pp.5945-5958.

Xu, H. and Van Deventer, J.S.J., 2000. The geopolymerisation of alumino-silicate minerals. International journal of mineral processing, 59(3), pp.247-266.

Yao, Z.T., Ji, X.S., Sarker:K., Tang, J.H., Ge, L.Q., Xia, M.S. and Xi, Y.Q., 2015. A comprehensive review on the applications of coal fly ash. Earth-science reviews, 141, pp.105-121.

Yoon, I.S., Çopuroğlu, O. and Park, K.B., 2007. Effect of global climatic change on carbonation progress of concrete. Atmospheric environment, 41(34), pp.7274-7285.

Yousuf, M., Mollah, A., Hess, T.R., Tsai, Y.N. and Cocke, D.L., 1993. An FTIR and XPS investigations of the effects of carbonation on the solidification/stabilization of cement-based systems-Portland type V with zinc. Cement and Concrete Research, 23(4), pp.773-784.

Yu, F., Sun, D., Wang, J. and Hu, M., 2019. Influence of aggregate size on compressive

strength of pervious concrete. Construction and Building Materials, 209, pp.463-475.

Zhang, D., 2013. “Ash fouling, deposition and slagging in ultra-supercritical coal power plants,” in Ultra-Supercritical Coal Power Plants: Materials, Technologies and Optimisation. Woodhead Publishing, pp. 133–183. doi: 10.1533/9780857097514.2.133.

Zheng, L., Wang, W. and Shi, Y., 2010. The effects of alkaline dosage and Si/Al ratio on the immobilization of heavy metals in municipal solid waste incineration fly ash-based geopolymer. Chemosphere, 79(6), pp.665-671.

Appendices

Appendix A

This Section contains extra information regarding extra experimental and literature Figures used in this study.

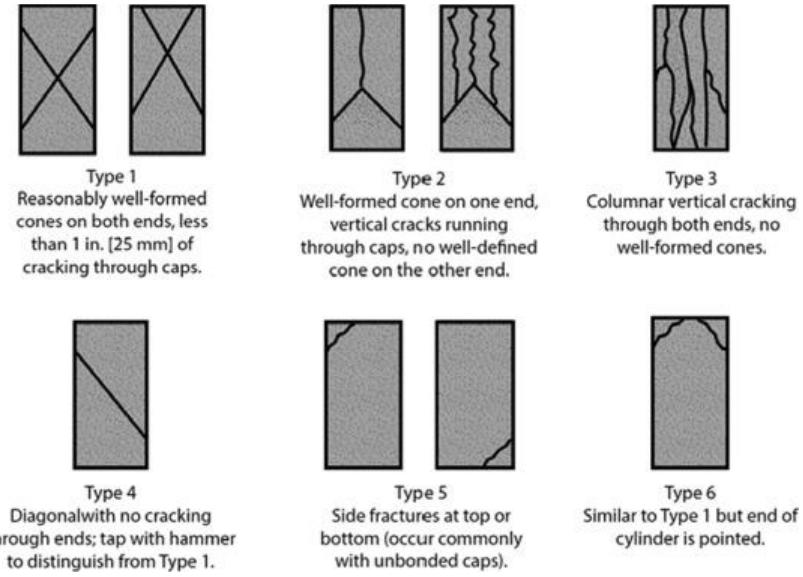

Figure A-1: CFA-based geopolymer concrete cylinder failure type compared to ASTM C39 failure

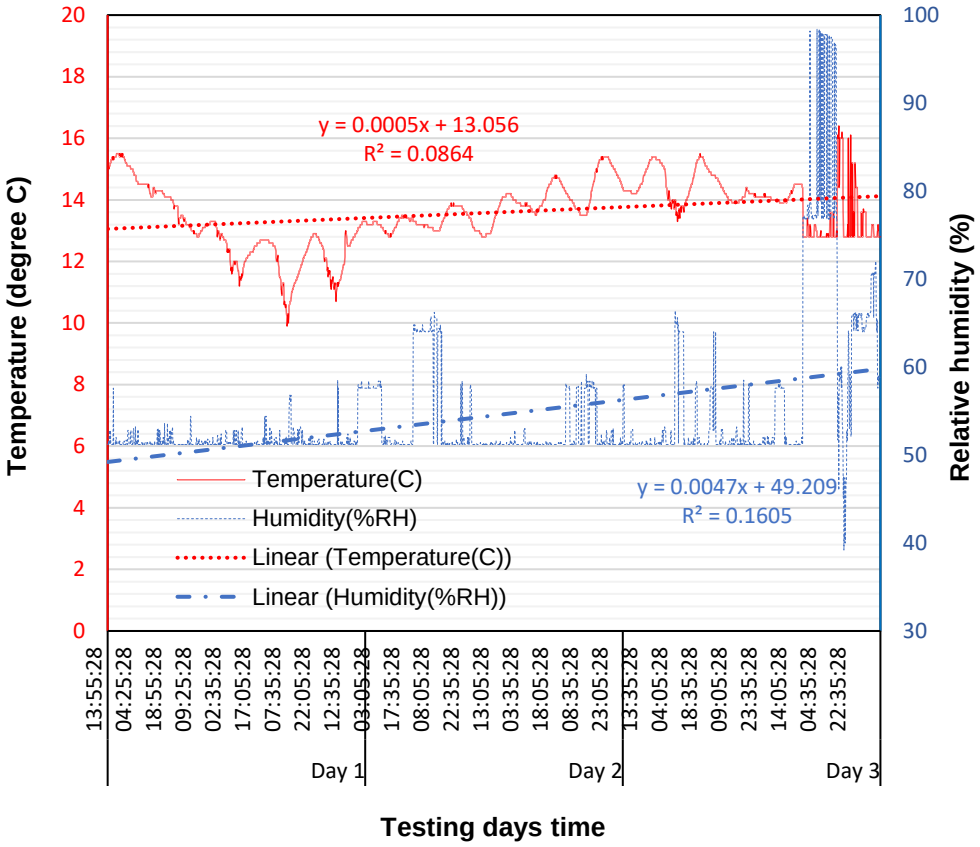

Figure A-2: Experimental temperature and humidity recording during efflorescence test

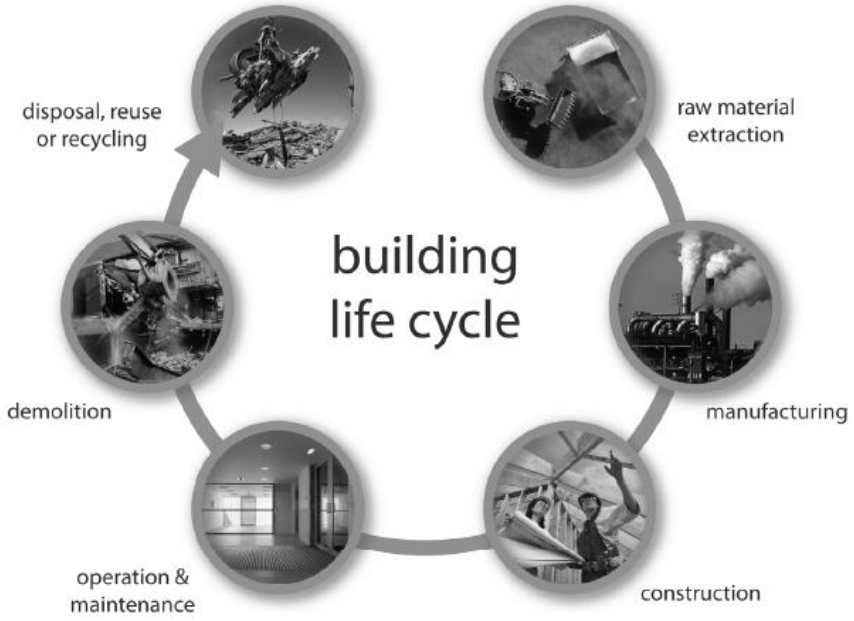

Figure A-3: Stage involved in the building life cycle (Source: Crawford, 2011).

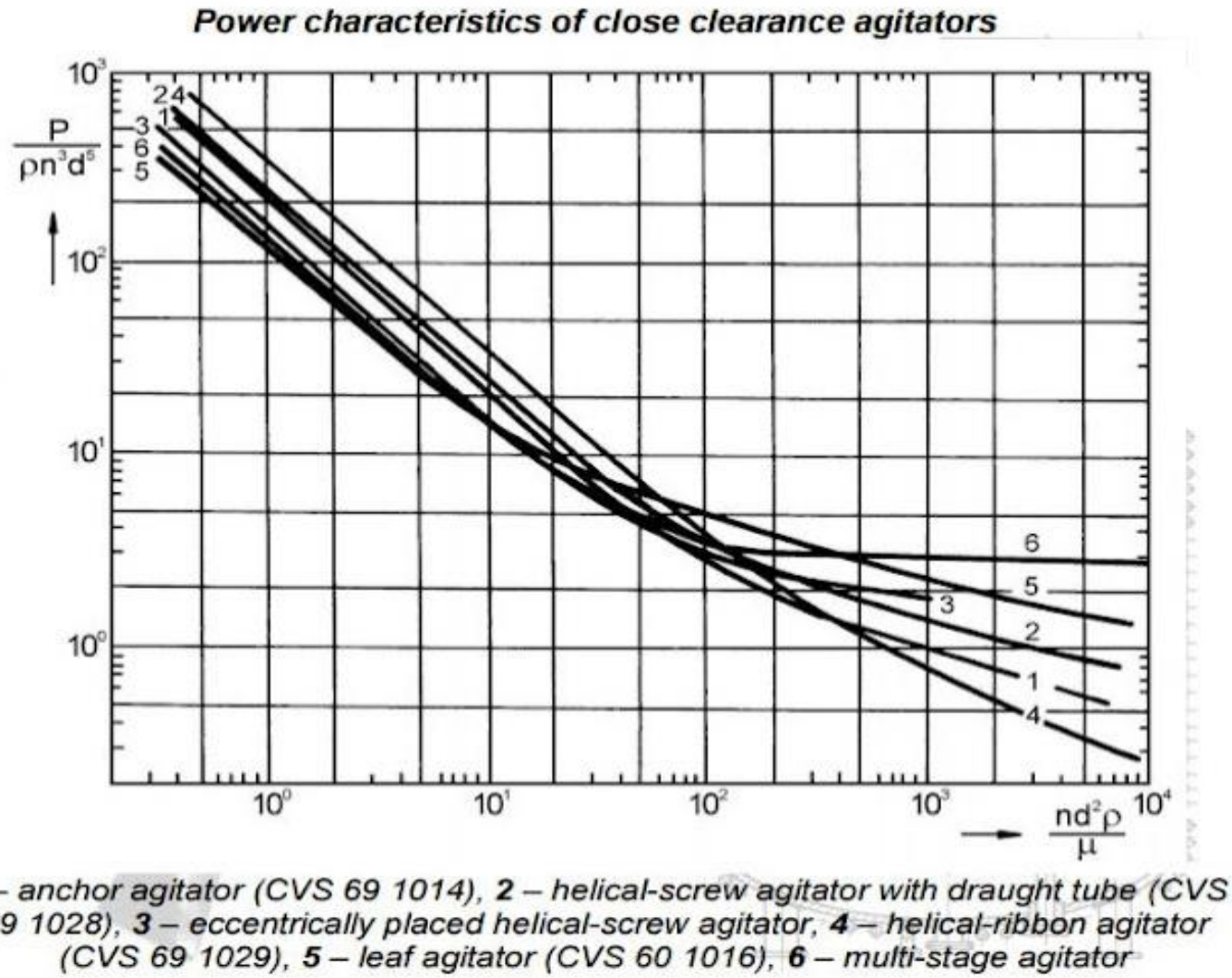

Figure A-4: Power characteristics of close clearance agitator curve for anchor agitator (Available at https://www.pharmacalculations.com/2016/05/types-of-agitators.html, Accessed on 12 November 2022).

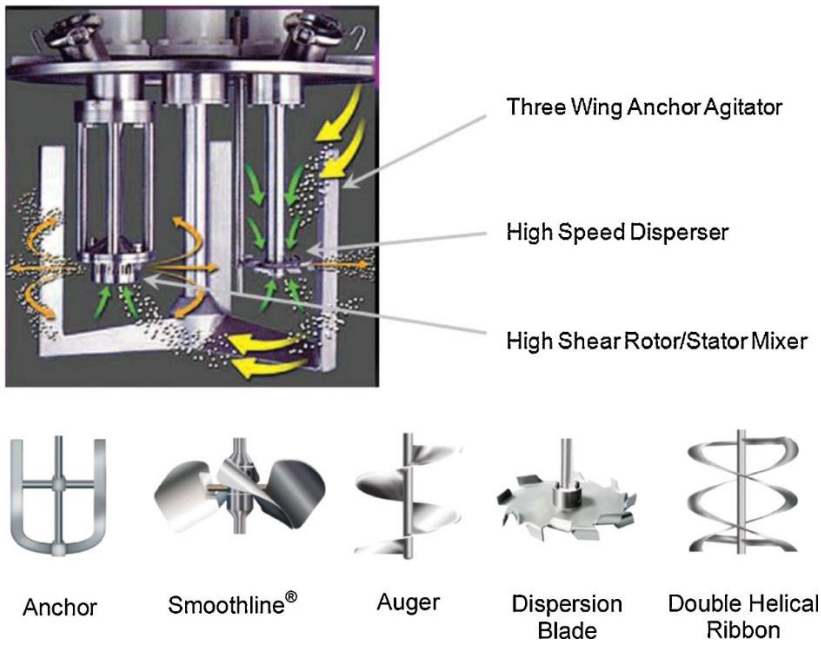

Figure A-5: An example of suitable a suitable model for the synthesis of CFA-based geopolymer concrete geopolymer stirred-tank reactor at large-scale capacity (modified from source: Ghanem et al, 2014).

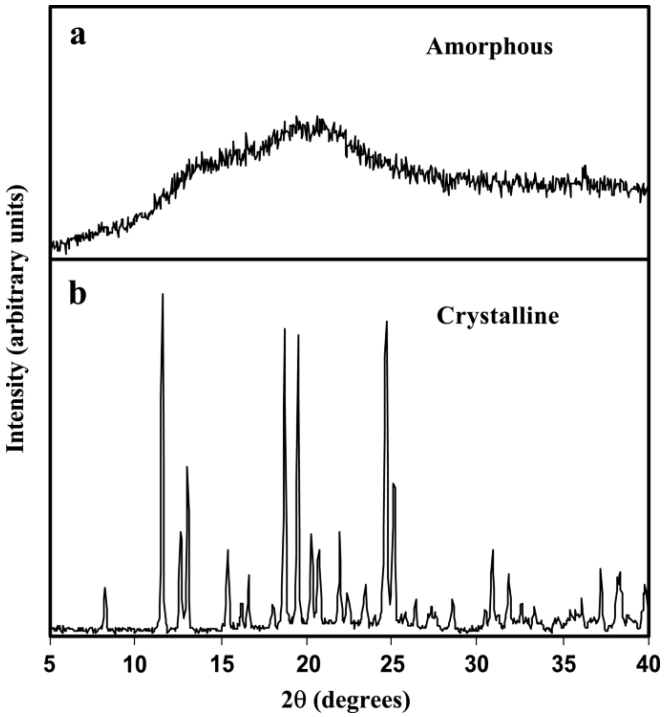

Figure A-6: Identification of powder X-ray patterns; amorphous (a) and crystalline (b) (Source: Nunes et al., 2005).

Millimeters	µm	Phi (ϕ)	Wentworth size class	
		-20		
4096		-12	Boulder (-8 to -12ϕ)	
1024		-10		
256		-8	Pebble (-6 to -8ϕ)	
64		-6		
16		-4	Pebble (-2 to -6ϕ)	Gravel
4		-2		
3.36		-1.75		
2.83		-1.50	Gravel	
2.38		-1.25		
2.00		-1.00		
1.68		-0.75		
1.41		-0.50	Very coarse sand	
1.19		-0.25		
1.00		-0.00		
0.84		0.25		
0.71		0.50	Coarse sand	
0.59		0.75		
1/2 – 0.50	500	1.00		
0.42	420	1.25		
0.35	350	1.50	Medium sand	Sand
0.30	300	1.75		
1/4 – 0.25	250	2.00		
0.210	210	2.25		
0.177	177	2.50	Fine sand	
0.149	149	2.75		
1/8 – 0.125	125	3.00		
0.105	105	3.25		
0.088	88	3.50	Very fine sand	
0.074	74	3.75		
1/16 – 0.0625	63	4.00		
0.0530	53	4.25		
0.0440	44	4.50	Coarse silt	
0.0370	37	4.75		
1/32 – 0.0310	31	5		
1/64 0.0156	15.6	6	Medium silt Fine silt	
1/128 0.0078	7.8	7	Very fine silt	
1/256 – 0.0039	3.9	8		Mud
0.0020	2.0	9		
0.00098	0.98	10		
0.00049	0.49	11	Clay	
0.00024	0.24	12		
0.00012	0.12	13		
0.00006	0.06	14		

Figure A-7: Wentworth grain-size scale for siliciclastic sediment (Available at http://www-odp.tamu.edu/publications/197_IR/chap_02/c2_f6.htm, Accessed on the 30th of September 2022).

Figure A-8: Fire test sample mould with Y6 reinforcement steel (a) and fire sample after finished (b).

Figure A-9: Top face of radon measurement RAD 7 (a) and 100 mm cubic CFA-based geopolymer paste block inside a gamma vacuum chamber.

Figure A-10:CFA-based geopolymer paste after Vicat apparatus test

Appendix B.

This Section contains additional results data of the experiment and analytical techniques as well as that of literature which served during the decision making.

Table B-1: Embodied energy and Carbon dioxide emission related to 1 Kg of different materials produced (Source: Scrivener, 2014)

Material	Embodied Energy, MJ/Kg	CO_2 emissions Kg CO_2 eq
Normal concrete	0.95	0.13
Fire clay bricks	3.00	0.22
Road & Pavement	2.41	0.14
Glass	15.00	0.85
Wood (plain timber)	8.50	0.46
Wood (multilayer board)	15.00	0.81
Steel (from ore)	35.00	2.80

Table B-2: Scale-up for kinematic similarity index n values (Available at https://www.pharmacalculations.com/2016/05/types-of-agitators.html, Accessed on 12 November 2022).

Requirements	n Value
For equal liquid motions	1
For equal liquid suspension of solids	3/4
For equal rate of mass transfer	2/3

Table B-3: Cost and shipping cost and other activities costs associated with the JS 1000 concrete mixer.

JS 1000 concrete batch mixer set, activity	**Cost, R**
Purchased price	R 103 654.20
Shipping	R 74 009.10
Installation	R 38 144.75
Insurance	R 4 871.75
Taxes	R 15 548.13
Engineering	R 14 096.97
Some overhead expenses	R 36 278.97
Bare module cost (including JS 1000 concrete batch mixer set)	**R 286 603.86**
Total module cost (Bare module cost + unforeseen costs and contractor fees)	**R 338 192.56**

Table B-4: Sieve analysis results and cumulative percentage of coarse aggregate

SABS Sieves, mm	Retained by sieve			Cumulative percentage passing sieve
	On specific sieve		Cumulative percentage of the total mass	
	Mass, g	Percentage of the total mass		
20	12	0.77	0.77	99.23
14	75	4.80	5.57	94.43
10	1080	69.11	74.68	25.32
7.1	386	24.70	99.38	0.62
5	8	0.51	99.89	0.11
2	0.5	0.03	99.92	0.08
1	0	0.00	99.92	0.08
0.6	0	0.00	99.92	0.08
0.3	0	0.00	99.92	0.08
0.15	0.75	0.05	99.97	0.03
0.075	0.5	0.03	100.00	0.00
Pan	0	0.00	100.00	0.00
Total	1562.75	100	599.54	220.08
Fitness modulus=		6.00		

Table B-5: Sieve analysis and cumulative fine aggregates

SABS Sieves, mm	Retained by sieve			Cumulative percentage passing sieve
	On specific sieve		Cumulative percentage of the total mass	
	Mass, g	Percentage of the total mass		
20	0	0.00	0.00	100.00
14	0	0.00	0.00	100.00
10	0	0.00	0.00	100.00
7.1	0	0.00	0.00	100.00
5	0	0.00	0.00	100.00
2	2	0.29	0.29	99.71
1	43	6.23	6.52	93.48
0.6	83	12.03	18.55	81.45
0.3	202	29.28	47.83	52.17
0.15	296	42.90	90.72	9.28
0.075	64	9.28	100.00	0.00
Pan	0	0.00	100.00	0.00
Total	690	100	163.91	836.09
Fitness modulus=		1.64		

Table B-6: Process equipment building material to be considered during installation.

Equipment name	Construction Material type	Construction material to be avoid	Comment
Paving moulds	Plastic or steel	-	-
Water measurement bucket	Plastic or steel	-	-
Sodium hydroxide preparation tank	Plastic	Aluminium based drum	Na_2O can react with Al_2O_3
Sodium hydroxide solution measuring bucket	Plastic	Aluminium based drum	Na_2O can react with Al_2O_3
Sodium silicate measuring drum	Plastic or steel	-	
Alkaline storage drum	Plastic	Aluminium based drum	-

Na_2O and Al_2O_3 are sodium and aluminium oxides respectively.

Table B-7: CFA-based geopolymer paste and concrete Tensile-to-compression strength ratio

CFA-based geopolymer strength	Tensile strength, MPa	Tensile to compression strength ratio, %
GPP, room with plastic cover	2.8	6.7
GPC, room with plastic cover	4.0	12.8
GPC, 24 hr 60 oC oven curing	4.5	11.7
GPC, room no with plastic cover	2.8	11.0

Table B-8: Carbon dioxide greenhouses equivalent over Global warning potential period of 100 years and their emissions sources (Source: Available at: https://www.epa.gov/ghgemissions/overview-greenhouse-gases#CO2-references, Accessed on 8th of August 2022).

Greenhouse gases	Chemical Formulas	Global Warming Potential (100-year) CO2 eq	Atmospheric lifetime (years)	Emission sources
Carbon dioxide	CO_2	1	Depend	Burning fossil fuels (coal, natural gas, and oil), solid waste, trees and other biological materials, as well as a result of certain chemical reactions
Methane	CH_4	25	12	production and transport of; coal, natural gas and oil. Livestock and agricultural practices. Land use and decay of organic waste in municipal solid waste landfills.
Nitrous oxide	N_2O	298	114	Agricultural, land use, and industrial activities; combustion of fossil fuels and solid waste and during the treatment of wastewater
Fluorinated gases	HFCs	up to 14,800	Up to 270	household, commercial, and industrial applications and processes.
	PFCs	up to 12,200	2,600 to 50,000	
	NF_3	17,200	740	
	SF_6	22,800	3,200	

Depend= CO_2 in the atmosphere is a component of the global carbon cycle, and its fate depends on geochemical and biological processes. Even though some excess carbon dioxide will be absorbed quickly (for example, by the ocean surface), some will remain in the atmosphere for thousands of years due to the very slow process by which carbon is transferred to ocean sediments.

Table B-9: EDS elemental atomic and weight percentage of pure CFA and synthesised CFA-based geopolymer formulations before and after durability tests.

CFA & CFA-based geopolymer formulations		Chemical elements atomic (Atomic) weight (Wt) concentrations (%)												Total
		C	O	Na	Mg	Al	Si	S	K	Ca	Ti	Fe	Cu	
CFA	Atomic	34.59	45.94	0	0.25	7.54	9.64	0.14	0.19	0.86	0.31	0.46	0.09	100
	Wt	24.11	42.65	0	0.35	11.8	15.7	0.25	0.44	1.99	0.86	1.5	0.35	100
GP, room with plastic cover	Atomic	13.81	56.44	1.89		12.59	14.18	0	0.1	0.63	0.11	0.26	0	100
	Wt	8.73	47.55	2.28	0	17.89	20.97	0	0.21	1.33	0.29	0.75	0	100
GPM, room with plastic cover	Atomic	12.84	55.37	3.57	0.26	9.13	16.53	0	0.2	1.25	0.3	0.55	0	100
	Wt	7.94	45.61	4.22	0.33	12.69	23.9	0	0.41	2.58	0.74	1.59	0	100
GPC 24 hr 60 oC oven curing	Atomic	22.99	51.22	2.86	0.3	6.91	12.03	0.12	0.33	2.37	0.24	0.51	0.12	100
	Wt	14.91	44.23	3.55	0.39	10.06	18.24	0.2	0.7	5.13	0.62	1.53	0.42	100
GPC, room with plastic cover	Atomic	22.37	51.65	3.34	0.39	7.54	12.07	0.13	0.21	1.5	0.29	0.49	0	100
	Wt	14.62	44.96	4.18	0.52	11.07	18.45	0.23	0.44	3.28	0.75	1.5	0	100
GPC, room with no plastic cover	Atomic	30.04	48.12	3.11	0.44	6.38	9.94	0.13	0.15	1.07	0.21	0.33	0.08	100
	Wt	20.61	43.98	4.08	0.62	9.83	15.94	0.24	0.33	2.46	0.58	1.05	0.29	100
GPC, room with plastic cover after water soaked	Atomic	30.14	48.13	2.32	0.33	6.13	9.67	0.15	0.22	2.2	0.23	0.48	0	100
	Wt	20.46	43.51	3.01	0.46	9.34	15.35	0.27	0.49	4.97	0.62	1.5	0	100
GPC, room with plastic cover after fire	Atomic	26.08	50.48	2.43	0.25	6.25	11.62	0.15	0.19	1.83	0.21	0.41	0.09	100
	Wt	17.38	44.81	3.1	0.34	9.36	18.11	0.26	0.41	4.06	0.56	1.28	0.32	100

Appendix C

This Section provides additional information about the initial form of the Equation used including its derived form or other additional equations.

$$Impact\ category\ emission\ =\ Indicator\ (emission\ factor)\ \times amount\ used$$ Equation C.1

$$\begin{pmatrix} Final\ system \\ energy \end{pmatrix} - \begin{pmatrix} Initial\ system \\ energy \end{pmatrix} = \begin{pmatrix} net\ energy\ transferred \\ to\ the\ system \end{pmatrix}$$ Equation C.2

$$Initial\ system\ energy = U_i + E_{ki} + E_{pi}$$ Equation C.3

$$Final\ system\ energy = U_f + E_{kf} + E_{pf}$$ Equation C.4

$$Energy\ transferred = Q - W$$ Equation C.5

$$(U_f - U_i) + (E_{kf} - E_{ki}) + (E_{pf} - E_{pi}) = Q - W$$ Equation C.6

$$\Delta U + \Delta E_k + \Delta E_P = Q - W$$ Equation C.7

$$V_{lab} = \left(\frac{3.14 \times D_T}{4}\right) \times H$$ Equation C.8

Appendix D

Editor's Certificate